Low Loss Silicate Based Dielectric Materials for Wireless Communication

THESIS SUBMITTED TO

THE UNIVERSITY OF KERALA

FOR THE AWARD OF THE DEGREE OF

DOCTOR OF PHILOSOPHY

IN PHYSICS

UNDER THE FACULTY OF SCIENCE

BY

TONY JOSEPH

MATERIALS AND MINERALS DIVISION
NATIONAL INSTITUTE FOR INTERDISCIPLINARY
SCIENCE & TECHNOLOGY (CSIR)
THIRUVANANTHAPURAM- 695 019
KERALA, INDIA.

2011

Dedicated to.....

My beloved parents

DECLARATION

I hereby declare that the Ph.D thesis entitled **"Low loss silicate based dielectric materials for wireless communication"** is an independent work carried out by me at the Materials and Minerals Division, National Institute for Interdisciplinary Science and Technology (CSIR), Thiruvananthapuram, under the supervision of Dr. M. T. Sebastian, it has not been submitted any where else for any other degree, diploma or title.

Thiruvananthapuram
February 2011 Tony Joseph

राष्ट्रीय अंतर्विषयी विज्ञान तथा प्रौद्योगिकी संस्थान
(वैज्ञानिक एंव प्रौद्योगिकी अनुसंधान परिषद्)
(पहले क्षेत्रीय अनुसंधान प्रयोगशाला)
NATIONAL INSTITUTE FOR INTERDISCIPLINARY SCIENCE AND TECHNOLOGY
(Council of Scientific & Industrial Research)
(formerly Regional Research laboratory)
इन्डस्ट्रियल इस्टेट डाक घर, तिरुवनन्तपुरम 695 019, भारत
Industrial Estate P.O., Thiruvananthapuram 695 019, India

CERTIFICATE

This is to certify that the work embodied in the thesis entitled **"Low loss silicate based dielectric materials for wireless communication"** has been carried out by **Mr. Tony Joseph** under my supervision at the Materials and Minerals Division of National Institute for Interdisciplinary Science and Technology (Formerly Regional Research Laboratory), Thiruvananthapuram.

Thiruvananthapuram
February 2011

Dr. M. T. Sebastian

ACKNOWLEDGMENTS

I present this thesis, in the name of God, the Almighty, and my Source of Wisdom, who showers his unperturbed blessings undeservingly upon me throughout my life.

I wish to express my deepest gratitude to my thesis supervisor, Dr. M. T. Sebastian for suggesting an interesting problem, intellectual support, encouragement and enthusiasm expressed throughout the course of this research work.

I am highly thankful to Dr. Suresh Das, Director; Prof. T. K. Chandrashekar and Dr. B. C. Pai, former Directors, NIIST, Trivandrum for providing all the research facilities for Ph. D work.

I gratefully acknowledge Dr. Jose James (Scientist, NIIST) and Dr. Manoj Raama Varma (Scientist, NIIST) for fruitful scientific discussions and advices during my work.

I am deeply indebted to Dr. K. G. K. Warrier (Head, Materials and Minerals Division, NIIST, Thiruvananthapuram), Dr. U. Syamaprasad, Dr. Peter Koshy and Dr. P. Prabhakar Rao (Scientists, MMD, NIIST, Thiruvananthapuram) for their help given during the course of this work. The helps provided by other scientists of NIIST are also thankfully acknowledged.

The creative suggestions, valuable advice and help given by my seniors in the lab, N. Santha, Dr. Dr. L. A. Khalam (Lecturer, Iqbal College, Thiruvananthapuram), Dr. P. S. Anjana, (Lecturer, All Saints College, Thiruvananthapuram), Dr. G. Subodh (University of Stuttgart, Germany), Dr. Sumesh George and Mrs. Sherin Thomas are greatly acknowledged.

I thank my fellow labmates in Fine Ceramic group: Ms. T. S. Sasikala, Mr. Dhanesh Thomas, Mr. M. A. Sanoj, Mr. K. M. Manu, Ms. K. S. Deepa, Mr. K. Jithesh, Ms. J. Chameswary, Ms. P. Nisha, Ms. C. P. Reshmi, Ms. P. Neenu Lekshmi, Ms. Anlin Lazar K, Ms. Nina Joseph, and Mr. V. Jobin for their support and stimulating discussions. I am also thankful to my former colleagues in fine ceramics, Mr. V. K Sajith, K. S. Sandhya, Ms. Ali Fathima, Ms. S. Renjini, Ms. Sreena and Ms. B. Sayoojyam for their love and support.

I cherish the companionship of Mr. Alex, Mr. Jinish Antony, Mr. M. Shantil, Mr. Deepak D Prabhu, Mr. A. Aravind and Mr. Biju Francis who made my days at NIIST and Thiruvananthapuram a memorable one.

I am indebted to Mr. M. R. Chandran, Mr. P. Gurusamy, Mr. Veluswamy and Mr. P. Mukundan for extending the SEM, XRD and thermal measurement facility for my research work. I am thankful to all the office and library staff at NIIST for all their help and cooperation.

I wish to express my deep sense of gratitude to Prof. P. Mohanan (Department of Electronics, CUSAT, Cochin) and Dr. Jacob Philip (Sophisticates Test Instrument Centre, CUSAT, Cochin) for creative scientific discussions on dielectric and thermal conductivity measurements.

I would like to extend my sincere gratitude to Dr. H. Sreemoolanadhan (Scientist, VSSC) and Dr. R. Ratheesh (Scientist, C-MET, Thrissur) for the dielectric measurements as well as suggestions during my research.

I would like to express my thanks to Prof. H. Jantunen (University of Oulu, Oulu, Finland), Dr. Rick Ubic (Boise State University, Boise, ID, USA), Prof. Sander van Smaalen (University of Bayreuth, Bayreuth, Germany), Dr. Mohan Jacob (Australia) and Dr. D. Guha (Institute of Radio Physics and Electronics) for their collaborations with Dr. M. T. Sebastian, which helped me a lot during my Ph. D work.

The favors rendered by Mr. Rajesh (C-MET, Thrissur), Ms. S. Uma, and Mr. Sujith Raman (CUSAT, Cochin), are greatly acknowledged.

I fall in short of words in expressing my gratitude to my parents for their prayers and love throughout my education. I also wish to thank my siblings Teena and Terry for their affection and inspiration. At this time of happiness a special acknowledge is rendered to my grandma who is no more with me.

The financial assistance from Council of Scientific and Industrial Research in India (CSIR), New Delhi is gratefully acknowledged.

Finally, I need to express my appreciation to all those who have helped and inspired me during my doctoral study. The support from all these people gave me a lot of confidence throughout those countless hard-working days.

Tony Joseph

CONTENTS

List of Tables

List of Figures

ABBREVIATIONS

3G	third generations
CMS	calcium magnesium silicate, $CaMgSi_2O_6$
CTE	coefficient of thermal expansion
DGEBA	diglycidyl ether of bisphenol A
DR	dielectric resonator
DTA	differential thermal analysis
EMI	electromagnetic interference
HDPE	high density polyethylene
HTCC	high temperature co-fired ceramics
ICDD	international centre for diffraction data
LAN	local area network
LBS	lithium borosilicate
LMZBS	lithium magnesium zinc borosilicate
LSI	large scale integration
LTCC	low temperature co-fired ceramics
Mbps	mega bytes per second
PCB	printed circuit board
PS	polystyrene
PTFE	polytetrafluroethylene
PVA	polyvinyl alcohol
Q-factor	quality factor
SEM	scanning electron microscope
SPDR	split post dielectric resonator
S parameter	scattering parameter
SZS	strontium zinc silicate, $Sr_2ZnSi_2O_7$
TE mode	transverse electric mode
TGA	thermo gravimetric analysis
UTS	ultimate tensile strength
UTM	universal testing machine
WLAN	wireless local area network
XRD	X-ray diffraction

PREFACE

The recent growth in telecommunication systems and computers increased the demand for advanced materials with improved performance. Communication systems operating in the microwave and millimeter frequency range require materials for various applications like electronic packaging and dielectric resonators. The actual applications of dielectric materials in electronic packaging include printed circuit boards, substrates, encapsulations, interlayer dielectrics, die attach and so on. As the operating frequency is shifting to millimeter wave region, it is essential to use low permittivity materials for dielectric resonator applications. The development of dielectric ceramics with low permittivity, low dielectric loss together with good thermal stability remains as a challenging problem in the area of dielectric materials research.

The thesis entitled "Low loss silicate based dielectric materials for wireless communication" is a detailed investigation carried out on the synthesis, characterization, structure and microwave dielectric properties of certain silicates like alkaline earth orthosilicates and those belonging to akermanite-type and clinopyroxene group of silicates. The entire work has been divided into six chapters. The first chapter gives a general introduction of various applications of the dielectric ceramics and their importance in the field of wireless communication. Different application of dielectric materials like dielectric resonators, electronic packaging and substrates are elucidated along with the material requirements for these kinds of applications. The importance of low temperature co-fired ceramics as well as polymer-ceramic composites for applications as substrate materials are also discussed along with their merits and demerits. The preparation and characterization techniques used for the dielectric resonators and low temperature co-fired ceramics and polymer ceramic composite ares given in chapter two. The important properties of the materials measured include relative permittivity, dielectric loss or quality factor, temperature coefficient of resonant frequency, coefficient of thermal expansion, thermal conductivity etc.

The third chapter gives the structure and microwave dielectric properties of certain silicates. An introduction of Silicates and their various classifications based on oxygen sharing of $[SiO_4]^{4-}$ tetrahedra are also included in this chapter. The structure

and properties of three different classes of silicates are investigated (1) Sr-akermanite-type having the general formula $A_2BSi_2O_7$ where A = Ca, Sr, Ba and B = Zn, Mg, Ni, Co, Mn (2) alkaline earth orthosilicates, A_2SiO_4 where A= Ca, Sr, Ba and (3) clinopyroxenes having the formula $CaBSi_2O_6$ where B = Zn, Mg, Ni, Co, Mn. All the silicates studied are found to have low values of relative permittivity (~ 10) and varying values of quality factor and temperature coefficient of resonant frequency.

The investigations carried out in the third chapter indicate that two materials $CaMgSi_2O_6$ and $Sr_2ZnSi_2O_7$ may be suitable for dielectric resonator as well as substrate applications. The fourth chapter deals with lowering the sintering temperature of the above mentioned silicates for their applications as low temperature co-fired ceramics. The sintering temperature of the silicates is reduced by forming composites with low melting Lithium based borosilicate glasses. Their microwave dielectric properties are found to be suitable for forming hard substrates. The low sintering temperature (< 950 ^oC) enables the use of highly conductive metals like Ag, Au, Cu etc. for the metallization procedures. The chemical compatibility of the developed compositions for low temperature co-fired ceramic applications with Ag is also investigated in this chapter. The coefficients of thermal expansion of the compositions developed are measured and are found to be near to that of Silicon.

The individual properties of polymers and ceramics can be combined thereby offering excellent properties suitable for electronic packaging applications, which are discussed in the fifth chapter. The $Sr_2ZnSi_2O_7$ powder is mixed with different polymers such as polystyrene, high density polyethylene and Diglycidyl ether of bisphenol A and their electrical, thermal and mechanical properties are studied. The obtained values of relative permittivity, dielectric loss, thermal conductivity and coefficient of thermal expansion are compared with those of the theoretical predictions. The properties obtained for the polymer/ceramic composites indicate the possibility of using these composites for the development of soft substrates. The sixth chapter deals with major achievements of the investigations that have been carried out and the scope for future research based on the results of the present work.

Chapter 1

Dielectric Materials for Wireless Communication

1.1 Introduction

Wireless communication is, by any measure, the fastest growing segment of the communications industry. As such, it has captured the attention of the media and the imagination of the public. Cellular systems have experienced exponential growth over the last decade and there are currently around 4.5 billion users worldwide and about 650 million in India. Indeed, cellular phones have become a critical business tool and part of everyday life in most developed countries, and are rapidly replacing outdated wire line systems in many developing countries. In addition, wireless local area networks currently supplement or replace wired networks in many homes, businesses, and campuses. Many new applications, including wireless sensor networks, automated highways and factories, smart homes and appliances, and remote telemedicine, are emerging from research ideas to concrete systems. The explosive growth of wireless systems coupled with the propagation of laptop and palmtop computers indicate a bright future for wireless networks, both as stand-alone systems and as part of the larger networking infrastructure. However, many technical challenges remain in designing robust wireless networks that deliver the performance necessary to support emerging applications (Tse *et al.*, 2005).

As a first step to wireless communication, an elaborate set of signal combinations was developed to convey complex messages and observation stations were built on hilltops and along roads to relay these messages over large distances. These early communication networks were replaced first by the telegraph network (invented by Samuel Morse in 1838) and later by the telephone. In 1895, a few decades after the telephone was invented, Marconi demonstrated the first radio transmission from the Isle of Wight to a tugboat 18 miles away, and radio communication was born. Wired Ethernet technology was introduced in 1970's, which steered many commercial companies away from radio-based networking. Wired Ethernets today offer data rates of 100 Mbps. In 1985 the Federal Communications Commission (FCC) enabled the commercial development of wireless LANs. The current generation of wireless LANs has data rate capacity of several tens of Mbps and a coverage area of around 150 m. Despite the big data rate differences, wireless LANs are becoming the preferred Internet access method

in many homes, offices, and campus environments due to their convenience and freedom from wires.

Table 1.1 Licensed spectrum allocated to major commercial wireless systems

Wireless system	Frequency range
AM radio	535-1605 KHz
FM radio	88-108 MHz
Broadcast TV	54-88 MHz, 174-216 MHz
Broadcast TV (UHF)	470-806 MHz
3G broadband wireless	746-764 MHz, 776-794 MHz
1G and 2G digital cellular phones	806-902 MHz
Satellite digital radio	2.32-2.325 GHz
Satellite TV	12.2-12.7 GHz
Fixed wireless services	38.6-40 GHz

By far the most successful application of wireless networking has been the cellular telephone system. The roots of this system began in 1915, when wireless voice transmission between New York and San Francisco was first established. Cellular telephone systems are extremely popular and lucrative worldwide: these are the systems that ignited the wireless revolution. Cellular systems provide two-way voice and data communication with regional, national, or international coverage. Cellular systems were initially designed for mobile terminals inside vehicles with antennas mounted on the vehicle roof. Today these systems have evolved to support lightweight handheld mobile terminals operating inside and outside buildings at both pedestrian and vehicle speeds. The basic premise behind cellular system design is frequency reuse, which exploits the fact that signal power falls off with distance to reuse the same frequency spectrum at spatially-separated locations. The first generation of cellular systems (1G) used analog communications, wince they were primarily designed in the 1960's, before digital communications became prevalent. Second generation (2G) systems moved from analog to digital due to its many advantages. The components are cheaper, faster, smaller, and require less power. Voice quality and capacity are improved compared to analog systems. Digital systems can also offer data services in addition to voice, including short messaging, email, internet access, and imaging capabilities (camera phones).While 2G

networks focus primarily on voice communications, text messaging and simple web browsing, the latest third generation (3G) devices offer near-broadband speeds for web browsing and multimedia integration. The significant difference between 2G and 3G networks is the faster data speeds offered by 3G. For voice use and text messaging, the differences between a 2G and 3G phone are minimal. But the 3G standard allows data, pictures and videos to be uploaded and downloaded quickly (Goldsmith, 2005).

Commercial satellite systems are another major component of the wireless communication infrastructure. The most appealing use for satellite system is broadcasting of video and audio over large geographic regions. Satellites are best tailored for broadcasting, since they cover a wide area and are not compromised by an initial propagation delay. Moreover, the cost of the system can be amortized over many years and many users, making the service quite competitive with terrestrial entertainment broadcasting systems.

Table 1.2 Unlicensed spectrum allocated to the wireless systems.

Wireless system	**Frequency range**
Cordless phones, 1G WLANs	902-928 MHz
Bluetooth, WLANs	2.4-2.4835 GHz
Wireless PBX	5.725-5.85 GHz
Indoor systems	5.12-5.25 GHz
Short outdoor and campus applications	5.25-5.35 GHz
Long outdoor and point-to-point links	806-902 MHz

Most wireless applications reside in the radio spectrum between 30 MHz and 30 GHz. These frequencies are natural for wireless systems since they are not affected by the earth's curvature, require only moderately sized antenna, and can penetrate the ionosphere. The required antenna size for good reception is inversely proportional to the square of signal frequency, so moving systems to higher frequency allows for more compact antennas. However, received signal power with non-directional antennas is proportional to the inverse of frequency squared, so it is harder to cover large distances with higher frequency signals. The following table shows the licensed spectrum allocated

to major commercial wireless systems in the U.S. today. There are similar allocations in Europe and Asia.

Unlicensed spectrum is allocated by the governing body within a given country. Often countries try to match their frequency allocation for unlicensed use so that technology developed for that spectrum is compatible worldwide. The following table shows the unlicensed spectrum allocations in the U.S.

1.2 Microwave communication

The frequency spectrum used for radio communication has gotten very crowded, especially below 300 MHz. Hence it was necessary to make use of the high frequencies in the electromagnetic spectrum for wireless communication. The term microwave seems to have first appeared in the paper by Nello Carrara in the first issue of Alta Frequenza in 1932. The term microwave refers to alternating current signals with frequencies between 300 MHz to 300 GHz (Pozar, 1997). Radiations of this type are excited by transitions between molecular rotational energy levels. Microwaves having frequencies greater than 30 GHz are generally referred to as millimeter waves. Fig. 1 shows the entire electromagnetic spectrum with a special reference to microwaves (Sebastian, 2008). It is clear that most of the microwave systems are located in the frequency range 300 MHz to 30 GHz.

Microwaves have many benefits compared to the low frequency radio waves. One of the huge advantages is the increased bandwidth. For example, a broadcast AM radio operating at 1000 kHz can have 100 radio stations of band width 10 kHz. But if the operating frequency is 4 GHz, 4000 radio stations of the same bandwidth can be allocated. The huge amount of spectrum available at microwave frequencies permits the transmission of very large amount of information. Microwaves are easier to control because a small antenna could direct the waves as well. One advantage of such control is that the energy could be easily confined to tight beam. This beam could be focused on another antenna several kilometers away, making it difficult for someone to intercept the conversation. Another characteristic is that because of their high frequency, greater amount of information could be put on them. These advantageous make microwaves

extremely useful for RADAR as well as communications (Schwartz, 2005). The explosive growth in the microwave communication industry led to tremendous demand for novel low dielectric loss microwave components. In wireless communication systems, a variety of dielectric ceramics have been utilized for microwave dielectric applications (Sebastian, 2008).

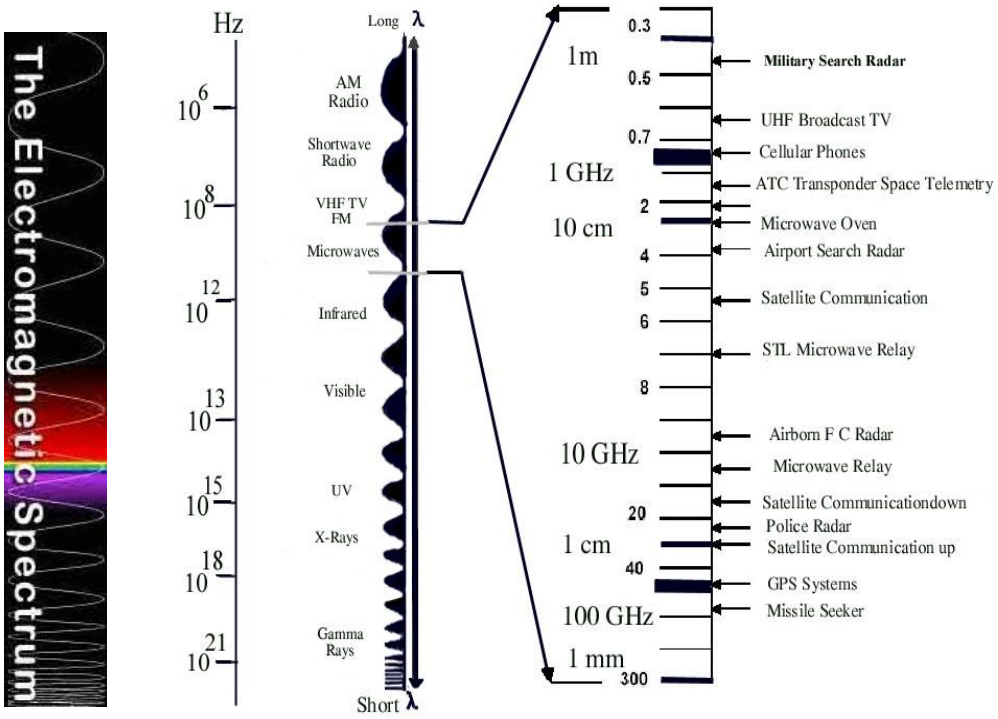

Figure 1.1 The electromagnetic spectrum and various wireless communication systems using microwaves.

1.3 Dielectric materials

The term dielectric is a difficult one to define with any precision and is often interchanged with insulator or non-conductor. Fundamentally, a dielectric is an insulating but polarisable material used either actively or passively in an electric field. Such materials usually find applications as either capacitors or microwave resonators. When a dielectric is introduced between two plates of a capacitor, the capacity of the capacitor will increase by a factor called relative permittivity or dielectric constant (ε_r). The capacitance increases because the material effectively cancels part of the applied field

and thus "storing" part of the field or charge. Fig. 1.2 shows the parallel plate capacitor without and with the presence of a dielectric material between the plates.

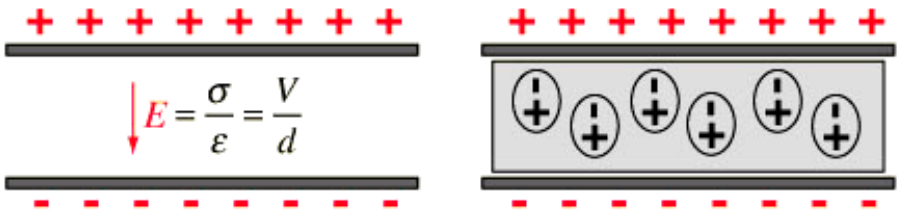

Figure 1.2 Effect of a dielectric material of relative permittivity ε_r on the capacitance of a parallel plate capacitor. If the capacitance without dielectric medium is C_0, the new capacitance, $C = \varepsilon_r \times C_0$.

1.4 Fundamentals of Dielectric Properties

The dielectric properties of a material are defined by a parameter called permittivity. The permittivity is a complex parameter, which depends upon the materials ability to be polarized under the application of an electric filed. Polarization can be defined as the charge displacement in a dielectric material to produce a net dipole moment under the presence of an electric field. The dipole moment per unit volume of the material is called the polarization vector $\vec{P}$. Different polarization mechanisms can occur depending on frequency, temperature, and composition. Therefore the permittivity will also be a function of frequency, temperature and composition. The real part of permittivity represents the material's ability to store electrical charge, whereas the imaginary part implies the dielectric loss factor of the material. Both relative permittivity and dielectric loss factor are dimensionless quantities.

1.4.1 Complex permittivity

If a sinusoidal voltage is applied across a capacitor in vacuum with the form $V(t) = V_0 \exp(i\omega t)$, a charging current $I(t)$ results, where $I(t) = i\omega C\, V(t)$, which is 90° advanced in phase in relation to the applied voltage. When the same alternating field is applied to a capacitor containing a lossy dielectric (see Fig. 1.3) the charging current is no longer 90° advanced from the voltage. For such a case permittivity takes a complex form as $\varepsilon^* = \varepsilon' + i\varepsilon''$, where ε' is the real part of the complex permittivity (relative permittivity) and characterizes a materials ability to store a charge, and ε'' is the

imaginary part of the relative permittivity which is a measure of the heat related loss in the material (Harrop, 1972). The parallel plate capacitor containing the lossy dielectric has a resulting current when an alternating field is applied. This current consists of I_C (the capacitive component of the current) and I_R (the loss component of the current) with the total current equal to the sum $I_T = Ic + I_R$ with I_T related to the voltage by

$$I_T(t) = (i\omega\varepsilon' + \omega\varepsilon'')\, C_0 V(t) \qquad (1.1)$$

And therefore

$$I_C(t) = \omega C_0 \varepsilon'\, V(t) \qquad (1.2)$$

$$I_R(t) = \omega C_0 \varepsilon''\, V(t) \qquad (1.3)$$

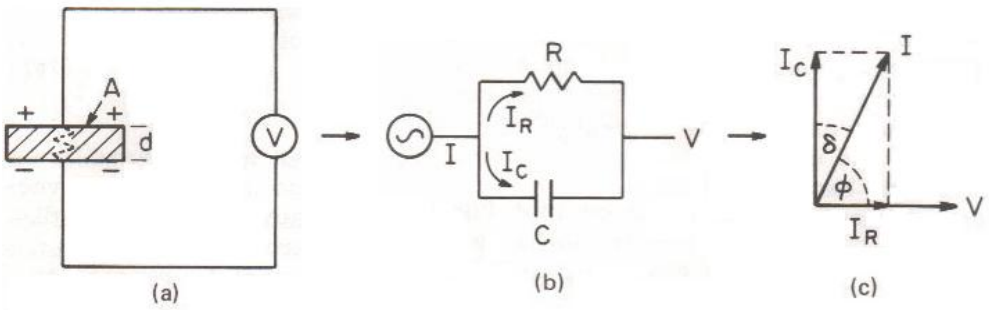

Figure 1.3 (a) A lossy dielectric between a parallel plate capacitor (b) equivalent circuit (c) phase diagram.

As shown in Fig. 1.3(c), the phase difference between the total current $I_T(t)$ and voltage V(t) is 90 - δ, where δ is the loss angle. This angle also represents the phase difference between the applied electric field and polarization of the material. The tangent of this angle is the ratio of the imaginary part to the real part of the complex permittivity (Tan $\delta = \varepsilon''/\varepsilon'$). The inverse of dielectric loss is called quality factor (Q = 1/ Tan δ), which is also used to express the dielectric loss. As already mentioned, the dielectric properties are intimately related to the polarization of a material by the equation

$$\mathbf{P} = \chi_e \varepsilon_0 \mathbf{E} = (\varepsilon_r - 1)\varepsilon_0 \mathbf{E} \qquad (1.4)$$

where P is the polarization in a material, E is the electric field strength, and ε_0 is the permittivity of free space. As a result an understanding of the mechanisms of polarization

that can occur in materials is necessary to understand the dielectric properties of these materials.

1.4.2 Different polarization mechanisms in dielectrics

Dielectric polarization is the displacement of charged particles under the action of an electric field so that there is a net electric dipole moment per unit volume of the material. At the microscopic level, several dielectric mechanisms can contribute to dielectric behavior. They are interfacial, dipolar, ionic and electronic. Dipole orientation and ionic conduction interact strongly at microwave frequencies. Atomic and electronic mechanisms are relatively weak and usually constant over the microwave region. Each dielectric mechanism has a characteristic "cutoff frequency". As frequency increases, the slow mechanisms drop out in turn, leaving the faster ones to contribute to ε_r. The loss factor (tan δ) will correspondingly peak at each critical frequency. The magnitude and "cut off frequency" of each mechanism is unique for different materials (West, 1984).

(a) Space charge/Interfacial polarization

Space charge or interfacial polarization occurs when charge carriers are present which can migrate to an appreciable distance through a dielectric and which becomes piled up at physical barriers such as grain boundary, interphase boundary etc. This type involves a long-range ion movement, which give rise to a high relative permittivity. This process always results in a distortion of the macroscopic field and is important only at low frequencies which may extend upto 10^3 Hz.

(b) Orientational/dipolar polarization

This type of polarization occurs only in polar substances. In zero electric field, the dipoles will be randomly oriented and thus carry no net polarization. When an electric field is applied, the dipoles will tend to align in the direction of the applied field and the materials will acquire a net moment. This is called orientational polarization. In other words, the perturbation of thermal motion of the ionic or molecular dipoles produces a net dipolar orientation in the direction of the applied field. Two mechanisms can be operative in this case. (a) In linear dielectrics (non-ferroelectrics) dipolar polarization

results from the motion of the charged ions between the interstitial positions in ionic structures parallel to the applied field direction. The mechanism is active in the 10^3-10^6 Hz range. (b) Molecules having permanent dipole moment may be rotated about an equilibrium position against an elastic restoring position. Its frequency of relaxation is very high of the order of ~10^{11} Hz. The dipolar polarization contributes to the relative permittivity in the sub-infrared range of frequencies.

(c) Ionic polarization

Ionic polarization is due to a relative displacement of the atomic components of the molecule in the presence of an electric field. In this case the material should have an ionic character. The applied external field displaces the ions slightly from their rest positions and thereby inducing net dipoles. The mechanism contributes to the relative permittivity at infrared frequency range (~ 10^{12}-10^{13} Hz).

(d) Electronic polarization

The electronic polarization arises from the displacement of electron cloud with respect to the nucleus. This occurs at high frequencies of about 10^{16} Hz. Electronic polarization is present in all materials and, it does not contribute to conductivity or dielectric loss in most dielectrics. The relative permittivity at optical frequencies arises almost entirely from the electronic polarizability. Electronic polarization is responsible for the optical refractive index, η and is a part of relative permittivity in all materials.

At microwave frequencies the mechanisms due to ionic and electronic polarization contribute to the dielectric properties. Orientation polarization is temperature dependent whereas electronic and ionic polarizations are temperature independent and are functions of molecular structure (West, 1984).

1.4.3 Frequency dependant polarization

The frequency dependent response is due to many factors. For electronic and atomic polarization, the inertia of orbiting electrons must be accounted for. Due to this inertia effect, these polarization mechanisms will be small for any frequency other than the resonant frequency. Far below this frequency little contribution to ε' and ε'' is given

from these mechanisms. At the resonant frequency a peak in ε″ will occur and a dispersion will occur in ε′ (West, 1984; Herbert, 1985).

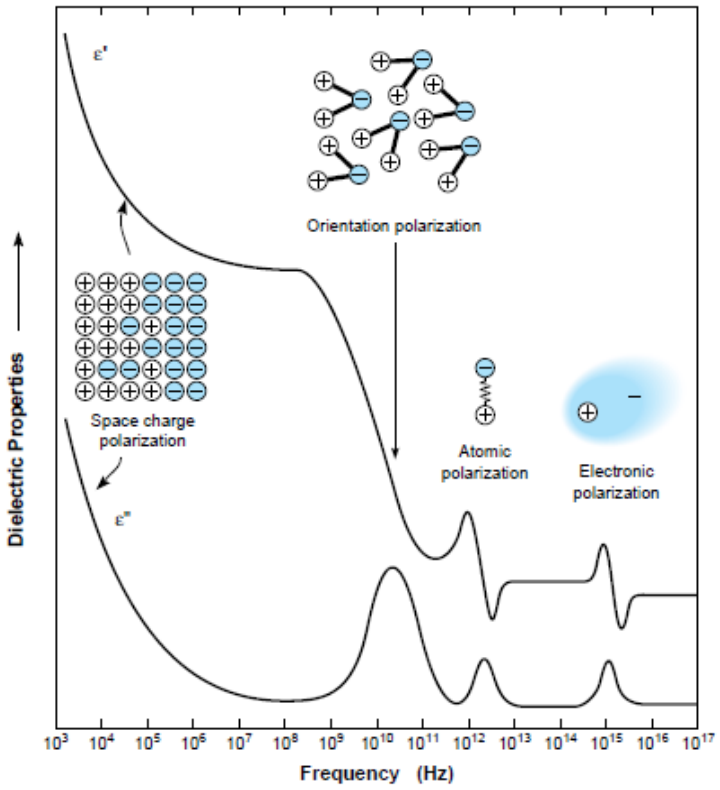

Figure 1.4 Frequency dependence of polarization and its effects on ε′ and ε″(www.crops.org).

Materials which undergo orientation polarization will experience dispersion at the relaxation frequency. In these materials a large change in ε′ and ε″ will occur at this frequency. At the relaxation frequency, the oscillation of the applied field is "too fast" for the molecules to have time to fully rotate. As a result, ε′ will decrease when the relaxation frequency is reached since less of the applied field is canceled by the dipoles as the frequency is increased. A peak in ε″ also occurs at this frequency since the most energy is dissipated at that point. This is due to the fact that at low frequencies rotation is slow and hence minimum energy is dissipated. Above the relaxation frequency the molecules only rotate a small distance and again minimum energy is dissipated. The maximum lies in-between these two extremes at the relaxation frequency. A relaxation of this type can be described by the Debye equations in some materials (Chen *et al.*, 2004)

$$\varepsilon' = \frac{\varepsilon_u + (\varepsilon_r - \varepsilon_u)}{1 + \omega^2 {\tau_e}^2} \tag{1.5}$$

$$\varepsilon'' = \frac{(\varepsilon_r - \varepsilon_u)\,\omega\tau_e}{1 + \omega^2 {\tau_e}^2} \tag{1.6}$$

where ε_r and ε_u are the relative permittivity of a material before and after the relaxation event respectively, ω is the frequency, and τ is the relaxation time. These equations can only be applied to some materials since they correspond to a material which only has one relaxation time. Often materials will have a distribution of relaxation times. Several different relaxation times can occur since materials are often heterogeneous, with the environment around ions and molecules being quite different due to temperature variations or other effects. For such materials equation (1.5) must be modified as

$$\varepsilon^* = \varepsilon_\infty + (\varepsilon_S - \varepsilon_\infty)\int_0^\infty \frac{G(\tau)}{1 + i\,\omega\,\tau_e}\,d\tau \tag{1.7}$$

where ε_S is the relative permittivity in the presence of static electric field, ε_∞ is the relative permittivity as ω tends to infinity and G (τ) is a distribution function of relaxation times. Materials which have an interfacial polarization mechanism present may also undergo an anomalous dispersion, similar to the dipolar relaxation. This relaxation can also often be described using Debye's equations (Chen *et al.*, 2004).

1.4.4 Prediction of relative permittivity

The relative permittivity of an insulator is related to the polarizability of atoms comprising it. The permittivity ε_r can be calculated theoretically using Clausius–Mossotti equation for cubic or isotropic materials (Frohlics, 1950)

$$\frac{(\varepsilon_r - 1)}{(\varepsilon_r + 2)} = \left(\frac{4\pi}{3}\right)\left(\frac{\alpha_D}{V_m}\right) \tag{1.8}$$

Rearranging

$$\varepsilon_r = \frac{3V_m + 8\pi\alpha_D}{3V_m - 4\pi\alpha_D} \quad (1.9)$$

where V_m is the molar volume and α_D is the sum of the dielectric polarizability of individual ions. The V_m of the dielectric material can be obtained from X-ray diffraction studies. The ε_r depends on the dielectric polarizability of the constituent ions and the crystal structure. Based on the additive rule, Shannon states that the molecular polarizability α_D of a complex material can be broken up into the molecular polarizability of simpler compounds (Shannon, 1993). For example

$$\alpha_D(A_2BO_4) = 2\ \alpha_D(AO) + \alpha_D(BO_2) \quad (1.10)$$

where A and B are the cations. Furthermore, it is possible to break up the molecular polarizability of complex compounds into ions according to

$$\alpha(A_2BO_4) = 2\ \alpha(A^{2+}) + \alpha(A^{4+}) + 4\ \alpha(O^{2-}) \quad (1.11)$$

The dielectric polarizability of several ions are reported by Shannon (Shannon, 1993). The calculated ε_r usually agrees well with porosity-corrected experimental values for well-behaved ceramics. It may be noted that deviations from calculated values can occur due to deviations from cubic symmetry, presence of ionic or electronic conductivity, H_2O or CO_2 in channels, rattling of ions, presence of dipolar impurities or ferroelectric behavior and also the fact that the sample is ceramic and not a single crystal. The deviations in the reported values of dielectric polarizability and even a small error in determining the cell volume can significantly affect the calculated value of the permittivity.

1.4.5 Dielectric loss

The dielectric loss tangent (tan δ) of a material denotes quantitatively dissipation of the electrical energy due to different physical processes such as electrical conduction, dielectric relaxation, dielectric resonance and loss from non-linear processes (Choi *et al.*, 2006). Origin of dielectric losses can also be considered as being related to delay between the electric field and the electric displacement vectors (Krzmanc, 2005). The total dielectric loss is the sum of intrinsic and extrinsic losses. Intrinsic dielectric losses are the

losses in the perfect crystals which depend on the crystal structure and can be described by the interaction of the phonon system with the ac electric field. The intrinsic dielectric losses depend on the crystal symmetry, ac field frequency and temperature. These intrinsic losses fix the lower limit of losses in defect-free single crystals or ideal pure materials (Gurevich *et al.*, 1986; 1991). Extrinsic losses are associated with imperfections in the crystal lattice such as impurities, microstructural defects, grain boundaries, porosity, microcracks, order–disorder, random crystallite orientation, dislocations, vacancies, dopant atoms etc. The extrinsic losses are caused by lattice defects and therefore can in principle be eliminated or reduced to the minimum by proper material processing. The losses due to different types of defects show different frequency and temperature dependence. The crystals belonging to different symmetry groups have very different temperature and frequency dependences of dielectric loss (Gurevich *et al.*, 1986). Manufacturers of dielectric ceramics often use the name ‘‘quality factor’’ for the reciprocal of the tan δ. One should carefully distinguish this quantity from the Q-factor of a resonator which is defined as

$$Q_0 = 2\pi \frac{\text{Maximum energy stored per cycle}}{\text{Average energy dissipated per cycle}} \tag{1.12}$$

The term ‘‘quality factor’’ is more commonly associated with microwave resonators. Quality factor is a measure of the power loss of a microwave system. For the microwave resonator, losses can be of four types: (a) dielectric, (b) conduction,(c) radiation and (d) external. The measurement conditions can be adjusted such that the losses due to conduction and radiation can be neglected.

1.4.6 Factors affecting dielectric loss

Microwave dielectric loss is influenced by a number of factors, such as permittivity (Harrop, 1969), onset of phase transitions (Colla *et al.*, 1993; Reaney *et al.*, 1994), processing conditions, raw material impurities (Templeton *et al.*, 2000) and order/disorder behavior and porosity (Sagala *et al.*, 1992). The dielectric loss is the result of a combined contribution of the degree of crystal structure imperfection, microstructural inhomogeneity and interaction with the phonons. Ceramics with

microstructural inhomogeneities such as space charges or dipoles which lie either between matrix grains and inclusions or at grain boundaries have higher losses. Such inhomogeneities may arise due to secondary phases, impurity segregation, incomplete densification etc. It is found that the quality factor of a ceramic is increased with increase in bulk density, provided the densification is promoted by solid state diffusion mechanism. Hence glassy phase formation should be avoided during sintering to get high quality factor. Because of the natural difficulties involved in getting ceramics with reproducible microstructures, it is essential that the ceramic is at least composed of a single phase with homogeneous microstructure to have as high Q as possible.

The structural factors that are involved in loss mechanism include lattice defects, distortion of symmetry, mass of ions, cation ordering etc. The dielectric loss tangent of microwave dielectrics (tan δ) is brought about by the effect of anharmonic terms in the potential energy on the mean separation of a pair of atoms and is increased by lattice imperfections in the crystal. The dielectric loss caused by the anharmonic terms increases at higher temperatures. The random distribution of ions is also considered to be a kind of imperfection. The Q factor of the ordered ceramics would be much greater than the less ordered ceramics. Any type of defects such as grain boundaries, stacking faults, chemical or structural disorder, point defects, planar defects, line defects, inclusions, secondary phases, twinning, porosity etc. contribute to dielectric losses. In the microwave region, the intrinsic loss is mainly due to the interaction of the applied field with phonons. This leads to dampening of the phonon modes of fundamental lattice.

1.4.7 Effect of porosity on the dielectric properties

The value of relative permittivity decreases with increase in porosity since air has $\varepsilon_r = 1$. Usually it is very difficult to obtain the ceramic with 100% densification and hence a correction for porosity becomes necessary. The variation of relative permittivity with porosity has been considered by using a number of approximations (Kingery *et al.*, 1976). The models consider the dielectrics as a composite system of two phases (dielectric material and porosity) with different values of relative permittivity. Penn *et al*. obtained the following equation for the porosity correction of relative permittivity of a dielectric material (Penn *et al.*, 1997)

$$\varepsilon_m = \varepsilon_c\left(1-\frac{3P(\varepsilon_c-1)}{2\varepsilon_c+1}\right) \quad (1.13)$$

where ε_m is the measured ε_r, ε_c is the corrected ε_r and P is the fractional porosity. The dielectric loss increases with porosity due to the fact that it causes irregular reflection of the electromagnetic waves and hence loss of energy. The correction for porosity of the loss tangent can also be obtained as (Penn *et al.*, 1997)

$$\tan\delta = (1-P)\tan\delta_0 + A'P\left(\frac{P}{(1-P)}\right)^{2/3} \quad (1.14)$$

where tan δ is the measured value of dielectric loss, tan δ_0 is the loss tangent of fully dense material and A′ a constant.

1.4.8 Effect of humidity on the dielectric properties

The tan δ increases with increasing porosity due to collection of moisture in the pores. Humidity effects on low frequency dielectric properties of porous materials have been studied (Field, 1946). Jonscher (Jonscher, 1996) identified low frequency loss mechanism in porous materials in the presence of moisture, and Tinga et al. (Tinga *et al.*, 1973) studied the effect in some materials at microwaves. It is clear that the relaxation process centered at low frequency is responsible for high dielectric loss over a wide frequency range extending into the microwave range. The humidity effects on low frequency dielectric properties of porous materials have been associated to the liberation of ions tightly bound in the dry condition. In contact with an adsorbed water film, these ions become free to move over extended regions. This mechanism would produce an interfacial polarization process giving rise to a low frequency peak. Charge carriers could also be produced by an electrochemical process of dissociation of water into a proton and a hydroxyl ion (Molla *et al.*, 1999).

1.5 Applications of microwave dielectrics

In the next recycling-oriented society, new technologies are required for survivals of human beings on earth. These technologies include for energy and natural resources conservation, waste disposal techniques, reduction of global warming and so on. To

achieve this advanced functions of materials are essential. The microwave dielectrics can play a crucial role in fulfilling the needs of next generation as it can have a lot of applications. Microwave materials can be used for the following functions: (1) electromagnetic resonance, (2) electromagnetic-wave shortening, (3) electromagnetic-wave delay, (4) temperature variation of resonant frequency, (5) electric magnetic-wave absorption, and (6) other functions: such as transparency and refractive index. Function (1) has been used for resonator and filter, and might be used for energy transfer in future. Function (2) has been used for miniaturization of microwave communication equipments. Function (3) is useful for millimeter wave equipments. Function (4) has been used for zero temperature coefficients of resonant frequency and relative permittivity, and might be used for temperature sensor. Function (5) has been used for darkroom for radio wave and wave absorber. Functions (6) have been used for dielectric wave guide for millimeter wave communications, and for transparent ceramics with high refractive indexes, and wide range transparency up to middle IR region.

From a historical perspective, guided electromagnetic wave propagation in dielectric media received much attention in the early days of research in microwaves. The dielectric ceramics play a prominent role in telecommunication and satellite broadcasting industry for its potential advantages such as reliability, ease of integration, good dielectric properties and excellent performance (Wersing, 1996). In electronic industry, dielectric materials are being used as electronic packages, substrates, dielectric resonators, dielectric waveguides, dielectric antennas, capacitors etc.

1.5.1 Electronic packaging applications

The effectiveness, with which an electronic system performs its electrical functions, as well as the reliability and cost of the system, are strongly determined not only by the electrical design, but also by the packaging materials. Electronic packaging refers to the packing of integrated circuit chips (dies), the interconnections for signal transmission, power and ground, the encapsulations for protecting the chips and interconnections from moisture, chlorides and other species in the environment, the heat sinks to remove heat from the chips, the power supply and the housing for electromagnetic interference (EMI) shielding. Dielectric properties of packaging

significantly influence the performance of high speed microelectronic devices. Electrical characteristics of microelectronic devices, such as signal attenuation, propagation velocity and cross talk are influenced by the dielectric properties of the package substrate and encapsulation material. The electrical properties in material selection include relative permittivity, loss tangent, frequency and temperature stability of dielectric properties, dielectric strength and electrical resistivity. An important role of packaging materials is to ensure the electrical insulation of the silicon chip and of circuit pins. Ideally, a low conductivity is needed to avoid current leakage, a low relative permittivity to minimize the capacitive coupling effects and reduce signal delay and a low loss factor to reduce electrical loss (Sun *et al.*, 2005). The temperature coefficient of the relative permittivity of microwave substrates are very important in many outdoor wireless applications for the reduction or control of temperature-induced drift in circuit operating characteristics. High electrical resistivity and dielectric strength are also required for microelectronic applications (Chung, 1995; Pecht *et al.*, 1999).

The actual applications of materials in electronic packaging include interconnections, printed circuit boards, substrates, encapsulations, interlayer dielectrics, die attach, electrical contacts, connectors, thermal interface materials, heat sinks, solders, brazes, lids, housings, and so on. The important considerations of the electronic packaging are discussed below.

(a) Printed Circuit boards (PCB)

A PCB is a sheet for the attachment of chips, whether mounted on substrates, chip carriers, or otherwise, and for drawing of interconnections. It is a polymer-matrix composite that is electrically insulating and has conductor lines (interconnections) on one or both sides. Multilayer boards have lines on each inside layer so that interconnections on different layers may be connected by short conductor columns called electrical vias. PCB for the mounting of pin-inserting type packages need to have lead insertion holes punched through the circuit board. PCBs for the mounting of surface-mounting-type packages need no holes. The main ingredients in a PCB composite are the polymer matrix (e.g., epoxy) and reinforcing fibers (e.g., glass, Kevlar). The conventional method of fabricating a PCB involves the lamination of fiber prepregs. In addition to the

interconnections, metal layers and columns can be incorporated in a board for the purpose of restraining the thermal expansion and heat dissipation.

(b) Substrates

Substrates provide the mechanical base and electrical insulating material on which thick-film materials are fabricated. A substrate is usually an electrical insulator, although, with the use of a dielectric film on the surface, an electrical conductor can also be used. Substrate materials include ceramics (e.g., Al_2O_3, AlN, mullite, glass ceramics), polymers (e.g., polymide), semiconductors (e.g., silicon) and metals (aluminum). The most common substrate material is Al_2O_3. The competition between ceramics and polymers for substrates is increasingly keen. Both are electrically insulating; ceramics are advantageous in that they tend to have a high thermal conductivity than polymers; polymers are advantageous in that they tend to have lower relative permittivity than ceramics. To decrease relative permittivity, ceramics with pores are being developed, but their brittleness, roughness and low thermal conductivity are undesirable. A high thermal conductivity is attractive for heat dissipation; a low relative permittivity is attractive for a small capacitive effect and hence a small signal delay. A detailed description of substrates and their various requirements are included in a later section of the chapter.

(c) Interconnects

An interconnection is a conductor line for signal transmission, power, or ground. It is usually in the form of a film of thickness > 1 μm. It can be on a chip, a substrate or a PCB. The film is made by either screen printing or plating. Metals are mostly used for interconnections. The choice of metal depends on the depends on the need for withstanding air oxidation in the process of co-firing with the ceramic. Copper is an excellent conductor, but it oxidizes readily when heated in air. Other options for highly conducting metals are Silver and Gold. Refractory metals such as tungsten and molybdenum, are suitable for interconnections heated to high temperatures (>1000 ^oC), for example during Al_2O_3 substrate processing.

(d) Interlayer dielectrics

An interlayer dielectric is a dielectric film separating the interconnection layers, such that the two kinds of layers alternate and form a thin film multilayer. The dielectric is a polymer, usually spun on or sprayed; or a ceramic, usually applied by chemical vapor deposition (CVD). The most common multilayer involves polyimide as the dielectric and copper interconnections, plated, sputtered, or electron-beam deposited. A less common multilayer uses SiO_2 (CVD) as the dielectric and aluminum as the interconnections. The multilayer sits on ceramic multilayer substrates, usually Al_2O_3, with tungsten interconnections. The purpose of thin film multilayer is to enhance the packing efficiency of the interconnections.

(e) Die attach

A die attach is a material for joining a die (a chip) to a substrate. It can be a metal alloy (a solder paste), a polymeric adhesive or a glass. Die attach materials are usually applied by screen printing. A solder is attractive in its high thermal conductivity, which enhances heat dissipation. A polymer or glass has poor thermal conductivity, but this problem can be alleviated by the use of thermally conductive fillers, such as silver particles.

(f) Encapsulation

An encapsulation is an electrically insulating conformal coating on a chip for protection against moisture and mobile ions. An encapsulation can be a polymer (e.g., epoxy, polyimide, polyimide siloxane, silicone gel, parylene, and benzocyclobutene), which can be filled with SiO_2, BN, AlN, or any other electrically insulating ceramic particles for decreasing the thermal expansion and increasing the thermal conductivity. The decrease of the thermal expansion is needed because a neat polymer typically has a much higher coefficient thermal expansion than a semiconductor chip. An encapsulation can also be a ceramic like SiO_2, Si_3Ni_4, silicon oxynitride etc. In the process of electronic packaging, encapsulation is a step performed after both die bonding and wire bonding, and before the packaging using a molding material.

(g) Lid

A lid is a cover for a chip for physical protection. The chip is typically mounted in a well in a ceramic substrate and the lid covers the well. A lid is preferably a metal because of the need to dissipate heat. It is typically joined to the ceramic substrate by soldering, using a solder perform (e.g., Au-Sn) shaped like a gasket. To avoid a mismatch in the coefficient of thermal expansion, a metal (or alloy) with a matching coefficient of thermal expansion to that of ceramic is used (e.g., Kovar, 54Fe-29Ni-17Co) for the lid. Although Kovar has a low value of coefficient of thermal expansion (5.3×10^{-6} ppm/^{o}C at 20-200 ^{o}C), it suffers from a low thermal conductivity of 17 W/mK.

(h) Heat sink

A heat sink is a thermal conductor that serves to conduct (mainly) and radiate heat away from the circuitary. It is typically bonded to a printed circuit board. The thermal resistance of the bond and that of the heat sink itself govern the effectiveness of heat dissipation. A heat sink that matches the coefficient of thermal expansion of the circuit board is desirable for resistance to thermal cycle.

In general, the integrated circuit chips (dies) are attached to a substrate or a printed circuit board on which the interconnection lines have been written (usually by screen printing) on each layer of the multilayer substrate or board. In order to increase the interconnection density, another multilayer involving thinner layers of conductors and interlayer dielectrics may be applied to the substrate before the attachment of the chips.By means of soldered joints, wires connect between electrical contact pads on the chip and electrical contact pads on the substrate or board. The chip may be encapsulated with a dielectric for protection. It may also be covered by a thermally conducting lid. The substrate or board is attached to a heat sink. A thermal interface material may be placed between the substrate and heat sink to enhance the quality of thermal contact. The whole assembly may be placed in a thermally conducting housing.

There are numerous variations to the packaging described above. In the most conventional one, chips are attached to a ceramic substrate via soldered joints, while the substrate is in turn mounted via soldered joints to a printed circuit board (also known as a

card). In another variation, the chip is attached directly on the card, resulting in a direct chip attachment module (DCAM). In yet another variation, the chip is attached via a cardlet, one of many small cards, attached to a large card, resulting in a multichip module laminate (MCML). An MCML obviates the need for a sophisticated mother card, allows denser packaging than DCAM, and is less expensive than a multichip module involving ceramic substrates. A conventional packaging process involves putting the interconnections on a flat substrate before putting on the chips-a process known as chip last. A new process, chip first, saves the total number of processing steps by putting the chips in wells of chosen depths in a substrate before putting the interconnections on the plane of the well tops.

1.5.2 Substrate applications

A substrate, also called a chip carrier, is a sheet on which one or more chips are attached and interconnections are drawn. The first substrates were made with steatite ceramics, which were sintered in air at temperatures in the range of 1200-1350 ^{o}C. These substrates were metalized with various pastes, such as gold, silver, palladium, and platinum. The steatite ceramics were soon replaced with alumina materials and were metalized with Mo, W, and Mo-Mn pastes. The latter three pastes have to be sintered in reducing atmosphere (Levinson, 1987). A substrate can be formed either by a single layer or by many layers. In the case of a multilayer substrate, interconnections are also drawn on each layer inside a substrate, such that the interconnections in different layers are connected, if desired by electrical vias. Substrates may function as a simple passive carrier providing strength as in many hybrid microelectronic applications or may be a key active component of the circuit as in silicon solar cells. All thick-film substrates should have the ability to withstand high temperatures and have high electrical resistivity, mechanical strength, dielectric breakdown voltage and thermal shock resistance. In addition to these general requirements, other important properties that depend on the application include thermal conductivity, thermal expansion, surface smoothness, relative permittivity and dielectric loss. Dielectric substrate materials are classified into hard substrates and soft substrates.

1.5.2.1 Hard substrates

Hard substrates are ceramics such as alumina, aluminum nitride and beryllium oxide which can withstand extreme heat during wire bonding (Chung, 1995). The market for these ceramic substrates has increased in recent years with the development of electronic industry. The development of hybrid circuits has given rise to the need for a substrate with a very smooth surface, available as thin flat plates and mechanically strong. A high thermal conductivity is also necessary since the miniaturization of components leads to high energy densities. For electronic applications steatite and alumina have been used as the substrate for its high mechanical strength and low dielectric losses. The physical and dielectric properties of various dielectric substrates are shown in Table 1.3.

Table 1.3 Physical properties of selected substrate materials.

Property	**Al_2O_3**	**BeO**	**AlN**	**Silicon**	**Borosilicate**
CTE ($ppm/^oC$)	6.6	7.2-8.0	3.8-4.4	3.5	3.3
Thermal conductivity ($Wm^{-1}K^{-1}$)	29-37	260-290	140-260	125	1.2
ε_r (at 1 MHz)	9.7-10.5	6.5-7.0	8.0-9.2	11.8	4
tan δ (at 1 MHz)	0.0002	0.0004	0.0005	0.005	0.0004

Ceramic substrates are the preferred substrate for most thick-film applications due to dimension stability and inertness at typical thick-film firing temperatures. They have high electrical resistivity of the order of 10^{13} Ω-cm and dielectric breakdown voltages greater than 200 kV/cm, making them ideal for high-voltage circuitry. Among the various commercially available substrate materials, alumina has become the most widely used one because it combines electrical, mechanical and economical advantages. However, alumina in its pure form has a very high sintering temperature above 1700^oC. Berylia possess a high thermal conductivity value (an order of magnitude higher than alumina). The combination of high strength and thermal conductivity give BeO a good thermal shock resistance. The CTE value is slightly higher than alumina and relative permittivity

is slightly lower. The disadvantages with berylia are the high cost and potential toxicity problem associated with its use. The high thermal conductivity of AlN can also be utilized for substrate applications. However, they also possess a high processing temperature. Also, they are reactive to some conventional glass binders thus causing difficulties in cofiring process. Last two decades have witnessed an immense research on the development of low permittivity materials. Forsterite (Mg_2SiO_4), Cordierite ($Mg_2Al_4Si_5O_{18}$), Mullite (Al_2SiO_5), Wollastonite ($CaSiO_3$), and Spinel aluminates ($MgAl_2O_4$ and $ZnAl_2O_4$) has been developed as hard substrates (Herbert, 1985; Ohsato, Tsunooka, Kan, Ohishi, Miyauchi, Tohdo, Kawai, *et al.*, 2004; Surendran *et al.*, 2005; Ohsato *et al.*, 2006; Sebastian, 2008). The problem with these materials is their high sintering temperature, thus restricting the use of highly conductive metals like Ag, Au, Cu etc. for the metallization process. These metals have low melting points (~ 1000 ^oC) and hence cannot be co-fired with conventional materials. A new technology called low temperature co-fired ceramic technology (LTCC) is used to overcome this difficulty, which will be discussed later in this chapter. Thus the search for new materials with good thermal and dielectric properties and also having good co-firing properties are still in progress.

1.5.2.2 Soft substrates

Soft substrates are used in applications where packaged parts are soldered on the board (Chung, 1995). Generally, the polymers or polymer based composites are used as soft substrates. Polymers like polytetrafluroethylene (PTFE), polyethylene, polystyrene, poly-ether-ether-ketone and epoxy shows excellent dielectric properties. However, their low thermal conductivity and high thermal expansion limits their application as substrate in electronic modules (Bur, 1985). A third category of substrate materials is the composites in which the soft substrates are loaded with particles of hard ceramics, thus reducing the thermal expansion and improving the thermal conductivity of soft substrates. A detailed description of the composites and their properties are included in a later section of the chapter.

1.5.2.3 Material requirements

(a) Dielectric properties

The international technology roadmap for semiconductor (ITRS) predicts the necessity of low permittivity materials for interlayer dielectrics as the components in the electronic modules increases according to Moor's law. The ITRS lists the development of low permittivity materials as one of the key five difficult challenges for the semiconductor industry (Hatton *et al.*, 2006). Moor's law predicts that the number of components in a module doubles in two years. The propagation delay time (t_d) of electromagnetic waves in a dielectric is given by the equation,

$$t_d = \frac{l\sqrt{\varepsilon_r}}{c} \tag{1.15}$$

where l is the line length, ε_r is the relative permittivity of the substrate and c is the speed of light (Sebastian, 2008). Therefore a low value of ε_r ensures a small propagation delay. High electrical resistivity is also needed to prevent electrical leakage current between the conductor tracks. The dielectric loss of the substrate should also be as low as possible to avoid electrical losses, especially at very high frequencies. The interaction of the signal with a lossy substrate will produce heat and hence signal attenuation (Sebastian, 2008).

(b) Thermal properties

An electronic material experiences a range of steady-state temperatures, temperature gradients, rates of temperature change, temperature cycles and thermal shocks through manufacturing, storage and operation. Thermal properties that are significant in enduring such life cycle profiles include thermal conductivity/diffusivity, specific heat capacity and coefficient of thermal expansion (CTE). High thermal conductivity is required to ensure that the temperature of the IC's and other components mounted on the substrate does not increase beyond a particular level. The CTE of the substrate material should be matching to that of Si, which is ~ 4 ppm/^{o}C. Also it should be noted that the dielectric properties should not exhibit large variations with operating temperature.

(c) Mechanical properties

The mechanical properties affect the material's ability to sustain loads due to vibrations, shock and thermomechanical stresses during manufacture, assembly, storage and operation. Key properties that are of importance for electronic packaging applications include the modulus of elasticity, tensile strength, Poisson's ratio, flexural modulus, fracture toughness, creep resistance and fatigue strength.

(d) Chemical properties

Chemical properties of the substrate materials are important because of the need to survive manufacturing, storage, handling and operating environments. The chemical properties of significance are water absorption, flammability and corrosion resistance. The electrical properties of electronic materials often change as a result of water absorption, swelling and other dimensional instabilities. The corrosion leads to the formation of more stable compounds and can degrade the physical properties of the materials (Chung, 1995).

(e) Compatibility with the electrode material

In a multilayer ceramic substrate it is usually required to co-fire the ceramic with the conductor paste in order to get desired conductor patterns on or within the substrate. In the case of high temperature co-fired ceramics (HTCC), the conductors used are W, Mo etc. along with the ceramic tapes of Al_2O_3 and in the low temperature co-fired ceramic (LTCC) technology, noble metals like Ag, Au, Cu etc, which are highly conducting are used with the ceramic tapes with low sintering temperature (usually a combination of ceramic and glass). Since the ceramic tapes and metal pastes are co-fired, it is of prime importance that a chemical compatibility exists between them. The metal should in no way react with the ceramic material to form unwanted secondary phases, which might degrade the electrical, thermal and mechanical properties of the substrate.

1.5.3 Dielectric resonators (DR)

A dielectric resonator is an electronic component that exhibits resonance for a narrow range of frequencies, generally in the microwave band. Dielectric ceramics are widely used as dielectric resonators and dielectric filters which are mounted to electronic devices such as in mobile phones, personal radios and satellite receivers. It was established that through multiple internal reflections, a piece of dielectric with a suitable relative permittivity can confine microwave energy at a few discrete frequencies, provided that the energy is fed in the appropriate direction. The electromagnetic wave moving from the electrically dense high dielectric region to the electrically thin air meets very high impedance at the dielectric-air interface and reflects back to the dielectric itself. As the relative permittivity increases the impedance offered by the boundary also increase to allow better confinement of energy within the dielectric body. The reflection coefficient approaches unity when the relative permittivity approaches infinity. The trapped electromagnetic waves will form standing waves to generate resonance (Fig. 1.5).

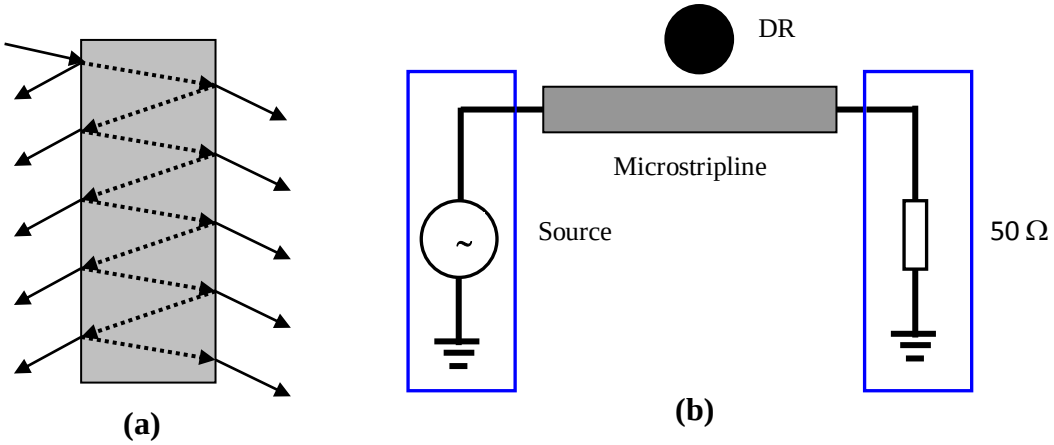

Figure 1.5 (a) Sketch of multiple internal reflections in DR (b) DR as a circuit element coupled to a microstripline.

If the transverse dimensions of the dielectric are comparable to the wave length of the microwave, then certain field distributions or modes will satisfy Maxwell's equations and boundary conditions and only those modes satisfying this condition will be excited. The frequency of the generated resonating modes depends on the dimensions and relative permittivity of the dielectric specimen. For microwaves the free space wavelength (λ_o) is

of the order of a few centimeters and on entering the material with ε_r in the range 20-100, the wavelength (λ_d) inside the dielectric will be in millimeters. Hence proper resonance occurs only when the transverse dimensions of the dielectric sample are of the same order (in millimeters) for resonance to occur (Sebastian, 2008). Fig. 1.5 (b) shows the coupling of a DR to a microstripline.

Table 1.4 Important groups of microwave ceramics (Wersing, 1996).

Ceramic	ε_r	τ_f (ppm/^{o}C)	**Quality factor (Q)**	
			At 2 GHz	**At 20 GHz**
$Ba_2Ti_9O_{20}$	40	2	15000	2000
$Zr_{0.8}TiSn_{0.2}O_4$	38	0	15000	3000
$BaTi_u[(Ni_xZn_{1-x})_{1/3}Ta_{2/3}]_{1-u}O_3$	30	-3 to +3	26000	5000
$Ba[Sn_x(Mg_{1/3}Ta_{2/3})_{1-x}]O_3$	25	0	> 40000	10000
Nd_2O_3-BaO-TiO_2-B_2O_3	~90	0	3000	--
$BiNbO_4$	~40	-30	4000	--

Table 1.4 lists those microwave ceramics that have gained the most technical importance so far. $BaTi_4O_9$ was one of the first microwave ceramics to fulfill the technical requirements, with ε_r = 38, τ_f =15ppm/^{o}C. and Q = 5000 at 2 GHz. Shortly after this, it was shown that $Ba_2Ti_9O_{20}$ ceramics possess even better properties. As Table 1.4 shows, one obtains equally good values for ε_r, and Q in the ceramic system zirconium titanate stannate (ZTS). In addition, one can also make τ_f zero or even negative for ZTS ceramics. This has led to the widespread use of ceramics from this system, such that ZTS ceramics are today termed standard microwave ceramics. The highest dielectric quality factors Q have been found among microwave ceramics based on $Ba(Zn_{1/3}Ta_{2/3})O_3$ (BZT) and on $Ba(Mg_{1/3}Ta_{2/3})O_3$ (BMT). Therefore, these ceramics are usually denoted as 'high Q' microwave ceramics (Wersing, 1996). Nowadays low relative permittivity materials have been receiving more attention since the utilizable electromagnetic spectrum is expanding to millimeter wave region. At these frequencies, the DRs having relative permittivity > 20 will be too small to be handled and hence the only solution is to go for materials having low relative permittivity (< 10) for using as DRs. Various silicates like forsterite (Mg_2SiO_4) and willemite (Zn_2SiO_4) are suitable for DR application at

millimeter wave frequencies, but with some modification of their τ_f values (Sebastian, 2008).

1.5.3.1 Equivalent circuit of DR

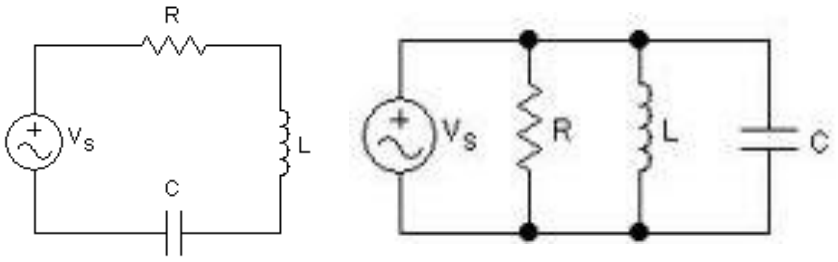

Figure 1.6 Equivalent LCR circuit for a resonator. (a) series circuit and (b) parallel circuit.

As shown in Fig. 1.6, depending on the selection of reference plane, a resonator can be represented by a series equivalent circuit or a parallel equivalent circuit. If the reference plane is chosen at a place where the electric field integration is zero (or the magnetic field integration is maximum), the resonator can be represented by a series LCR circuit. If the reference plane is chosen at a place where the electric field integration is maximum, the resonator can be represented by a parallel LCR circuit. The following discussions focus on parallel LCR circuit.

From the fundamental rules of resonant electrical circuits, the electric energy stored in the capacitor is given as (Harrop, 1972)

$$W_e(t) = \frac{1}{2} C[v(t)]^2 = \frac{1}{2} C|V|^2 \cos^2(\omega t) \quad (1.16)$$

and magnetic energy stored in the inductor is

$$W_m(t) = \frac{1}{2} L\,[i(t)]^2 = \frac{|V|^2}{2\omega^2 L} \sin^2(\omega t) \quad (1.17)$$

At resonance, capacitive and inductive reactances become equal and opposite to vanish. Hence the impedance of the circuit equals the ohmic resistance and maximum energy storage takes place within the body of the dielectric resonator. At this condition

$$\omega = \omega_{res} = \frac{1}{\sqrt{LC}} \tag{1.18}$$

The maximum stored energy W_{max} will be the sum of that stored in capacitor (W_e) and inductor (W_m). Since the average energy values are equal to one half of their peak values,

$$W_{max} = 2W_e = 2W_m = W_e + W_m \tag{1.19}$$

In terms of the average stored energies, the definition of Q at resonance becomes (Sucher, 1963)

$$Q = \left[\frac{\omega(W_e + W_m)}{P_d} \right]_{\omega=\omega_{res}} \tag{1.20}$$

If the operational frequency is not equal to the resonant frequency, the peak of the stored electric energy is not equal to the peak of the stored magnetic energy. Therefore, the definition of Q is not unique at any frequency other than ω_{res}. For a parallel equivalent circuit, if the working frequency is greater than the resonant frequency ($\omega > \omega_{res}$), the electric field energy is larger than the magnetic field energy; if the working frequency is lower than the resonant frequency ($\omega < \omega_{res}$), the magnetic field energy is higher than the magnetic field energy. For a series equivalent circuit, contrary conclusions can be obtained (Chen *et al.*, 2004).

1.5.3.2 Material requirements

Certain criteria are to be met for using the dielectric material for DR applications. They are in terms of relative permittivity, quality factor and temperature dependence of resonant frequency. The value of relative permittivity depends on the frequency of application, whereas a high quality factor is always desired. For best performance of a DR as a circuit element, it is always important that the resonating frequency is independent of the operating temperature.

(a) Relative permittivity

The use of dielectrics in microwave communication reduces substantially the overall dimensions of microwave circuits (Sebastian, 2008). A high ε_r facilitates circuit miniaturization because the wavelength inside the DR is inversely proportional to the square root of its permittivity as given by the equation.

$$\lambda_d = \frac{\lambda_o}{\sqrt{\varepsilon_r}} \tag{1.21}$$

where λ_d is the wavelength in the dielectric, λ_0 is the wavelength in air (actually in vacuum). The dimension of the dielectric sample must be an integral multiple of half-wavelength in the dielectric to resonate in the simplest fundamental mode. If that wavelength is reduced, then the physical dimensions of the resonator must be reduced as well. When microwaves enter a dielectric material, they are slowed down by a factor roughly equal to the square root of the permittivity which implies that the wavelength decreases by the same amount and the frequency is unaffected as shown in Fig. 1.7.

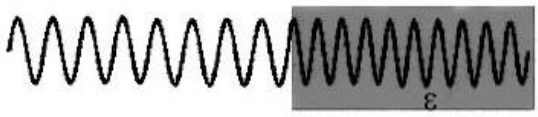

Figure 1.7 The wave length reduced by a factor $(\varepsilon_r)^{1/2}$ when the wave enters in the dielectric medium.

As the operating frequency becomes higher and higher, the wavelength becomes very small which in turn reduces the size of the DR further. Thus if a high permittivity material is used for very high frequency applications, the size of the DR becomes too small thereby making it difficult to be handled. Thus it is always desired to have materials with low relative permittivity, preferably less than 20, for millimeter wave applications of DR.

(b) High quality factor (low dielectric loss)

Normally a quality factor greater than 2000 is required for practical applications. The figure of merit for assessing the performance or quality of a resonator is Q factor. It

is a measure of energy loss or dissipation per cycle as compared to the energy stored in the fields inside the resonator. The Q factor is defined by (Bahl *et al.*, 1988)

$$Q_0 = 2\pi \frac{\text{Maximum energy stored per cycle}}{\text{Average energy dissipated per cycle}} \tag{1.22}$$

$$Q = \frac{2\pi W_o}{PT} = \frac{\omega_o W_o}{P} \tag{1.23}$$

where W_0 is the stored energy, P is power dissipation, ω_o is resonant radian frequency and period $T=2\pi/\omega_0$. When a resonant circuit or cavity is used as a load in a microwave circuit, several different Q factors can be defined. First Q accounts for internal losses. It is the unloaded Q factor Q_0. Next external quality factor (Q_e), accounts for external losses. When the resonator is used in actual circuit, the loaded Q factor, Q_L which is the overall Q factor and includes both internal and external losses has to be considered. The dielectric Q factor (Q_d) for a homogeneous dielectric material is given by

$$Q_d = \frac{1}{\tan\delta} \tag{1.24}$$

For a dielectric loaded cavity where cavity containing an aperture

$$\frac{1}{Q_0} = \frac{1}{Q_c} + \frac{1}{Q_d} + \frac{1}{Q_r} \tag{1.25}$$

where Q_c is the conduction Q factor, Q_d is the dielectric Q factor and Q_r the radiation Q factor. When the resonator is connected to load

$$\frac{1}{Q_L} = \frac{1}{Q_e} + \frac{1}{Q_o} \tag{1.26}$$

where Q_L is the loaded Q factor, Q_e the external Q factor and Q_0 the unloaded Q factor. Q_L is determined experimentally from the shape of the resonance peak, as illustrated in Fig.1.8. Loaded quality factor refers to a resonator coupled with external circuit. Its relationship with unloaded quality factor depends on the coupling coefficients. A peak occurs in the transmitted signal amplitude at the resonant frequency, and the peak has

some finite breadth. A bandwidth (BW) is defined as the width of resonance curve at half power points (3 dB down from the peak). The peak frequency (resonant frequency) f divided by the 3 dB width is equal to Q_L.

$$Q_L = \frac{\omega_o}{\Delta\omega} = \frac{f_r}{\Delta f} \tag{1.27}$$

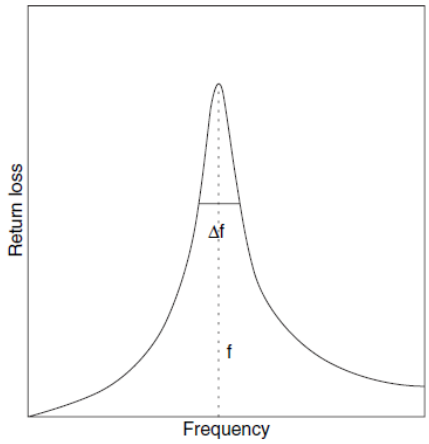

Figure 1.8 The$TE_{01\delta}$ resonant peak and associated parameters.

The resonator BW is inversely proportional to the Q-factor. Thus high Q resonators have narrow BW. If the coupling is low (coupling coefficients << 1), then the unloaded Q-factor is approximately equal to the loaded Q-factor. In practice, resonators are often used with adjustable couplings which allow such approximation without the need for measuring coupling coefficients. If conduction, radiation and external losses are negligible, then $Q_L=1/\tan\delta$. When we measure the dielectric loss, at a particular frequency, we get the total loss tangent and we cannot distinguish the contributing factors (Sebastian, 2008).

(c) Small temperature coefficient of resonant frequency (τ_f)

The coefficient of temperature variation of the resonant frequency (τ_f) determines the frequency stability. It is defined as

$$\tau_f = \frac{1}{f_r} \times \frac{\Delta f}{\Delta T} \tag{1.28}$$

where f_r is the resonant frequency at room temperature, Δf is the variation of resonant frequency from room temperature for a change in temperature ΔT. The τ_f depends on the temperature variation of ε_r and coefficient of linear thermal expansion according to the expression

$$\tau_f = -\alpha_L - \frac{\tau_\varepsilon}{2} \tag{1.29}$$

The value of τ_f should be near to zero for practical applications. However, it is desired to have a small positive or negative τ_f (between -10 and +10 ppm/^oC) to compensate for the temperature variation of the resonant frequency due to subtle variations in circuit design by different manufacturers (Joseph, Sebastian, *et al.*, 2010).

1.5.3.3 Modes and mode nomenclature

A microwave resonator has infinite number of resonant modes, each of them corresponding to a particular resonant frequency, at which the electric stored energy is equal to the magnetic one. The excited modes can be classified into three distinct types: TE, TM and hybrid. The fields for TE and TM modes are axisymmetric whereas hybrid modes are azimuthally dependent. The hybrid modes can again be categorized into HE and EH. According to the mode nomenclature (Kobayashi *et al.*, 1980), the variation of fields along the azimuthal, radial and Z-direction inside the resonator, are denoted by adding mode indices as subscripts to each family of modes. This nomenclature is historically based on the mode nomenclature of cylindrical dielectric waveguides. The TE, TM, HE and EH modes are classified as $TE_{nmp+\delta,}$ $TM_{nmp+\delta}$,$HE_{nmp+\delta,}$ and $EH_{nmp+\delta}$respectively. The first index denotes the number of full-period field variations in azimuthal direction, the index m (m = 1, 2, 3 …..) denotes the order of variation of the field along the radial direction and the index p+δ (p = 0, 1, 2……) denotes the order of variation of the fields along the Z-direction.

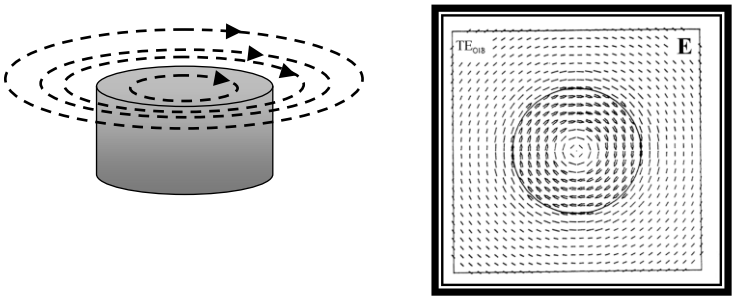

Figure 1.9 Electric field distribution of $TE_{01\delta}$ mode in equatorial plane.

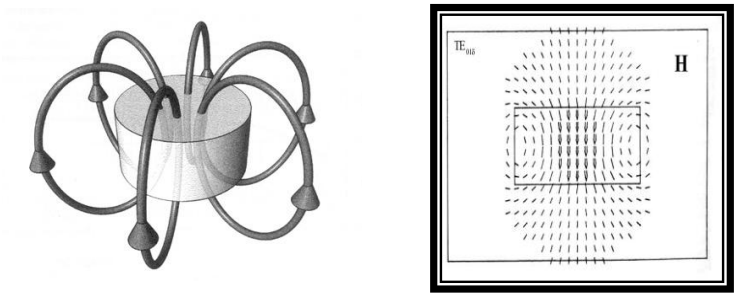

Figure 1.10 Magnetic field distribution of $TE_{01\delta}$in the meridian plane.

The resonant mode most often used in shielded microwave circuits is $TE_{01\delta}$. It is a transverse electrical mode having azimuthal symmetry $\partial/\partial\varphi = 0$, and less than a half cycle variation in field in the z-direction. Here, the third index denotes the fact that the dielectric resonator is shorter than one-half wavelength. The actual value of δ depends on the relative permittivity of the resonator and the substrate. Figs. 1.9 and 1.10 respectively shows the typical field distributions for $TE_{01\delta}$ of a cylindrical dielectric resonator (Kajfez, 1998). The magnitude of the electrical field component is zero at the centre of the resonator and has a maximum value at around x = 2r/3 where r is the radius of the disk. Outside the resonator, the field decays exponentially. The field variation as a function of radial distance remains the same in different planes parallel to the equatorial plane (Kaul, 1997). This mode does not have an electric field component perpendicular to the sample surface and hence the electric filed distribution is unaffected by the presence of air between the sample and the metal plate. This makes it easy to identify from the other

modes. For high relative permittivity materials it is the most dominant mode (1st mode) provided L (thickness of DR) less than D (diameter of DR), whereas for low permittivity materials it will the 3rd or 4th one (Chen *et al.*, 2004).

1.5.3.4 Types of DR

The disk shaped dielectric material is the simplest form of a dielectric resonator. The usual geometries of DRs are discs, rings and parallelepipeds as shown in Fig. 1.11. By inserting a metal or ferrite screws into the central hole of a ring resonator, the resonant frequency of modes can be tuned. Similar techniques are used to suppress the modes adjacent to the desired mode, to avoid interference and to reduce the dielectric loss. The mode spectrum and resonant frequencies of DRs greatly depend on the aspect ratio (diameter D/length L). The dimensions of the specimen are important to achieve wide separation of modes. The proper aspect ratios are 1.0 to 1.3 and 1.9 to 2.3. In practice the specimen diameters in the range 7 to 25 mm have been found most suitable. Fig 1.11 shows different types of dielectric resonators.

Figure 1.11 Different types of dielectric resonators (courtesy:www.ntktech.com)

1.5.3.5 Applications of DR: Filters, oscillators and antennas

Dielectric resonators are inevitable components in microwave subsystems which are used in low loss filters, oscillators and antennas. DR series are widely used in voltage controlled oscillators and filters for cellular phone, cordless phone and so on. DRs find applications in low noise block (LNB) converters for digital broadcasting systems, microwave filters, security systems, detectors, auto cruise control (ACC) of radar

systems, wireless communication equipments, cellular base stations, global positioning systems, satellite multiplexing filter devices, high stability dielectric resonator oscillators, microwave duplexers, etc. All these applications of DRs may be categorized based on their ability as a frequency determining component.

1.5.4 Capacitor application

Capacitors are the indispensable components in all the electronic devices. Basic function of the capacitor is to charge and discharge during its operation. The value of permittivity determines the charge storage capacity of the capacitor. The capacitance C is given by the equation,

$$C = \frac{\varepsilon_0 \varepsilon_r A}{d} \tag{1.30}$$

where ε_o and ε_r are the permittivity of the vacuum and relative permittivity of the dielectric material, A is the area of the electrode material and d is the thickness of the dielectric material. Hence, high permittivity dielectric material is preferred for miniaturization of the electronic devices (Herbert, 1985).

1.6 Low temperature co-fired ceramics (LTCC)

1.6.1 Introduction

The current trend in the microelectronics industry is to reduce the overall size of the electronic packages. This means that more complex packages have to be made with higher interconnect density, smaller components but with same or greater reliability. Among the various fabrication methods of electronic devices, low temperature co-fired ceramic (LTCC) technology has become an attractive manufacturing platform with high speed and good functionality for compact, light weight and integrated electronic components, modules, substrates and devices (Tummala, 1991; Sebastian *et al.*, 2008). Next to RF laminates and passive integration on high ohmic silicon, LTCC is an established technology for the realization of highly integrated modules for mobile communication devices.

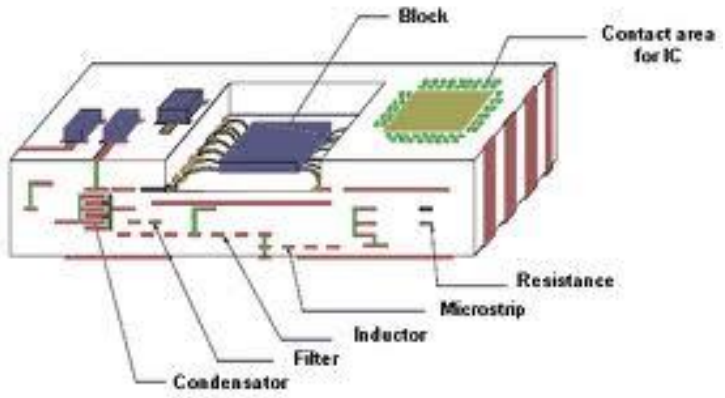

Figure 1.12 A schematic representation of an LTCC multilayer module (courtesy: www.mshak.am).

The size, cost and performance of integration, packaging and interconnection technologies are critical factors for the success of a microwave product (Jantunen *et al.*, 2003). In both military and commercial applications, lower weight and smaller size requirements are necessitating increased density in electronic packaging. To realize extremely miniaturized RF modules, one technology trend is to decrease the line width and spacing of metal lines to reach a higher wiring density. Another trend is to increase the precision of the processes in order to enable the substrate integration of functions with a higher demand of accuracy. Cross-talk noise between lines and electric signal delay are suppressed by positioning the electric-signal wiring on low-ε_r material layers. Downsizing or lowering the profile of substrates (eg. decrease number of capacitance layers) can be achieved by forming internal capacitors on high-ε_r material layers. One way to achieve greater density is through integration of numerous components within a single package. Fig. 1.12 shows the structure of an LTCC multilayer module. LTCC has the unique ability to integrate a broad variety of components such as inductors, capacitors and filters into a very compact arrangement, thereby leaving valuable circuit surface areas for active components (Sprague, 1990; Alexander, 1993; Goldberg, 1995). The target firing temperature is in the range 850-940 ^{o}C because this is the most suitable range for commercial LTCC metal pastes and tapes.

1.6.2 LTCC technology-History

The origin of multilayer ceramic substrate technology was at RCA Corporation in the late 1950's and the basis of current process technologies (green sheet fabrication technology and multilayer laminate technology using the doctor blade method) was discovered at this time (Mistler *et al.*, 2000). Progress was made using these technologies with IBM taking the lead, and the circuit board for IBM's mainframe computer commercialized in the early 1980's was the inheritance. Since this multilayer board was co-fired at the high temperature of 1600 ^{o}C with the alumina insulating material and conductor material (Mo, W, Mo-Mn), it is called high temperature co-fired ceramic. From the middle of the 1980's, fine wires were used in order to increase wiring density in circuit boards for high density mounting. But the attenuation of signal occurs due to the electrical resistance of the wiring. Hence it is necessary to use materials with low electrical resistance (like Cu or Au). Poor connection of interconnects may result if the thermal expansion of the board is not close to that of the silicon (~ 4 ppm/^{o}C). Hence insulating materials with low thermal expansion (ceramics) are desirable. Further, to achieve high speed transmission of signals, it is necessary that the ceramic has a low relative permittivity. In the early 1990's, many Japanese and American electronics and ceramics manufacturers had developed multilayer boards (LTCC) that met these requirements (Imanaka, 2005). Among them, Fujitsu and IBM were the first to succeed with commercial applications of multilayer substrates using copper wiring material and low relative permittivity ceramics. From the latter half of the 1990's to the present, the focus of applications has shifted to high frequency wireless for the electronic components, modules and so on used in mobile communication devices. For the multilayer circuit board, the low thermal expansion of ceramics was its biggest merit for the purpose of high density mounting of LSI components. For high frequency applications, its low transmission loss is its key feature, and the low dielectric loss of ceramic gives it an advantage over other materials. The process, design aspects and requirements for LTCC technology is discussed in the review "Low loss dielectric materials for LTCC applications: A review" authored bySebastian and Jantunen (Sebastian *et al.*, 2008).

1.6.3 Materials selection and requirements

Although the LTCC technology for high frequency applications demonstrates some very advantageous features, its development is still in the early stages. The main problem relate to the rigorous demands placed on the materials requirement. In general, it is believed that the main difficulties in the development of new LTCC materials are not related to their dielectric properties but to their sintering behaviour, thermo-mechanical properties, chemical compatibility, production cost and the range of variation of each parameter (Sebastian *et al.*, 2008).

1.6.3.1 Densification temperature

To produce a module, the LTCC materials are co-fired with an inner electrode structure and, as a consequence, the sintering temperature must be lower than the melting point of the electrode. In addition, a chemical compatibility between the LTCC material and the electrode must exist. Silver is a usual choice for the electrode, which means the sintering temperature is commonly adjusted to about 900 ^{o}C. It should be noted that any densification or crystallisation of the composite at lower temperatures, such as below 800 ^{o}C, is undesirable as this can prevent the evaporation of the organics and solvents used in conductive pastes, causing residual carbon traces in the microstructure. Any residual carbon that may form during binder decomposition if left in the LTCC would adversely affect the dielectric properties. This means that the densification of the ceramic should start above this temperature (Sebastian *et al.*, 2008).

1.6.3.2 Dielectric properties

(i) Relative permittivity (ε_r)

LTCCs are basically composite structures of glass and ceramics and therefore, controlling their relative permittivity depends largely on the combination of constituent materials of the composite and its material composition. Generally, low relative permittivity materials with ε_r = 4 -14 are used for substrate layers while high permittivity materials are opted to enable miniaturised, embedded capacitors, inductors, filters and antennas (Kagata *et al.*, 1992; Wahlers, 2001). Since propagation delay decreases with

decrease in relative permittivity (refer to Eqn. 1.15), substrates with low relative permittivity are essential to increase the speed of signal.

(ii) Dielectric loss (tan δ)

In order to reduce the dielectric loss of LTCC composites, it is effective to construct them with low dielectric loss materials. The dielectric loss value of common LTCC materials, is expressed with the Q value (1/tan δ) multiplied by the measurement frequency, which should be greater than 5000 GHz. At least three types of dielectric loss for glasses have been distinguished: resonance type vibrational losses at very high frequency, migration losses caused by the movement of mobile ions and deformation losses by defect or deformation of the basic silicon oxide network (Navias *et al.*, 1946; Shand, 1958). Resonance type vibrational losses are particularly important in the microwave region. The selection of glass should be done carefully as it affects the dielectric, mechanical and thermal properties of the glass/ceramic composites. A detailed description of the glasses and their properties are given in a later section of this chapter.

(iii) Temperature stability of dielectric properties (τ_f and τ_ε)

The temperature dependence of the resonance frequency is important for LTCC applications. The coefficient of temperature variation of the resonant frequency (τ_f) value of 10 ppm/^{o}C causes a 0.11 % shift of the resonant frequency (5.5 MHz at 5.2 GHz) within the temperature range -30 ^{0}C to +80 ^{0}C. Though novel LTCC materials with zero τ_f (e.g. Heraeus CT2000, $\tau_f \leq 10$ ppm/^{o}C) have been developed, the component designer must be aware that the structure itself may affect its τ_f (Thomas, 2010).

1.6.3.3 Thermal properties

The circuit boards and packages undergo heat stress during assembly processes, reliability tests and also during device operation. Thus in addition to the dielectric properties, designers must also consider the thermal properties of the LTCC composites. The important thermal properties under consideration are thermal conductivity and coefficient of thermal expansion.

(a) Thermal conductivity

The thermal conductivity of LTCC materials should be moderately good.The removal of heat generated by the device during operation is critical for the efficient functioning of the package. It is therefore necessary to maintain the temperature below 100 ^{o}C for efficient and reliable operation of the device. The heat removal has become even more critical in recent years because of the ever-growing need to fabricate high density and high power devices that can operate at high speed. Advancement in technology and the continuing trends toward miniaturization of devices in the future will place even more stringent requirements on heat dissipation characteristics of the packaging LTCC. The thermal conductivity of an LTCC is 2 W/mK, versus 0.5 W/mK for organic materials. A common method to improve thermal dissipation is to use a heat spreader, but a more advantageous alternative provided by LTCC technology is to place metallic via arrays (thermal conductivity 50 W/mK) under high power components (Imanaka, 2005).

(b) Thermal expansion

The coefficient of thermal expansion (CTE) of a material is a measure of the characteristic change in its dimension for each degree change in temperature, as the material is uniformly heated or cooled. Thus, CTE can be written as:

$$\alpha_l = \frac{\Delta L}{L\,\Delta T} \tag{1.31}$$

where ΔL represents the change in length over a temperature span ΔT, starting from an initial length L. It is strongly temperature dependent property and for most of the ceramics a near linear range can be achieved between ~ 25 ^{o}C-300 ^{o}C, within which the expansion coefficient varies little. The CTE is an important parameter as it affects the Si based ICs attached. Therefore, the substrate is expected to exhibit CTE values close to that of Si in order to avoid deformations such as crack and delaminations. between the substrate and the attached components due to shrinkage mismatch. Thermal expansion coefficient is a directional or anisotropic factor because of its strong dependence on the crystal structure, bond strength and density.

1.6.3.4 Chemical compatibility with electrode material

The LTCC should not react with the conductive material used. The formation of additional phases in the ceramic should be minimised since the reaction of the composites with the conducting electrode, degrades the performance of the microwave modules. A critical issue in manufacturing LTCC microelectronics is the precise and reproductive control of shrinkage on sintering. In the screen-printing of the conductive patterns, instead of pure metals, pastes containing conductive particles in glassy additives are used. Thus when developing LTCC materials, one has to take into account of the reactions not only with the conductive material like silver but also with other additives of the conductor paste.

1.6.4 Fabrication of LTCC

In the fabrication of desirable LTCC substrates, a complete densification and sufficient crystallization are generally necessary to achieve the required mechanical and dielectric properties. Porosity and low degree of crystallinity would lead to relatively poor mechanical properties and residual glass would decrease the Q value at microwave frequency. Attempts to achieve the above requirements are made with the help of glass systems including a high softening glass, nucleating agents, sintering aids and properties and structure modifiers (Jean *et al.*, 1992; Jean *et al.*, 1996; 1996; Jean *et al.*, 1997).

Three approaches have been used to obtain glass-ceramic compositions suitable for fabricating self-supporting LTCC substrates. In the first type, the glass-ceramics, fine powder of a suitable glass composition is used that has the ability to sinter well to full density in the glassy state and simultaneously crystallize to become glass-ceramic. A typical example of this type is the glass system $MgO\text{-}Al_2O_3\text{-}SiO_2$ having cordierite as the principal crystalline phase (Knickerbocker *et al.*, 1993). The second type, the glass-ceramic composites, consists of a mixture of a suitable glass and one or few ceramic powders, such as alumina in nearly equal proportions. Usually a volume content of more than 50% of a glass with a soften temperature of 20-50 ^{o}C below the sintering temperature of the composite is used. In the third type, the glass bonded ceramics, only very low volume content (5-15%) of a glass with a very low softening temperature (< 400

^{o}C) is used to densely sinter the composite. Table 1.5 shows examples of systems belonging to these three categories along with their manufacturers and important properties.

Table 1.5 Some of the common LTCC dielectric and their properties.

LTCC dielectric material	ε_r (1 MHz)	CTE (ppm/^{o}C)	Bending strength (MPa)	T_s (^{o}C)	Conductor material	Company
Glass-ceramics						
MgO-Al_2O_3-SiO_2	5.3-5.7	2.4-5.5	180-230	850-950	Cu	IBM
CaO-Al_2O_3-SiO_2-B_2O_3	6.7	4.8	250	950	Cu, Ni	Taiyo Yuden
Glass-ceramic composites						
SiO_2-B_2O_3 + Al_2O_3	5.6	4.0	240	1000	Cu	Fujitsu
MgO-Al_2O_3-SiO_2-B_2O_3 + silica	4.3-5.0	3-8	150	850-950	Ag, Ag/Pd	Hitachi
Glass-bonded ceramic						
$BaNd_2Ti_4O_{12}$ + Bi_2O_3-B_2O_3-SiO_2-ZnO	60	9-10	300	900	Ag, Au, Ag/Pd/Pt	Siemens

1.6.5 Glass-ceramic composites

Out of the above three variations, the glass-ceramic composites are most suitable for developing the LTCC substrate. This method is easy and cost effective. In the glass-ceramic composites, the densification is achieved by the process of liquid phase sintering. The glass serves as a flow medium dispersing and rearranging the crystalline particles in the glass melt. Although reactive processes such as dissolution and precipitation occur at the glass ceramic interfaces, these are not essential for the densification process. The densification is mainly due to nonreactive liquid phase sintering. In most cases, the reaction between the glass and the ceramic lead to the formation of new crystalline phases which affects the properties of the composites adversely. The effectiveness of sintering aids depends on several factors such as sintering temperature, viscosity, solubility and glass wettability (Kingery, 1959). The main requirement for liquid phase sintering is that the liquid phase should wet the grains of the ceramics. Generally the chemical reaction between sintering aids and the ceramics can provide the best wetting

condition (Jean *et al.*, 2000). However, a chemical reaction results in the formation of the secondary phase. It was shown that one can exploit different mechanisms of liquid phase sintering depending on the amount of the glass powder in the composite mixture. To obtain full density in the ceramic glass composite, a sufficient quantity of glass (20-50 %) is required. Too little glass can result in poor densification which produces low mechanical strength and poor hermeticity of the final products. Too much glass (> 50%) is also undesirable, because it cause shape distortion during firing and also deteriorates the microwave dielectric properties.

1.6.6 Selection of Glass

Table 1.6 Common LTCC glasses and their physical and dielectric properties.

Glass code	Composition (mole%)	Density (g/cc^3)	Softening Temp. (^oC)	ε_r	Tan δ	Reference
B	B_2O_3	2.46	450	2.5	0.00550 (1 MHz)	(Navias *et al.*, 1946)
PBS	40:PbO,40:B_2O_3, 20:SiO_2	4.31	448	12.9	$7.1x10^{-3}$ (12 GHz)	(Sebastian *et al.*, 2008)
BBS	30:BaO,60:B_2O_3, 10:SiO_2	3.40	627	7.20	$4.4x10^{-3}$ (15 GHz)	(Sebastian *et al.*, 2008)
ZBS	60:ZnO,30:B_2O_3, 10:SiO_2	3.60	582	7.50	$1.07x10^{-2}$ (15 GHz)	(Wu *et al.*, 1999)
LBS	35.5:Li_2O, 31.66:B_2O_3, 33.2:SiO_2	2.34	513	6.44	$3x10^{-3}$ (1 MHz)	(Jantunen *et al.*, 2000)
MBS	40:MgO, 40:B_2O_3, 20:SiO_2	3.18	950	5.0	$2.3x10^{-3}$ (1 MHz)	(Thomas and Sebastian, 2008)
LMZBS	20:Li_2O, 20:MgO, 20: ZnO, 20:B_2O_3, 20:SiO_2	2.75	900	6.90	$1x10^{-3}$ (1 MHz)	(Renjini *et al.*, 2009)

The selection of glass is very important in controlling the properties of the ceramic-glass composites. Among the glasses, silica glass has the lowest dielectric loss in the microwave region (Hippel, 1954; Kinser, 1971). The dielectric loss of fused quartz is less than 0.001 in the frequency range from 10^2 to 2.5×10^{10} Hz. Although the loss level

is attractive, silica is not an effective flux for microwave dielectrics if used alone. To lower the melting point, the rigid bonds in SiO_2 may be broken by modifiers, particularly alkali ions, but this results in higher losses (Sebastian *et al.*, 2008). For binary glasses based on SiO_2, tan δ for borosilicate is about 0.001 at 3 GHz. Ternary glasses based on borosilicates also shows low loss in the microwave region. Some of the alumina silicate based glasses such as cordierite and celsian also show low loss factors in the microwave region. The magnitude of tan δ for cordierite glass ceramics at 10 GHz increases with the increase in glass content of the glass-ceramic composite. Also tan δ for the mineral celsian which contains TiO_2 decreased at 10 GHz with increasing crystallization temperature. This was probably due to a decrease in the residual glassy phase which contributes to the interfacial polarization (Takada *et al.*, 1994). Table 1.6 gives the physical and dielectric properties of various glasses used in the present investigation.

The constituent oxides in glass composition are broadly classified into oxides that make networks, modifier oxides that break network and intermediate oxides that can become oxides of either type. Since modifier oxides break network, they lower the softening point of the glass and increases its fluidity. B_2O_3, SiO_2, GeO_2, P_2O_5 and a few others are the common network formers. Glasses made solely from network formers often have limited utility. For example, pure B_2O_3 glass (T_g ~ 450^oC) is not water resistant and pure SiO_2 glass while valued for its chemical durability and thermal shock resistance, possess high processing temperatures (above 1750^oC). Thus majority of useful glasses contain additives that serve to alter the processing and properties. These are commonly termed as network modifiers and intermediates. Network modifiers provide extra oxygen ions but do not participate in the network, thereby raising the O/Si ratio of the glass. The extra oxygen allows the bridging oxygen between two tetrahedral to be disrupted and two non-bridging oxygen to terminate each tetrahedron. The effects of modifiers are directly analogous to the decreasing SiO_4 interconnectivity observed in crystalline silicates with increasing O/Si ratio. In glasses the loss of connectivity results in greatly decreased viscosities and T_g's for modified silicates and reduces the processing temperatures of silicate glasses into more practical ranges. While alkaline oxides (Na_2O, Li_2O, K_2O) are very effective modifiers, they result in glasses that are not chemically durable (Sebastian *et al.*, 2008).

1.6.7 Other applications of LTCC technology

Nowadays there are many new microelectronics and non-microelectronics applications of the LTCC technology. LTCC is very good for high voltage, high pressure or vacuum applications. The technology is applied to build microsystems for miniature fuel cell energy conversion systems, drug delivery, biological parameter monitoring, gas or liquid chromatographs, cooling and heat exchangers, MOEMS and MEMS packaging, particle separators, polymerise chain reaction (PCR) (Chou *et al.*, 2002), micro total analysis systems (μTAS) and photonic devices (Soucy *et al.*, 2000). Important new applications of LTCC are microfluidic systems used mostly for chemical analysis. Micro-high performance liquid chromatography (μ- HPLC) made in LTCC demonstrates very good properties of ceramics at high pressures. The properties of LTCC/chemiresistor smart channels are comparable to the performance of silicon-based ones. LTCC structure can be used as a focusing electrode in the field emitter arrays (Chenggang *et al.*, 2002). LTCC materials are applied for fiber optic and electro-optic packages. Silicon MEMS packaging is another very wide field of LTCC application. Another interesting application of LTCC is three-dimensional shells used for example in spherical stepper motor or radar sensor (Li *et al.*, 2002).

1.7 Composites

1.7.1 Introduction

The term ‘composites’ describes a mixture of two or more materials, each being present in significant quantities and each imparting a unique property to the mixture. By combining two or more constituents, it is possible to create materials with unique combinations of properties that cannot be achieved in another way. Composite technology, where a novel artificial material is fabricated by combining for example, ceramic and another ceramic or a polymer material in an ordered manner or just by mixing is being used widely for electronic, sonar, medical diagnostics and NDT purposes. The composite electro-ceramics introduce not only new functionalities but also fabrication flexibility. The best example is printed circuit boards (PCBs), for which dielectric properties and the CTE are critical. Polymer-matrix composites in the form of

E-glass fiber-reinforced polymer PCBs are well established packaging materials. Similarly, a variety of particles are added to polymers to reduce the CTE and increase the thermal conductivity, or both. These materials are usually referred to as particle-reinforced polymer-matrix composites.

1.7.2 Properties of the composites

1.7.2.1 Sum of properties

In the case of sum property, the composite property coefficient depends on the corresponding coefficients of its constituent phases. For example, the relative permittivity of the composite depends on the relative permittivity of its constituent phases.

1.7.2.2 Combination of properties

In the combination of properties, composites exhibit characteristics that are beyond the limits of constituent phases and therefore simple mixing rules do not apply. In such a case two or more coefficients, like Young's modulus (E) and density (ρ), are combined to produce third characteristic acoustic wave velocity $v = (E/\rho)^{1/2}$. Highly anisotropic wave propagation is obtained with composites with e.g. needle/fiber reinforced composites where the orientation of the filler with respect to the plane-wave plays crucial role in the overall wave velocity. Significantly higher wave velocities can be obtained when the needles/fibers are orientated along the direction of the propagation. The wave speed of the composite is approaching to the acoustic wave speed of the filler as a function of filler loading while in the case of perpendicularly aligned fillers the wave speed can be even lower than that of the matrix

1.7.2.3 Product of properties

The product properties are more complex. The product properties of a composite involve different properties in its constituent phases and the interaction between the phases often causing unexpected results. For e.g., in a magneto-electric composite, the magneto-strictive strain in one phase creates an electric polarization in an adjacent piezoelectric phase. A product property utilizes different properties of the two phases of a composite to

produce yet a third property through the interaction of the two phases. By combining different properties of two or more constituent phases, interesting product properties are sometimes obtained with a composite. In some cases, product properties are found in composites that are entirely absent in the phases making up the composite. Table 7 lists some of such product properties.

Table 1.7 Examples of product properties

Property of phase 1	Property of phase 2	Property of the composite
Thermal expansion	Electrical conductivity	Thermistor
Magnetostriction	Piezoelectricity	Magnetoelectricity
Hall effect	Electrical conductivity	Magnetoresistance
Photoconductivity	Electrostriction	Photostriction
Superconductivity	Adiabatic demagnetization	Electrothermal effect
Piezoelectricity	Thermal expansion	Pyroelectricity

1.7.3 Connectivity

Making ceramic polymer composites not only involves choosing the right material but also coupling them with best possible design. The concept of connectivity was first established by Newnham et al. (Newnham *et al.*, 1978). Connectivity is a key feature in the development of multi phase solids since the physical properties can be changed in different orders of magnitude depending on how connections are made (McLachlan *et al.*, 1990). The interspatial relationship in a multiphase material has maximum importance because it controls the mechanical, electrical, magnetic and thermal fluxes between the phases. In a composite each phase may be self-connected in either one, two or three dimensions. In a two phase composite there are 10 different combinations of connectivity and they are 0-0, 0-1, 0-2, 0-3, 1-1, 1-2, 1-3, 2-2, 2-3 and 3-3 connectivity. These connectivity patterns are illustrated in Fig. 1.13 using cube as building block. The most commonly studied composites are 0-3 and 1-3 configurations. 0-3 configuration can be easily prepared at relatively low cost (Dias *et al.*, 1996).

The preparation of 0-3 ceramic/polymer composites involves proper selection of the ceramic and the polymer. Normally ceramic is prepared in the powder form by grinding and hence adequate grain sizes are obtained. The polymer, determines the way

in which the materials can be mixed. If the polymer is an epoxy, the mixing can be done by hand at room temperature using adequate amount of resin, hardener and ceramic. In the case of a thermo plastic polymer the blending process can be done in two different ways. In the first case the polymer is heated above the glass transition temperature, in a kneading machine, and then ceramic powder is added gradually and will be mixed till a reasonable blend is obtained. In the second method, the polymer is dissolved in a solvent and the powdered ceramic is added to it and then the solvent is allowed to evaporate by a curing process.

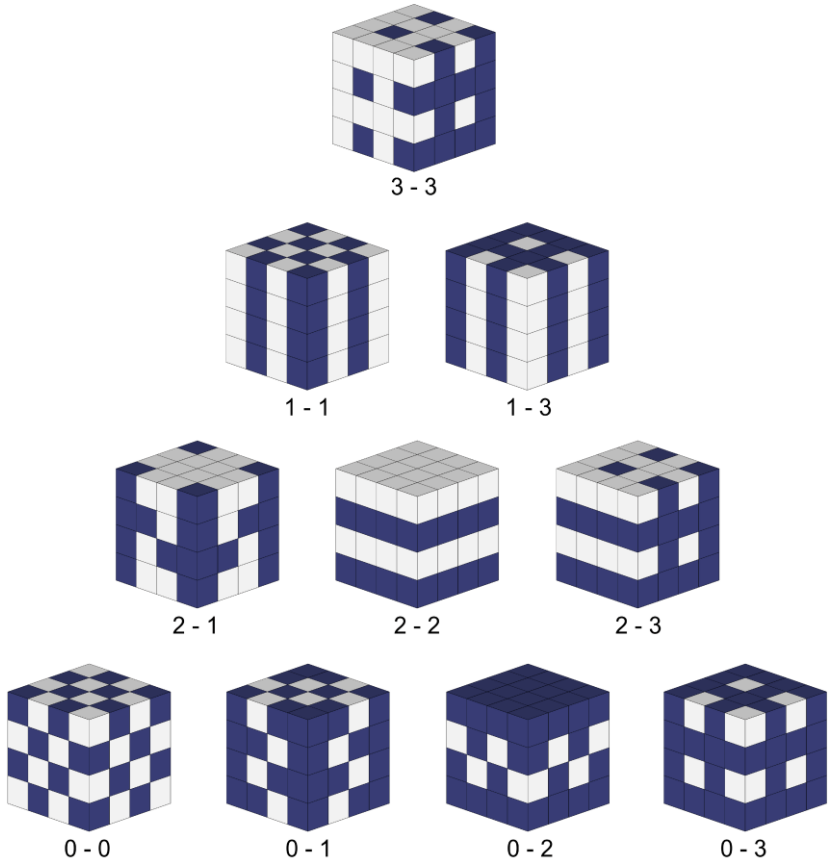

Figure 1.13 Connectivity patterns in a di-phasic composites systems(Newnham *et al.*, 1978).

Ceramic composites with different connectivity can also be made by different techniques like, extrusion, tape casting and replamine process. Extrusion processing can be used to prepare a 3-1 composite. A ceramic slip is extruded through a die giving a three dimensionally connected pattern with one dimensional holes, which can be filled later with a different material. A 2-2 pattern can be produced by tape casting of

multilayer capacitors with alternating layers of metal and ceramic. In this arrangement both the phases are self connected in two dimensions, however, not connected in the Z direction. In 3-2 pattern one phase is three dimensionally connected while the other in two. This pattern can be obtained by modifying the 2-2 pattern by inserting holes in one of the phases and the second phase can connect through the holes resulting in a three dimensional connectivity.

Considering the physical properties, the 3-3 pattern is the most complicated and interesting one. In this pattern two phases form interpenetrating three dimensional net works. These patterns can be found in living systems such as coral, where organic tissue and inorganic skeleton interpenetrate one another and also in bone and wood. Experimentally 3-3 connectivity composites can be produced by replamine form process (Dias *et al.,* 1996). In this process a suitably shaped coral is used as a template material for the ceramic. First of all the coral is vacuum impregnated with casting wax, afterwards the coral is leached away chemically leaving the negative of the coral shape. The positive of the template is filled with the solution containing ceramic and wax. After heating at 300 ^{o}C, the remaining ceramic structure can be sintered at high temperatures. A polymer of suitable viscosity can be impregnated into this three dimensional structure and a 3-3 composite can be obtained. Metal-ceramic 3-3 composites can be prepared by infiltrating ceramic foams with molten alloys. The ceramic forms are prepared by gel casting technique and molten alloys are infiltrated into the ceramic foam (Binner *et al.*, 2009).

1.7.4 Polymers for microelectronic applications

Polymers play a crucial role for applications such as substrate and electronic packaging. Polymers have the advantages of low temperature processability and flexibility. They also have interesting dielectric properties for a range of frequencies. Most of the polymers have low values of relative permittivity and dielectric loss at microwave frequencies, which is usually required for substrate as well as packaging applications. In general the polymers can be classified into two categories (i) thermoplastic polymers (ii) thermoset polymers (Cahn *et al.*, 1993). Thermosetting plastics are polymer materials that irreversibly cure to a stronger form. The cure may be done through heat, through a chemical reaction (two-part epoxy, for example), or

irradiation such as electron beam processing. A thermoplastic is a plastic that melts to a liquid when heated and freezes to a brittle, very glassy state when cooled sufficiently. Most thermoplastics are high-molecular-weight polymers whose chains associate through weak Van der Waals forces (polyethylene); stronger dipole-dipole interactions and hydrogen bonding (nylon); or even stacking of aromatic rings (polystyrene). Thermoplastic polymers differ from thermosetting polymers as they can be re-melted and remolded. Thermoplastics are elastic and flexible above a glass transition temperature T_g. There are number thermoplastic polymers like; polyethylene, polystyrene, polypropylene, poly-ether-ether-ketone (PEEK) etc used for making composites. Thermoset materials are usually liquid or malleable prior to curing and designed to be molded into their final form. The most commonly used thermoset matrices are, epoxy resins, polyimide, bakelite etc (Cahn *et al.*, 1993).

1.7.5 Polymer/Ceramic Composites

The importance of polymers in electronic applications lies in the fact that, though they are not intrinsically functional, they can be doped and made functional and their soft or pliable nature enables flexible free-standing substrates in a variety of different shapes. Until now, the needs of substrate materials were covered by soft thermoplastics based on polytetrafluoroethylene (PTFE) or ceramic substrates, but neither satisfies both the required dielectric and mechanical characteristics. The presence of Teflon in the formulation of such polymeric substrates makes the metallization process during the manufacture of large sized boards difficult. In addition, there is a polymeric transition at room temperature, so the variation of the relative permittivity with temperature is not linear. Recently, there has been a huge interest in polymer ceramic composites because they enable inexpensive industrial level realization of 3D microwave devices and packages with advanced electric and mechanical properties. Particularly, composites using thermoplastic polymers such as PTFE, polyethylene, polystyrene, silicone rubber etc have drawn much industrial and academic interest because they have the additional advantage of a simple, 3D fabrication process such as injection moulding of electronic components.

The almost limitless possibilities to combine two or more materials at the micro or nanoscopic level lead to a large range of properties. Polymer-ceramic composites consisting of ceramic particles filled in a polymer matrix are now widely used in the electronic industry as substrates for high frequency uses, since they combine the electrical properties of ceramics and the mechanical flexibility, chemical stability and processing possibility of polymers (Soane *et al.*, 1989). The presence of filler in a semicrystalline polymer can cause many changes to the physical properties of the polymer. Several reports are available which investigates the use of silica filled polymer composites for packaging applications. However, because of the low thermal conductivity of silica filler, researchers are extending their work to develop new fillers with high thermal and electrical performance (Sebastian *et al.*, 2010). There are many possible candidates for ceramic fillers having both high thermal conductivity and high electrical resistivity such as diamond, beryllia, boron nitride, aluminum nitride etc. The thermal properties of the polymers can be improved with a sufficiently high (> 40%) volume percentage of filler (Yu *et al.*, 2000). However, higher filler content results in low strength, poor fluidity, poor flexibility and defects in the composite and have adverse effect on the dielectric properties. Hence by the proper design of these composites, we can utilize the ease of processing and low relative permittivity of polymers and high thermal conductivity, low thermal expansion coefficient and thermal stability of ceramics.

Recently, a large number of polymer-ceramic composites has been introduced for telecommunication and microelectronic applications. The composites with a three-dimensionally connected polymer phase loaded with isolated ceramic particles called composites of 0-3 connectivity is the most attractive for practical applications. Composites of 0-3 connectivity enable flexible forms and very different shapes with very inexpensive fabrication methods including simple mixing and molding (Sebastian *et al.*, 2010). Composites used in microelectronic packaging have to simultaneously fulfill diverse requirements such as low dielectric loss (tan δ), moderate relative permittivity (ε_r), low temperature coefficient of relative permittivity ($\tau\varepsilon_r$), low moisture absorption, low coefficient of thermal expansion and high dimensional stability and mechanical stiffness.

Polymer/ceramic composites are potential materials group suitable for producing demanding and functional packages that combine the electrical properties of ceramics and the mechanical flexibility, chemical stability, and processing possibilities of polymers. The connectivity between the two phases in the composites is very important in achieving the desired properties. The preparation of 0-3 type composite materials by combining a dielectric or a ferroelectric ceramic and a polymer for suitable properties means not only choosing the right materials, processed in a particular way, but also coupling them with the best possible structure. The interspatial relationships in a multiphase (Newnham *et al.*, 1978) material control the mechanical and electrical properties, and thermal fluxes between the phases. The filler particle size, interfacial properties, percolation level, and porosity effects can also play a role in the composite properties. Interfacial effects can occur between the ceramic grains and the polymer matrix, leading to large dielectric relaxations normally at low frequencies. However, the response of the composite may have a property that is not displayed in the individual phases. The properties of the polymer-ceramic composites are determined by the number of phases and the way in which the phases are interconnected. The response of a polymer-ceramic composite to an external excitation (electric field, temperature, stress etc) depends on the response of the individual phases, their interfaces as well as the connectivity concept. Although a very large number of ceramic with low loss are available, they are generally very brittle. This leads to a difficulty in the fabrication of complex shapes or machining the ceramic substrates during circuit fabrication. These difficulties can be avoided by using 0-3 polymer-ceramic composites as an alternative, which offer excellent material characteristics such as low temperature processability, flexibility, machinability, chemical resistance, tailored dielectric properties etc. Ceramic filled polymers are used in electronic packaging for device encapsulation. Encapsulation of electronic devices protects them from an adverse environment and increases their long term reliability.

1.7.6 Advantages of polymer/ceramic composites

Composite materials are traditionally designed for use as structural materials. With the rapid growth of the electronics industry, composite materials are finding more

and more electronic applications. The design criteria for this group of composites are different because of the vast difference in property requirements between structural composites and electronic composites. While structural composites emphasize high strength and high modulus, electronic composites emphasize high thermal conductivity, low thermal expansion, low relative permittivity, high/low electrical conductivity, and/or electromagnetic interference (EMI) shielding effectiveness, depending on the particular electronic application. The applications of polymer/ceramic composites in microelectronics include interconnections, printed circuit boards, substrates, encapsulations, interlayer dielectrics, die attach, electrical contacts, connectors, thermal interface materials, heat sinks, lids and housings. The applications of printed circuit boards can be divided into two areas: information technology and communication industries. Both applications have identical technical demands for the future evolution to high-frequency appliances. As the working frequency of electronic appliances increases, signal intensity losses become more sensitive. Circuit substrates with poor dielectric properties will maintain an unfavourable signal conveying efficiency. Therefore, demand is high in high frequency appliance markets for small relative permittivity and low dissipation energy substrates. Polymer/ceramic composites also offer excellent material characteristics including low temperature processability, flexibility, high temperature resistance, outstanding solvent resistance etc.

Chapter 2

Experimental Techniques

2.1 Introduction

The word “Ceramics” originated from the Greek word “Keramos” meaning fired clay. The definition broadened to “art and science of making and using solid articles formed by the action of heat on earthly raw materials” (Richerson, 2006). Later on Kingery made a new definition as “ceramic materials is anything that is not an organic material or a metal” (Kingery, 1960). Most of the people associate the word ceramic with pottery sculpture, sanitaryware, tiles etc. However, this view point is incomplete as it contains only the traditional or silicate based ceramics only. Today the field of ceramics can be divided into traditional and advanced ceramics. Traditional ceramics are characterized by silicate based porous microstructures that are coarse, non uniform and multiphase. They are formed by mixing clays and feldspar followed by forming either by slip-casting or on potter’s wheel, then firing and finally glazing (Bersaum, 1997). Advanced ceramics consist of oxides, carbides and even completely synthetic materials which have no natural equivalents. The microstructure of these ceramics is at least an order of magnitude finer, homogeneous and less porous compared to the traditional counter parts. Regarding the applications of ceramics, traditional ceramics are quite common from sanitaryware to fine Chinas. The applications of advanced ceramics include thermal insulation, refractoriness, ferroelectric materials, semi conducting materials, insulators in electronic applications, microwave dielectrics, magnetic and superconducting, catalysis, anticorrosion properties etc. Among these microwave dielectrics have extreme importance because of the present explosive growth in wireless communication.

2.2 Synthesis of ceramics

Ceramic fabrication techniques generally include various powder processing methods with powder synthesis, forming and sintering. The powder synthesis process of ceramics involves several techniques like (a) solid state reaction route (b) mechanical methods and (c) chemical routes (Arai, 1996). Powders with different properties can be produced using different processing methods. A careful selection of the preparation technique is required to prepare powders consisting of particles with specific properties to yield the bulk component. The synthesis of specific powders and better control of

chemical and physical characteristics of ceramic powders can deliver improved and reproducible properties. The most common method of preparing ceramic powders is by solid-state reaction methods, because it is the simplest, easier and cost effective method to make bulk amount of ceramics. However, it is established that the surface area of the ceramic powder derived through solid state reaction technique is relatively lower and hence the particles can offer lesser points of contacts which are vital for effective sintering reactions to take place (Schmalzried, 1974). The inhomogeneity of particle size distribution and high temperature of formation are the major drawbacks of solid state ceramic techniques (Nanni *et al.*, 1999). However, it is less expensive and hence it is more popular. In the mechanical methods, small particles are produced from larger ones by mechanical forces, a process referred to as comminution. The process of comminution involves operations such as crushing, grinding and milling. Mechanical treatment of ceramic powders can reduce particle size and enables to obtain nano-structured powders, which are of considerable interest in the current trend of miniaturization and integration of electronic components. However, this technique lacks the synthesis of phase pure ceramics, which is essential for the fabrication of DRs and ceramic substrates with optimum dielectric properties. Hence alternate chemical techniques like molten salt, co-precipitation, sol-gel, hydrothermal, polymer precursor and combustion methods have also been employed to synthesize dielectric ceramics (West, 1984). But the sinterability of bulk ceramics prepared using chemically derived powders was found to be very poor and hence none of these techniques could give a higher quality factor for dielectric resonators compared to the DRs obtained through solid state technique. Moreover the stringent operation conditions involved in the reaction sequence as well as the high cost of chemicals limit the usage of chemical methods for the industrial fabrication of DRs and ceramic substrates. Hence in the present study we have employed the conventional solid state synthesis of ceramics for the fabrication of dielectric resonators and substrates, because this method is cost effective and can lead to better dielectric properties, which is the primary interest in the fabrication of electronic devices employing dielectrics.

2.3 Solid state synthesis

The solid state ceramic route is considered to be one of the oldest and easiest materials synthesizing techniques for the synthesis of complex oxide materials. Metal oxides containing more than one type of cation are of interest from both academic and commercial point of view. This is because complex metal oxides exhibit a number of features that are not found in simple oxides. The conventional ceramic synthesis route involves basically four steps (a) intimate mixing of the stoichiometric oxides, (b) high temperature firing/calcination (c) intermediate grinding and (d) sintering. On heating at high temperatures, a new material is formed (see Fig. 2.1) to reduce the free energy, at the points of contact through solid state diffusion. This new product layer (of a few Å) eventually acts as a potential barrier between the two grains and thus impeding further grain to grain material transport. This demands the need of new point of contacts to be introduced which is usually achieved through grinding or ball milling. This frequent grinding coupled with multiple calcination maximizes the product to reactant ratio. The solid state synthesis requires high temperature to form the product which leads to agglomerated particles.

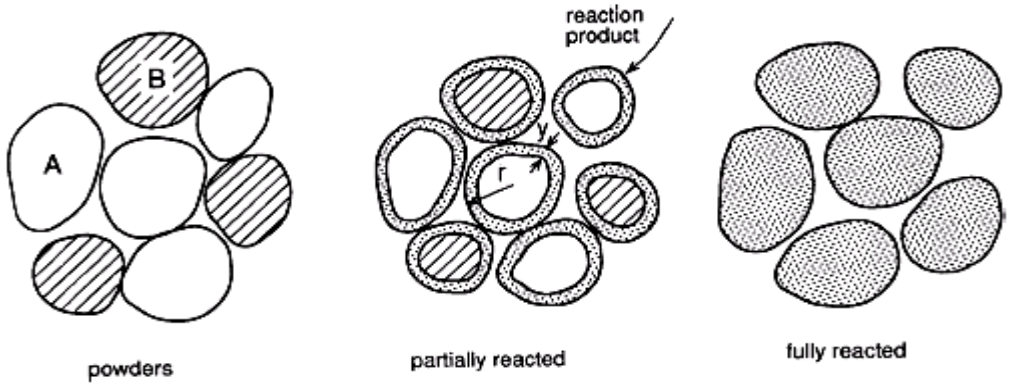

Figure 2.1 Reaction between two kinds of particles to form a product at the points of contact.

The solid-state reaction method, which is employed in the present work, involves the following steps

2.3.1 Selection of appropriate starting materials

Fine grain powders to maximize surface area, reactive starting reagents and well defined compositions are the three criteria that must be taken into account while selecting appropriate starting materials. The oxides of the constituent cations are used in this method. In some instances, notably Ba, the oxide is not suitable because it is either unstable or highly hygroscopic. In such cases, the carbonate or nitrate is used, because they will decompose to oxides on heating and are more reactive. The impurities are detrimental to dielectric properties and they affect reactivity of the fired ceramics too. Hence raw material purity of greater than 99.9% is essential for obtaining phase pure compounds.

2.3.2 Stoichiometric mixing

The raw materials need to be intimately mixed to increase the points of contact between reactant oxides, which in turn act as 'product layer formation centers'. The mixing and milling eliminates agglomerates and reduces particle size. If agglomerates are present they densify more rapidly resulting in pores. During the mixing process, agglomerates are broken and defects are introduced into the grains that enhance diffusion mechanism. Therefore the mixture of powders is ground well and thoroughly mixed using distilled water or acetone. Ball mills are used for the mixing purpose. In the present investigation, the mixture of constituent powders taken in polythene bottles were ball milled for sufficient duration in distilled water medium using Yttria Stabilized Zirconia (YSZ) balls. In the milling process, the particles experience mechanical stresses at their contact points due to compression, impact or shear with the milling medium or with other particles. The mechanical stress leads to elastic and inelastic deformation. If the stresses exceed ultimate strength of the particle, it will fracture the particles. The mechanical energy supplied to the particle is used not only to create new surfaces but also to produce other physical changes in the particle (Beke, 1964). The rate of milling is determined by the relative size, specific gravity and hardness of the media and particles. The shape of the milling media (balls) is an important factor in ball milling as it determines the product size distribution. Using spherical ball the size distribution is broad since two balls have only one point of contact between them. On the other hand using cylindrical balls with

'dome ends' the particle size distribution is more uniform with narrow distribution curves (Rose *et al.*, 1958). This is due to the fact that cylindrical balls offer a line of contact between them.

2.3.3 Calcination

Calcination is the intermediate heat treatment at a lower temperature prior to sintering. Calcination processes are endothermic decomposition reactions in which an oxysalt, such as a carbonate or hydroxide, decomposes, leaving an oxide as a solid product and liberating a gas. The kinetics of solid state reactions occurring during calcination may be controlled by any one of the three processes: (i) the reaction at the interface between the reactant and the solid product, (ii) heat transfer to the reaction surface or (iii) gas diffusion or permeation from the reaction surface through the porous product layer. The calcination conditions such as temperature, duration of heating and atmosphere are important factors controlling shrinkage during sintering. Though the final phases of interest may not be completely formed, the calcination yields a consistent product.

2.3.4 Grinding

The calcined powders are invariably agglomerated which need to be ground to fine powder. Grinding can be accomplished by any suitable means. It prepares the reacted material for ceramic forming. The grinding also helps to homogenize the compositional variations that may still exist or that may arise during calcination. Generally, grinding down to somewhere around 0.1 to 1 μm is advisable. If the grinding is coarser the ceramic can have large intergranular voids and low fired density. If grinding is too fine, the colloidal properties may interfere with subsequent forming operations. Generally for grinding purpose ball mill or mortar with pestle is used. The milling process can dramatically improve the quality of the powder, improving the bulk and green density and enhancing sintering. In large scale operation a grinding medium is chosen that suffers very little wear.

2.3.5 Addition of polymeric binder

The principal functions of a ceramic binder are to impart sufficient strength and appropriate elastic properties for handling and shaping during the post forming stage. They coat the ceramic particles and provide lubrication during pressing and a temporary bond after pressing. The selection of binder and other additives must be compatible with the chemistry of the ceramic and the purity requirements of the application. In modern ceramics technology, in die pressing, a narrow range of water-soluble organic binders, such as poly vinyl alcohol is most often applied to improve the rheological properties of the powder compact (Onoda *et al.*, 1973). The polymeric dispersions and organic binders provide the pressed ceramic powders with optimal properties from the point of view of thickening abilities and mechanical strength of the pressed samples (McHale, 1991). The commonly used polymers for ceramic binding purpose are poly vinyl alcohol (PVA), poly ethylene glycol (PEG), carboxymethylcellulose etc. most of which are water thinnable polymeric dispersions. The amount of organic binder required for pressing is quite low, typically ranging from 0.5 to 5 wt%. The binder concentration for each process is about 3 % in dry process, 3-17 % in wet processing and 7-20 % in plastic forming (McHale, 1991). The recent research trends suggest that the PVA and PEG are ideal binder additives for fabrication of microwave dielectric ceramics (Alford *et al.*, 2000).

The binder must be removed prior to densification of the ceramic. Organic binders can be removed by thermal decomposition. For example, PVA burn out on heating above 400^{o}C. If reaction between the binder and the ceramic occurs below the binder decomposition temperature or if the ceramic densifies below this temperature, the final part will be contaminated or may even be cracked or bloated. If the temperature is raised too rapidly or if the atmosphere in the furnace is reducing, the binder may char rather than decompose, leaving behind carbon.

2.3.6 Powder compaction (uniaxial pressing)

Most ceramic-forming processes start with a powder and consist of compaction of the powder into a desired shape. The main objective is usually to achieve the greatest degree of particle packing and a high degree of homogeneity. A typical pressing

operation has three basic steps: (i) filling the mold or die with powder (ii) compacting the powder to a specific size and shape and (iii) ejecting the compact from the die. The most common and widely used method of powder compaction is uniaxial pressing. It involves the compaction of powder into a rigid die by applying pressure in a single axial direction through a rigid punch or piston (Ichinose, 1987; Richerson, 2006). Compaction is done slowly to facilitate the escape of the entrapped air. The pressure gradient in powder compact as a function of the distance from the upper punch is given by the formula

$$P_x = P_a \exp\left[-4\mu K \frac{L}{D}\right] \tag{2.1}$$

where μ is the coefficient of friction, P_a is the applied pressure, L is the length and D is the diameter of the powder compact. It is evident that the pressure distribution of a powder compact is more uniform when the length to diameter ratio is smaller (Castro, 2000). For microwave dielectric measurements, the samples having a D/L ratio ~ 2 are prepared and hence the pressure distribution is more or less uniform in the powder compacts. A pressure of 50-150 MPa is ideal in ceramic forming.

Friction between the powder and die wall decreases the pressure available for compaction with increasing distance from the pressing punch. Since compact density is directly related to forming pressure, a forming pressure gradient becomes a density gradient in the compact. Friction is influenced by the die material and its surface finish, nature of the powder and the organic additives used. Highly polished Tungsten Carbide or steel are used as the die material, which helps in great deal in reducing the friction. Internal lubricants such as Stearic acid dissolved in Propane 2-ol can reduce the friction with the die and ease the processing.

2.3.7 Sintering

The firing process or sintering is usually the final stage in ceramic manufacturing. Sintering refers to the densification of a particulate ceramic compact by the removal of pores between the starting particles (accompanied by shrinkage of the component), combined with growth together and strong bonding between adjacent particles when subjected to high temperatures (Kingery, 1960). It involves heat treatment of powder

compacts at elevated temperatures, where diffusional mass transport is appreciable which results in a dense polycrystalline solid (Kang, 2002). The criteria that should be met before sintering can occur are (i) a mechanism for material transport must be present (ii) a source of energy to activate and sustain this material transport must be present. The primary mechanisms for transport are diffusion and viscous flow. Heat is the primary source of energy, in conjunction with energy gradients due to particle-particle contact and surface tension. Thermodynamically, sintering is an irreversible process in which a free energy decrease is brought about by a decrease in surface area. The principal goal of sintering is the reduction of compact porosity. The development of microstructure and densification during sintering is a direct consequence of mass transport through several possible paths and one of these paths is usually predominant at any given stage of sintering (Coble, 1961). They are (i) evaporation/condensation (ii) solution/precipitation (iii) lattice diffusion and (iv) surface diffusion or grain boundary diffusion. Several variables influence the rate of sintering. Some of them are initial density, material, particle size, sintering atmosphere, temperature, time and heating rate. The sintering phenomena are of two types. The first one is solid-state sintering, where all densification is achieved through changes in particle shape, without particle rearrangement or the presence of a liquid phase. The other one is liquid-phase sintering, where some liquid is present, which aids compaction.

2.3.7.1 Solid state sintering

Solid-state sintering involves material transport by volume diffusion. Diffusion may consist of movement of atoms or vacancies along a surface or grain boundary or through the volume of the material. Surface diffusion (vapour –phase transport) does not result in shrinkage whereas, volume diffusion along grain boundaries or through lattice dislocations result in shrinkage (Coble, 1961). The driving force for solid-state sintering is the difference in free energy or chemical potential between the free surfaces of particles and the points of contact between adjacent particles. The linear shrinkage of the material caused by the lattice diffusion from line of contact between two particles to the neck region can be expressed as:

$$\frac{\Delta L}{L_0} = \left(\frac{K\gamma a^3 Dt}{KTd^n} \right)^m \qquad (2.2)$$

where $\Delta L/L_o$ = linear shrinkage (equivalent to the sintering rate); γ = surface energy; a^3 = atomic volume of the diffusing vacancy; D = self-diffusion coefficient; k = Boltzmann constant; T = temperature; d = particle diameter; t = time and K = constant dependent on geometry. The exponent n is close to 3 and m is generally in the range of 0.3 to 0.5. From Eq. (2.2) it can be clearly understood that the particle diameter has a major effect on the rate of sintering. The smaller the particles, the greater the sintering rate. Fine particle size powder can be sintered more rapidly at a lower temperature than coarser powder. The various stages involved in the sintering process are as follows:

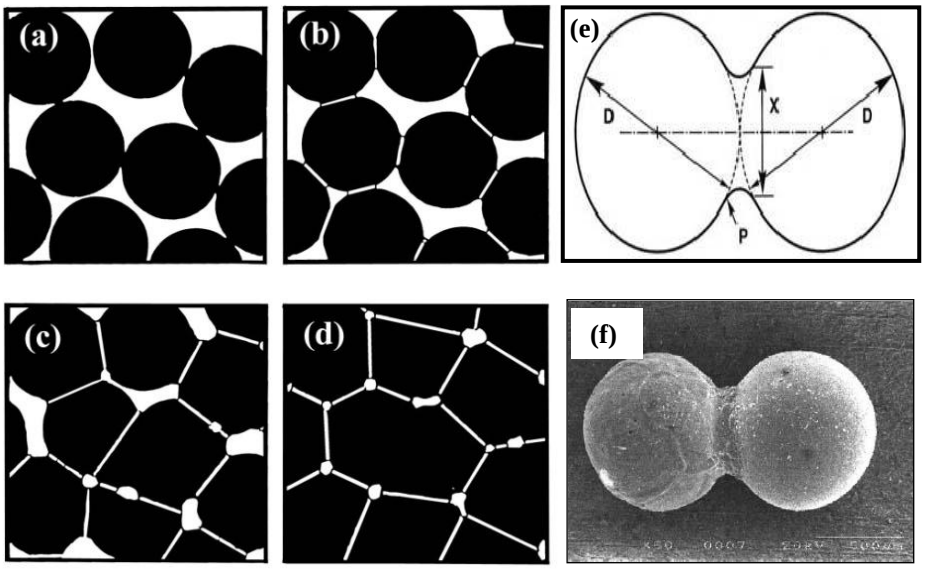

Figure 2.2 Different stage of sintering (a) & (b) Initial stage, (c) Intermediate stage and (d) Final stage of sintering (e) Neck formation during first stage and (f) SEM picture of neck formation in sintered alumina (German, 1996).

(a) Initial stage of sintering

It involves rearrangement of particles and initial neck formation at the contact point between each particle. The rearrangement consists of slight movement or rotation of adjacent particles to increase the number of points of contact. Bonding occurs at the points of contact where material transport can occur and where surface energy is highest.

After the initial stage, the densification of the sintering component increases by ~10% and it is reached very quickly (seconds or minutes) after exposing powder to high temperature because of the large surface area and the high driving force for sintering (Kingery *et al.*, 1955).

(b) Intermediate stage of sintering

The second stage of sintering is referred to as intermediate sintering. The physical changes that occur at this stage are: the size of the necks between the particles grow, porosity decreases and the centers of the original particles move closer together. The grain boundaries begin to move so that one grain begins to grow while the adjacent grain is consumed. This allows geometry changes that are necessary to accommodate further neck growth and removal of porosity. Intermediate sintering continues as long as pore channels are interconnected and ends when pores become isolated. Most of the shrinkage during sintering occurs during this stage. The shrinkage in the intermediate stage can result in additional densification by as much as 25%, or to a total of about 95% of theoretical density (Gupta, 1978).

(c) Final stage of sintering

It involves the final removal of porosity by vacancy diffusion along the grain boundaries. Therefore the pores must remain close to the grain boundaries. Pore removal and vacancy diffusion are aided by the movement of grain boundaries and controlled grain growth. However, if grain growth is too rapid, the grain boundaries can move faster than the pores and leave them isolated inside the grain. As the grain continues to grow, the pore becomes further separated from the grain boundary and has decreased chance of being eliminated. Therefore, grain growth must be controlled to achieve maximum removal of porosity. The final sintering stage begins at about 93-95% of theoretical density, when porosity is already isolated (Kingery, 1954). Ideally, at the end of this stage all porosity is eliminated. The complete elimination of porosity in the final stage of sintering can only happen when all pores are connected to fast, short diffusion paths along grain boundaries (or, equivalently, if the grain boundaries remain attached to the pores).

Other factors which affect the rate of sintering are particle packing, particle shape and particle size distribution. If particle packing is not uniform in the greenware, it will be difficult to eliminate all the porosity during sintering. If the concentration of elongated particles is high, it can result in bridging during the forming process producing large irregularly shaped pores that are difficult to remove after sintering. Particles of same size are difficult to pack efficiently and they form compacts with large pores and a high volume percentage of porosity. However, commonly available powder has a range of particle sizes from submicron upward. Better overall packing can be achieved during compaction, but isolated pores due to bridging and agglomeration are usually quite large and result either in porosity or large grain size after sintering.

2.3.7.2 Liquid phase sintering

Liquid-phase sintering (LPS) is an important means of manufacturing dense ceramic components from powder compacts. It involves the presence of a viscous liquid at the sintering temperature and is the primary densification mechanism for most silicate systems. In two phase systems involving mixed powders, liquid formation is possible because of different melting ranges for the components or the formation of low melting phase, including a glassy phase. The major advantages of LPS are enhanced sintering kinetics and tailored properties. However, apart from these merits, the ceramics sintered by LPS are susceptible to shape deformation. In order to attain densification by LPS certain criteria must be satisfied. They are (i) a liquid must be present at the sintering temperature, (ii) there must be good wetting of the liquid on solid or the contact angle must be low and (iii) there must be appreciable solubility of solid in liquid. Commercial ceramics tend to have a small amount of reactive liquid that accelerates the densification rather than facilitate viscous flow. When the liquid coats each grain, the material can often be sintered to a higher density at a lower temperature with less of a tendency for exaggerated grain growth. Less than 1 volume % of the liquid phase is sufficient to coat the grains if the liquid is distributed uniformly and the grain size is about 1μm. Secondly, the liquid must have a solubility for the solid. Finally, the diffusive transport for the solid atoms dissolved in the liquid should be high enough to ensure rapid sintering. The wetting liquid concentrates at the particle contacts and forms a meniscus; this exerts an

effective compressive pressure on the compact resulting in a rapid rearrangement of particles into a higher density configuration. Densification during LPS can be achieved by the following three rate-controlling mechanisms:

(a) Particle rearrangement

In the initial stages of liquid phase sintering, a number of consecutive and simultaneous processes such as melting, wetting, spreading, liquid redistribution etc. may occur. Both solid and liquid are subjected to rearrangement because of the unbalanced capillary forces. Liquid films between the particles act as a lubricant and the particle rearrangement takes place in the direction of reducing porosity. The driving force for the rearrangement arises due to the imbalance in capillary pressure as a result of particle size distribution, irregular particle shape, local density fluctuation in the powder compact and anisotropic material properties. As the density increases, particles experience increasing resistance to further rearrangement due to crowding by neighboring particles until the formation of a close packed structure.

(b) Solution-precipitation

When the rearrangement becomes insignificant, additional densification can be achieved by dissolution of the solid at grain contacts thus resulting in the center-to-center approach of particles. The main driving force for this process is capillary forces. The dissolved solute transfers to the uncompressed part of the grain structure by diffusion through a liquid phase. This mass transfer results in contact-point flattening and hence a linear shrinkage in the powder compact. The dissolution rate of the solid decreases as the contact area increases due to simultaneous reduction of effective stress at the contact area. At the later stage of solution precipitation, the interconnected pore structures pinch off to form isolated or closed pores.

(c) Pore removal

This is the final stage of LPS which starts after pore closure. During this stage a maximum relative density upto 95% is attained. The closed pores usually contain gaseous species from sintering atmosphere, vaporized liquid and decomposed solid. Several

processes can occur simultaneously during the final stage LPS which includes growth and coalescence of grains and pores, dissolution of liquid into solid, phase transformations and formation of reaction products between liquid and solid.

2.4 Preparation of glass

Most of the ceramics possess high sintering temperatures (above 1200 ^{o}C). As discussed in chapter 1, the most effective method to lower the processing temperature of the ceramic is to add low melting, low loss glasses. Traditionally, glasses are produced by cooling a liquid fast enough to prevent detectable crystallization. From this kinetic point of view, glass formation can be considered as the avoidance of crystallization. In the present investigation, glasses such as B_2O_3 (B), 30BaO-60B_2O_3-10SiO_2 (BBS), 60ZnO-30B_2O_3-10SiO_2 (ZBS), 40PbO-20B_2O_3-40SiO_2 (PBS), 40MgO-40B_2O_3-20SiO_2 (MBS), 35.14Li_2O-31.66B_2O_3-33.2SiO_2 (LBS), and 20Li_2O-20MgO-20ZnO-20B_2O_3-20SiO_2 (LMZBS) are used. Initially high purity oxides such as B_2O_3, Li_2CO_3, SiO_2, ZnO, $BaCO_3$, Bi_2O_3 and $(MgCO_3)_4$ $Mg(OH)_2$ $5H_2O$ (99.9 % Aldrich chemical company, U.S.A) are accurately weighed and thoroughly mixed. After mixing they are dried and melted in platinum crucibles above their melting points. The high temperature favors the materials to react with one another and also encourages the escape of gas bubbles from the melt which is usually referred to as refining the glass. Upon completion of the refining process, the glass is suddenly cooled from the melting temperature to room temperature (process known as quenching) where the glass has higher viscosity. Finally the so formed glass is powdered for further mixing with ceramics.

2.5 Preparation of polymer-ceramic composites

Composite materials play a key role in the modern science and technology, especially in the area of electronics. Polymer based composite materials has a number of applications. Low dielectric loss ceramic loaded polymers can be used in electronic packaging and substrate applications. Mainly two preparation methods are used for the preparation of polymer ceramic composites (i) Melt mixing and (ii) Molding, out of which melt mixing is a very suitable method for mixing of thermoplastic polymers and ceramic powder.

2.5.1 Melt Mixing

Melt mixing technique can be employed to make composite if the polymers are thermoplastic with low viscosity during melting and low melting point (< 300 ^{o}C). The melt mixing technique has been used to fabricate composite based on high density polyethylene (HDPE) and polystyrene (PS). A kneading machine was used to fabricate ceramic polymer composites. It consists of variable speed mixer having two counter rotating sigma blades and heating facility up to 300 ^{o}C. Fig. 2.3 shows the photograph of kneading machine and sigma blades. Desired amount of polymer were taken in Kneading machine and slowly the temperature is increased. As the temperature is increased the polymer starts melting and viscous fluid is formed.

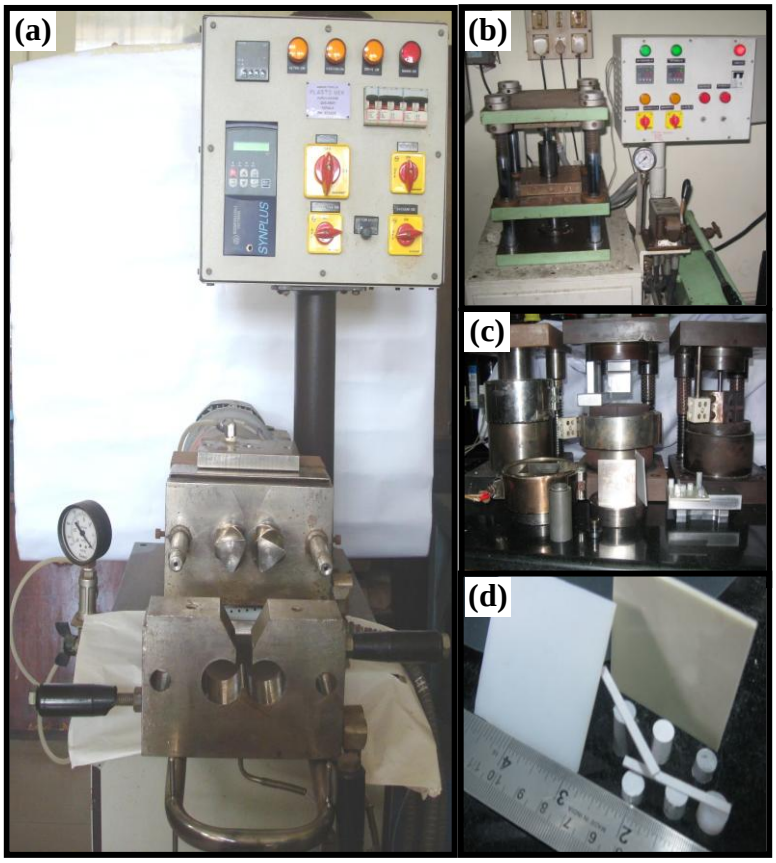

Figure 2.3 Photographs of (a) Kneeding machine, (b) Hot press, (c) Die set used for hot pressing the samples and (d) polymer/ceramic composite samples.

Then the selected amount of ceramic was added in very small amount keeping the temperature constant and rotating the sigma blades. The temperature is about 150 to 165

^{o}C for high density polyethylene (HDPE) and polystyrene (PS). The rotation of the sigma blades causes uniform mixing of polymer and ceramic. Thus obtained composite were hot pressed under a pressure of 50 MPa and 150 ^{o}C for 15 min. The hot press and the die set used for the preparation of the polymer/ceramic composites are shown in Fig. 2.3(b,c).

2.5.2 Molding

Molding technique is used for making polymer composites involving thermosetting polymers like epoxy resin. This has an additional advantage of room temperature processing. The epoxy used in the present study was diglycidyl ether of bisphenol A (DGEBA). The curing agent used was polyamines. The epoxy to hardener ratio is 10:1. The starting materials, epoxy and ceramic powders were mixed separately using an agate and mortar for 45 minutes with an intermediate heat treatment of about 50 ^{o}C. The intermediate heat treatment lowers the viscosity of epoxy and thereby promotes the uniform dispersion of ceramic powders. The hardener was added to the epoxy-ceramic composite and mixed for 10 minutes. The presence of hardener also lowers the viscosity of the epoxy and fills up the gap between the ceramic fillers. The composite was then poured into corresponding die and kept in evacuated dessicator for 5 hours. The composite was then shaped for testing.

2.6 Preparation of multilayer ceramic-The tape casing process

Multilayer ceramic substrates (hard substrates) are developed using a process called “tape casting process”, also known as doctor blade or knife casting. This technique has been used by the paper and plastic industries for many years. This method was introduced for ceramic materials for the first time by Glenn Howatt in 1947 and ever since it has been used to produce multilayer capacitors, ceramic substrates, High Temperature Co-fired Ceramic (HTCC) and Low Temperature Co-fired Ceramic (LTCC) applications and also for piezoelectric applications. The tape casting method is able to produce flexible, self-supporting green ceramic sheets with a wide thickness range (10 µm–1 mm) and it can be arranged as a continuous process, although a small scale laboratory route for cost effective tests is possible. The tapes also have smooth surfaces

suitable for accurate printing to form e.g. conductive patterns (Mistler *et al.*, 2000). The method consists of a slurry preparation and its casting followed by component preparation (Chung, 1995). The basic formula for the tape casting slurry includes the ceramic powder, solvents and organic additives. In the fired product the ceramic material is all that remains and thus the solvents and additives have to be removed in earlier process steps. These ingredients are added only to facilitate the fabrication of the tape with an appropriate thickness and density and to make the tape strong enough for subsequent processing (Imanaka, 2005).

There are many different possible formulations of the solvent/additive system for the tape casting slurry. The role of the solvents is to dissolve the organic additives, provide suitable viscosity for the slurry and also slightly disperse the ceramic powder particles. The solvents should also evaporate at moderate temperatures immediately after the casting process.

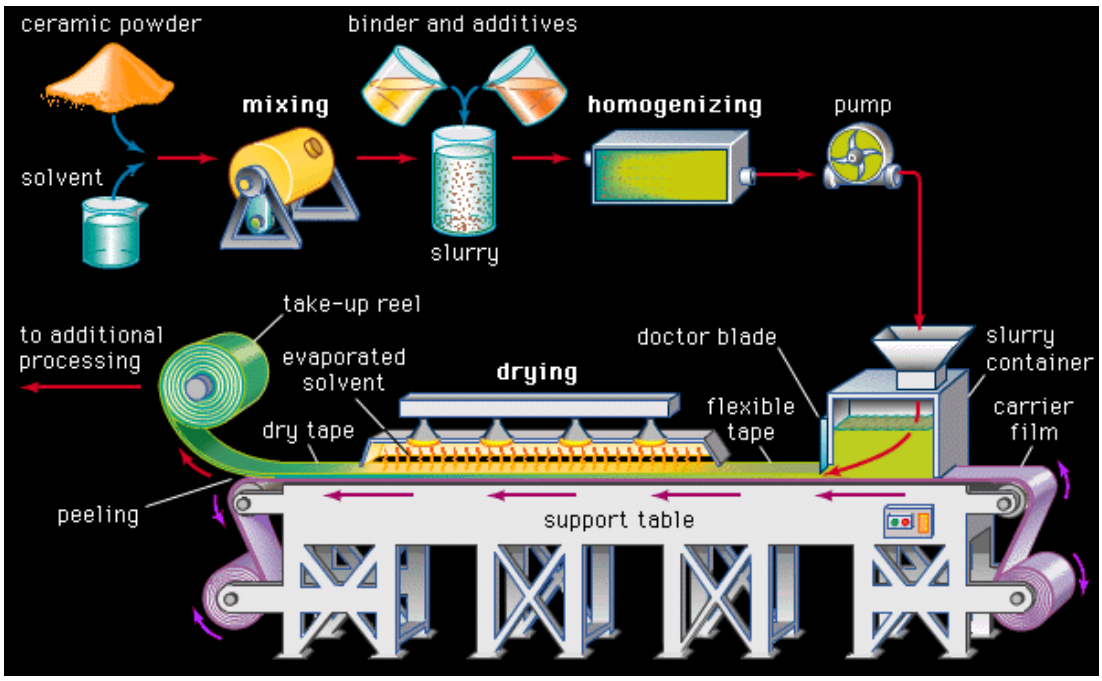

Figure 2.4 The tape casting process (courtesy: Britannica Encyclopedia)

The organic additives consist of dispersant, binder and plasticizer, which are added in consecutive phases as shown in Fig. 2.4. The dispersant provides a stable suspension of the ceramic powder helping to produce a uniform and homogeneous tape.

The binder coats the ceramic powder particles and holds them together and the plasticizer imparts the flexibility necessary for the multilayer component preparation. The amounts of additives and solvents should be kept to a minimum because large excess amounts can cause burnout difficulties, carbon residuals and a low fired density. Typically, the binder system is based on either acrylic or poly(vinyl butyral) (PVB) plastics and non-aqueous solvents. Both these systems have been successfully used to prepare the commercial LTCC tapes and also electroceramic sheets (Mistler *et al.*, 2000). Before slurry preparation the properties of the most important component, the ceramic powder, have also to be measured. This normally includes particle size and distribution as well as specific surface area (SSA) determinations. These characteristics govern how the particles pack together in the green state and determine the formulation of organics and solvents added to the slurry (Mistler *et al.*, 2000). After preparation, the slurry is spread onto a temporary substrate such as glass or carrier film by forcing it to pass through a gap of accurate width, which is the determining factor for the thickness of the tape. In this state the casting speed and the viscosity of the slurry are also important.

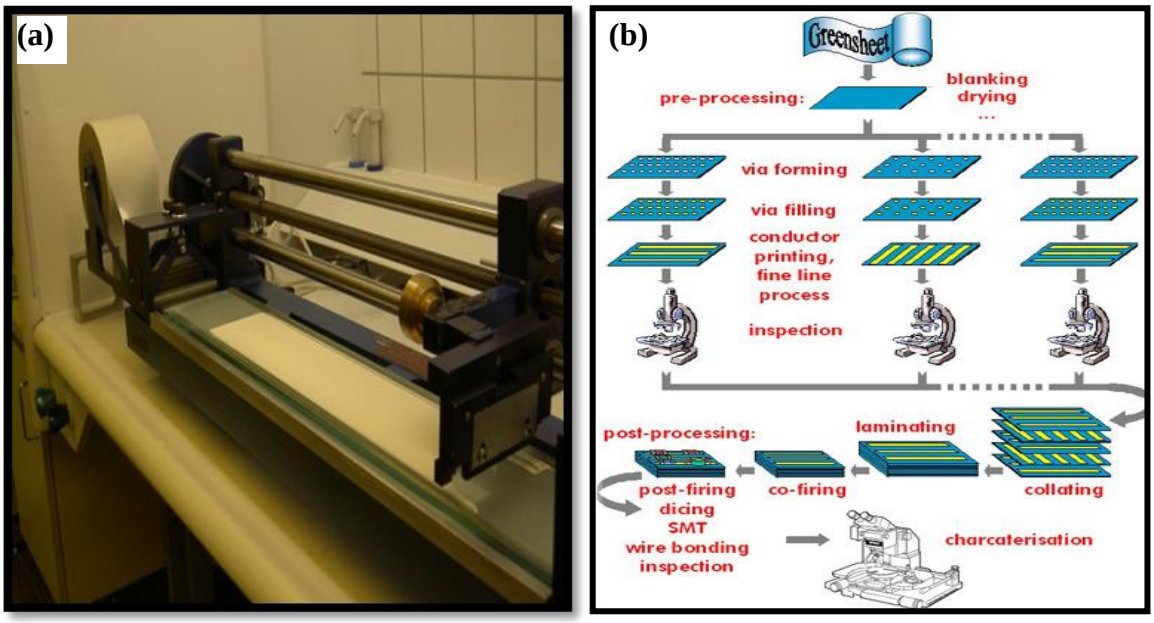

Figure 2.5 (a) A typical tape casting machine (b) Processing of green ceramic tapes to form a multilayer substrate (www.ltcc.de/en/services_man.php).

A typical tape casting machine is shown in Fig. 2.5 (a). After drying the tape in air, it is further processed to form multilayer components as shown in Fig. 2.5 (b). The tape is first blanked to size and required vias are formed using, typically, punching or drilling. After via filling and screen printing of the conductive patterns on each separate layer, they are stacked together, laminated and co-fired. (Imanaka, 2005). The mechanical strength, flexibility, surface smoothness, dimensional stability, sinterability and good binder burnout behavior are requirements which ensure that the tape can be handled, that accurate patterns on its surface can be printed and that the firing state can be carried out to produce a dense and accurately dimensioned product. In an ideal lamination, the boundary between two adjacent tapes should be undetectable after compression. This can only be guaranteed by use of the correct lamination parameters and sufficient slurry formulation and preparation. Because these depend very much on materials and production parameters, they have to be defined empirically from case to case and are therefore often a proprietary secret for commercial materials.

2.7 Structural and microstructural characterization of ceramics

2.7.1 X-ray diffraction

Figure 2.6 A typical XRD machine (courtesy: www.cise.columbia.edu)

The crystal structure of the powdered ceramic specimens in this investigation was first analyzed by X-ray diffraction (XRD) techniques. The X-ray diffraction method is most useful for qualitative, rather than quantitative analysis. An X-ray diffractometer utilizes a powdered sample, a goniometer, and a fixed-position detector to measure the diffraction patterns of unknown samples. The powdered sample provides (theoretically) all possible orientations of the crystal lattice, the goniometer provides a variety of angles of incidence, and the detector measures the intensity of the diffracted beam. The resulting analysis is described graphically as a set of peaks with percentage intensity on the Y-axis and goniometer angle on the X-axis. The exact angle and intensity of a set of peaks is unique to the crystal structure being examined (Bacon, 1966). A monochromator is used to ensure that a specific wavelength reaches the detector, eliminating fluorescent radiation. The resulting trace consists of recording of the intensity against counter angle (2θ). The trace can then be used to identify the phases present in the sample. Diffraction data from many materials have been recorded in a computer searchable Powder Diffraction File (PDF). Comparing the observed data with that in the PDF allows the phases in the sample to be identified (Bish *et al.*, 1989; Cullity *et al.*, 2001). In this investigation XRD spectra were recorded using CuKα radiations (Philips Corp, Almelo, Netherlands)

2.7.2 Scanning electron microscopic methods

The scanning electron microscope (SEM) is critical in all fields that require characterization of solid materials. In the present investigation SEM is used to analyze the microstructure of sintered and thermally etched surface of ceramic samples. SEM generates high-resolution images of shapes of objects. A schematic diagram of SEM is shown in Fig. 2.7.

In this method, an electron beam is produced at the top of the microscope by an electron gun. The electron beam, which typically has an energy ranging from a few hundred eV to 100 keV, is focused by one or two condenser lenses into a beam with a very fine focal spot sized 0.4 nm to 5 nm. The beam passes through pairs of scanning coils or pairs of deflector plates in the electron optical column, typically in the objective lens, which deflect the beam horizontally and vertically so that it scans in a raster fashion

over the sample surface. When the primary electron beam interacts with the sample, the type of signals gathered include secondary electrons, characteristic x-rays, and back scattered electrons. In SEM these signals come not only from the primary beam impinging upon the sample, but from other interactions within the sample near the surface. The SEM is capable of producing high-resolution images of a sample surface in its primary use mode, namely secondary electron imaging (SEI). Due to the manner in which this image is created, SEM images have great depth of field yielding a characteristic three-dimensional appearance useful for understanding the surface structure of a sample. The resolution of SEM can fall somewhere between less than 1 nm and 20 nm. An electrically conductive (usually gold) coating must be applied to electrically insulating samples. In this study we have used a Scanning Electron Microscope of JEOL JSM-5600LV, Tokyo, Japan for the microstructural evolution of ceramic samples prepared.

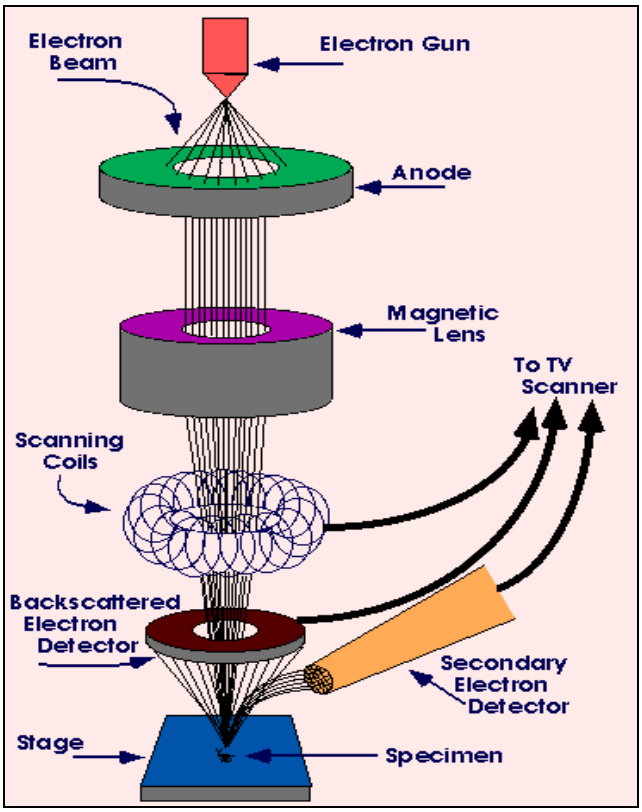

Figure 2.7 Schematic representation of SEM (courtesy: www.purdue.edu)

2.8 Microwave Characterization

2.8.1 Introduction

Microwave materials have been widely used in a variety of applications ranging from communication devices to military satellite services, and the study of materials properties at microwave frequencies and the development of functional materials have always been among the most active area of materials science. In recent years, the increasing demands for the development of high speed, high frequency circuits and systems require complete understanding of the properties of materials functioning at microwave frequencies. All these aspects make the characterization of material properties an important field in microwave electronics. There have been many extensive review papers on the microwave methods for materials property characterization (Afsar *et al.*, 1986; Weil, 1995; Krupka and Weil, 1998). The microwave methods for materials characterization generally fall into non-resonant method and resonant methods (Sebastian, 2008). Non-resonant methods are often used to get a general knowledge of electromagnetic properties over a frequency range while the resonant methods are used to get accurate knowledge of dielectric properties at a single frequency or several discrete frequencies. By modifying the general knowledge of materials properties over a certain frequency range obtained from non-resonant methods along with the accurate knowledge of materials properties at several discrete frequencies obtained from resonant methods, accurate knowledge of materials properties over a frequency range can be obtained.

In non-resonant methods, the properties of materials are fundamentally deduced from their impedance and wave velocities in the material. Non-resonant methods mainly include reflection methods and transmission/reflection methods. In reflection methods, the properties of a sample are obtained from the reflection due to the impedance discontinuity caused by the presence of sample in a transmission structure. In a transmission/reflection method, the material under test is inserted into a segment of transmission line and the properties of the materials are deduced on the basis of the reflection from the material and the transmission through the material.

Resonant methods usually have higher accuracies and sensitivities than non-resonant methods, and are most suitable for low-loss samples. Resonant methods generally include resonator method and resonant-perturbation method. The resonator method is based on the fact that the resonant frequency and quality factor of a dielectric resonator with given dimensions are determined by its permittivity and permeability. This method is usually used to measure low loss dielectrics whose permeability is μ_0. In a resonant perturbation method, the sample is inserted into a resonator, and the properties of the sample are calculated from the changes of the resonant frequency and the quality factor of the resonator caused by the sample. The perturbation methods are highly suitable for materials of small size since the material should not alter the field configuration considerably. These techniques are suitable for relative permittivity less than 10, although this range can be extended by an exact solution of the resonator containing the specimen. Hence this technique is not commonly used for DR characterization. However, this method is suitable for low loss, low permittivity substrate characterization.

2.8.2 Microwave network and scattering parameters

The concept of microwave network is developed from the transmission line theory, and is a powerful tool in microwave engineering. Microwave network method studies the responses of a microwave structure to external signals, and it is a complement to the microwave field theory that analyzes the field distribution inside the microwave structures. In the network approach, we do not care the distributions of electromagnetic fields within a microwave structure, and we are only interested in how the microwave structure responds to external microwave signals. Two sets of physical parameters are often used in network analysis. One set of parameters are voltage and current. The other set of parameters are the input wave (the wave going into the network) and the output wave (the wave coming out of the network). Different network parameters are used for different sets of physical parameters. For e.g., impedance and admittance matrixes are used to describe the relationship between voltage and current, while scattering parameters are used to describe the relationships between the input and output waves.

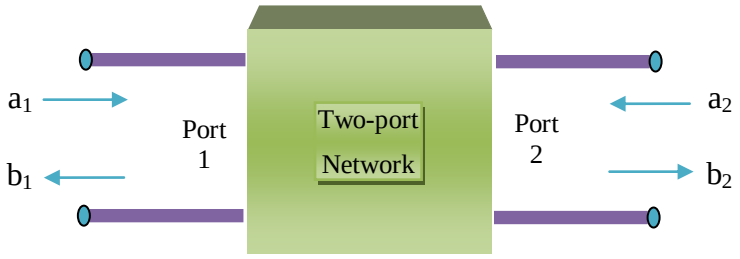

Figure 2.8 A two-port network with "a"s (waves going into the network) and "b"s (waves going out of the network) defined.

As shown in Fig. 2.8, the responses of a network to external circuits can be described by the input and output microwave waves. The input waves at port 1 and port 2 are denoted as a_1 and a_2 respectively, and the output waves from port1 and port 2 are denoted as b_1 and b_2 respectively. These parameters may be voltage or current, and in most cases, we do not distinguish whether they are voltage or current. The relationship between the input wave [a] and output wave [b] are often described by scattering parameters [S]

$$[b] = [S]\,[a] \tag{2.3}$$

where $[a] = [a_1, a_2]^T$, $[b] = [b_1, b_2]^T$, and the scattering matrix [S] is in the form

$$[S] = \begin{bmatrix} S_{11} & S_{12} \\ S_{21} & S_{22} \end{bmatrix} \tag{2.4}$$

For a scattering parameter S_{ij}, if $a_i = 0$ $(i \neq j)$, from equation (2.3), we have

$$S_{jj} = \frac{b_j}{a_j} \quad (j = 1,2) \tag{2.5}$$

$$S_{ij} = \frac{b_i}{a_j} \quad (i \neq j; i = 1,2; j = 1,2) \tag{2.6}$$

Equation (2.5) shows that when port j is connected to a source and the other port is connected to a matching load, the reflection coefficient at port j is equal to S_{jj}:

$$\Gamma_j = S_{jj} = \frac{b_j}{a_j} \tag{2.7}$$

Equation (2.6) shows that when port j is connected to a source, and port i is connected to a matching load, the transmission coefficient from port j to port I is equal to S_{ij}:

$$\Gamma_{j\to i} = S_{ij} = \frac{b_i}{a_j} \tag{2.8}$$

Therefore a knowledge of the scattering parameters S_{ij} (i=1,2 ; j=1,2) provides information about the reflection as well as transmission coefficients at the ports of a network connected to an external circuit and hence are crucial in determining the microwave properties of the material under test (Chen *et al.*, 2004).

2.8.3 Network analyzer

Network Analyzer is the major instrument used in this investigation for the characterization of low loss microwave dielectric ceramics as well as polymer/ceramic composites. It is widely used to measure the four elements in a scattering matrix: S_{11}, S_{12}, S_{21}, and S_{22}. As shown in the Fig. 2.9, a network analyzer mainly consists of a source, signal separation devices, and detectors. A network analyzer can measure the four waves independently: two forward travelling waves a_1 and a_2, and two reverse travelling waves b_1 and b_2. The scattering parameters can thus be obtained by the combinations of these four waves according to equations (2.5) and (2.6). The four detectors, labeled a_1, a_2, b_1 and b_2 are used to measure the four corresponding waves respectively, and the signal separation devices ensure the four waves be measured independently.

Two types of network analyzers are available, scalar and vector network analyzers. Scalar network analyzer measures only the magnitude of reflection and transmission coefficients while the vector network analyzer measures both the magnitude and phase. Both the magnitude and phase behavior of a component can be critical to the performance of a communication system. A vector network analyzer can provide information on a wide range of these devices, from active devices such as amplifiers and

transistors, to passive devices such as capacitors and filters. A more detailed information about network analyzers can be found in (Ballo, 1998). The present work employs both scalar and vector network analyzers.

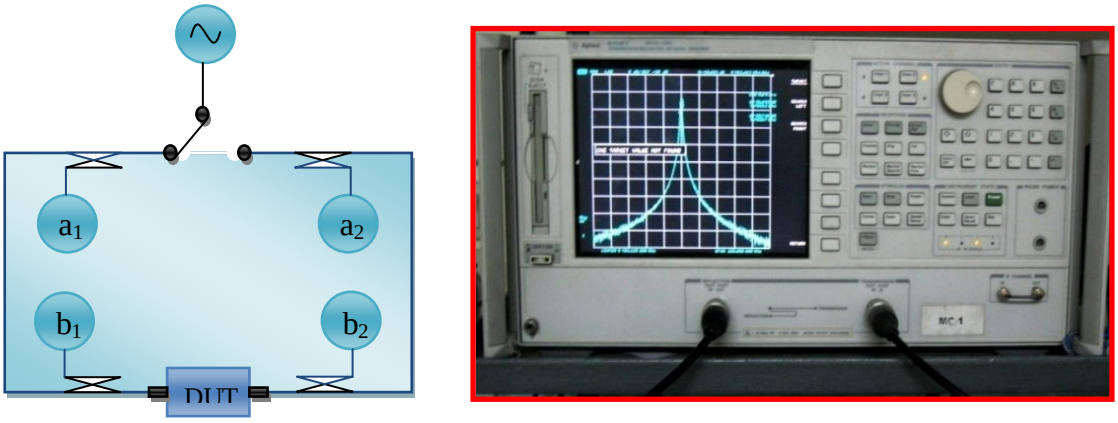

Figure 2.9 (a) The block diagram for a network analyzer (DUT: device under test) (b) HP 8753 ET vector network analyzer.

2.8.4 Measurement of relative permittivity (ε_r)

In this method developed by Hakki and Coleman (Hakki *et al.*, 1960) a circular disc of material whose ε_r to be measured is inserted between two mathematically infinite conducting plates, as shown in Fig. 2.10 (a). If the dielectric material is isotropic then the characteristic equation for this resonant structure operating in the TE_{0ml} mode is written as

$$\alpha \frac{J_0(\alpha)}{J_1(\alpha)} = -\beta \frac{K_0(\beta)}{K_1(\beta)} \tag{2.9}$$

where $J_0(\alpha)$ and $J_1(\alpha)$ are Bessel functions of the first kind of orders zero and one respectively. The $K_0(\beta)$ and $K_1(\beta)$ are the modified Bessel functions of the second kind of order zero and one respectively. The parameters α and β are given by the equations

$$\alpha = \frac{\pi D}{\lambda_o} \left[\varepsilon_r - \left(\frac{l\lambda_o}{2L} \right)^2 \right]^{1/2} \tag{2.10}$$

$$\beta = \frac{\pi D}{\lambda_o}\left[\left(\frac{l\lambda_o}{2L}\right)^2 - 1\right]^{1/2} \tag{2.11}$$

where l = the longitudinal variations of the field along the axis, L = Length of the DR, D = Diameter of the DR, λ_0 = free space resonant wave length.

The characteristic equation (2.9) is a transcendental equation and hence a graphical solution is necessary. Corresponding to each value of β there is infinite number of α_n that solves the characteristic equation. Hakki and Coleman (Hakki *et al.*, 1960; Courtney, 1970) obtained a mode chart showing the variation of α values as a function of β and are shown in Fig. 2.10 (b).

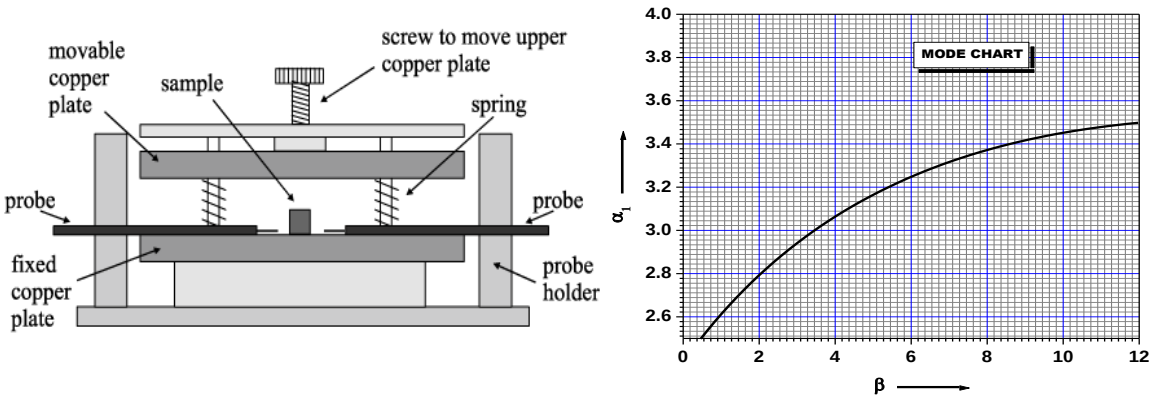

Figure 2.10 (a) Hakki-Coleman method for measuring ε_r by end shorted method (Hakki *et al.*, 1960; Courtney, 1970) (b) Mode chart of Hakki–Coleman giving α_1 as functions of β.

The relative permittivity of the resonator can be calculated using the mode chart parameters (α_1 and β_1), the resonant frequency (f_r) and the dimensions of the dielectric puck using the equation

$$\varepsilon_r = 1 + \left[\frac{c}{\pi D f_r}\right]^2 \left(\alpha_1^2 + \beta_1^2\right) \tag{2.12}$$

The horizontally oriented E-field co-axial probes for coupling microwaves to the DRs, were proposed by Courtney (Courtney, 1970) which enabled to span a wide range of frequencies, since there is no cut-off frequency for coaxial lines. The TE_{011} mode is

used for the measurements since this mode propagates inside the sample but is evanescent outside the geometry of DR. Therefore, a large amount of electrical energy can be stored in the high Q dielectric resonators (Kobayashi *et al.*, 1980). However, in the open space post resonator setup, a part of electrical energy is radiated out as evanescent field and hence the axial mode number is usually expressed as δ since it is less than 1 (i.e. $TE_{01\delta}$). In the end shorted condition the E-field becomes zero close to the metal wall and electric energy vanishes in the air gap (Cohn *et al.*, 1966).

In the experimental setup, a vector network analyzer is used for taking measurements at microwave frequencies. The network analyzer was interfaced with computer for quick and accurate measurement. The specimen is placed approximately symmetrical with two E-probes. The resonant modes are visualized by giving a wide frequency range by adjusting the network analyzer. To select the TE_{011} resonance from the several modes having non-zero E_z components, the upper metal plate is slightly tilted to introduce an air gap. As the plate is tilted the entire TM modes move rapidly to the higher frequencies while the TE_{011} mode remains almost stationary. It is well known that in exact resonance technique, TE_{011} is least perturbed by the surroundings. After identifying the TE_{011} resonant frequency or central frequency (f_r), the span around f_o is reduced as much as possible to get maximum resolution. The 3 dB bandwidth of the curve decreases and a stage of saturation is reached when the width will remain the least possible. The coupling loops are fixed at this position and the centre frequency can be noted corresponding to the maxima as f_o. By knowing the diameter 'D' and length 'L' of the sample β is calculated using equation 2.11. From the mode chart, the value of α_1 corresponding to β_1 value is noted. The permittivity ε_r is calculated using Eqn. 2.12.

2.8.5 Measurement of quality factor

In the present study the Q_u of the DR samples are measured by using a method proposed by Krupka *et al.* (Krupka, Derzakowski, Riddle and Baker-Jarvis, 1998) (See Fig. 2.11). This is a two-port transmission method, and the quality factor is obtained from the scattering parameter S_{21}. In this method, the DR specimen to be characterized is placed inside a cylindrical copper/invar cavity whose inner surface is silver coated to reduce radiation loss. The diameter of the cavity is designed almost four times of the

sample diameter to reduce the effect of cavity shielding. Samples with diameter/length (D/L) ratio of 1.8 - 2.2 are preferable to get maximum mode separation and to avoid interference from other modes. The DR specimen is kept over a quartz spacer placed at the inner bottom surface, which enables to avoid the conduction loss. The cavity is provided with a tunable upper lid. This enables to tune the height of air layer in the metallic cavity and hence to provide more accuracy in the determination of the resonant mode and quality factor.

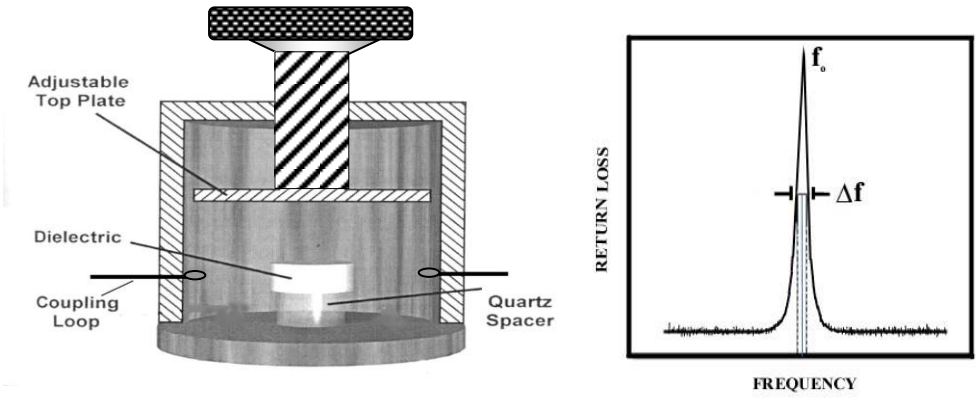

Figure 2.11 (a) The cavity set up for the measurement of Q factor (b) Nature of return loss (S_{21}) Vs frequency graph for calculating the loaded Q factor from resonant mode.

Microwaves are fed into the sample using two loop coaxial antennas which provides a magnetic coupling to excite the transmission mode resonance spectrum of dielectric cylinder. Observe S_{21} (return loss) versus frequency spectrum. In principle the cavity has infinite number of modes, when excited with microwave spectrum of frequencies. $TE_{01\delta}$ mode is identified as the fundamental mode with least perturbation when the tunable top lid is adjusted properly. After identifying the $TE_{01\delta}$ mode, the lid is fine tuned to get maximum separation between $TE_{01\delta}$ and any nearby cavity modes, to attain maximum possible accuracy in the Q_u measurement. Measure $TE_{01\delta}$ mode frequency (f_0) and the 3 dB bandwidth (Δf) from the resonance spectrum shown in Fig. 2.11 (b) to calculate the loaded Q factor as

$$Q_L = \frac{f_o}{\Delta f} \qquad (2.13)$$

By assuming that the two couplings between the cavity and the two transmission lines are weak and equal, the unloaded quality factor (Q_u) can be calculated using the equation (Chen *et al.*, 2004)

$$Q_u = \frac{Q_L}{1-\left|S_{21,f_0}\right|} = \frac{Q_L}{1-10^{S_{21f_0}(dB)/20}} \tag{2.14}$$

where S_{21,f_0} is the S_{21} value at the resonant frequency. Practically the unloaded Q factor will be nearly equal to loaded Q factor for extremely loose coupling (for low loss samples). In the microwave frequency range the dielectric loss increases with frequency and hence there exists an inverse relationship between quality factor and resonant frequency. Hence the quality factor of dielectric resonators is conventionally represented in units of $Q_u \times f$, rather than Q_u.

2.8.6 Measurement of temperature coefficient of resonant frequency (τ_f)

Stability of resonant frequency with temperature is an important property of a DR to operate in microwave devices. τ_f is defined as

$$\tau_f = \frac{1}{f}\frac{\Delta f}{\Delta T} \tag{2.15}$$

The unit of τ_f is parts per million per degree Celsius. In order to measure τ_f, DR is kept in a cavity, same as that used for quality factor measurement. Then the entire set up is heated in the temperature range of 25 to 75 ^oC. The probe of the thermocouple is kept just inside the isothermal enclosure so that it does not disturb the resonant frequency. Shift in the resonant frequency of $TE_{01\delta}$ is noted at every 2 ^oC increment in temperature. The variation of resonant frequency is noted using an interfaced computer and τ_f is calculated.

2.8.7 Split post dielectric resonator (SPDR)

Split post dielectric resonator methods are suitable for the characterization of dielectric sheet samples, including dielectric substrates for planar circuits. The resonator mainly consists of two dielectric discs in a metal enclosure. The dielectric discs are thin

and the height of metal enclosure is relatively small, so the evanescent electromagnetic field character is strong not only in the air-gap region outside the cavity but also in the cavity region for radii greater than the radius of the dielectric resonator. Therefore the electromagnetic fields are also attenuated in the cavity so it is usually not necessary to take then into account in the air gap. This simplifies the numerical analysis and reduces possible radiation. In a split-post dielectric resonator (SPDR) method (Krupka, 2003), the measurement fixture usually has a cylindrical structure working at a TE mode, and the resonator is split into two parts at the electric current node along a plane perpendicular to the cylinder axis. The sample under test is placed in the gap between the two parts of the resonator, usually at the place of maximum electric field. The loading of a dielectric sheet sample changes the resonant properties of a split resonator, and the dielectric properties of the sample can be derived from the resonant properties of the resonator loaded with sample and the dimensions of the resonator and the sample.

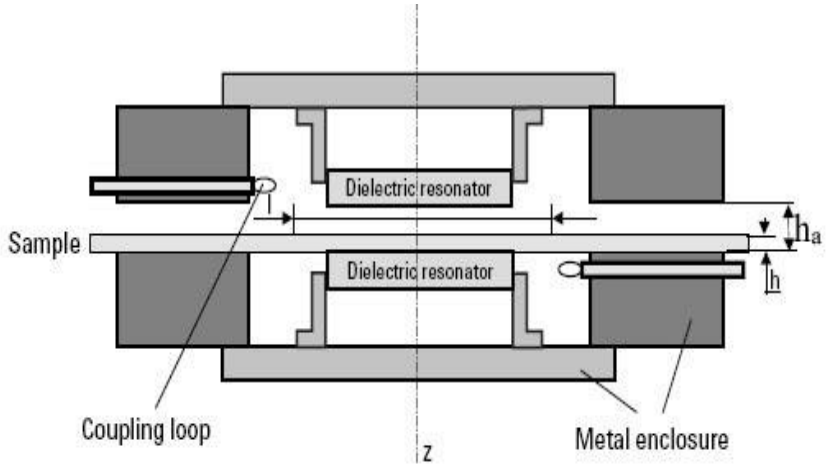

Figure 2.12 Schematic representation of a split post dielectric resonator (Krupka *et al.*, 2001).

The proposed geometry of a split-dielectric resonator fixture for the measurement of the complex permittivity of dielectric sheet samples is shown in Fig. 2.12. Split-post dielectric resonator usually operates with the $TE_{01\delta}$ mode, which has only azimuthal electric field component, so the electric field remains continuous on the dielectric interfaces. The field distributions are affected by the introduction of the sample, which in turn changes the resonant frequency, and the unloaded Q-factor of the sample. The dielectric properties of the sample are derived from the changes of resonant frequency

and unloaded quality factor due to the insertion of the sample. For low-loss materials, the influence of losses on the resonant frequencies is negligible, so the real part of permittivity of the sample under test is related to the resonant frequencies and physical dimensions of the cavity and sample only. In this method, calibration technique is used and we compare the difference of resonant frequency of the split dielectric resonator before and after the sample is inserted. The relative permittivity of the sample is an iterative solution to the following equation (Krupka *et al.*, 2001)

$$\varepsilon_r = 1 + \frac{f_o - f_s}{h f_o K_\varepsilon(\varepsilon_r, h)} \tag{2.16}$$

where h is the thickness of the sample under test, f_o is the resonant frequency of empty resonant fixture, f_s is the resonant frequency of the resonant fixture with dielectric sample, K_ε is a function of ε_r and h and has been evaluated using Rayleigh-Ritz technique (Krupka *et al.*, 2001). The dielectric loss tangent of the sample can be determined by

$$\tan\delta = (Q_u^{-1} - Q_{DR}^{-1} - Q_C^{-1})/\rho_{es} \tag{2.17}$$

In equations (2.16) and (2.17)

$$p_{es} = h\varepsilon_r K_1(\varepsilon_r, h) \tag{2.18}$$

$$Q_c = Q_{c0} K_2(\varepsilon_r, h) \tag{2.19}$$

$$Q_{DR} = Q_{DR0} \cdot \frac{f_o}{f_s} \cdot \frac{p_{eDR0}}{p_{eDR}} \tag{2.20}$$

where p_{es} and p_{eDR} are the electric-energy filling factors for the sample and for the split resonator respectively; p_{eDR0} is the electric-energy filling factor of the dielectric split resonator for empty resonant fixture; Q_{c0} is the quality factor depending on metal enclosure losses for empty resonant fixture; Q_{DR0} is the quality factor depending on dielectric losses in dielectric resonators for empty resonant fixture; and Q_u is the unloaded quality factor of the resonant fixture containing the dielectric sample. The values of p_{eDR}, p_{es} and Q_c for a given resonant structure can be calculated using numerical techniques. The sample should be flat and must be positioned such that it extends beyond the

diameter of two cavity sections. The position of the sample in z-direction is not sensitive to the measurement results. This provides the accuracy of a resonator technique without having to machine the sample. Typical uncertainty of the permittivity measurements of a sample of thickness h can be estimated as $\Delta\varepsilon/\varepsilon = \pm (0.0015+\Delta h/h)$ and uncertainty in loss tangent measurements $\Delta (\tan \delta) = 2\times10^{-5}$.

2.9 Radio frequency dielectric measurements

Figure 2.13 Photograph of Hioki 3532-50 LCR Tester *(taken from: www.testequity.com)*

LCR meters are generally used for measurement of the capacitance conductance, impedance, and dissipation factor of dielectric ceramics in the radio frequency region by the well-known parallel plate capacitor method. The parallel plate capacitor method involves sandwiching a thin sheet of the material between two electrodes to form a capacitor. This is done by uniformly coating silver paste on both sides of cylindrical specimens of diameter ~ 10 mm and thickness ~ 1mm. The capacitance of a parallel-plate capacitor in vacuum is compared with one in the presence of the material for which the dielectric properties are to be measured. Then relative permittivity is calculated using the equation

$$C = \frac{\varepsilon_r \varepsilon_o A}{d} \qquad (2.21)$$

where C is the capacitance of material, ε_r and ε_o are the relative permittivity of material and free space respectively. In the present study, the dielectric properties at radio

frequency were measured using LCR meter (HIOKI 3532-50 LCR Hi TESTER, Japan) (parallel plate capacitor method).

2.10 Thermal characterizations

The determination of reaction during firing can best be accomplished by using techniques that measure chemical and physical changes as the sample being tested. Thermal analysis is defined as a group of methods by which the physical or chemical properties of a substance, a mixture and/or a reactant are measured as a function of temperature or time while the sample is subjected to a controlled heating/cooling.

2.10.1 Thermo gravimetric analysis (TGA)

Thermo gravimetric analysis is a technique in which the weight of a sample is continuously measured as the sample is subjected to a selected firing profile that is usually linear (Pennisi, 1991). In a thermo gravimetric analysis the mass of a sample in a controlled atmosphere is recorded continuously as a function of temperature or time as the temperature of the sample is increased. Thermo gravimetric methods are largely limited to decomposition and oxidation reactions and also to physical processes such as vaporization, sublimation and desorption.

2.10.2 Differential thermal analysis (DTA)

Differential thermal analysis (DTA) (Pennisi, 1991) employs two thermocouples connected differentially so that their electromotive force outputs are in opposition. DTA is a technique in which the difference in temperature between a substance and a reference material is measured as a function of temperature while the substance and reference material are subjected to a controlled temperature program. Information on the inorganic compounds such as dehydration, oxidation, reduction and solid-state reactions is provided by DTA.

2.10.3 Dilatometry

Dilatometry (Pennisi, 1991; Menard, 1999) is the continuous measurement of the length of the sample as the specimen is subjected to a controlled linear heating rate. In

this technique, dimensional changes in a sample are the primarily measured, with negligible force acting on it, while the sample is heated, cooled, or studied at a fixed temperature. The data obtained includes the shrinkage of a composition and more importantly the onset and completion of the sintering cycle. The thermal expansion of the samples, which is an important parameter for electronic packaging application of the dielectric materials, is also studied using the dilatometer. The value of coefficient of thermal expansion is calculated using the relation

$$\alpha_l = \frac{1}{L}\frac{\Delta L}{\Delta T} \qquad (2.22)$$

Where, L is the original dimension of the sample and ΔL is the change in length when the change in temperature is ΔT. In the present study, Dilatometer DIL 402 PC, NETZSCH (Selb, Germany) is employed for both thermal expansion and shrinkage measurements.

Figure 2.14 Photograph of dilatometer DIL 402 PC, NETZSCH (taken from: www.netzsch-thermal-analysis.com)

2.10.4 Thermal conductivity

We used an improved photopyroelectric technique (Marinelli *et al.*, 1990; Menon *et al.*, 2000) to determine the thermal conductivity of the composites. A 70 mW He-Cd laser of wavelength 442 nm, intensity modulated by a mechanical chopper (model

SR540) was used as the optical heating source. A PVDF film of thickness 28 μm, with Ni-Cr Coating on both sides, was used as pyroelectric detector. The output signal was measured using a lock in amplifier (model SR 830). Modulation frequency was kept above 60 Hz to ensure that the detector, the sample and backing medium were thermally thick during measurements. The thermal thickness of the composites was verified by plotting photopyroelectric (PPE) amplitude and phase with frequency at room temperature. Thermal diffusivity (γ) and thermal effusivity (e) were also measured from PPE signal phase and amplitude. (Sebastian *et al.*, 2003) From the values of γ and e, the thermal conductivity of the samples was obtained.

2.11 Mechanical properties

The ultimate tensile strength of the composite samples was measured using Shimadzu, AGS 1000 model Universal Testing machine (UTM). The calibration was done as per the ASTM procedure (D638) at a cross head of 2mm/min at room temperature. The micromechanical properties of the polymer/ceramic composites were measured using microhardness tester (Clemex 4, Germany). Both the surfaces of the samples were polished to have optically flat surface for indentation. The specimen was subjected to a load of 50 g and dwell time of 10 s. For pure ceramic sample, the load was increased to 500 g. A total of five readings were taken to get average hardness.

2.12 Error calculations in dielectric property measurements

The measurement of microwave dielectric properties was done with two decimal point accuracy. Usually three samples were prepared in a batch corresponding to a particular composition and the measurements were made at least twice per each specimen. The error in ε_r is calculated using the root sum of squares (RSS) method. The accuracy of ε_r measurement is restricted to the accuracy in measurement of resonant frequency and dimensions of the sample. Hence the possible errors in the measured value of permittivity of a sample of height (L), radius (r) and resonant frequency (f_r) given by

$$\Delta\varepsilon_r = \left[\left(\frac{\partial\varepsilon_r}{\partial L}\ \Delta L\right)^2 + \left(\frac{\partial\varepsilon_r}{\partial r}\ \Delta r\right)^2 + \left(\frac{\partial\varepsilon_r}{\partial f_r}\ \Delta f_r\right)^2\right]^{1/2} \qquad (2.23)$$

If the independent sources of error corresponds to one standard deviation, then the error in ε_r will also corresponds to one standard deviation (Jarvis *et al.*, 1998). The errors in unloaded quality factor (Q_u) and temperature coefficient of resonant frequency (τ_f) were calculated using RSS method by taking partial derivative of these parameters with respect to independent variables. The low frequency relative permittivity was measured using LCR meter. The error in the measurement of relative permittivity depends on the error in the evaluation of sample dimensions. Since a digital vernier is used for the determination of the dimensions, the maximum error in the measurement is only 0.01mm. Hence the maximum error in the relative permittivity is less than 2%.

2.13 Calculation of relative density of composites

The relative density of the specimen was measured by the Archimedes method. The theoretical density (D) of the composite can be calculated using the equation (Takada *et al.*, 1994)

$$D = \frac{W_1 + W_2}{W_1/D_1 + W_2/D_2} \tag{2.24}$$

where W_1 and W_2 are the weight percentage of the two phases with densities D_1 and D_2 respectively.

Chapter 3

Microwave Dielectric Properties of Some Silicates

3.1 Introduction

Microwave dielectric ceramics have been widely used in various wireless communication systems such as resonators, filters, antennae, and substrates (Sebastian, 2008). These applications particularly depend on the relative permittivity (ε_r) of the microwave dielectric ceramics. For example, materials having $\varepsilon_r > 80$ can aid miniaturization of mobile phone handsets, while those having $\varepsilon_r = 25\text{-}50$ and high quality factor values ($Q_u \times f$) are suitable for increasing signal/noise ratio for the main application in mobile phone base stations. Dielectric ceramics with $\varepsilon_r < 20$ and high $Q_u \times f > 100000$ GHz are desirable for high frequency applications like microwave and millimeter wave communication. Recent developments of the microwave technologies, such as wireless LAN, intelligent transport system, and microwave integrated circuits, has led to an increase of researches on microwave and millimeter-wave dielectric materials (Ohsato, Tsunooka, Kan, Ohishi, Miyauchi, Tohdo, Okawa, *et al.*, 2004). Particularly, the investigations on the materials useful for millimeter-wave communication have been increasing because of the large amount of information that can be transmitted at high speed in this frequency region (Cava, 2001; Fuji *et al.*, 2006). The utilizable region for frequency has been expanding to the millimeter-wave region because of the shortage of radio frequency (RF) resources. Millimeter wave communication has the advantages of improved resolution and directivity that can be obtained for a given antenna aperture. It can provide wider bandwidth, high level of frequency re-use and un-licensed wide-open spectrum and can also be used for the remote sensing of atmospheric gases in earth and planetary atmosphere and identification of potential threat materials in security applications(Vizard, 2006).

For the millimeter-wave communication applications, low relative permittivity (ε_r) materials are essential to increase the signal propagation velocity, to reduce the transmission attenuation and also reduce the cross coupling effect with a conductor. The resonant frequency decreases with increase in ε_r as well as with the increase in dimensions of the resonant structure. Hence for millimeter wave communication applications ε_r should be in the range 6-20. This helps to achieve a resonator of reasonable size for ease of fabrication as well as handling. Low dielectric loss (tan δ) is

another critical requirement of materials useful for millimeter wave communication systems. Usually, in the high frequency region, the dielectric losses increase. Thus the development of microwave dielectric with very high quality factor ($Q = 1/\tan \delta$) is necessary. Quality factor is a system property related to the efficiency of use of power supplied to the device. A high value of quality factor can also ensure excellent frequency selectivity. A near-zero temperature coefficient of resonant frequency (τ_f) is also important because it can offer the stability of the frequency against temperature. Usually a value of τ_f in the range -10 to +10 ppm/^oC is preferred to account for the subtle differences in the circuit design, construction and packaging of the similar components produced by different manufacturers. These stringent requirements limit the number of dielectric materials available for millimeter wave applications.

In the case of low relative permittivity materials, silicates have received much attention because of the covalent nature of Si-O bond in the SiO_4 tetrahedron. In 1980 Linus Pauling reported that 50% of the Si-O bond in SiO_4 tetrahedron is of covalent nature. The report was based on the electronegativity difference between Si and O (Pauling, 1980). The covalent nature of Si-O bond ensures low values of relative permittivity as well as dielectric loss. Microwave dielectric properties of many of the silicates are reported earlier (Sebastian, 2008). Tsunooka et al. reported the effects of TiO_2 on the sinterability and dielectric properties of high-Q forsterite ceramics (Tsunooka *et al.*, 2003). High $Q_u \times f \sim 230000$ GHz and low $\varepsilon_r \sim 7$ were obtained for a composition containing forsterite and 1 wt% of TiO_2. The composition containing 24 wt% TiO_2 has $Q_u \times f = 82000$ GHz, $\varepsilon_r = 11$ and $\tau_f = 0$ ppm/^oC (Ohsato *et al.*, 2006). The effect of calcination and sintering durations and the effect of Mn^{2+} substitution at Mg-site on the microwave dielectric properties of forsterite have also been reported (Sugiyama *et al.*, 2006; Ando *et al.*, 2007). Willemite is another silicate which has a low ε_r value of 6.6 and a high $Q_u \times f$ value upto 219000 GHz (Guo *et al.*, 2006; Dong *et al.*, 2008). The dielectric properties of several other silicates such as $MgSiO_3$, $CaSiO_3$, $CaMgSi_2O_6$, $CaAl_2Si_2O_8$, $NaAlSi_3O_8$, $Mg_2Al_4Si_5O_{18}$, $Ca_3(Zr_{1-x}Sn_x)Si_2O_9$, $Ba_2(Mg_{1-x}Zn_x)Si_2O_7$, $Sr_xBa_{1-x}Al_2Si_2O_8$, $Ca_xBa_{1-x}Al_2Si_2O_8$, $Sm_2Si_2O_7$, Li_2MgSiO_4etc were also investigated (Krzmanc, 2005;

Krzmanc *et al.*, 2007; Sun *et al.*, 2007; Terada *et al.*, 2007; Yokoi *et al.*, 2007; Song *et al.*, 2008; Wang *et al.*, 2008; George, Anjana, *et al.*, 2009; Renjini *et al.*, 2009).

3.2 Silicate basics

3.2.1 Silicate minerals

The silicate minerals form a group of inorganic compounds of great chemical, as well as structural complexity. The relative abundance of elements in the earth's crust determines what minerals will form and what minerals will be common. The earth crust consists of 27% Silicon and 45.6% Oxygen. The other main elements include 8% Aluminium, 6% Iron, 5% Calcium, 3% Magnesium, 2% Sodium and 2% Potassium. The main component of the crust is therefore SiO_x, with some elements substituting for Silicon and counter ions. Because Oxygen and Silicon are the most abundant elements, the silicate minerals are the most common.

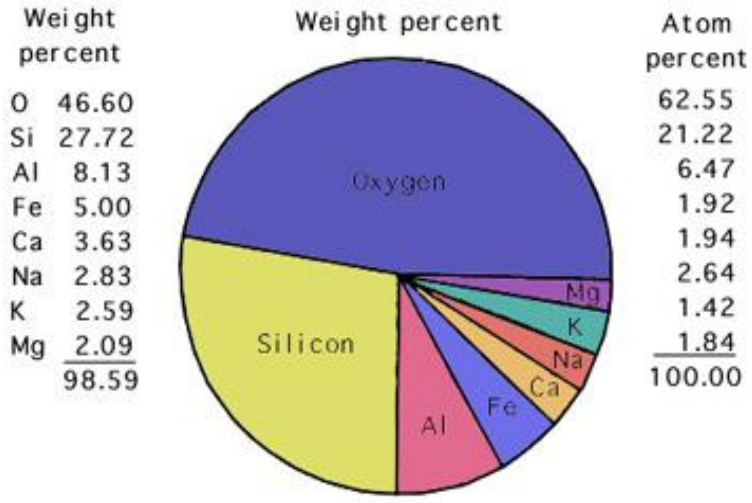

Figure 3.1 The eight most common elements in the earth's crust (Mason *et al.*, 1982).

3.2.2 Structure of silicates

In order to discuss the silicates and their structures it is first necessary to understand that the way atoms are packed together or coordinated by larger anions, like oxygen depends on the radius ratio of the cation to the anion, R_c/R_a. Table 3.1 gives the

coordination number (CN) for various range of values of R_c/R_a. The packing schemes for each coordination number are also indicated in the table.

Table 3.1 Coordination number (CN) and packing schemes based on cation to anion radius ratio.

R_c/R_a	CN	Type
1.0	12	Hexagonal or Cubic Closest Packing
1.0 - 0.732	8	Cubic
0.732 - 0.414	6	Octahedral
0.414 - 0.225	4	Tetrahedral
0.225 - 0.155	3	Triangular
<0.155	2	Linear

Since oxygen is the most abundant element in the crust, it will be the major anion that coordinates the other cations. The radius ratio of Si^{+4} to O^{-2} is 0.26, which requires that Si^{+4} be coordinated by four O^{-2} ions in tetrahedral coordination. In order to neutralize the +4 charge on the Si cation, one negative charge from each of the Oxygen ions will reach the Si cation. Thus, each Oxygen will be left with a net charge of -1, resulting in a SiO_4^{-4} tetrahedral group that can be bonded to other cations. It is this SiO_4^{-4} tetrahedron that forms the basis of the silicate minerals. Since Si^{+4} is a highly charged cation, Pauling's rules state that it should be separated as far as possible from other Si^{+4} ions. Thus, when these SiO_4^{-4} tetrahedrons are linked together, only corner oxygen will be shared with other SiO_4^{-4} groups. Several possibilities exist and give rise to the different silicate groups.

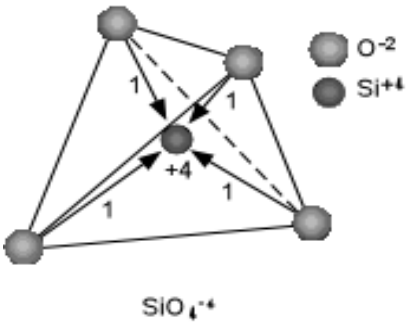

Figure 3.2 The SiO_4 tetrahedra: the building block of silicates (courtesy: www.tulane.edu).

3.2.3 Classification of silicates

The one common component of all silicates is the tetrahedral SiO_4^{-4} structural subunit. The basic tetrahedral grouping of four oxygens about each Si provides the strongest, most stable bonds within the silicate species. This very stable configuration is compatible with both the radius ratio rule and the strong covalent $3sp^3$ bonding. Silica tetrahedral units SiO_4^{-4} may occur within silicate structures as independent units or they may polymerize in varying degree through the sharing of common Oxygens. When SiO_4^{-4} tetrahedra polymerize, it is always through common sharing of Oxygens, never by sharing of edges or faces of the tetrahedra. The whole silicate family can be classified into six distinct groups as shown in Fig. 3.3 based on the manner in which SiO_4^{-4} tetrahedral units associate.

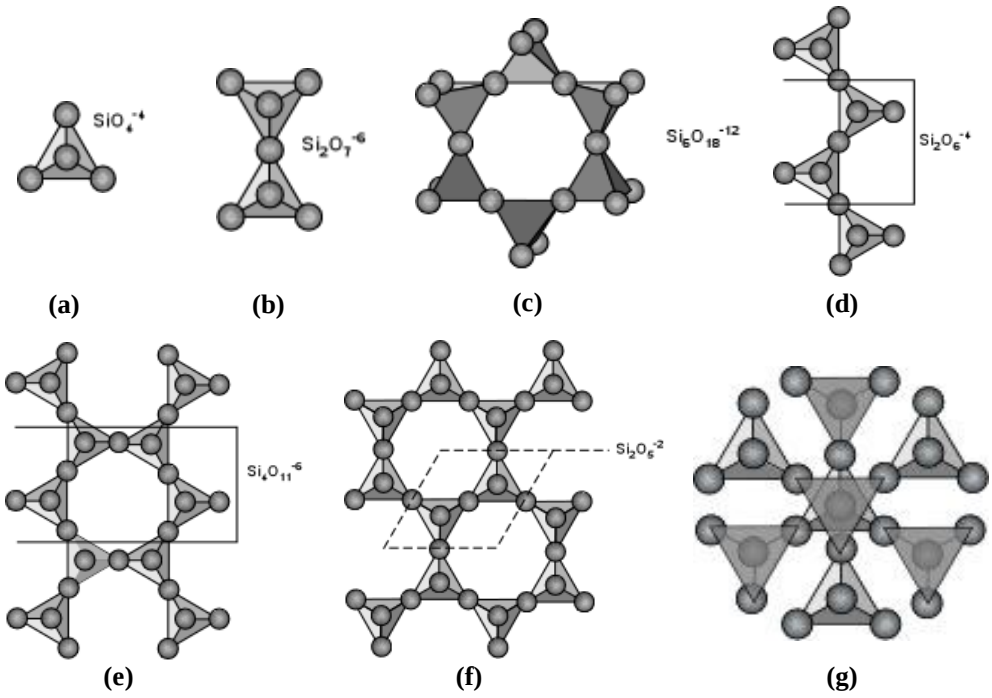

Figure 3.3 Classification of silicates based on different combination of SiO_4 tetrahedra (courtesy: www.tulane.edu).

(a) Nesosilicates (Island Silicates)

If the corner Oxygens are not shared with other SiO_4^{-4} tetrahedrons, each tetrahedron will be isolated. Thus, this group is often referred to as the island silicate

group. The basic structural unit is then SiO_4^{-4}. In this group the oxygens are shared with octahedral groups that contain other cations like Mg^{+2}, Fe^{+2}, or Ca^{+2}. E.g. Olivine, $(Mg,Fe)_2SiO_4$.

(b) Sorosilicates (Double Island Silicates)

If one of the corner Oxygens is shared with another tetrahedron, this gives rise to the sorosilicate group. It is often referred to as the double island group because there are two linked tetrahedrons isolated from all other tetrahedrons. In this case, the basic structural unit is $Si_2O_7^{-6}$. A good example of a sorosilicate is the mineral hemimorphite- $Zn_4Si_2O_7(OH)\cdot H_2O$. Some sorosilicates are a combination of single and double islands, like in epidote, $Ca_2(Fe^{+3},Al)Al_2(SiO_4)(Si_2O_7)$-(OH)

(c) Cyclosilicates (Ring Silicates)

If two of the Oxygens are shared and the structure is arranged in a ring, such as that shown in Fig. 3.3 (c), we get the basic structural unit of the cyclosilcates or ring silicates. Shown in Fig. 3.3 (c) is a six membered ring forming the structural group $Si_6O_{18}^{-12}$. Three membered rings, $Si_3O_9^{-6}$, four membered rings, $Si_4O_{12}^{-8}$, and five membered rings $Si_5O_{15}^{-10}$ are also possible. A good example of a cyclosilicate is the mineral Beryl, $Be_3Al_2Si_6O_{18}$.

(d) Inosilicates (Single Chain Silicates)

If two of the Oxygens are shared in a way to make long single chains of linked SiO_4 tetrahedra, we get the single chain silicates or inosilicates. In this case the basic structural unit is $Si_2O_6^{-4}$ or SiO_3^{-2}. This group is the basis for the pyroxene group of minerals, like the orthopyroxenes $(Mg,Fe)SiO_3$ or the clinopyroxenes $Ca(Mg,Fe)Si_2O_6$.

(e) Inosilicates (Double Chain Silicates)

If two chains are linked together so that each tetrahedral group shares three of its Oxygens, we can form double chains, with the basic structural group being $Si_4O_{11}^{-6}$. The amphibole group of minerals are double chain silicates, for e.g. the tremolite-ferroactinolite series, $Ca_2(Mg,Fe)_5Si_8O_{22}(OH)_2$.

(f) Phyllosilicates (Sheet Silicates)

If three of the oxygens from each tetrahedral group are shared such that an infinite sheet of SiO_4 tetrahedra are shared we get the basis for the phyllosilicates or sheet silicates. In this case the basic structural group is $Si_2O_5^{-2}$. The micas, clay minerals, chlorite, talc, and serpentine minerals are all based on this structure. In this structure, Al can be substituted for Si in one of the tetrahedral groups. A good example is biotite, $K(Mg,Fe)_3(AlSi_3)O_{10}(OH)_2$.

(g) Tectosilicates (Framework Silicates)

If all of the corner Oxygens are shared with another SiO_4 tetrahedron, then a framework structure develops. The basic structural group then becomes SiO_2. The minerals quartz, cristobalite, and tridymite are all based on this structure. If some of the Si^{+4} ions are replaced by Al^{+3} then this produces a charge imbalance and allows for other ions to be found coordinated in different arrangements within the framework structure. Thus, the feldspar and feldspathoid minerals are also based on the tectosilicate framework.

3.3 Microwave dielectric properties of $(Sr_{1-x}A_x)_2(Zn_{1-x}B_x)Si_2O_7$ ceramics (A = Ca, Ba and B = Co, Mg, Mn, Ni)

3.3.1 Introduction

In recent years, there are several reports based on mixed alkaline earth and transition metal disilicates, which have akermanite-type and melilite-type crystal structures. They are represented as $A_2BSi_2O_7$, where A is an alkaline earth and B is a transition metal. In this case, the basic structural unit is $Si_2O_7^{-6}$ and hence they belong to the class of sorosilicates. The most common crystal structure is the tetragonal akermanite-type with space group $P\bar{4}2_1m$ (no. 113), while a few others have monoclinic crystal structure with space group C2/c (no. 15) (Kimata, 1982; Adams *et al.*, 1996; Tovar *et al.*, 1998; Kusaka *et al.*, 2001; Kaiser *et al.*, 2002). However, there are only a few studies related to their microwave dielectric properties (Yokoi *et al.*, 2007). In contrast, far more attention was paid to the synthesis, structural modifications and

photoluminescence studies of these materials (Kimata, 1982; Adams *et al.*, 1996; Tovar *et al.*, 1998; Lin *et al.*, 1999; Kusaka *et al.*, 2001; Kaiser *et al.*, 2002; Bali *et al.*, 2003; Aitasalo *et al.*, 2006; Ochi, 2006; Hao *et al.*, 2007; Yokoi *et al.*, 2007). The tetragonal crystal structure of $A_2BSi_2O_7$ was first reported by Kimata where A = Ca and B = Co (Kimata, 1982). The $Ca_2MgSi_2O_7$, $Ca_2ZnSi_2O_7$, $Sr_2MgSi_2O_7$, $Sr_2ZnSi_2O_7$ etc., which belong to the $A_2BSi_2O_7$ series have a tetragonal crystal structure (Kusaka *et al.*, 2001; Ochi, 2006; Hao *et al.*, 2007). Some of the silicates in the $A_2BSi_2O_7$ series like $Ba_2CoSi_2O_7$, $Ba_2ZnSi_2O_7$, $Ba_2CuSi_2O_7$ and $Ba_2MgSi_2O_7$ crystallize in the monoclinic structure (Adams *et al.*, 1996; Kaiser *et al.*, 2002; Yokoi *et al.*, 2007). There are also reports that $Ba_2CoSi_2O_7$ crystallizes in both tetragonal and monoclinic structure (Adams *et al.*, 1996; Lin *et al.*, 1999). The crystal structure of the tetragonal form of $A_2BSi_2O_7$ is shown in Fig. 3.4. It contains discrete $Si_2O_7^{6-}$ units formed by two corner sharing SiO_4 tetrahedra. The B atoms lie in the tetrahedra formed by oxygen atoms while that of A^{2+}cations have eight-fold oxygen coordination (Hao *et al.*, 2007). In the present work, the dielectric properties of $A_2BSi_2O_7$ ceramics are described, where A = Ca, Ba, Sr and B = Co, Mg, Mn, Ni, Zn.

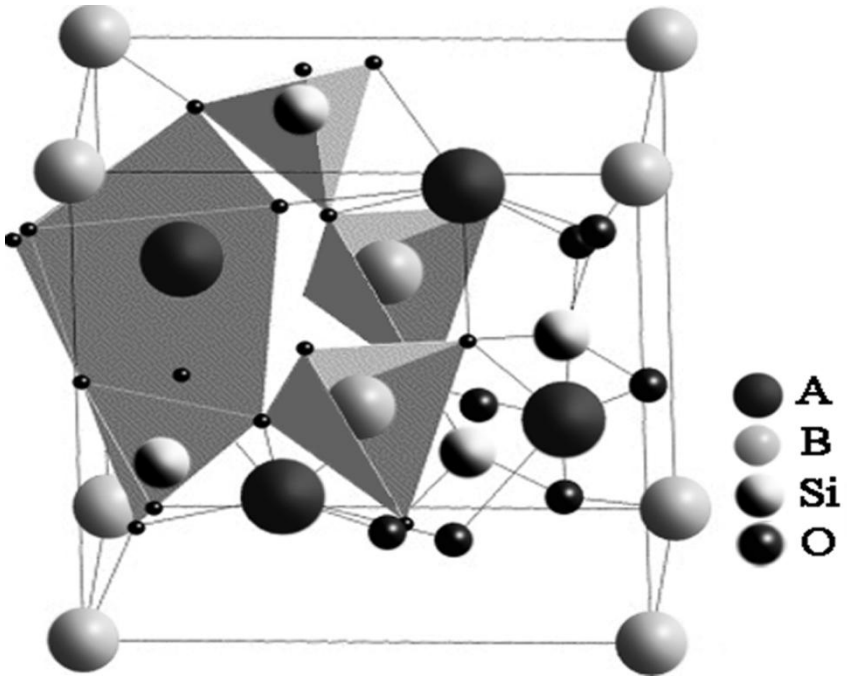

Figure 3.4 The crystal structure of the tetragonal form of $A_2BSi_2O_7$ (Hao *et al.*, 2007).

3.3.2 Experimental

The $A_2BSi_2O_7$ (A = Ca, Sr, Ba and B=Mg, Mn, Co, Ni, Zn) ceramics were prepared by the conventional solid-state ceramic route using powders of $CaCO_3$ (99+%), $SrCO_3$ (99.9%+), $BaCO_3$ (99%+), ZnO (99.9%), Co_3O_4 (99%+), $MnCO_3$ (99.9%+), $(MgCO_3)_4Mg(OH)_2.5H_2O$ (99%), NiO (99%), SiO_2 (99.6%) (all Aldrich Chemical Company Inc., Milwaukee). The stoichiometrically weighed raw materials were mixed by ball milling using zirconia balls in distilled water for 24 hours. The yielded powder mixtures were heated in the temperature range 1100-1250 ^oC/4h depending on the composition. The calcined powders were mixed with 4 wt% of PVA (molecular weight 22000, BDH Lab Suppliers, England), and were pressed into disks of 11 mm in diameter and 5-6 mm height under a uniaxial stress of about 100 MPa. The green compacts were initially fired at a rate of 3 ^oC/min up to 600 ^oC and then at a rate of 8 ^oC/min up to the sintering temperature. The sintering temperature was chosen to get highest density for all compositions. $SrTiO_3$ prepared by the same procedure using $SrCO_3$ and TiO_2 (Aldrich - 99.8%) was used to tune the value of τ_f.

The crystalline phases of the sintered samples after crushing and grinding were determined by powder X-ray diffraction technique (Philips Corp, Almelo, Netherlands) using CuKα radiation. The bulk densities of sintered samples were measured by the Archimedes method. The theoretical density, D of the mixture $A_2BSi_2O_7/SrTiO_3$ was calculated using the equation (2.24). SEM microstructure was recorded from the surface of thermally etched samples (JEOL JSM-5600LV, Tokyo, Japan). The thermal etching was done by heating the polished sample about 50 ^oC less than the sintering temperature. For low frequency (1 MHz) dielectric measurements, cylindrical specimens were electroded by uniformly coating silver paste on both sides and measurements done using an LCR meter as described in chapter 2. The microwave dielectric properties were measured in the frequency range 10-18 GHz using $TE_{01\delta}$ mode with a vector network analyzer (Agilent, Model No: E8362B, USA) were measured using the techniques explained in section 2.7. The measured values of relative permittivity were corrected for porosity using the equation (1.13).

3.3.3 Results and Discussion

(i) Phase Analysis

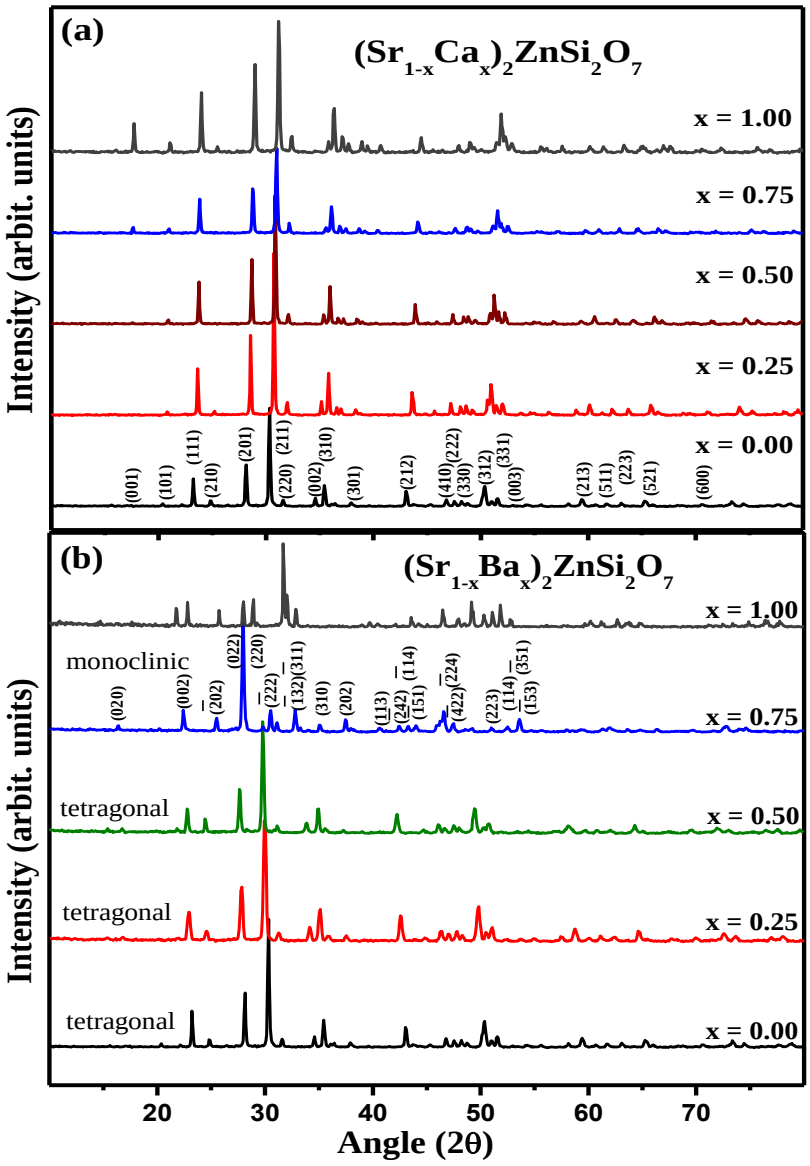

Figure 3.5 The XRD patterns of (a) $(Sr_{1-x}Ca_x)_2ZnSi_2O_7$ and (b) $(Sr_{1-x}Ba_x)_2ZnSi_2O_7$ ceramics for values of x = 0, 0.25, 0.5, 0.75, 1.

In the present study, $Sr_2ZnSi_2O_7$ is taken as the starting material and partial substitutions were made at the Sr and Zn-site to study the effect on the structure and dielectric properties. The sintering temperatures of all the compositions are optimized for

the highest density. Fig. 3.5 shows the XRD patterns of $(Sr_{1-x}A_x)_2ZnSi_2O_7$ (A = Ca, Ba) ceramics sintered at the optimized temperatures for values of x in the range 0 to 1. Fig. 3.5 (a) represents the diffraction patterns of $(Sr_{1-x}Ca_x)_2ZnSi_2O_7$ for values of x = 0, 0.25, 0.5, 0.75 and 1. The patterns obtained can be indexed according to the ICDD file card no: 39-0235 for $Sr_2ZnSi_2O_7$ (x = 0) having akermanite-type structure (tetragonal) with the space group $P\bar{4}2_1m$ (no. 113). It is apparent that all the compositions form a solid solution. As a consequence of substitution, the peaks shift to higher angles as the amount of Ca^{2+} increases. This is expected since the ionic radius of Ca^{2+} ion is 1.12 Å, which is smaller than that of Sr^{2+} ions (1.26 Å) in eight fold coordination (Shannon, 1976).

Fig. 3.5 (b) shows the XRD patterns for $(Sr_{1-x}Ba_x)_2ZnSi_2O_7$ in the range $0 \leq x \leq 1$. Solid solutions are formed for $0 \leq x \leq 0.50$ with the tetragonal structure similar to that of $Sr_2ZnSi_2O_7$. This is also supported by the observed shift of the diffraction peaks towards lower angles in the range $0 \leq x \leq 0.50$. This shift in the diffraction peaks is due to the substitution of larger Ba^{2+} ions (1.42 Å for coordination number 8) for Sr^{2+} ions. When x = 0.75, a structural change is observed from tetragonal to monoclinic. The XRD pattern for x = 0.75 is indexed according to the ICDD file card no: 86-0769 for $Ba_2CoSi_2O_7$ having a monoclinic structure with space group C2/c (no.15). Hence the structure of the composition $(Ba_{0.75}Sr_{0.25})_2ZnSi_2O_7$ is suggested as similar to that of the monoclinic $Ba_2CoSi_2O_7$. An entirely different XRD pattern with unidentified peaks is obtained for the composition x = 1 which cannot be accounted for either tetragonal or monoclinic structure.

The effect of B-site substitution on the crystal structure of $Sr_2(Zn_{1-x}B_x)Si_2O_7$ (B = Co, Mg, Mn and Ni) is shown in Fig. 3.6 (a-d). The B-site cations lie in the tetrahedra formed by oxygen atoms and have a coordination number of 4. Fig. 3.6 (a) depicts the diffraction patterns of $Sr_2(Zn_{1-x}Co_x)Si_2O_7$ for $0 \leq x \leq 1$. Solid solutions are formed in the entire composition range of x, with the tetragonal symmetry similar to that of $Sr_2ZnSi_2O_7$. The diffraction patterns do not show any observable shift with the increase in Co^{2+} content. This is well understood since the ionic radius of Co^{2+} (0.58 Å for coordination number 4) is close to that of Zn^{2+} ion (0.60 Å for coordination number 4). Fig. 3.6 (b,c) show the XRD patterns of compositions $Sr_2(Zn_{1-x}Mg_x)Si_2O_7$ and $Sr_2(Zn_{1-x}Mn_x)Si_2O_7$ in

the range $0 \leq x \leq 1$. Solid solutions with tetragonal crystal symmetry are formed in the whole composition range of x for the substitutions of both Mg and Mn ions at the Zn-site.

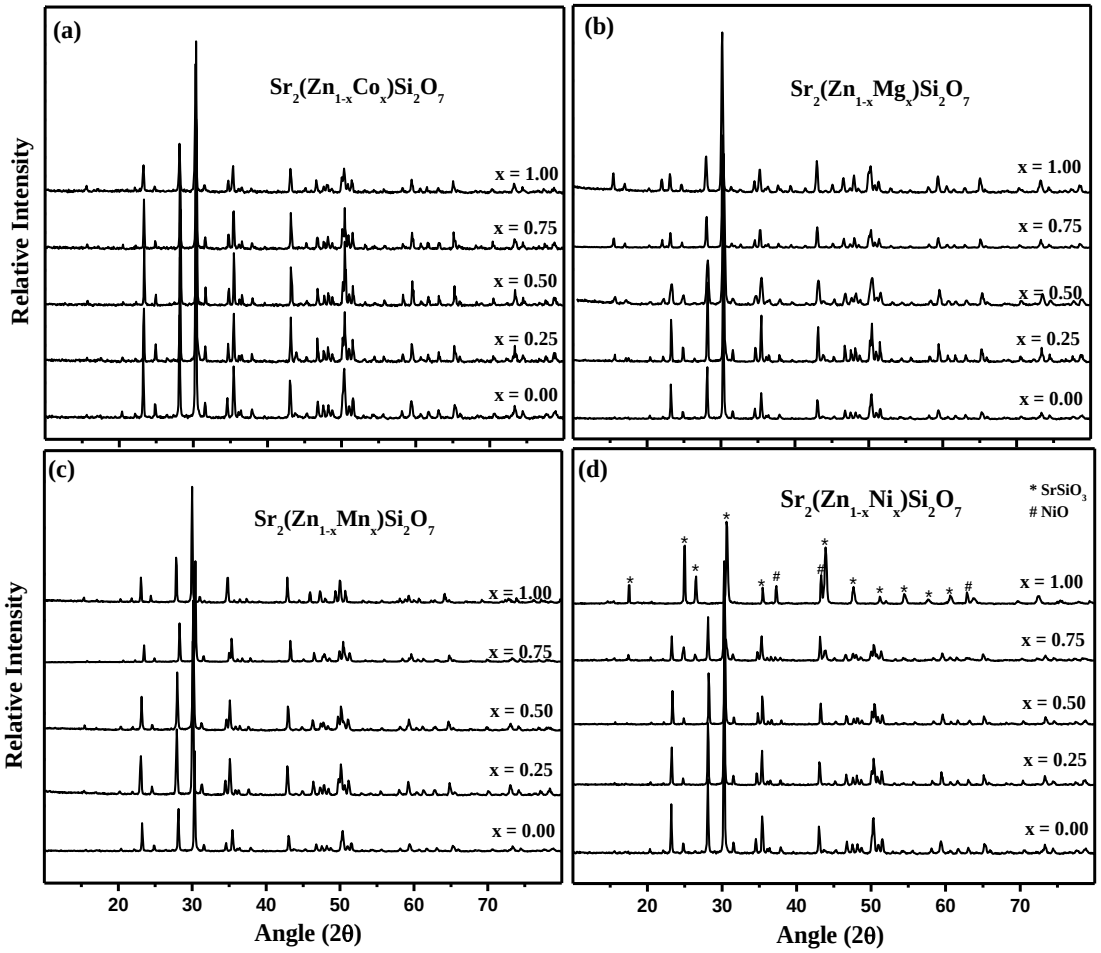

Figure 3.6 The XRD patterns of (a) $Sr_2(Zn_{1-x}Co_x)Si_2O_7$ (b) $Sr_2(Zn_{1-x}Mg_x)Si_2O_7$ (c) $Sr_2(Zn_{1-x}Mn_x)Si_2O_7$ (d) $Sr_2(Zn_{1-x}Ni_x)Si_2O_7$ ceramics for values of x = 0, 0.25, 0.5, 0.75, 1.

The diffraction peaks do not show any marginal shift with the increase in Mg^{2+} ion content, whereas a small shift towards smaller angles can be found in the case of Mg^{2+}ions. This is due to the fact that Mg^{2+} and Mn^{2+} have ionic radii 0.57 Å and 0.66 Å respectively for coordination number 4. When Zn is replaced by Ni, solid solutions of $Sr_2(Zn_{1-x}Ni_x)Si_2O_7$ are obtained in the range $0 \leq x \leq 0.50$ with tetragonal symmetry as shown in Fig. 3.6 (d). A small shift of the diffraction peaks towards higher 2θ values is observed and is attributed to the substitution of smaller Ni^{2+} ions (0.55 Å for coordination

number 4) at the Zn-site (Shannon, 1976). However, for x > 0.50, a mixture of $SrSiO_3$ and NiO is obtained indicating the absence of the formation of a solid solution.

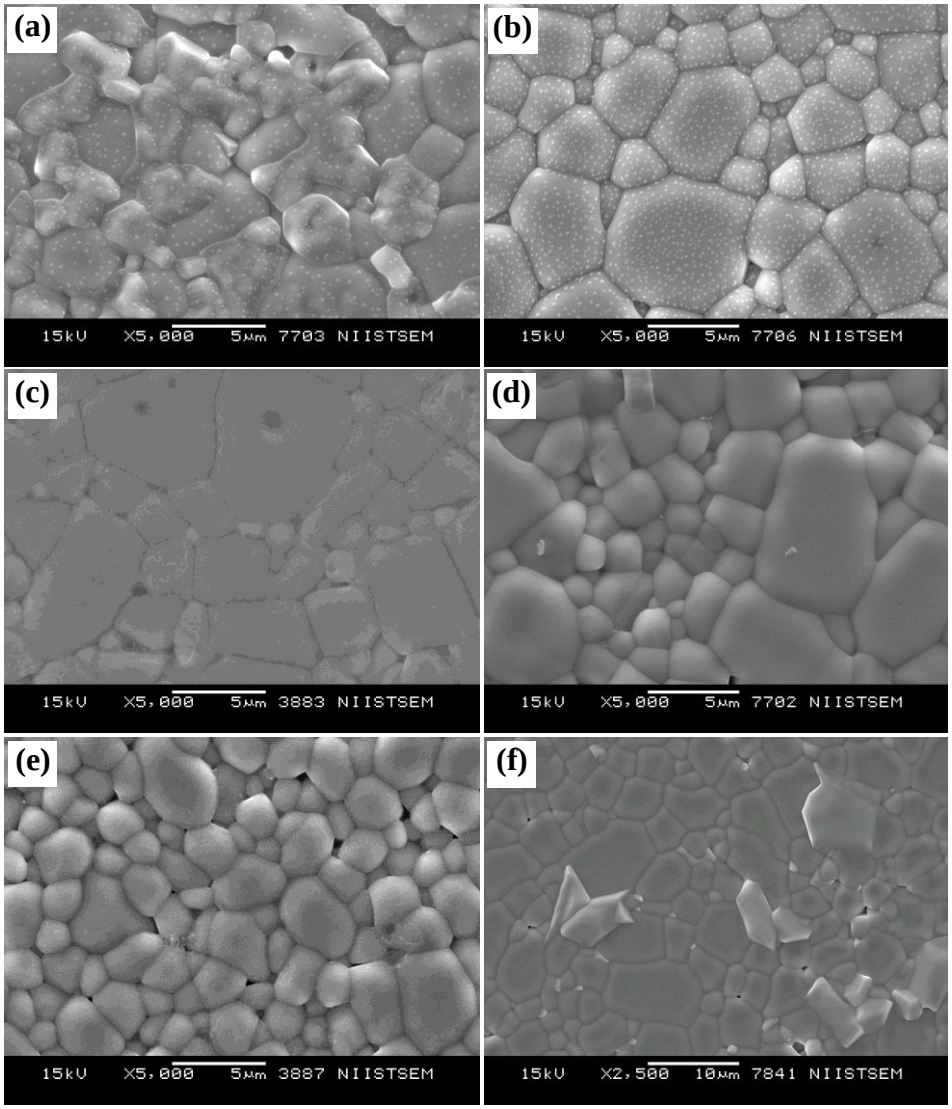

Figure 3.7 SEM images of (a) $Sr_2ZnSi_2O_7$ sintered at 1475 ^oC/2h (b) $Sr_2(Zn_{0.5}Co_{0.5})Si_2O_7$ sintered at 1425 ^oC/2h (c) $Sr_2(Zn_{0.5}Mg_{0.5})Si_2O_7$ sintered at 1500 ^oC/2h (d) $(Sr_{0.5}Ca_{0.5})_2ZnSi_2O_7$ sintered at 1375 ^oC/2h (e) $(Sr_{0.75}Ba_{0.25})_2ZnSi_2O_7$ sintered at 1375 ^oC/2h (f) $Sr_2ZnSi_2O_7$ + 2wt% $SrTiO_3$ sintered at 1450 ^oC/2h.

Fig. 3.7 (a-e) shows the SEM images of various compositions belonging to $A_2BSi_2O_7$ ceramics. Fig. 3.7 (a) represent the surface image of $Sr_2ZnSi_2O_7$ sintered at 1475 ^oC/2h. Well packed grains can be clearly seen without the presence of much porosity. The grain size varies considerably between 1-5 µm. The same is the case with the image of $Sr_2(Zn_{0.5}Co_{0.5})Si_2O_7$ sintered at 1425 ^oC/2h, where extremely small grains

having size less than 1 µm are present along with grains of size ~ 5 µm. The packing of the grains seems to be good, but not as good as $Sr_2ZnSi_2O_7$ ceramics. A similar conclusion can also be obtained from the SEM image of $Sr_2(Zn_{0.5}Mg_{0.5})Si_2O_7$ sintered at 1500 ^oC/2h. Fig. 3.7 (d-e) shows the SEM images of $(Sr_{0.5}Ca_{0.5})_2ZnSi_2O_7$ and $(Sr_{0.75}Ba_{0.25})_2ZnSi_2O_7$ heat treated at their optimized sintering temperature. The grain size varies randomly for both the ceramics. However for $(Sr_{0.75}Ba_{0.25})_2ZnSi_2O_7$ ceramics a much more uniform distribution of grain size in the range 0.5-4 µm is observed as compared to $(Sr_{0.5}Ca_{0.5})_2ZnSi_2O_7$ ceramics. For the latter one, the image 3.7 (d) gives a broad distribution of grain size from 0.5-8 µm. Though the grain size observed is not uniform, well packing of the grains could be achieved for all the composition with only a limited amount of porosity. Each of the micrographs has a uniform contrast and hence the possibility of the presence of any additional phases can be neglected, which is in accordance with the X-ray diffraction studies.

(ii) Variation of cell parameters with substitution

The $(Sr_{1-x}A_x)_2(Zn_{1-x}B_x)Si_2O_7$ system has a tetragonal akermanite-type symmetry with space group $P\bar{4}2_1m$ (no. 113). Hence the relation between lattice parameters 'a', 'c' and the lattice spacing d is described by the equation

$$\frac{1}{d^2} = \frac{h^2 + k^2}{a^2} + \frac{l^2}{c^2} \qquad (3.1)$$

The (hkl) represents the Miller indices. The values of 'a' were calculated using the lattice spacing (d) corresponding to (hk0) reflections, whereas that of 'c' using the d values of the reflections from the (00l) planes. The different values obtained for a were plotted against the Nelson-Riley function (Cullity *et al.*, 2001), which is given by

$$NRF = \frac{\cos^2\theta}{\sin\theta} + \frac{\cos^2\theta}{\theta} \qquad (3.2)$$

The Nelson-Riley function was taken along the X-axis and the values of a corresponding to different (hk0) reflections were taken along the Y-axis. The Y intercept

of the plot was selected as the most appropriate value of 'a'. The similar procedure was also done for the calculation of 'c'.

Table 3.2 Lattice parameters and XRD density values of $(Sr_{1-x}A_x)_2(Zn_{1-x}B_x)Si_2O_7$ ceramics calculated from the XRD pattern (A=Ca and B = Co, Mg, Ni)

$(Sr_{1-x}A_x)_2(Zn_{1-x}B_x)Si_2O_7$		'a' (Å)	'c' (Å)	Cell volume a^2c (Å^3)	X-ray density (g/cm^3)
A = Sr, B = Co	x = 0.00	8.021(2)	5.194(3)	334.2	4.06
	x = 0.25	8.017(0)	5.208(1)	334.7	4.04
	x = 0.50	8.013(0)	5.189(1)	333.2	4.04
	x = 0.75	8.002(1)	5.162(1)	330.5	4.06
	x = 1.00	7.995(0)	5.149(1)	329.1	4.06
A = Sr, B = Mg	x = 0.25	8.008(2)	5.200(9)	333.5	3.97
	x = 0.50	8.001(1)	5.159(1)	330.3	3.90
	x = 0.75	7.958(9)	5.162(2)	326.9	3.84
	x = 1.00	7.928(9)	5.166(0)	324.7	3.76
A = Sr, B = Mn	x = 0.25	8.029(0)	5.165(2)	333.0	4.05
	x = 0.50	8.066(2)	5.171(3)	336.4	3.98
	x = 0.75	8.074(7)	5.156(1)	336.1	3.96
	x = 1.00	8.123(5)	5.166(3)	340.9	3.88
*A = Sr, B = Ni	x = 0.25	8.018(2)	5.164(0)	332.0	4.07
	x = 0.50	8.021(0)	5.149(1)	331.3	4.06
A = Ca, B = Zn	x = 0.25	7.953(0)	5.134(1)	324.7	3.94
	x = 0.50	7.916(2)	5.078(1)	318.2	3.77
	x = 0.75	7.873(0)	4.976(8)	308.4	3.63
	x = 1.00	7.821(3)	4.958(8)	303.3	3.43
*A = Ba, B = Zn	x = 0.25	8.059(0)	5.223(3)	339.2	4.24
	x = 0.50	8.096(0)	5.303(1)	347.6	4.38

* Solid solutions having tetragonal structure are formed only for x = 0.25 and 0.50

Table 3.2 gives the extrapolated values of lattice parameters of $(Sr_{1-x}A_x)_2(Zn_{1-x}B_x)Si_2O_7$ ceramics. The theoretical density values given in the table are calculated using the cell volume $V = a^2c$ and the formula weight of the corresponding composition. Fig. 3.8 shows the nature of variation of the lattice parameters 'a' and 'c' of $(Sr_{1-x}A_x)_2(Zn_{1-x}B_x)Si_2O_7$ solid solutions as a function of the composition x. As the amount of smaller

Ca^{2+} ions increases in the solid solution, both the cell parameters 'a' and 'c' decrease. An opposite effect can be observed with the increasing amount of bigger Ba^{2+} ions. In the case of Mn^{2+} substitution, as the value of x increases a small increase in the lattice parameter 'a' is observed. This is due to the higher ionic radius of Mn^{2+} compared to that of Zn^{2+} ion. The substitution of Co^{2+}, Mg^{2+} and Ni^{2+} ions at the Zn-site do not cause any significant changes in both of the lattice parameters (Shannon, 1976).

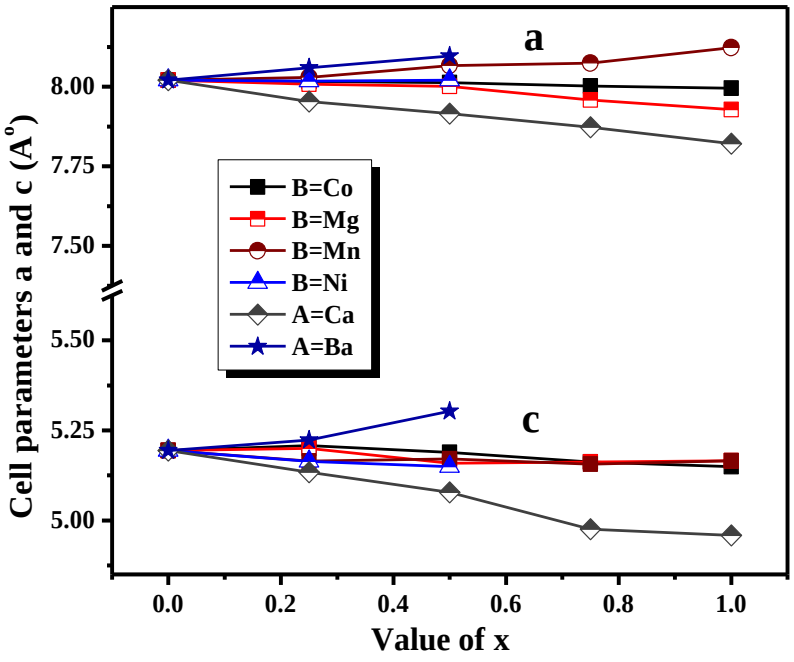

Figure 3.8 Variation of lattice parameters a and c of $(Sr_{1-x}A_x)_2(Zn_{1-x}B_x)Si_2O_7$ with value of x (A=Ca, Ba and B=Co, Mg, Mn, Ni).

Fig. 3.9 represents the variation of unit cell volumes of $(Sr_{1-x}A_x)_2(Zn_{1-x}B_x)Si_2O_7$ solid solutions (A = Ca, Ba and B = Co, Mg, Mn, Ni) with the value of x. The cell volume decreases from 334 $Å^3$ to 303 $Å^3$ in the case of Ca substitution due to the small ionic radius of Ca^{2+} as compared to Sr^{2+}ion. The decrease in the cell volume can also be seen in the case of Co, Mg and Ni substitution. The decrease in the cell volumes lies within the range of 10 $Å^3$ due to the matching ionic radii of Co^{2+}, Mg^{2+} and Ni^{2+} with Zn^{2+} ion. Ba^{2+} substitution at the A-site causes the cell volume to increase upto 347 $Å^3$ for x = 0.5. This can be well explained by the bigger ionic radius of Ba^{2+} compared to that of Sr^{2+} ion. Mn^{2+} substitution at the B-site also causes a small increase in the cell volume

from 334 Å^3 to 341 Å^3 (Shannon, 1976). The variation of the lattice parameters and cell volumes indicates the substitution of various ions at the respective sites, thereby forming solid solutions.

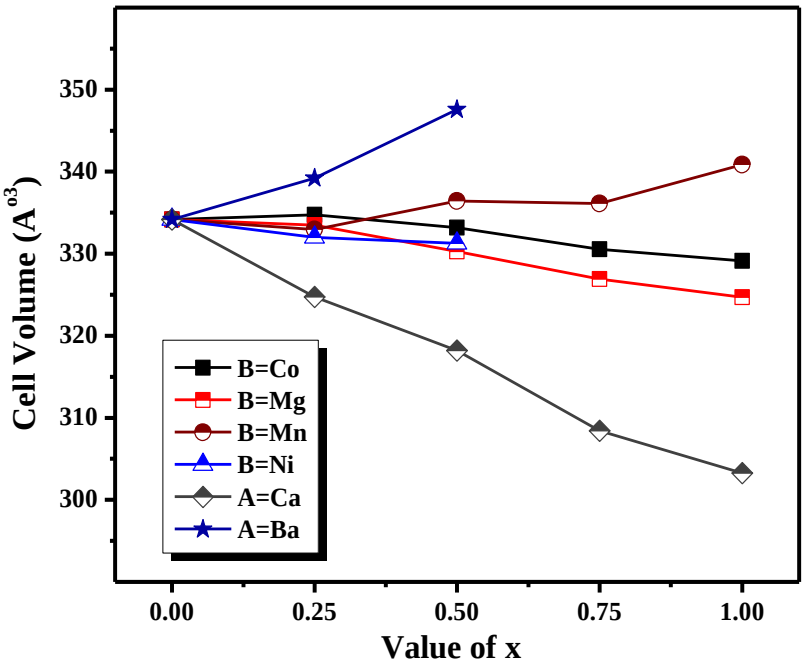

Figure 3.9 Variation of unit cell volumes of $(Sr_{1-x}A_x)_2(Zn_{1-x}B_x)Si_2O_7$ as a function of value of x (A=Ca, Ba and B=Co, Mg, Mn, Ni).

(iii) Microwave dielectric properties

Fig. 3.10 shows a typical case of optimization of the sintering temperature by studying the variation of relative density, relative permittivity, $Q_u \times f$ and τ_f. The relative density of $Sr_2ZnSi_2O_7$ increases from 94% at 1425 ^oC/2h and reaches a maximum value of 97% at 1475 ^oC/2h and then starts decreasing with further increase in sintering temperature (Fig. 3.10 (a)). The same trend is observed in the case of measured values of relative permittivity. The value of relative permittivity of $Sr_2ZnSi_2O_7$ ceramic sintered at 1425 ^oC is 7.8, and it increases to a maximum value of 8.1 when sintered at 1475 ^oC. With further increase in sintering temperature to 1500 ^oC, ε_r decreases to a value of 7.9. The porosity corrected values of relative permittivity of $A_2BSi_2O_7$ are given in Table 3.3 (Penn *et al.*, 1997).

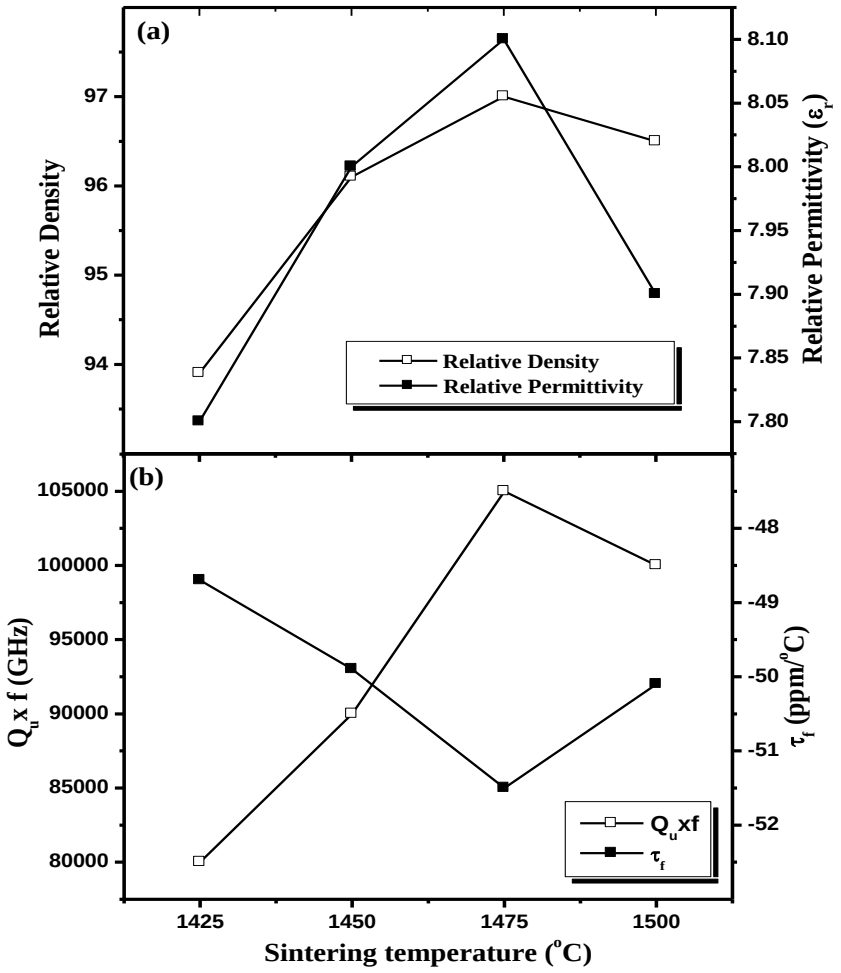

Figure 3.10 Variation of (a) Relative density and relative permittivity (b) $Q_u \times f$ and τ_f of $Sr_2ZnSi_2O_7$ ceramics with sintering temperature.

Fig. 3.10 (b) shows the variation of the $Q_u \times f$ and τ_f values of $Sr_2ZnSi_2O_7$ ceramics sintered at various temperatures. The value of $Q_u \times f$ reaches a maximum value of 105000 GHz (at 12.628 GHz) when sintered at 1475 ^oC, and thereafter it decreases. Thus the variation of $Q_u \times f$ values with sintering temperature is similar to that of relative density as shown in Fig. 3.10 (a). Hence the optimized sintering temperature for $Sr_2ZnSi_2O_7$ ceramics is chosen as 1475 ^oC/2h, where the sample has maximum relative density, relative permittivity and $Q_u \times f$ values. The sintering temperatures of all the other compositions are similarly optimized. Fig. 3.10 (b) also shows the variation of the τ_f values of $Sr_2ZnSi_2O_7$ ceramic with sintering temperatures. Remarkable variations in the τ_f

values are not recognized when sintered at different temperatures. The value of τ_f varies from -49 ppm/^oC to -52 ppm/^oC when sintered in the temperature range of 1425-1500 ^oC.

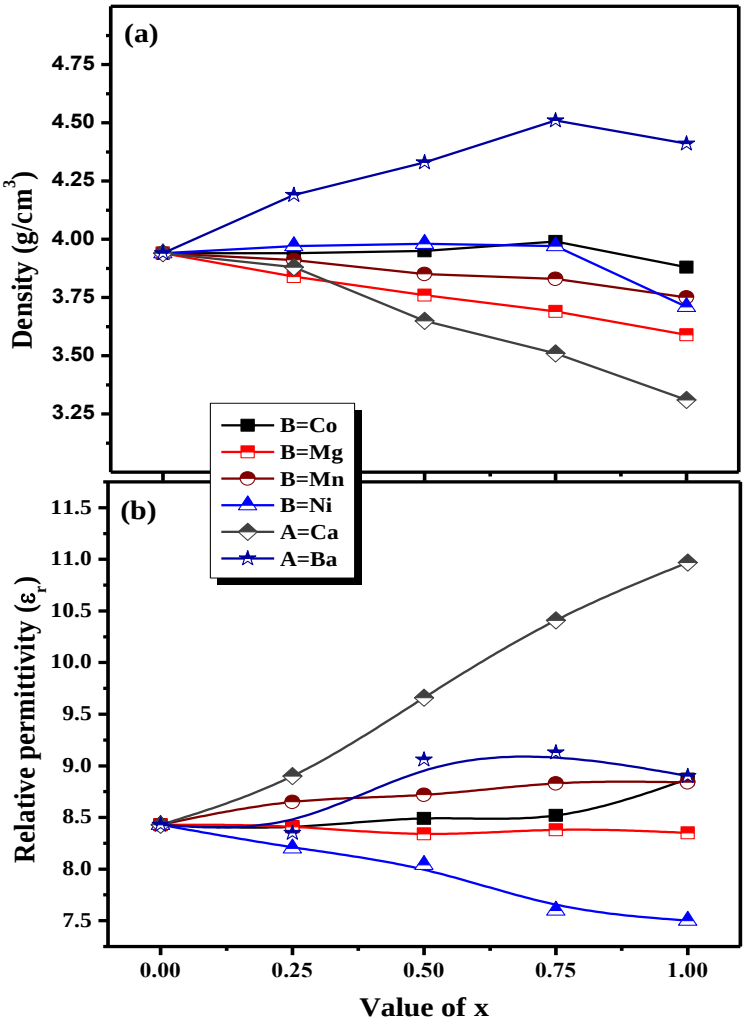

Figure 3.11 Variation of (a) density and (b) relative permittivity of $(Sr_{1-x}A_x)_2(Zn_{1-x}B_x)Si_2O_7$ as a function of value of x (A=Ca, Ba and B=Co, Mg, Mn, Ni).

The microwave dielectric properties of $(Sr_{1-x}A_x)_2(Zn_{1-x}B_x)Si_2O_7$ ceramics are also studied in the range $0 \leq x \leq 1$. The variation of density of $(Sr_{1-x}A_x)_2(Zn_{1-x}B_x)Si_2O_7$ ceramics as a function of composition x is shown in Fig. 3.11 (a). Substitution of Ca^{2+} and Mg^{2+} decreases the density of the solid solutions, whereas an increase in the density values is observed with the increase in Ba^{2+} content. All composition has a relative density greater than 95% of the theoretical values. The variation in the values of porosity

corrected relative permittivity (Penn *et al.*, 1997) as a function of composition x is shown in Fig. 3.11 (b). The relative permittivity increases from 8.4 for $Sr_2ZnSi_2O_7$ to 10.9 for $Ca_2ZnSi_2O_7$. This is not expected since the ionic polarizability of Ca^{2+} ion (3.16 Å^3) is less than that of Sr^{2+} ion (4.24 Å^3). A similar trend is also seen in the case of Co^{2+} substitution, an increase in the relative permittivity is observed even though the ionic polarizability (1.65 Å^3) is less than that of Zn^{2+} (2.04 Å^3). The substitution of Mg^{2+} and Mn^{2+} at the Zn-site lead to the variation of relative permittivity as predicted by the values of ionic polarizability. The relative permittivity increases with increase in the Ba^{2+} ion content in the range $0 \leq x \leq 0.75$ since the ionic polarizability (6.4 Å^3) is greater than that of Sr^{2+} ions (Shannon, 1993). At x = 1, the phase formed is not identified and hence the correction for porosity has not been made. In the case of $Sr_2(Zn_{1-x}Ni_x)Si_2O_7$ ceramics, the values of relative permittivity in the range $0.50 \leq x \leq 1.00$, shown in Fig. 3.11 (b) are also not corrected for porosity because of the formation of a mixture of $SrSiO_3$ and NiO phases.

Table 3.3 Sintering temperature, relative density and dielectric properties of $A_2BSi_2O_7$ ceramics.

$A_2BSi_2O_7$	**ST(^{o}C)**	**Relative Density**	**$Q_u \times f$ (GHz)**	**τ_f (ppm/^{o}C)**	**ε_r (porosity corrected)**	
					1MHz	**10-18(GHz)**
$Sr_2ZnSi_2O_7$	1475	97.3%	105000	-51.5	8.6	8.4
$Sr_2CoSi_2O_7$	1375	95.6%	34000	-56.7	9.3	8.9
$Sr_2MgSi_2O_7$	1550	95.5%	55000	-47.5	8.5	8.3
$Sr_2MnSi_2O_7$	1375	96.6%	32000	-58.8	9.0	8.8
$SrSiO_3$-NiO	1375	-	56500	-49.3	7.7*	7.5*
$Ca_2ZnSi_2O_7$	1300	96.5%	13500	-64.3	11.3	11.0
2BaO-ZnO-$2SiO_2$	1275	-	34000	-58.0	9.0*	8.8*

* Not corrected for porosity since they are mixture phases

Table 3.3 shows the dielectric properties of $A_2BSi_2O_7$ ceramics obtained in microwave frequency range when sintered at optimized temperatures. The relative permittivity values obtained at microwave frequencies (10-18 GHz) are compared with those obtained at 1 MHz. In most of the cases, only a small increase in relative permittivity is observed at 1 MHz than at microwave frequencies. The strong covalent

bonds in the SiO_4 tetrahedra, which are not easily susceptible to rattling, are responsible for the low relative permittivity and low loss factor.

The variation of the $Q_u \times f$ values of $(Sr_{1-x}A_x)_2(Zn_{1-x}B_x)Si_2O_7$ is shown in Fig. 3.12. All the substitutions decrease the quality factor. The effect is more prominent with Ca^{2+} substitution showing a very low value of $Q_u \times f \sim 13000$ GHz for $Ca_2ZnSi_2O_7$. No correlation between the $Q_u \times f$ values and size of the cations or valence is observed. Even a small deviation, either positive or negative of the ionic radius of the B-site substituted ions from 0.60 Å (for Zn) reduces the $Q_u \times f$ values. This is also true regarding the size of A-site cations in eight-fold coordination, where the reduction of $Q_u \times f$ is observed with the substitution of Sr^{2+} ions with smaller Ca^{2+} ions as well as bigger Ba^{2+} ions. The substitutions do not make much variation in the τ_f values as shown in Fig. 3.13. The values of τ_f vary between -48 to -64 ppm/^oC for various substitutions in the entire range of x. The Ca^{2+} substitution showed the largest variation in τ_f from -51.5 to -64.3 ppm/^oC in the composition range $0 \leq x \leq 1$.

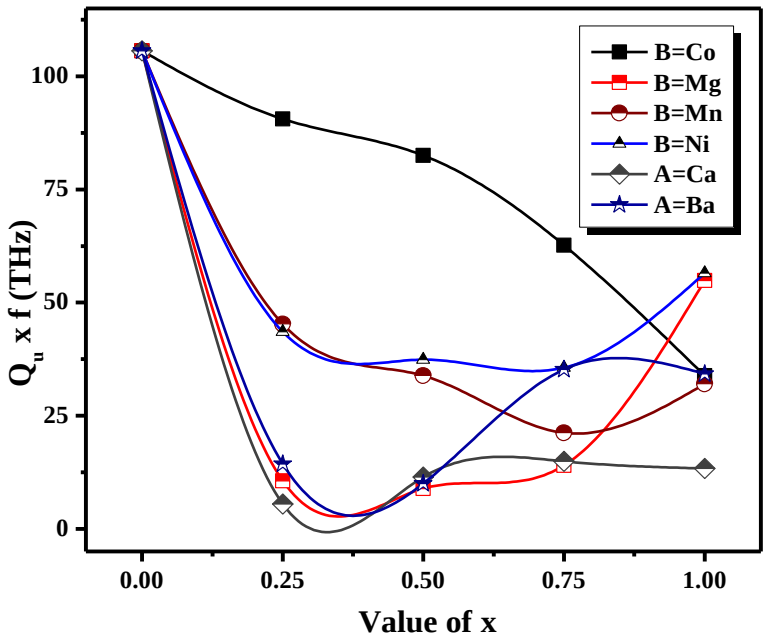

Figure 3.12 Variation of $Q_u \times f$ of $(Sr_{1-x}A_x)_2(Zn_{1-x}B_x)Si_2O_7$ with value of x (A=Ca, Ba and B=Co, Mg, Mn, Ni)

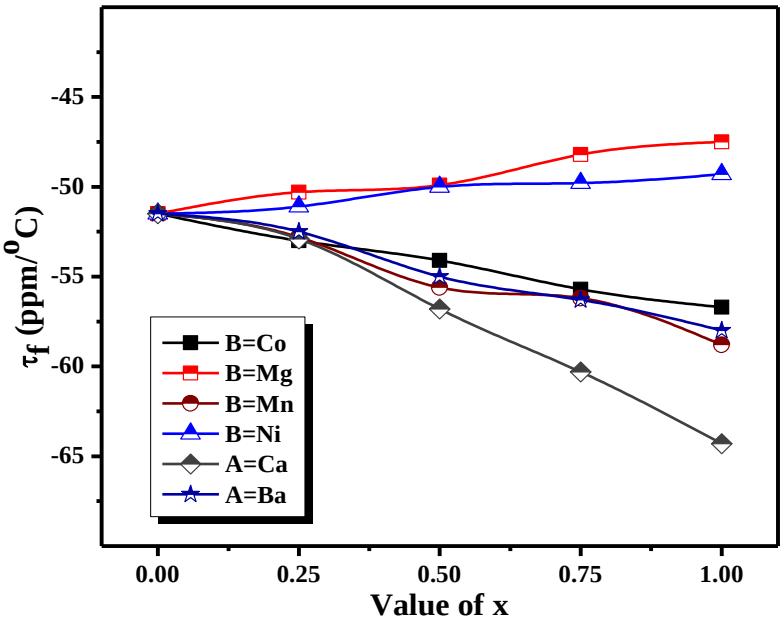

Figure 3.13 Variation of τ_f of $(Sr_{1-x}A_x)_2(Zn_{1-x}B_x)Si_2O_7$ ceramics with value of x (A=Ca, Ba and B=Co, Mg, Mn, Ni)

(iv) Effect of addition of $SrTiO_3$

The τ_f values of $A_2BSi_2O_7$ ceramics can be tailored by forming a mixture with materials having high positive values of τ_f such as $SrTiO_3$, $CaTiO_3$ (Wise *et al.*, 2002). The τ_f value of $Sr_2ZnSi_2O_7$ has been tailored by adding a small amount of $SrTiO_3$ having ε_r = 270, $Q_u \times f$ = 2000 GHz and τ_f= +1600 ppm/◦C (Wise *et al.*, 2001). Table 3.4 gives the microwave dielectric properties of $SrTiO_3$ added $Sr_2ZnSi_2O_7$ ceramics.

Table 3.4 Dielectric properties of $Sr_2ZnSi_2O_7$ + $SrTiO_3$ ceramics

Wt% of $SrTiO_3$	ST (°C)	ε_r	$Q_u \times f$ (GHz)	τ_f (ppm/°C)
0 wt %	1475	8.4	105000	-51.5
2 wt%	1450	8.8	60000	-13.0
4 wt%	1450	9.5	NR*	NR*

* NR: No Resonance

The relative permittivity of $Sr_2ZnSi_2O_7/SrTiO_3$ composites increases with the increase in $SrTiO_3$ content. This is due to the high relative permittivity of $SrTiO_3$. Addition of 2 wt% of $SrTiO_3$ to $Sr_2ZnSi_2O_7$ results in a decrease of τ_f value to -13

ppm/◦C with ε_r = 8.8, $Q_u \times f$ = 60000 GHz (at 12.585 GHz) when sintered at 1450 ^oC/2h. However, the sample $Sr_2ZnSi_2O_7$ + 4wt% $SrTiO_3$ sintered at 1450 ^oC/2h is lossy and do not resonate indicating that addition of larger amount of $SrTiO_3$ degrade quality factor. The XRD pattern of $Sr_2ZnSi_2O_7$ + 2wt% $SrTiO_3$ is shown in Fig. 3.14. The presence of diffraction peaks of $SrTiO_3$ (ICDD Card No: 96-0179) and $Sr_2ZnSi_2O_7$ indicates the absence of extensive chemical reaction between the two. The SEM image of the polished surface of $Sr_2ZnSi_2O_7$ + 2wt% of $SrTiO_3$ ceramics, sintered at 1450 ^oC shown in Fig. 3.7(f) also supports the result of XRD pattern. Two different types of grains can be seen indicating that the composite is a mixture of $SrTiO_3$ and $Sr_2ZnSi_2O_7$.

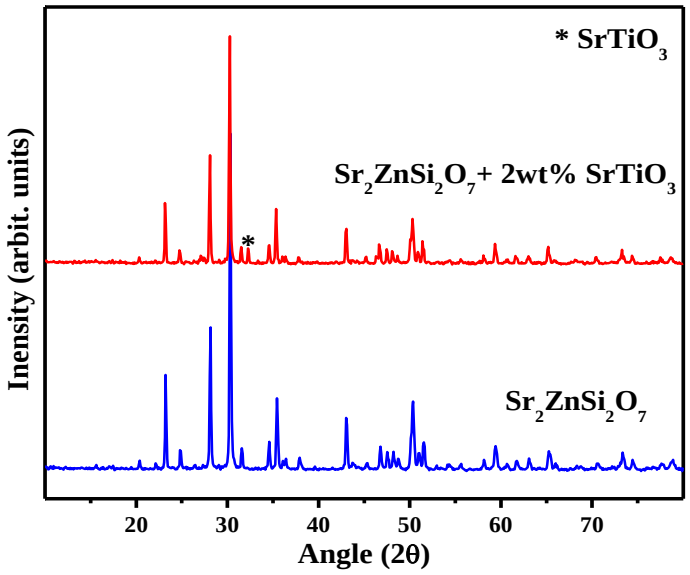

Figure 3.14 XRD patterns of $Sr_2ZnSi_2O_7$ sintered at 1475^{o}C/2h and $Sr_2ZnSi_2O_7$ + 2 wt% of $SrTiO_3$ sintered at 1450^{o}C/2h.

3.4 Microwave dielectric properties of alkaline earth orthosilicates A_2SiO_4 (A = Ba, Sr, Ca)

3.4.1 Introduction

As already mentioned, silicates have received considerable attention because of their potential for applications in the field of photoluminescence, electronic packaging and microwave communication. Silicates have also been extensively investigated among the host lattices for luminescent materials, especially the ones used in lamps because of

their stability, visible light transparency, and relatively ease of preparation (Pires *et al.*, 2001). For instance, zinc orthosilicates (Zn_2SiO_4) doped with Mn^{2+} is commercially used as a green phosphor, which has been studied by various experimental techniques since the 1930's. It has also been reported that Sr_2SiO_4 doped with Eu^{2+} is a promising yellow phosphor for white light emitting diodes (Li *et al.*, 2008). The dielectric properties of some of the orthosilicates have been well characterized and are found to be suitable for packaging as well as millimeter wave communication applications due to their low ε_r and high $Q_u \times f$ values. For e.g., some of the orthosilicates like Mg_2SiO_4 and Zn_2SiO_4 have excellent dielectric properties suitable for packaging and microwave communication applications (Sebastian, 2008). However, to the best of our knowledge, the dielectric properties of certain silicates belonging to the alkaline earth orthosilicate family such as Ba_2SiO_4, Sr_2SiO_4 and Ca_2SiO_4 are still unknown. So it would be of great use if we could extend our knowledge of the dielectric properties of materials, especially the silicates, which are yet unknown to the scientific community. This work is an attempt to discover the dielectric properties of orthosilicates Ba_2SiO_4, Sr_2SiO_4 and Ca_2SiO_4 and to study their suitability for electronic packaging applications.

Alkaline earth metals are forming orthosilicates with formula A_2SiO_4, but their crystal structures are different, which is mainly due to difference in cation radii and consequently different cation coordination. For e.g., in Be_2SiO_4 crystal structure, Be^{2+}cations are in tetrahedral coordination, but in orthorhombic Mg_2SiO_4, Mg^{2+}cations are octahedrally coordinated. Exceptional in this respect is calcium orthosilicate known of its rich polymorphism, in which the Ca^{2+}cations are in different coordination 6 or 8. Five crystalline phases were identified from room temperature to the melting point for Ca_2SiO_4: γ (orthorhombic), β (monoclinic), α_L' (orthorhombic), α_H' (orthorhombic) and α (trigonal/hexagonal) (Liu *et al.*, 2002). The structure of Sr_2SiO_4 and Ba_2SiO_4 are not well known whereas cation coordination is known and similarly as in K_2SiO_4, it is equal to 8. An orthorhombic form is the only stable modification of Ba_2SiO_4 (Catti *et al.*, 1983). Two modifications are observed for the orthosilicates of the intermediate-sized cation Sr^{2+}; the former should be presumably isostructural with β-Ca_2SiO_4 and the later with α_H'-Ca_2SiO_4 and Ba_2SiO_4, on the basis of their powder diagrams (Pieper *et al.*, 1972).

The α′ form of Sr_2SiO_4 was shown to be stabilized at room temperature by just very small amount of (2.5%) of Ba substitution (Pieper *et al.*, 1972).

3.4.2 Experimental

A_2SiO_4 (A = Ba, Sr, Ca) ceramics were prepared using high purity powders of $BaCO_3$, $SrCO_3$, $CaCO_3$ (99.9 %, Sigma Aldrich, Milwaukee, WI, U.S.A.) and SiO_2 (99.6 %, Sigma Aldrich). The stoichiometric amounts of raw materials were mixed by ball milling for 24 h using distilled water as a medium in polyethylene bottles. Calcination of the dried powders was then performed in the temperature range of 1150-1400 ^oC depending on the composition. The calcined powders were ground well and mixed with 4 wt% polyvinyl alcohol (molecular weight 22000, BDH Lab Suppliers, Poole, UK) and shaped into disks of different diameters and thicknesses for various measurements by applying a pressure of 150 MPa. The sintering was carried out at different temperatures in the range 1400-1600 ^oC for 4 h in order to attain maximum density for all the samples. The temperature corresponding to maximum density has been chosen as the optimized sintering temperature for each composition. The sintered samples were powdered and used to analyze the crystal structure and phase purity by the X-ray diffraction. The microstructure of the samples was recorded using a scanning electron microscope. The sintered density of the specimens was measured by the Archimedes method. The radio frequency measurements were carried out using a LCR meter and microwave measurements by a vector network analyzer-Agilent 8753 ET, Palo Alto, CA (see chapter 2). The coefficient of linear thermal expansion of the samples having a diameter of ~ 7 and thickness ~ 10 mm was measured by a dilatometer in the temperature range 30 to 600 ^oC.

3.4.3 Results and discussions

The XRD patterns of A_2SiO_4 (A = Ba, Sr, Ca) ceramics are shown in Fig. 3.15. Ba_2SiO_4 has an orthorhombic structure and belongs to the Pmcn (no. 62) space group with a = 5.805(3), b = 10.2(1), c = 7.499(1) and an X-ray density of 5.49 g/cm^3 as reported in the ICDD file card No. 70-2113. The observed diffraction pattern of Ba_2SiO_4 can be well matched with the above ICDD file, which is an indication of the absence of

any secondary phases. According to ICDD file card No. 76-1630, Sr_2SiO_4 has a monoclinic structure with space group $P2_1/n$ (no. 14) and a = 5.663(1), b = 7.084(2), c = 9.767 (2), β = 92.670 and an X-ray density of 4.54 g/cm^3. The obtained diffraction pattern for Sr_2SiO_4 in Fig. 3.15 (b) is indexed based on the pattern of the above file. The Ca_2SiO_4 has the same structure and symmetry as that of Sr_2SiO_4 as indicated by the X-ray diffraction pattern 3.15 (c). The indexing has been done based on the ICDD file card No. 86-0398.

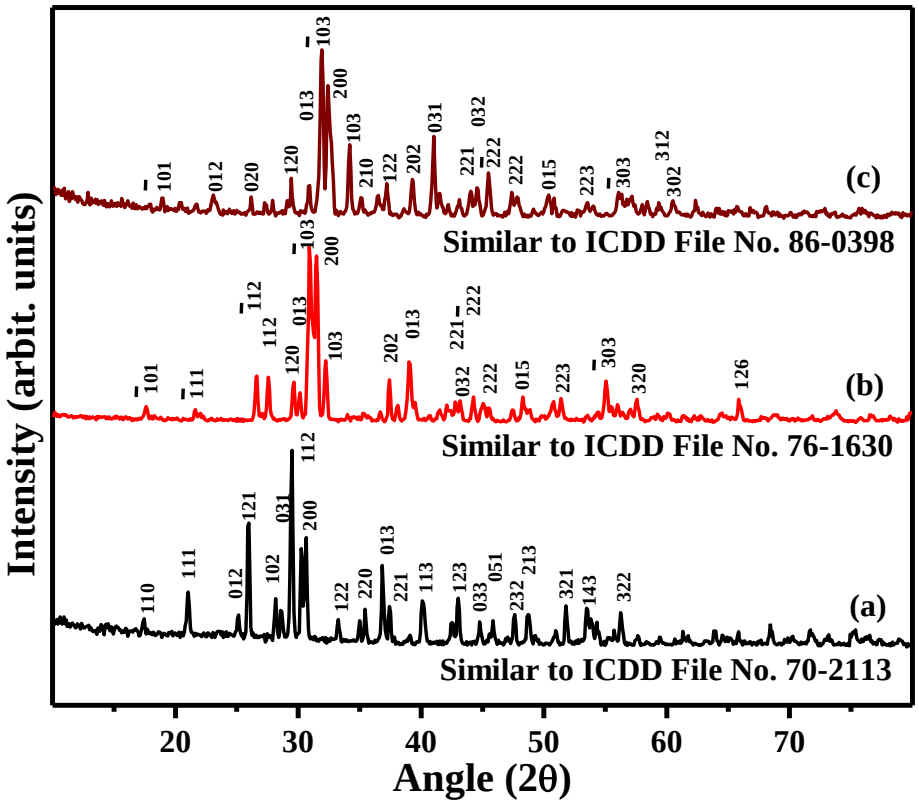

Figure 3.15 Powder X-ray diffraction patterns of (a) Ba_2SiO_4 sintered at 1525 ^oC/4h (b) Sr_2SiO_4 sintered at 1575 ^oC/4h and (c) Ca_2SiO_4 sintered at 1450 ^oC/4h.

The SEM images of Ba_2SiO_4 sintered at 1525 ^oC and Sr_2SiO_4 sintered at 1575 ^oC are shown in Fig. 3.16. The microstructure of Ba_2SiO_4 contains large grains of about 25 μm in size along with some small grains of size about 5 μm. The image of the fractured surface of Ba_2SiO_4 is also shown in Fig. 3.16 (b). Large grains can be seen along with some amount of entrapped porosity. Fig. 3.16 (c) depicts the microstructure of Sr_2SiO_4 ceramics, sintered at 1575 ^oC. All the grains are less than 10 μm in size and it seems that

some of grains have just started melting. The SEM picture of Ca_2SiO_4 ceramics is also shown in Fig. 3.16 (d). Very small grains of ~ 1-2 μm are observed along with a large amount of porosity.

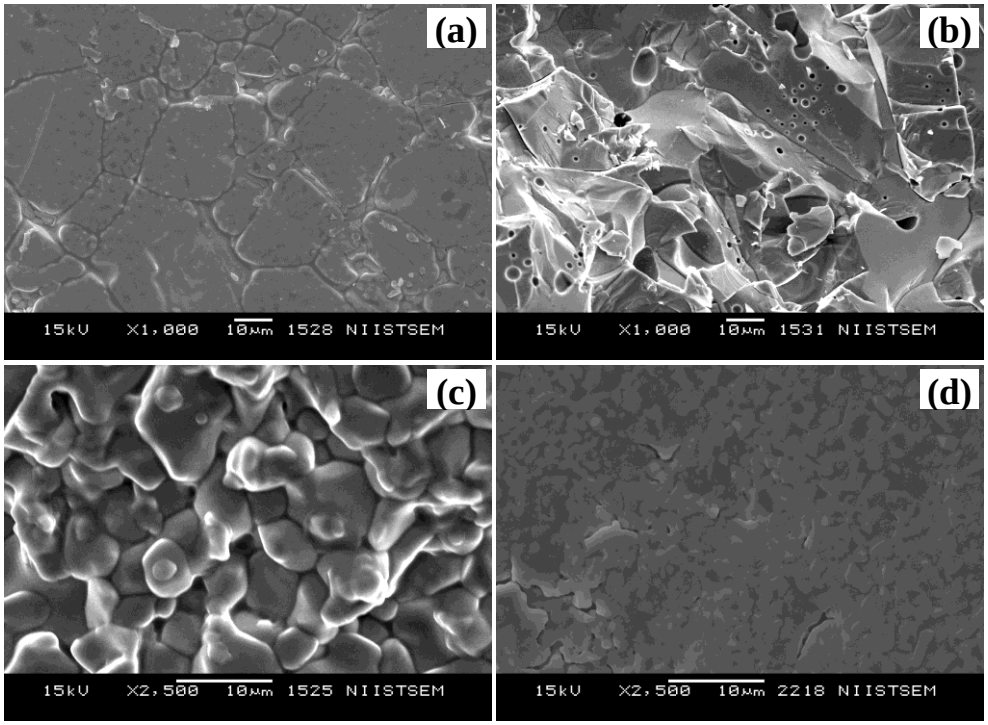

Figure 3.16 SEM images of (a) Ba_2SiO_4 sintered at 1525 ^oC/4h (b) fractured surface of Ba_2SiO_4 (c) Sr_2SiO_4 sintered at 1575 ^oC/4h (d) Ca_2SiO_4 sintered at 1450 ^oC/4h.

Fig. 3.17 shows the optimization of sintering temperature of A_2SiO_4 (A = Ba, Sr, Ca) ceramics. Optimization is done for highest density for all compositions. Usually highest density is associated with highest ε_r because of the elimination of porosity. High relative density also results in maximum values of $Q_u \times f$ due to the reduction in dielectric-air interface, which would cause irregular reflection of the microwaves thereby reducing the value of $Q_u \times f$. The porosity and hence the moisture taken up by the pores will be a minimum when the relative density is the highest, which is also a reason for the increase in the value of $Q_u \times f$. It is clear from Fig. 3.17 that the relative density of A_2SiO_4 ceramics increases with sintering temperature, becomes a maximum value and then deceases with further increase in the sintering temperature. This behavior is a result of grain growth and hence the elimination of porosity with the increase in sintering temperature. The optimized sintering temperatures of A_2SiO_4 ceramics are 1525 ^oC/4h, 1575 ^oC/4h and

1450 ^{o}C/4h for A = Ba, Sr and Ca respectively. In the case of Ba_2SiO_4 and Sr_2SiO_4 ceramics, the relative density achieved are 93.4% and 94.2% respectively. Still lower densification (89.5%) is achieved for Ca_2SiO_4, which may be due to the fact that Ca_2SiO_4 transforms to various polymorphic forms during the process of cooling(Liu *et al.*, 2002).

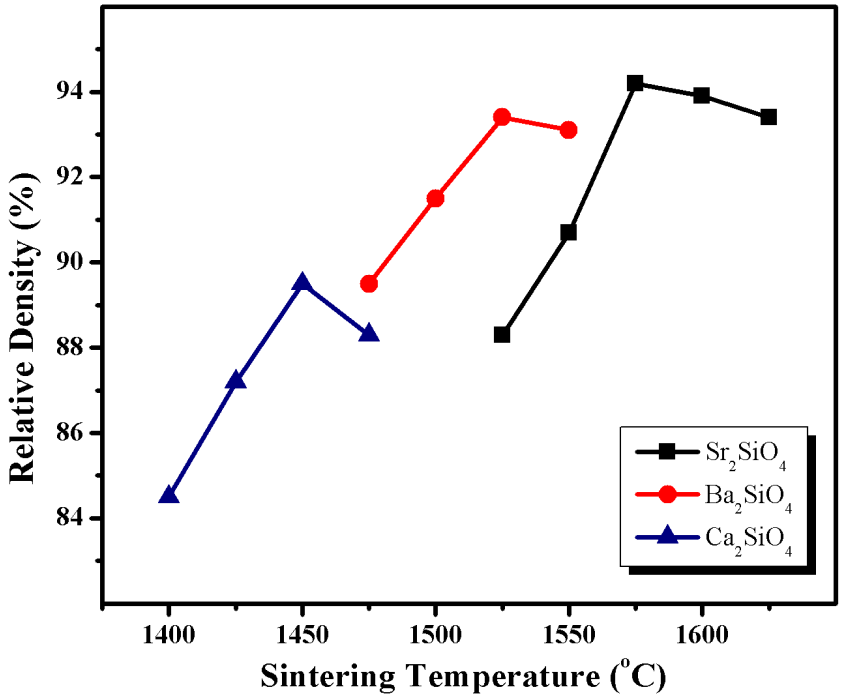

Figure 3.17 Optimization of sintering temperatures of Ba_2SiO_4, Sr_2SiO_4 and Ca_2SiO_4 based on relative density.

Table 3.5 shows the dielectric properties of A_2SiO_4 (A = Ba, Sr, Ca) ceramics both at radio and microwave frequencies when sintered at their respective optimized sintering temperatures. At 1 MHz the values of ε_r are 14.2, 11.6 and 9.4 for Ba, Ca and Sr based ceramics respectively. The value of ε_r decreases with the decrease of ionic radius of M^{2+}cation. The same trend can also be observed for ε_r at microwave frequencies, the values being 13.1, 9.6 and 8.1 respectively. The decrease in the values of ε_r as we move from Ba_2SiO_4 to Ca_2SiO_4 can be attributed to the decrease in the ionic polarizability of A^{2+} ion (Shannon, 1993). The values of ε_r at microwave frequencies are also found to be less than that at radio frequencies because of the fact that certain polarization mechanisms which are active at radio frequencies are absent at microwave frequency range (Sebastian, 2008). Since the relative density obtained for all the compositions are

less than 95%, a correction for porosity has been applied to the experimentally observed values of ε_r using the equation derived by Penn *et al*., and the porosity corrected ε_r values are given in table 3.5 (Penn *et al.*, 1997).

Table 3.5 Density, dielectric properties and thermal expansion data of M_2SiO_4 (M = Ba, Sr, Ca) ceramics when sintered at optimum temperatures.

A_2SiO_4	ST (^oC)	Density (g/cm^3)	1 MHz		ε_r (microwave)		$Q_u \times f$ (GHz)	τ_f ($ppm/^oC$)	α_l ($ppm/^oC$)
			ε_r	tan δ	measured	Porosity corrected			
Ba_2SiO_4	1525/4h	5.13	14.2	0.004	13.1	14.5	17900	-17	+10.3
Sr_2SiO_4	1575/4h	4.26	11.6	0.003	9.5	10.4	19100	-205	+6.2
Ca_2SiO_4	1450/4h	2.96	9.4	0.002	8.6	10.1	26100	-89	+7.0

The tan δ at 1 MHz is of the order of 10^{-3} for all the orthosilicates. At microwave frequencies, the $Q_u \times f$ values obtained are 17900 GHz, 19100 GHz and 26100 GHz for Ba_2SiO_4, Sr_2SiO_4 and Ca_2SiO_4 respectively. Despite its poor densification, Ca_2SiO_4 ceramic exhibits higher value of $Q_u \times f$ than the other two orthosilicates. It can be due to the low intrinsic loss of the Ca_2SiO_4 ceramics compared to Ba_2SiO_4 and Sr_2SiO_4. The τ_f of Ba_2SiO_4 is -17 $ppm/^oC$, whereas Sr_2SiO_4 and Ca_2SiO_4 exhibit high values of τ_f, -205 $ppm/^oC$ and -89 $ppm/^oC$ respectively. Therefore the τ_f of A_2SiO_4 ceramics should be modified using materials having high positive τ_f before any practical applications. Table 3.5 also gives the coefficient of thermal expansion (α_l) of A_2SiO_4 (A = Ba, Sr) ceramics. They exhibit small positive values of α_l, as expected, +10.3 $ppm/^oC$ for Ba_2SiO_4, +6.2 $ppm/^oC$ for Sr_2SiO_4 and +7.0 for Ca_2SiO_4.

3.5 Microwave dielectric properties of $CaBSi_2O_6$ (B = Mg, Co, Ni, Mn, Zn)

3.5.1 Introduction

$CaBSi_2O_6$ belongs to a class of minerals called pyroxenes, having the general formula $ABSi_2O_6$. The pyroxenes are an important group among the single chained inosilicates. They are common rock forming minerals and are represented in most igneous and many metamorphic rocks. Their presence in a rock indicates a high temperature of crystallization with a lack of water. The name pyroxene comes from the

Greek words for *fire* and *stranger* in a false allusion to their surprising presence in volcanic lavas. Pyroxenes are sometimes seen as crystals embedded in volcanic glass and the assumption was that they are impurities in the glass, hence the term "fire strangers". However the pyroxenes are simply early forming minerals that crystallized before the lava erupted. The typical pyroxene structure contains chains of SiO_3 tetrahedrons that every other one alternates from the left side to the right side of the chain. Each of the tetrahedrons has one flat edge that lies on the "base" of the structure as if the entire chain were a chain of connected three sided pyramids on a flat desert. The orderliness of the tetrahedrons means that they repeat every three tetrahedrons, ie. left-right-left. The chain structure explains the general prismatic to fibrous character of the members of this group. The slope of the tetrahedral pyramids helps to determine the cleavage angle of the pyroxenes at nearly 90^o degrees (actually 93^o and 87^o).

The pyroxene group is composed of minerals of the general formula $ABSi_2O_6$, where A and B are two divalent cations or a monovalent and a trivalent cation. If A and B are the same small-radius divalent cation like Fe or Mg or (syntheytically Co) the resultant structure is commonly orthorhombic, giving us the orthopyroxene group. At high temperature this structure inverts to C2/c high clinopyroxene which quenches to $P2_1/c$ low clinopyroxene. This give the primitive clinopyroxene group. At the pure Mg composition another orthorhombic structure with half the a-repeat of orthopyroxene is possible, and is called protoenstatitite. If A is a larger-radius cation like Ca or Na the structure is monoclinic C2/c. This gives the clinopyroxene group, the crystal structure of which is given in Fig. 3.18. If the B-site is too large the resultant structures are triclinic and giving the pyroxenoid group. The silicates, which are dealt with in this study, therefore belong to the clinopyroxene group, the most important one being diopside or $CaMgSi_2O_6$.

There are no reports on the microwave dielectric properties of the clinopyroxenes, except for $CaMgSi_2O_6$. Sun *et al.* studied the dielectric properties of $(Ca_{1-x}Mg_x)SiO_3$ for values of x in the range 0.1 to 0.9 (Sun *et al.*, 2007). The sintering temperature of $CaMgSi_2O_6$-$CaTiO_3$ has been reduced from 1300 ^oC to 880 ^oC by using the additive Li_2CO_3-V_2O_5 (Zhang *et al.*, 2008). Synthesis and microwave dielectric properties of $(Ca_{1-}$

$_xMg_x)SiO_3$ ceramics prepared by sol-gel process are also reported (Wang *et al.*, 2007). Numerous reports of glass-ceramics based on CaO-MgO-SiO_2 are also available (Kim *et al.*, 2008; Chang *et al.*, 2009; Kim, Hwang, *et al.*, 2009; Marques *et al.*, 2010). In this work we aim to study the microwave dielectric properties of $CaBSi_2O_6$ (B = Mg, Co, Ni, Mn, Zn) silicates prepared by the solid state ceramic route.

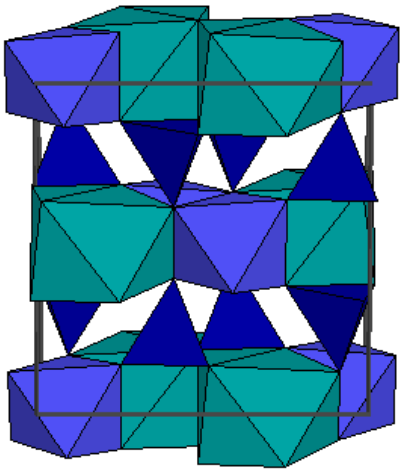

Figure 3.18 The crystal structure of clinopyroxenes (courtesy: www.ruby.colorado.edu).

3.5.2 Experimental

The $CaBSi_2O_6$ (B = Mg, Co, Ni, Mn, Zn) ceramics were prepared by conventional solid-state ceramic route. The chemicals used were $CaCO_3$, Co_3O_4, NiO, $MnCO_3$, ZnO, SiO_2, and $(MgCO_3)_4Mg(OH)_2.5H_2O$ (Aldrich Chemical Company, 99.9%). The raw materials were stoichiometrically weighed and were ball milled in polyethylene bottle using Yttria stabilized Zirconia balls in distilled water for 24 h. The slurry was dried at 100 ^oC in hot air oven and then calcined in the temperature range 1000-1150 ^oC/4h. The sintering was performed in the temperature range 1100-1325 ^oC/4h. In practice, the preparation conditions differ depending upon the composition, reactivity, grain growth etc. Hence it is necessary to optimize the processing conditions in order to get the final sintered compacts with desired properties.

The crystal structure and phase purity of the powdered samples were studied by X-ray diffraction technique and SEM micrographs recorded from the surface of thermally etched sample using scanning electron microscope. Low frequency dielectric properties

were measured using an LCR meter and the microwave dielectric properties (in the frequency range 7-12 GHz) using a scalar network analyzer (Aeroflex, IFR 6823 model). The relative permittivity and unloaded quality factor (Q_u) of the samples were measured by Hakki and Coleman and resonant cavity method respectively. The values of τ_f were measured in the temperature range 25-70 ^oC using the resonant cavity set up. The change in the resonance frequency is noted for every 2 ^oC rise in the temperature and the temperature coefficient of resonance frequency is calculated from the equation (2.15). The measured relative permittivity values were corrected for porosity using the equation (1.13) derived by Penn *et al.* (Penn *et al.*, 1997). The coefficients of thermal expansion of the samples were measured using a dilatometer (NETZSCH DIL 402 PC) in the temperature range 30-500 ^oC.

3.5.3 Results and Discussions

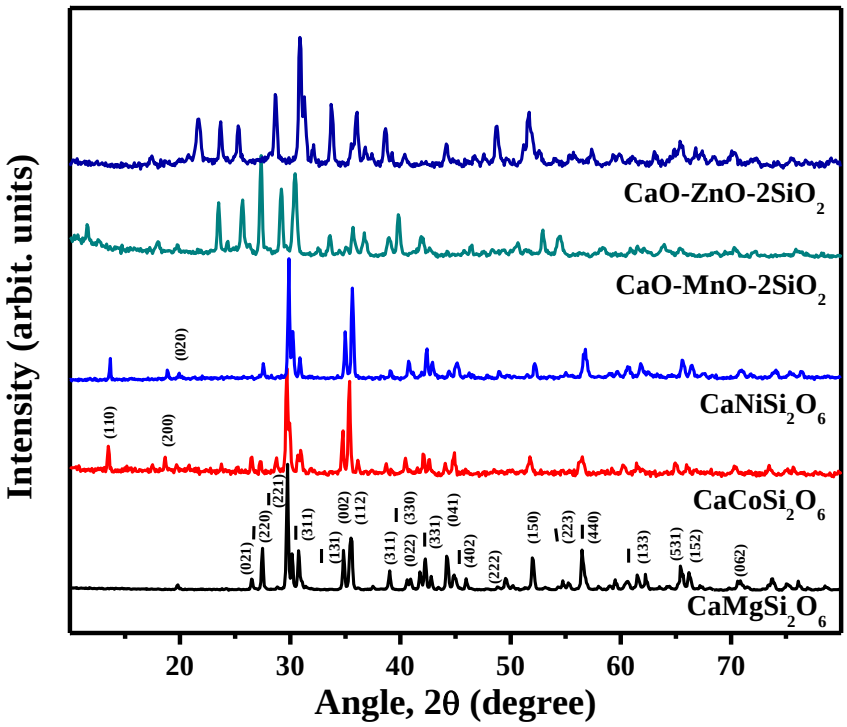

Figure 3.19 Powder X-ray diffraction patterns of $CaBSi_2O_6$ (B = Mg, Co, Ni, Mn, Zn) ceramics sintered at their respective sintering temperatures.

The powder X-ray diffraction patterns of $CaBSi_2O_6$ (B = Mg, Co, Ni, Mn, Zn) ceramics are shown in Fig. 3.19. The powder diffraction pattern of $CaMgSi_2O_6$ is indexed

based on ICDD file card no. 19-0239. All recognizable reflection peaks could be readily indexed to the C2/c monoclinic structure with lattice parameters of a = 9.748 Å, b = 8.926 Å, c = 5.250 Å and β = 105.8°, which is consistent with the standard data file. The diffraction patterns of $CaCoSi_2O_6$ and $CaNiSi_2O_6$ can be matched with the ICDD file card no. 84-1288 and 84-1287 respectively. They also have the same structure and space group as that of $CaMgSi_2O_6$. The lattice parameters of $CaCoSi_2O_6$ are a = 9.806 Å, b = 8.950 Å, c = 5.243 Å and β = 105.45°, where as that of $CaNiSi_2O_6$ are a = 9.734 Å, b = 8.891 Å, c = 5.228 Å and β = 105.87° according to the standard data files. Reflections from the planes (110), (200), (020) etc. are exhibited by $CaCoSi_2O_6$ and $CaNiSi_2O_6$ whereas they are absent for $CaMgSi_2O_6$. Variations in intensity of certain reflections are also observed depending on the element at the B-site. Fig. 3.19 also depicts the observed XRD patterns for B=Mn and B=Zn. The patterns are compared with the ICDD files 74-0336 for $CaMnSi_2O_6$ and 86-0748 for $CaZnSi_2O_6$. According the ICDD files $CaMnSi_2O_6$ and $CaZnSi_2O_6$ have monoclinic structure with C2/c space group similar to that of $CaBSi_2O_6$ (B = Mg, Co, Ni). However, the obtained diffraction patterns do not have any resemblance to the standard files. This indicates the absence of the formation of the phases $CaMnSi_2O_6$ and $CaZnSi_2O_6$.

Fig. 3.20 shows the SEM images of the $CaBSi_2O_6$ (B = Mg, Co, Ni, Mn, Zn) ceramics when heat treated at their respective sintering temperature. Fig. 3.20 (a) represents the polished and etched surface of $CaMgSi_2O_6$ ceramic, which exhibits grains of variable size starting from 5 µm to ~25 µm. Some porosity is also visible along the grain boundaries of the ceramic. Fig. 3.20 (b) shows the fractured surface of the $CaCoSi_2O_6$ ceramic. The fractured surface represents well packed grains of size less than 5 µm. Fig. 3.20 (c) depicts the surface of $CaNiSi_2O_6$ ceramic. Good microstructure is observed with grains of variable size. The smallest grain is about 1 µm in size while the largest grain is about 5 µm. Fig. 3.20 (d) shows the SEM image of $CaO\text{-}MnO\text{-}2SiO_2$, which exhibits grains of size starting from 5 µm to 20 µm for the largest grain. Some porosity is also visible in the photograph of $CaO\text{-}MnO\text{-}2SiO_2$. Fig. 3.20 (e) shows the fractured surface of the $CaO\text{-}ZnO\text{-}2SiO_2$ ceramic. The grain boundaries are not well visible and therefore represent a poor microstructure. Each of the images is of same

contrast and hence each composition $CaBSi_2O_6$ (B = Mg, Co, Ni, Mn, Zn) may represent a single phase material. The formation of the phases $CaBSi_2O_6$ (B = Mg, Co, Ni) belonging to monoclinic structure with C2/c space group could be well identified from the XRD patterns, where as those for B=Mn and Zn could not be recognized. More advanced studies will be required in this direction to identify the phases formed.

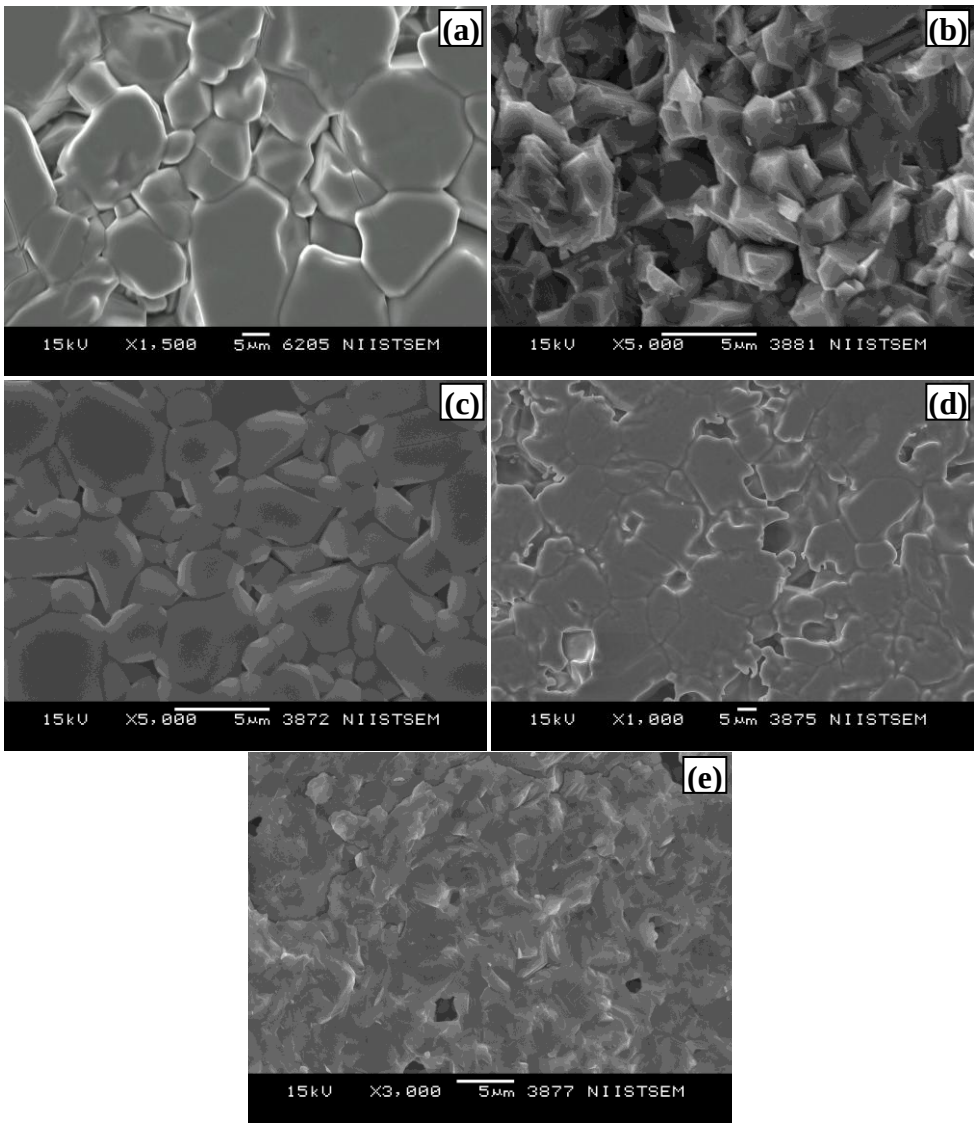

Figure 3.20 SEM images of (a) $CaMgSi_2O_6$ sintered at 1300 ^oC/2h (b) $CaCoSi_2O_6$ sintered at 1200 ^oC/2h (c) $CaNiSi_2O_6$ sintered at 1300 ^oC/2h (d) $CaO\text{-}MnO\text{-}2SiO_2$ sintered at 1200 ^oC/2h (e) $CaO\text{-}ZnO\text{-}2SiO_2$ sintered at 1150 ^oC/2h.

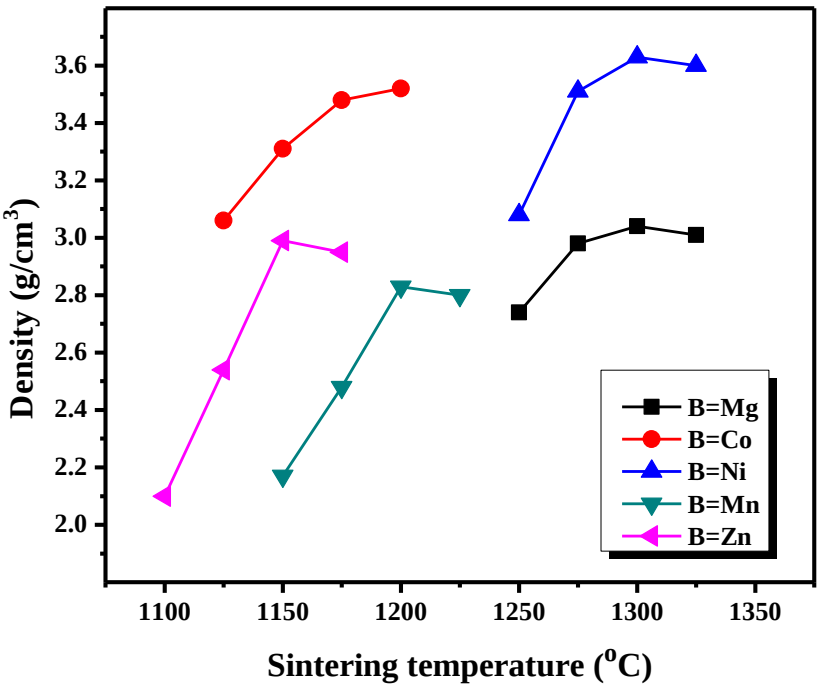

Figure 3.21 Optimization of sintering temperatures of $CaBSi_2O_6$ (B = Mg, Co, Ni, Mn, Zn) ceramics based on the their bulk density.

Fig. 3.21 represents the variation of density of $CaBSi_2O_6$ (B = Mg, Co, Ni, Mn, Zn) ceramics as a function of sintering temperature. The density of all the silicates is found to be increased with sintering temperature. The increase in sintering temperature enhances grain growth, which results in the elimination of porosity and hence improvement in density. The highest density achieved for $CaMgSi_2O_6$ is 3.04 g/cm^3, when sintered at 1300 ^oC/2h. The bulk density obtained at 1300 ^oC/2h is 93.5 % of the theoretical value. Further increase in sintering temperature causes a decrease in density of the $CaMgSi_2O_6$ ceramics. In the case of $CaCoSi_2O_6$, the density increases upto a sintering temperature of 1200 ^oC/2h and with further increase in sintering temperature, the sample melts. Thus the highest density achieved for $CaCoSi_2O_6$ is at 1200 ^oC/2h, which is 3.52 g/cm^3, 93.6 % of the theoretical value. Similarly for $CaNiSi_2O_6$, maximum density is achieved at 1300 ^oC/2h, which is 3.63 g/cm^3 (94.8%). The trend of variation of density with sintering temperature was also similar for $CaBSi_2O_6$ (B = Mn, Zn). But the densities of the silicates achieved were much less than the theoretical values. For instance $CaBSi_2O_6$ (B = Mn), when sintered at 1200 ^oC/2h, has a density of 2.83 g/cm^3, which is

only 79.1% of the anticipated value of 3.58 g/cm^3 for $CaMnSi_2O_6$. Similarly for B=Zn, the obtained density is 2.99 g/cm^3, which is only 77.7 % of the expected value of 3.85 g/cm^3 for $CaZnSi_2O_6$. The low values of relative density achieved are due to the absence of the formation of $CaMnSi_2O_6$ and $CaZnSi_2O_6$.

Table 3.6 Relative density, dielectric properties and thermal expansion data of $CaBSi_2O_6$ (B = Mg, Co, Ni, Mn, Zn) ceramics when sintered at optimum temperatures.

$ABSi_2O_6$	ST(°C)	Relative Density (%)	1 MHz		ε_r (8-12 GHz)		$Q_u \times f$ (GHz)	τ_f (ppm/°C)	α_l (ppm/°C)
			ε_r	tan δ	measured	porosity corrected			
B=Mg	1300/2h	93.5	9.11	0.006	7.5	8.3	53000	-45	+3.7
B=Co	1200/2h	93.6	8.94	0.001	7.7	8.5	28500	-55	0
B=Ni	1300/2h	94.8	9.05	0.005	7.7	8.3	23200	-41	+2.0
*B=Mn	1200/2h	--	7.96	0.009	7.2	--	18000	-31	--
*B=Zn	1150/2h	--	6.90	0.003	7.1	--	8000	-32	--

*The expected phases $CaMnSi_2O_6$ and $CaZnSi_2O_6$ are not formed.

Table 3.6 gives the densification, dielectric properties both at radio and microwave frequencies and thermal expansion data of the $CaBSi_2O_6$ (B = Mg, Co, Ni, Mn, Zn) ceramics sintered at their optimized temperatures. As already mentioned densities near to the theoretical values were achieved for B=Mg, Co and Ni, whereas for B=Mn and Zn the expected phases were not formed. The relative permittivity of the $CaBSi_2O_6$ (B = Mg, Co, Ni) were ~ 9 and dielectric loss tangent of the order of ~ 10^{-3} at radio frequencies (1 MHz). The predominantly covalent nature of Si-O bonds might be the reason for the low values of relative permittivity and loss tangent. The microwave dielectric properties were measured in the range 8-12 GHz. As expected the relative permittivity of $CaBSi_2O_6$ (B = Mg, Co, Ni) ceramics are less than those obtained at 1 MHz. This is due to the absence of polarization mechanisms which are active at radio frequencies (Sebastian, 2008). Since the relative density obtained for all the silicates are less than 95%, the values of ε_r are corrected for porosity using the equation derived by Penn *et al.*, which are also given in table 3.6 (Penn *et al.*, 1997). The porosity corrected values of relative permittivity of $CaBSi_2O_6$ (B = Mg, Co, Ni) ceramics are 8.3, 8.5 and 8.3 respectively. Higher value of relative permittivity is obtained for $CaCoSi_2O_6$

compared to $CaMgSi_2O_6$ and $CaNiSi_2O_6$. This might be due the fact that the ionic polarizability of Co^{2+} ion is higher than that of Mg^{2+} and Ni^{2+}. The ionic polarizability of Co^{2+}, Mg^{2+} and Ni^{2+} are 1.65, 1.32 and 1.23 $Å^3$ respectively (Shannon, 1993). Similar values of relative permittivity obtained for $CaMgSi_2O_6$ and $CaNiSi_2O_6$ can also be well understood based on approximately similar ionic polarizability of Mg^{2+} and Ni^{2+}. Since the relative permittivity obtained at microwave frequencies are less than 10 for all the silicates, high signal propagation speed can be achieved.

Excellent $Q_u \times f$ are also obtained for $CaBSi_2O_6$; 53000, 28500 and 23200 GHz respectively for B = Mg, Co and Ni. The high $Q_u \times f$ value of $CaMgSi_2O_6$ may be due to the low intrinsic loss of the $CaMgSi_2O_6$ ceramics compared to $CaCoSi_2O_6$ and $CaNiSi_2O_6$. The high $Q_u \times f$ values obtained for $CaBSi_2O_6$ (B = Mg, Co, Ni) ensures an efficient use of power supplied to the device and also ensures excellent frequency selectivity. The temperature coefficient of resonant frequency (τ_f) of the silicates are -45, -55 and -41 ppm/^oC respectively for B = Mg, Co and Ni. Generally silicates have a negative value of τ_f. The obtained values of τ_f are not suitable for immediate practical applications and therefore have to be tuned to near zero ppm/^oC by suitable additives having high positive τ_f such as TiO_2, $CaTiO_3$ or $SrTiO_3$ etc (Sebastian, 2008). The results of the measurement of coefficient of thermal expansion (α_l) of $CaBSi_2O_6$ (B = Mg, Co, Ni) ceramics are also shown in table 3.6. The measurement was conducted in the temperature range of 30-500 ^oC. The coefficients of thermal expansion of silicates are 3.7, 1.9 and 2.0 ppm/^oC respectively for $CaMgSi_2O_6$, $CaCoSi_2O_6$and $CaNiSi_2O_6$.

3.6 Conclusions

The $(Sr_{1-x}A_x)_2(Zn_{1-x}B_x)Si_2O_7$ ceramics (A = Ca, Ba and B = Co, Mg, Mn, Ni) were prepared by conventional solid state ceramic route. Solid solutions $(Sr_{1-x}A_x)_2(Zn_{1-x}B_x)Si_2O_7$ having a tetragonal structure were formed for substitutions A = Ca and B = Mg, Mn, Co in the range $0 \leq x \leq 1$. The composition $(Sr_{0.25}Ba_{0.75})_2ZnSi_2O_7$ has a monoclinic crystal structure. In the case of $Sr_2(Zn_{1-x}Ni_x)Si_2O_7$, a mixture of $SrSiO_3$ and NiO phases resulted when $x > 0.50$. The variation of cell parameters and cell volumes of solid solutions $(Sr_{1-x}A_x)_2(Zn_{1-x}B_x)Si_2O_7$ were studied as a function of the value of x. Excellent properties $\varepsilon_r = 8.4$, $Q_u \times f = 105000$ GHz (at 12.628 GHz) and $\tau_f = -51.5$ ppm/$\circ$C

were obtained for $Sr_2ZnSi_2O_7$ for samples sintered at 1475 ^oC/2h. The substitutions at Sr and Zn-sites lowered the $Q_u \times f$ values of $Sr_2ZnSi_2O_7$. The high value of $\tau_f = -51.5$ ppm/◦C of $Sr_2ZnSi_2O_7$ is lowered by adding small amount of $SrTiO_3$. $Sr_2ZnSi_2O_7$ + 2 wt% $SrTiO_3$ sintered at 1450 ^oC/2h has $\varepsilon_r = 8.8$, $Q_u \times f = 60000$ GHz (at 12.585 GHz) and $\tau_f = -13$ ppm/◦C and is a possible material for millimeter wave communication systems and microwave substrates.

The alkaline earth orthosilicates ceramics A_2SiO_4 (A = Ba, Ca, Sr) were prepared by the conventional solid state ceramic route. The formation of Ba_2SiO_4, β-Sr_2SiO_4 and β-Ca_2SiO_4 phases was confirmed by X-ray diffraction studies. The microstructure of Ba_2SiO_4 contained very large grains ~ 25 μm in size, Sr_2SiO_4 had grains of size ~ 10 μm, and very small grains (< 2 μm) for Ca_2SiO_4. The values of ε_r were decreased in the order Ba_2SiO_4 > Sr_2SiO_4 > Ca_2SiO_4 due to the decrease in the ionic polarizability of A^{2+} cations. The $Q_u \times f$ values obtained were 17900 GHz, 19100 GHz and 26100 GHz for Ba_2SiO_4, Sr_2SiO_4 and Ca_2SiO_4 respectively. The τ_f of Ba_2SiO_4 was -17 ppm/^oC, whereas Sr_2SiO_4 and Ca_2SiO_4 exhibited high values of τ_f, -205 ppm/^oC and -89 ppm/^oC respectively. Therefore further modification of τ_f is needed before any practical application of these alkaline earth orthosilicates. The values of α_l were +10.3 ppm/^oC for Ba_2SiO_4, +6.2 ppm/^oC for Sr_2SiO_4 and +7.0 for Ca_2SiO_4.

$CaBSi_2O_6$ (B = Mg, Co, Ni, Mn, Zn) ceramics were prepared by the conventional solid state ceramic route. The phase formation of $CaMgSi_2O_6$, $CaCoSi_2O_6$ and $CaNiSi_2O_6$ were identified using the X-ray diffraction analysis. X-ray studies show the absence of the formation of $CaMnSi_2O_6$ and $CaZnSi_2O_6$. The microstructures of the ceramics contain grains of randomly varying size falling in the range 1-25 μm. The $CaMgSi_2O_6$ ceramics sintered at 1300 ^oC/2h has $\varepsilon_r = 8.3$, $Q_u \times f = 53000$ GHz and $\tau_f = -45$ ppm/◦C in the frequency range 8-12 GHz. $CaCoSi_2O_6$ sintered at 1200 ^oC/2h has $\varepsilon_r = 8.5$, $Q_u \times f = 28500$ GHz and $\tau_f = -55$ ppm/◦C in the same frequency range. Similarly $CaNiSi_2O_6$ sintered at 1300 ^oC/2h has $\varepsilon_r = 8.3$, $Q_u \times f = 23200$ GHz and $\tau_f = -41$ ppm/◦C. in the frequency range 8-12 GHz. The silicates $CaMgSi_2O_6$, $CaCoSi_2O_6$ and $CaNiSi_2O_6$ show small positive values of coefficient of thermal expansion 3.7, 1.9 and 2.0 ppm/^oC respectively.

Chapter 4

Silicate Based Dielectrics for LTCC Applications

4.1 Introduction

The interest on advanced ceramic substrate materials for microwave integrated circuits (MIC) has been increasing in recent decades. Ceramic substrates find wide range of applications especially in wireless access circuits that use millimeter waves for the third generation cell phones, ultra high speed WLAN, optical communications, global positioning system, car anti-collision system on the intelligent transport system (ITS) etc (Sebastian, 2008). Glass filled ceramics, such as low-temperature co-fired ceramics (LTCCs), have found wide use in microelectronic industry as ceramic-packaging materials for integrated multilayer circuits (Jantunen *et al.*, 2002; Imanaka, 2005). The LTCC materials are commonly used in cast tape forms followed by tape lamination and sintering at low temperatures (less than 950 ^{o}C). The low sintering temperature enables the co-firing of substrates with highly conductive and inexpensive metals such as silver or copper. Although there are other multilayer substrate technologies available, such as organic laminates, the LTCC has a unique set of combined characteristics, such as low dielectric loss even at high frequencies, stability of frequency with temperature, low thermal expansion, high strength, and high thermal conductivity, which makes it very attractive as the operational frequencies shift to the microwave region.

Extensive studies have been carried out to develop cost-effective, high-performance, reliable multilayer microwave LTCC devices with embedded metal electrodes (Jantunen *et al.*, 2002; Choi *et al.*, 2003; Hu *et al.*, 2004; Imanaka, 2005). The co-fired ceramic multilayer technology allows the fabrication of three dimensional circuits in which resistors, inductors, capacitors and low loss interconnects are buried within a ceramic block (Kiang, 2003). In this technique, the dielectric layers are commonly fabricated by tape casting, followed by screen printing of the electrodes, lamination, and firing (Mistler *et al.*, 2000; Jantunen *et al.*, 2004; Hu *et al.*, 2005; Imanaka, 2005). Cast tapes used in this technique are fairly thin, flat, and self-supporting, with the thickness generally ranging from 0.010 to 1.27 mm (Mistler *et al.*, 2000; Hu *et al.*, 2005).

The major requirements of an LTCC substrate are described in chapter 1 (section 1.6.3). They are: (i) low dielectric constant $\varepsilon_r < 10$ (to increase the signal speed), (ii) low

dielectric loss (tan δ) or high quality factor (to increase selectivity), (iii) high thermal conductivity (to dissipate the heat generated), (iv) low or matching coefficient of thermal expansion to that of silicon, and (v) low temperature coefficient of resonant frequency τ_f. The key processing issue is however the co-firing, meaning that the sintering temperature of the LTCC tapes must be lower than the melting point of the metal electrodes (960 ^oC in the case of Ag electrode). It should also be noted that any densification of the ceramic at lower temperatures, such as below 800 ^oC, is undesirable as this can prevent the evaporation of the organics and solvents used in conductive pastes and binder and plasticisers causing residual carbon traces in the microstructures (Tummala, 1991; Gektin *et al.*, 1998). This means that the densification of the ceramic should starts above 800 ^oC. In addition, a chemical compatibility between the LTCC material and the electrode must exist.

A common way to develop LTCC's is the addition of low melting, low loss glasses to the main dielectric ceramic. This is one of the most effective and widely accepted method used for LTCC's since it is efficient and cost-effective (Sebastian *et al.*, 2008). Recent researches have shown that the glass addition is a useful method for producing low loss ceramics like Al_2O_3, $BaTiO_3$, CeO_2, $MgAl_2O_4$, $ZnTiO_3$, $MgTiO_3$-$CaTiO_3$ with low sintering temperatures (Mori *et al.*, 2006; Chaouchi *et al.*, 2007; Higuchi *et al.*, 2007; Hsiang *et al.*, 2008; Huang *et al.*, 2008; Anjana *et al.*, 2009). In the case of low ε_r dielectrics, the silicates have received much attention because of their small ε_r values. However, most of the silicates have high sintering temperatures. Efforts have been made to lower the sintering temperature of various low loss silicates like Zn_2SiO_4, Mg_2SiO_4, Li_2MgSiO_4, $Sm_2Si_2O_7$ etc. by the addition of low melting glasses (Sasikala *et al.*, 2008; Zhang *et al.*, 2008; George, Anjana, *et al.*, 2009; Kim, Nguyen, *et al.*, 2009; Renjini *et al.*, 2009; Zhang *et al.*, 2009; Joseph, Sebastian, *et al.*, 2010). In the present work the LTCC compositions based on two silicates, namely $CaMgSi_2O_6$ and $Sr_2ZnSi_2O_7$ ceramics are presented. As already discussed in chapter 3, these silicates have excellent dielectric properties in the microwave range of frequencies. These silicates in pure form are not suitable for LTCC applications due to their high sintering temperature and hence glass addition has been used to reduce the sintering temperature.

4.2 $CaMgSi_2O_6$ based ceramic/glass composites for LTCC applications

4.2.1 Introduction

$CaMgSi_2O_6$ belongs to the class of inosilicates and is a member of the pyroxene group. It has a monoclinic structure with space group C2/c. The $CaMgSi_2O_6$ is a low relative permittivity material with interesting microwave dielectric properties, which have already been discussed in chapter 3. $CaMgSi_2O_6$ ceramics, sintered at 1300^oC/2h has a densification of ~ 93% and has ε_r = 8.3, $Q_u \times f$= 53,000 GHz (10.20 GHz) and τ_f = −45 ppm/◦C. The high sintering temperature makes it impossible for using this ceramic for LTCC applications. Therefore the sintering temperature has to be reduced below 950 ^oC for the purpose of co-firing with highly conducting metal pastes used for conductor linings. For this purpose glass addition to the ceramic was adopted, as this technique is easy and cost effective. In the present work it is attempted to reduce the sintering temperature of $CaMgSi_2O_6$ ceramics by the addition of low melting borosilicate glasses like B_2O_3, BBS, MBS, LBS, ZBS, and LMZBS.

4.2.2 Experimental

(i) Preparation of ceramic and glass

The $CaMgSi_2O_6$ (CMS) ceramics were prepared by the conventional solid-state ceramic route as described in chapter 2. The chemicals used were $CaCO_3$, SiO_2, and $(MgCO_3)_4Mg(OH)_2.5H_2O$ (Aldrich Chemical Company, 99.9%). The glass powders used in this investigation were B_2O_3 (B), $30BaO\text{-}60B_2O_3\text{-}10SiO_2$ (BBS), $60ZnO\text{-}30B_2O_3\text{-}10SiO_2$ (ZBS), $40PbO\text{-}20B_2O_3\text{-}40SiO_2$ (PBS), $40MgO\text{-}40B_2O_3\text{-}20SiO_2$ (MBS), $35.14Li_2O\text{-}31.66B_2O_3\text{-}33.2SiO_2$ (LBS), and $20Li_2O\text{-}20MgO\text{-}20ZnO\text{-}20B_2O_3\text{-}20SiO_2$ (LMZBS). They were synthesized from high purity oxide chemicals $BaCO_3$, Li_2CO_3, PbO, $(MgCO_3)_4Mg(OH)_2.5H_2O$, ZnO, B_2O_3, and SiO_2 (Aldrich Chemical Company, 99.9%). The powders were mixed in the required ratio by weight in an agate mortar for 2 hours using distilled water as the medium. They were dried, melted in platinum crucible above their softening point, quenched and powdered (see chapter 2). Quenching is done by immediately cooling the melted glass to room temperature.

(ii) Preparation of ceramic/glass composite

The CMS is mixed with different wt % of glass powders in aqueous medium to form thick slurry. A 4 wt% solution of Polyvinyl Alcohol (molecular weight 22,000, BDH Lab Suppliers, England) was added as a binder. These slurries were then dried and ground and then pressed into cylindrical compacts of different thickness in a 11 mm diameter die under a pressure of 100 MPa. The green compacts are initially fired at a rate of 3 ^{o}C/min up to 600 ^{o}C and then at a rate of 12 ^{o}C /min to the sintering temperature. An intermediate soaking at 600 ^{o}C for 30 minutes was given to expel the binder. In practice, the preparation conditions differ depending upon the composition, reactivity, grain growth etc. Hence it is necessary to optimize the processing conditions in order to get the final sintered compacts with desired properties. Optimization is done by experimental iterations. The optimized sintering temperatures were in the range 900 ^{o}C to 1300 ^{o}C depending on the amount of glass loading.

(iii) Structure, microstructure and dielectric properties

The crystal structure and phase purity of the powdered samples were studied by X-ray diffraction technique and SEM micrograph was recorded from the surface of thermally etched sample using scanning electron microscope as explained in chapter 2. The densities of sintered samples were measured using Archimedes method. The theoretical density, *D* of the glass added $CaMgSi_2O_6$ was calculated using the equation (2.24).

For low frequency (50Hz-5MHz) and microwave dielectric measurements the methods described in sections 2.7 and 2.8 of chapter 2 are adopted. Low frequency measurements were carried out using a LCR meter. The variation of relative permittivity at 1 MHz was also measured in the temperature range -25 ^{o}C to 70 ^{o}C using the LCR meter. The microwave dielectric properties were measured in the frequency range 8-14 GHz by using a Scalar Network Analyzer (Aeroflex, IFR 6823 model) by employing Hakki and Coleman (Hakki *et al.*, 1960) and resonant cavity methods (Krupka, Derzakowski, Riddle and Jarvis, 1998) respectively. The measured relative permittivity values were corrected for porosity using the equation (1.18) (Penn *et al.*, 1997). The

thermal contraction of the green samples was studied using a dilatometer in the temperature range 30-1000 ^{o}C. The change in the linear dimensions of the samples was measured using the dilatometer in the temperature range 30-500 ^{o}C. The coefficients of thermal expansion (α_l) can then be calculated using equation (2.24). The measurement of microwave dielectric properties was carried out on several samples for consistency.

4.2.3 Results and discussions

(i) Effect of glass addition on the sintering temperature of $CaMgSi_2O_6$

$CaMgSi_2O_6$ (CMS) ceramics sintered at 1300 ^{o}C/2h has a densification of ~ 93% and has ε_r = 8.3, $Q_u \times f$= 53,000 GHz (10.20 GHz) and τ_f = −45 ppm/◦C (see chapter 3). To reduce the sintering temperature of CMS for making it useful for LTCC applications, different glasses such as B, BBS, MBS, ZBS, PBS, LBS, and LMZBS are used. The physical and dielectric properties of these glasses are reported earlier (Wu *et al.*, 1999; Park *et al.*, 2004; Surendran, Mohanan, *et al.*, 2004; Renjini *et al.*, 2009).

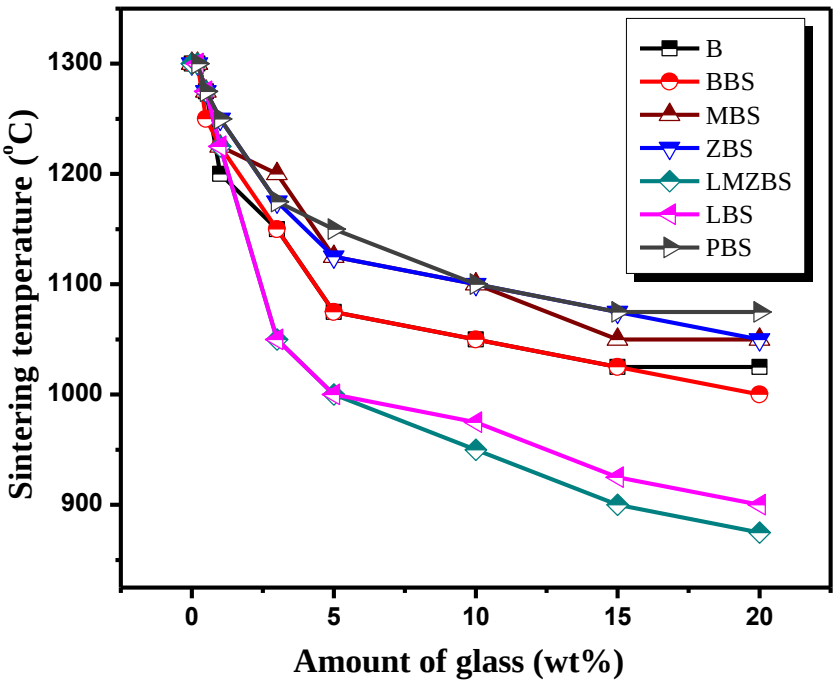

Figure 4.1 Variation of the sintering temperature of the CMS/glass composites with different wt% of glass addition.

The variation of sintering temperature of CMS/glass composites as a function of different wt% of added glasses is shown in Fig. 4.1. It can be seen that most of the glasses (except LBS and LMZBS) used in this study are not effective in lowering the sintering temperature. The addition of 15 wt% of LBS and LMZBS glasses reduced the sintering temperature of the ceramic/glass composite to 925^{o}C and 900^{o}C respectively. Therefore by using proper amount of LBS and LMZBS glasses, the sintering temperature of CMS can be reduced to below the melting point of Ag, which is very essential for the co-firing process of the ceramic with Ag. The liquid phases formed by the melting of the glasses, penetrate between grains and exert an attractive force, pulling them together. The combination of these forces and the lubricating effect of the liquid as it penetrate between grains leads to densification at lower temperatures and in shorter times by allowing pore elimination to proceed to completion. It may also be noted that only the Li containing glasses are effective in decreasing the sintering temperature of CMS. The alkali ion (Li^{+}) can act as a modifier, breaking the rigid bonds in SiO_2 thereby considerably reducing the sintering temperature of the ceramics (Hippel, 1954). Hence extensive studies have been done only for the composites containing LBS and LMZBS glasses.

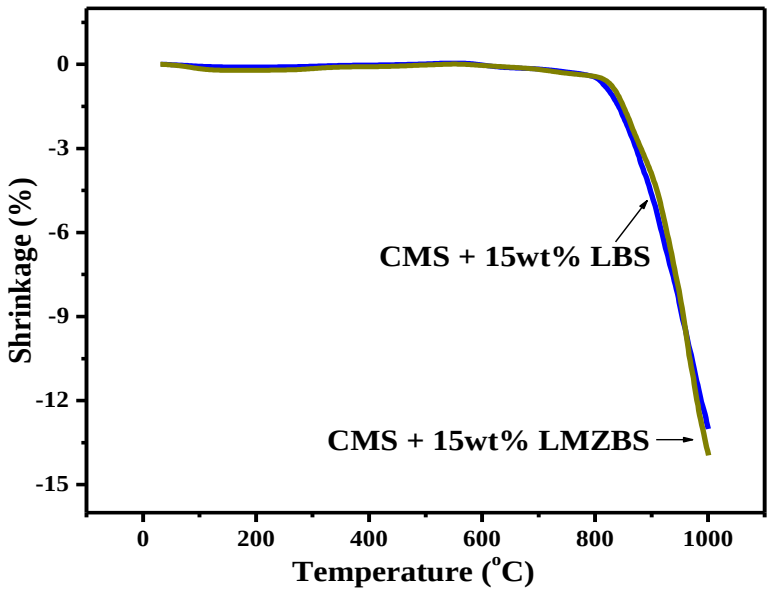

Figure 4.2 Percentage shrinkage of CMS+15 wt% LBS and CMS+15 wt% LMZBS composites as a function of temperature.

Fig. 4.2 shows the variation of linear dimension of CMS+15wt% LBS and CMS+15wt% LMZBS samples as a function of temperature. For both of the samples, the shrinkage starts around 800 ^{o}C, but was complete only beyond 1000 ^{o}C. However, the sintering temperatures chosen in this study was less than 1000 ^{o}C. This is because of the good dielectric properties, especially the $Q_u \times f$ values obtained at these temperatures, which will be explained later in this chapter.

(ii) Structure and microstructure

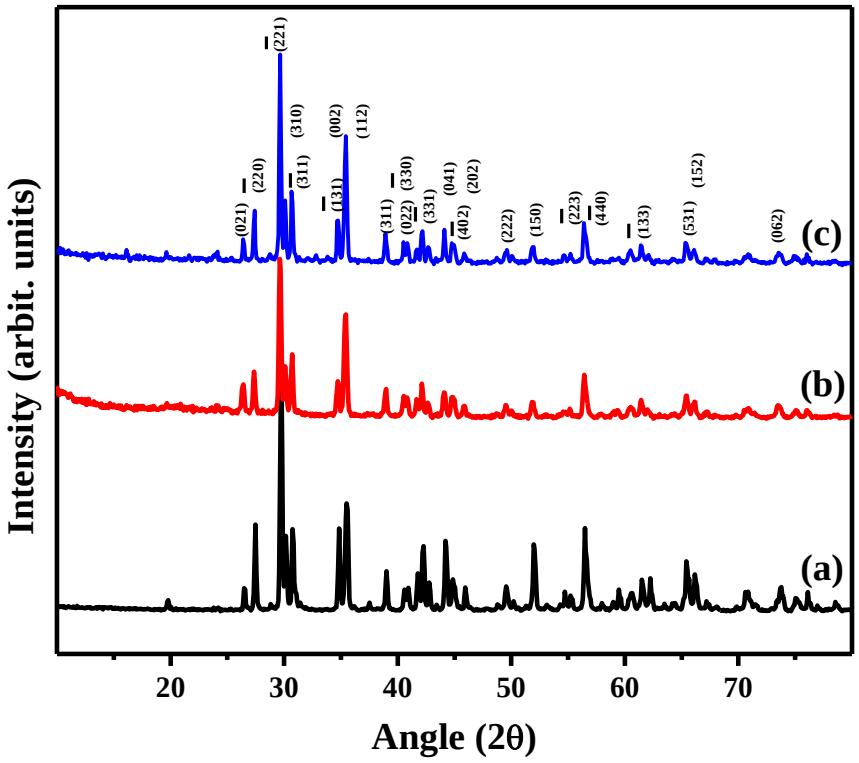

Figure 4.3 Powder XRD patterns for (a) CMS sintered at 1300 ^{o}C/2h (b) CMS+15 wt% LBS sintered at 925 ^{o}C and (c) CMS+15 wt% LMZBS sintered at 900 ^{o}C.

Fig. 4.3(a-c) shows the XRD pattern of pure CMS and its composites containing 15wt% of LBS and LMZBS glass. The powder diffraction pattern of CMS is indexed based on ICDD file card no. 19-0239. All recognizable diffraction peaks can be readily indexed to the C2/c monoclinic structure with lattice parameters of a = 9.748 Å, b = 8.926 Å, c = 5.250 Å and β = 105.8^{o}, consistent with the standard data file. Even though large amount of glasses (15 wt%) are present, no additional peaks are observed (Fig. 4.3

(b-c)), which means that there is no chemical reaction between the components of the glass and the ceramics. Hence, it may be concluded that the glass phases exist as liquid phase during sintering and retains its amorphous nature even after the temperature treatment.

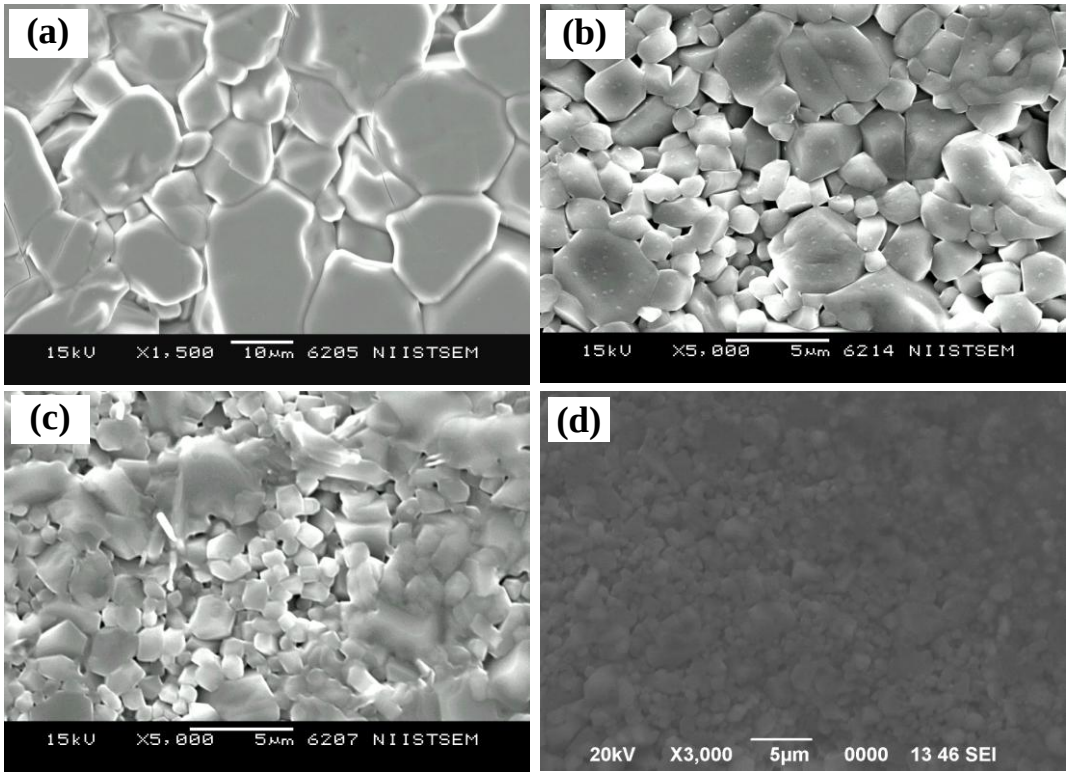

Figure 4.4 SEM images of (a) CMS sintered at 1300 ^{o}C/2h (b) CMS+5 wt% LMZBS sintered at 1000 ^{o}C/2h and (c) CMS+15 wt% LMZBS sintered at 900 ^{o}C/2h (d) CMS+15 wt% LBS sintered at 925 ^{o}C/2h.

The effect of liquid phase on the grain size of the CMS ceramics has been studied taking LMZBS glass as an example. Fig. 4.4(a-c) shows SEM images of pure CMS, CMS+5wt% LMZBS, and CMS+15wt% LMZBS respectively, sintered at optimum temperatures. From Fig. 4.4 (a) it is clear that pure CMS sintered at 1300 ^{o}C has an average grain size of 10 μm. The presence of liquid phase is apparent from Fig. 4.4(b-c). As the amount of liquid phase increases the grain size decreases considerably. It is because of the decrease in sintering temperature with the increase in glass phase (Huang *et al.*, 2003). Grains of size 1-3 μm are seen in the case of CMS+5wt% LMZBS, sintered at 1000 ^{o}C/2h (Fig. 4.4 (b)). Still smaller grains are observed by the addition of 15 wt% LMZBS glass with CMS sintered at 900 ^{o}C/2h. Most of the grains have a size in the

range of 0.2-2 μm. This large variation in grain size is possibly due to the large amount of liquid phase and differences in the sintering temperature. SEM image of CMS+15wt% LBS sintered at 925 ^{o}C/2h is shown in Fig. 4.4(d). The ceramic seems to have very small grains (<1 μm) with high degree of porosity, probably because of the evaporation of the low melting LBS glass.

(iii) Microwave dielectric properties

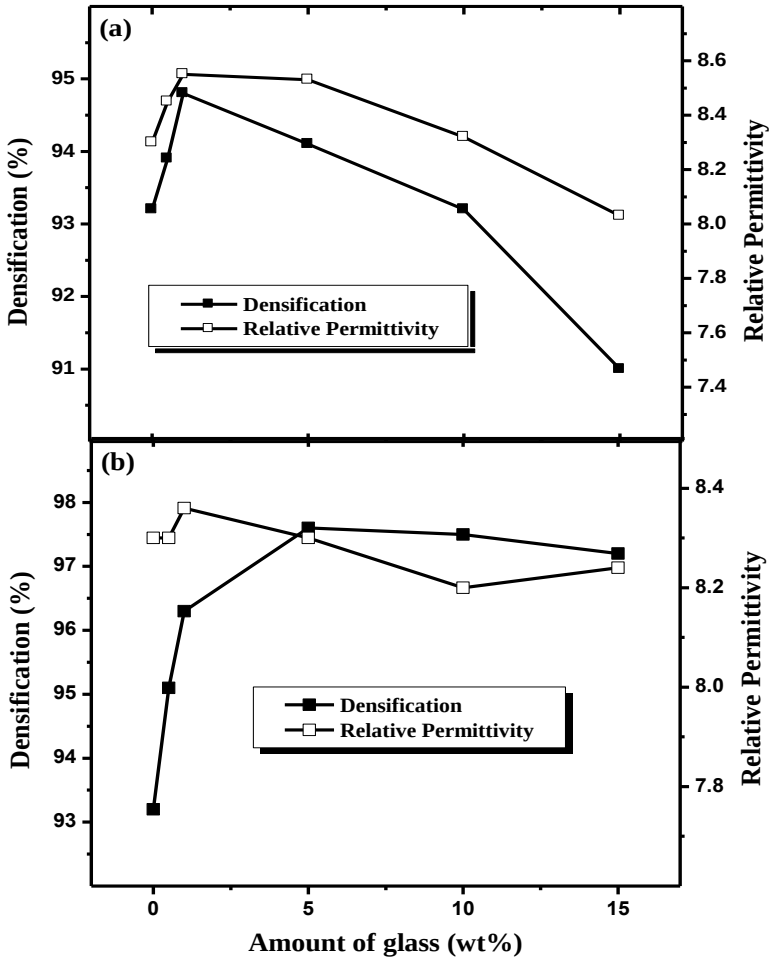

Figure 4.5 Variation of densification and porosity corrected relative permittivity of (a) CMS/LBS (b) CMS/LMZBS composites as a function of different wt% of glass addition.

Fig. 4.5 shows the variation of densification and relative permittivity with different wt% of glass addition. For pure CMS sintered at 1300 ^{o}C/2h, the densification is

about 93%. From Fig. 4.5(a) it is clear that the densification increases with LBS content to reach a maximum value of 95% for CMS+1wt% LBS composite. With further addition of LBS glass, the densification decreases to 91% for CMS+15wt% LBS, which is also evident from the SEM image shown in Fig. 4.4(d).

The variation of porosity corrected relative permittivity is also shown in Fig. 4.5(a). The variation shows the same trend as that of densification. For CMS/LMZBS composites, the densification reaches a maximum value of 97% for 5wt% of LMZBS addition. The values of relative permittivity are in the range 8.2 to 8.3 for the entire range of composition in the case of CMS/LMZBS composites. This is because of the good densification of CMS/LMZBS composites and also due to relatively high value of ε_r for LMZBS glass (7.4) than LBS glass (6.5).

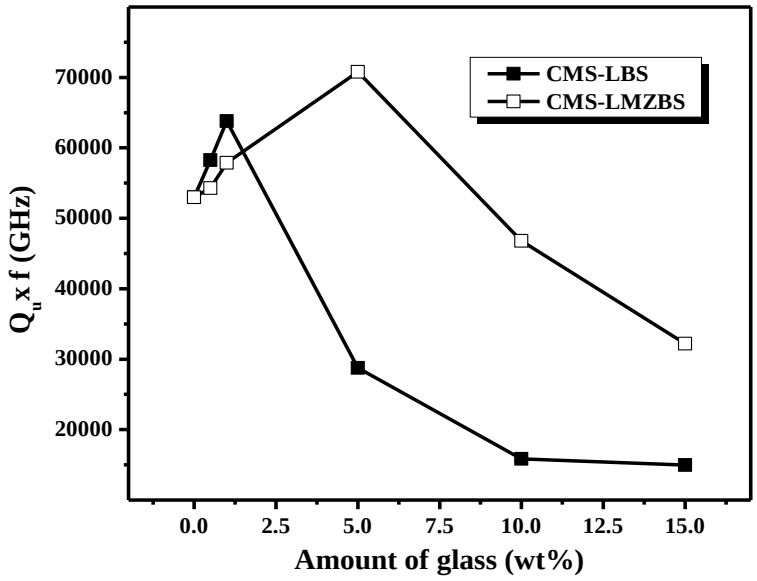

Figure 4.6 Variation of $Q_u \times f$ values of CMS/LBS and CMS/LMZBS composites as a function of different wt% of glass addition.

The variation of quality factor ($Q_u \times f$) of the ceramic/glass composite with the increase in glass content is shown in Fig. 4.6. In the case of CMS/LBS composite, the $Q_u \times f$ value increases to a maximum value of 64000 GHz at 10.27 GHz for 1wt% of LBS glass addition with ε_r = 8.5 and τ_f = −45 ppm/◦C. As the amount of LBS glass increases, the $Q_u \times f$ value decreases to 15000 GHz (10.17 GHz) for the composition CMS+15wt%

LBS, sintered at 925°C. This composition has ε_r = 8 and τ_f = −49 ppm/◦C. Fig. 4.6 also shows the variation of $Q_u \times f$ values of CMS/LMZBS composites. The best dielectric properties obtained are $Q_u \times f$ = 71000 GHz (10.22 GHz), ε_r = 8.3 and τ_f = −47 ppm/◦C, for the composite containing 5wt% of LMZBS glass. Further increase in the glass content causes the $Q_u \times f$ values to degrade sharply. In the case of CMS+15wt% LMZBS composite sintered at 900°C, the dielectric properties obtained are $Q_u \times f$ = 32000 GHz (10.15 GHz), ε_r = 8.2 and τ_f = −48 ppm/◦C.

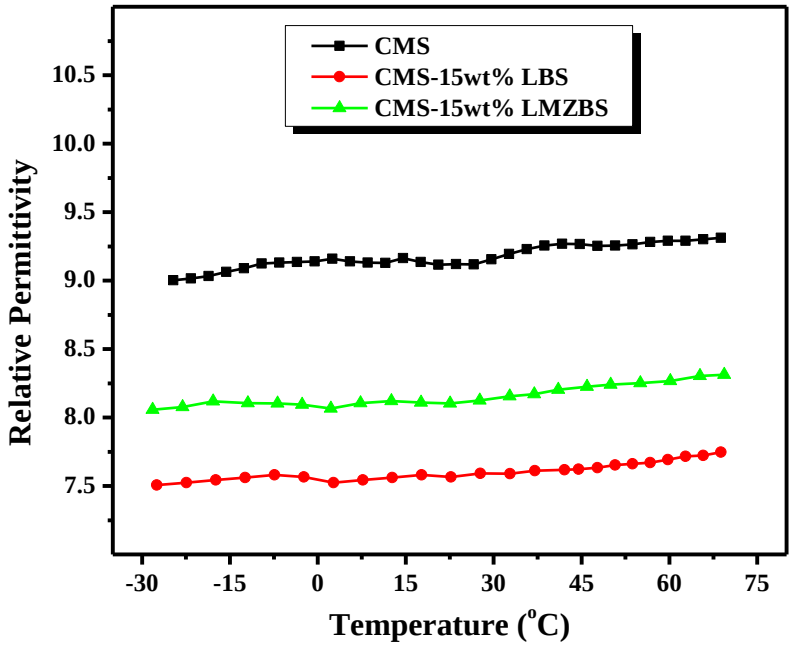

Fig. 4.7 Variation of relative permittivity of CMS and CMS+15 wt% glass composites at 1 MHz as a function of temperature.

In the case of both ceramic/glass composites, the variation of $Q_u \times f$ is similar to that of densification. Hence it is obvious that a limited amount of glass addition can improve the $Q_u \times f$ values. This can be due to the improved densification obtained with the help of LBS and LMZBS glasses. Addition of large amount of glass decreases the $Q_u \times f$ values due to a decrease in densification and also due to the fact that glasses have higher dielectric losses. A comparison of $Q_u \times f$ values of CMS/LBS and CMS/LMZBS composite indicates that better properties are obtained in the case of CMS/LMZBS

composites. The high Li content (35.14 wt%) of LBS glass must be the reason for the decreased $Q_u \times f$ values. This is due to the fact that the alkali ions, which are weakly held in the glassy network, absorb energy and eventually give rise to dielectric loss (Sebastian *et al.*, 2008). LMZBS glass has less Li content (20 wt%) compared to LBS and hence give better $Q_u \times f$ values. It is also reported that the presence of ZnO can improve the value of $Q_u \times f$ (Huang *et al.*, 2008). An increase in the negative direction of τ_f values is observed with an increase in the glass content. This is due to the negative τ_f values of both LBS and LMZBS glasses (Sebastian *et al.*, 2008).

The variation of relative permittivity (at 1 MHz) of CMS, CMS+15wt% LBS, and CMS+15wt% LMZBS as a function of temperature is shown in Fig. 4.7. A small increase in relative permittivity is observed for all compositions with an increase in temperature. The changes (%) observed in the value of relative permittivity as the temperature increases from -25 ^oC to 70 ^oC are only 3.4%, 3.1% and 3.3% for CMS, CMS+15wt% LBS, and CMS+15wt% LMZBS respectively. At very low temperatures the amplitude of thermal vibration of the ions gets reduced thereby reducing the polarization, which in turn decreases the relative permittivity. As the temperature increases the ions gain more energy and vibrate in higher amplitudes. This can be the reason for the small increase in the relative permittivity with temperature.

(iv) Compatibility with Ag

In order to study the reactivity of Ag with the glass added ceramics, 20 wt% of Ag was added to both CMS+15wt% LBS, and CMS+15wt% LMZBS compositions. Fig. 4.8 (b-c) shows the powder XRD patterns for CMS+15wt% LBS+20wt% Ag, and CMS+15wt% LMZBS+20wt% Ag. The XRD pattern of pure CMS is also given for a comparison (Fig. 4.8(a)). The powder diffraction pattern of Ag was indexed based on ICDD file card No. 4-783. All the major peaks of CMS as well as that of Ag are observed, indicating the absence of any chemical reaction between the ceramic/glass composite and the Ag particles. The SEM images of CMS+15wt% LBS+20wt% Ag and CMS+15wt% LMZBS+20wt% Ag, shown in Fig. 4.9 also indicate the absence of chemical reaction of Ag powder with the ceramic-glass composite. Bright spherical particles having uniform distribution and size ($\leq$1 μm) clearly indicate the presence of

unreacted Ag particles. Hence it may be concluded that Ag remains unreacted with the ceramic/glass composite, thereby making it possible for the co-firing of Ag electrodes with the CMS/glass composite.

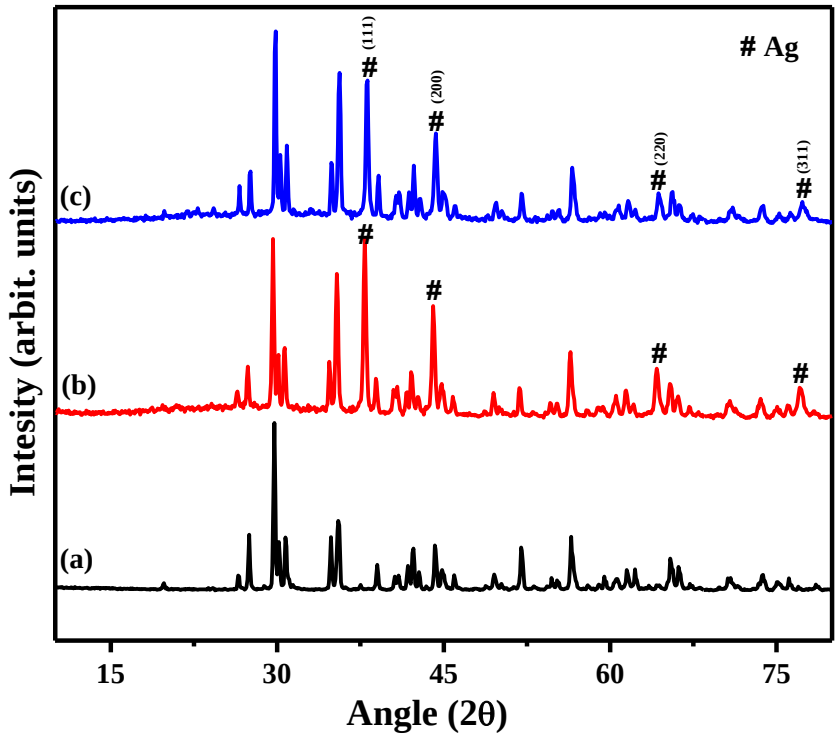

Figure 4.8 Powder XRD patterns for (a) CMS sintered at 1300 ^{o}C/2h (b) CMS+15 wt% LBS+20 wt% Ag sintered at 925 ^{o}C and (c) CMS+15 wt% LMZBS+20 wt% Ag sintered at 900 ^{o}C.

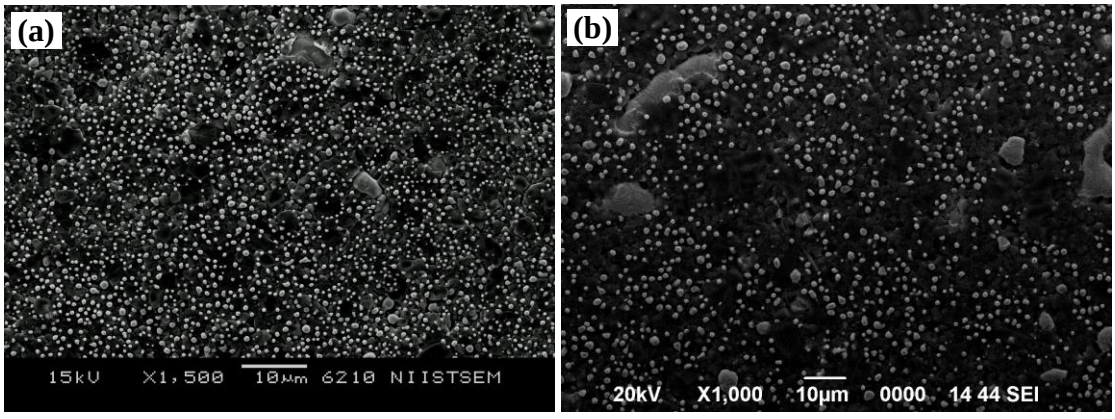

Figure 4.9 SEM images of (a) CMS+15 wt% LBS+20 wt% Ag sintered at 925^{o}C and (b) CMS+15 wt% LMZBS+20 wt% Ag sintered at 900^{o}C. Uniform distribution of fine Ag particles can be clearly seen.

(v) Coefficient of thermal expansion (α_l)

As already explained in chapter 1, the coefficient of thermal expansion (α_l) is an important parameter to be considered for the substrate application of ceramic materials. The value of α_l of the ceramic materials should be nearly equal to that of Si, which is ~ 4 ppm/^oC. Fig. 4.10 shows the variation of linear dimensions of CMS, CMS+15 wt% LBS and CMS+15 wt% LMZBS with operating temperature. All the samples show an increase in their linear dimensions with temperature. Glass added ceramics expand more than that of pure ceramic. Glasses in general have large value of thermal expansion compared to the ceramics, which when incorporated into the ceramics further increases the value of α_l of the ceramic. The values of α_l, calculated in the temperature range 30 ^oC to 500 ^oC using the equation (2.24) are +3.7, +5.14 and +5.85 for CMS, CMS+15wt% LBS, and CMS+15wt% LMZBS respectively. Therefore it can be concluded that the thermal expansion of the ceramic/glass composites are approximately equal to that of Si and hence are suitable for LTCC application.

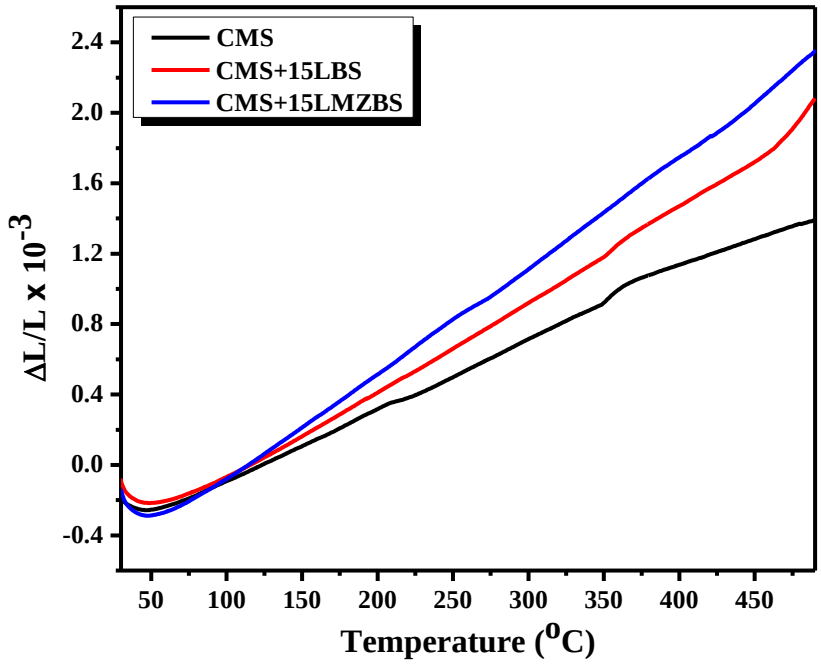

Figure 4.10 Variation of linear dimensions of CMS, CMS+15 wt% LBS and CMS+15 wt% LMZBS with operating temperature.

4.3 Tape casting and dielectric properties of $Sr_2ZnSi_2O_7$ based ceramic/glass composite for LTCC applications

4.3.1 Introduction

In the present work the $Sr_2ZnSi_2O_7$ (SZS) ceramics which has a tetragonal crystal structure with space group $P\bar{4}21m$ (no. 113) is used as a basic dielectric to develop a novel LTCC composition (Hao *et al.*, 2007). The SZS ceramics sintered at 1475 ^oC/2h has ε_r = 8.5, $Q_u \times f$= 105000 GHz (at 12.628 GHz) and τ_f = −51.5 ppm/^oC (Joseph *et al.*, 2009). Therefore as in the case of $CaMgSi_2O_6$, the sintering temperature of pure ceramic is not suitable for LTCC applications. On the basis of the results of $CaMgSi_2O_6$/glass composites, LMZBS ($20Li_2O$-$20MgO$-$20ZnO$-$20B_2O_3$-$20SiO_2$) glass is selected to reduce the sintering temperature of SZS ceramics. A detailed study of the effect of LMZBS glass on the microwave dielectric properties of SZS ceramics are presented in this study. An attempt is made to tune the τ_f of the glass ceramic composite using $SrTiO_3$. Moreover ceramic tapes were cast using a tape casting machine. The properties of the novel LTCC composition as well as the effect of tape casting, stacking and firing on its electrical properties are presented, the latter one being an important issue rarely reported. Furthermore, reactivity of pure Ag with the developed LTCC composition is also investigated.

4.3.2 Experimental

(i) Ceramic and glass preparation

The preparation of SZS and $SrTiO_3$ are explained in chapter 3. Solid-state ceramic route was used and the starting powders used were $SrCO_3$, ZnO and SiO_2, TiO_2 (99.8 %) (Aldrich Chemical Company, 99.9 %, St. Louis, MO). The glass powder used in this investigation was $20Li_2O$-$20MgO$-$20ZnO$-$20B_2O_3$-$20SiO_2$ (LMZBS). It was synthesized from high purity oxides (Li_2CO_3, $(MgCO_3)_4Mg(OH)_2.5H_2O$, ZnO, B_2O_3, and SiO_2, Aldrich Chemical Company, 99.9 %). The powders were mixed in the required ratio by weight in an agate mortar for 2 h using distilled water as the medium. The resulting slurry was dried in a oven to remove the water content and then melted in a platinum crucible at

1000 ^{o}C. It was then quenched down to room temperature to form the LMZBS glass, which was thoroughly ground to make a fine powder.

(ii) Preparation and characterization of dry pressed compacts

The SZS was mixed with different load of LMZBS glass powder in an agate mortar for 2 hours using aqueous medium to form thick slurry.A 4 wt% solution of polyvinyl alcohol was added as a binder. After drying and grinding in an agate mortar, cylindrical compacts were pressed (~ 11 × 6 mm) under a uniaxial pressure of 150 MPa. Optimization of the sintering temperature for all compositions was performed by experimental iterations. Five samples of the same composition were kept at five different temperatures and the densities of the resulting samples were measured. The temperature corresponding to the highest density is the optimized sintering temperature of that composition. The highest density is usually associated with highest relative permittivity as well as quality factor due to the fact that amount of porosity is a minimum. The theoretical density, D of the glass added SZS was calculated using the equation (2.24). The density of SZS and LMZBS were 8.1 g/cm^3 and 2.75 g/cm^3, respectively (Joseph *et al.*, 2009; Renjini *et al.*, 2009). The theoretical density values calculated using the above equation will give an account of the maximum density of different compositions that can be achieved by sintering. The bulk density of the samples obtained was measured by Archimedes method. The term relative density, which is the ratio of measured density to theoretical density, is used to give an account of the percentage density of the samples achieved. The shrinkage characteristics of the samples were measured using a dilatometer. The shrinkage characteristics give knowledge of the sintering temperature at which the densification process has started as well as completed. The crystal structure was studied by X-ray diffraction technique using Ni-filtered CuKα radiation and scanning electron microscope was used to investigate the microstructure of thermally etched samples. The X-ray diffraction patterns in conjunction with the SEM images were employed to identify the presence of different phases such as SZS, $SrTiO_3$ and Ag. The microwave dielectric properties were measured in the frequency range 10-15 GHz by using a scalar network analyzer (Aeroflex, IFR 6823 model, Cupertino, USA). The measured values of the relative permittivity were corrected for porosity using the

equation (1.18) (Penn *et al.*, 1997). The temperature-coefficient of resonant frequencies (τ_f) were measured by heating the samples in the temperature range 25–85 °C using the TE_{011} mode under the end-shorted condition.

(iii) Preparation and characterization of laminated tapes

The SZS + 15 wt% LMZBS powder was mixed with solvents and a dispersant in a ball mill for 24 h. It was then mixed with plasticizers and a binder for another 24 h. The solvents used were ethanol and xylene (Aldrich Chemical), the dispersant was Blown Z-3 Menhaden fish oil, the binder was polyvinyl butyral (B98), and the plasticizers were butyl benzyl phthalate (S160) and polyalkylene glycol (UCON 50HB2000). The average molecular weight of UCON 50HB2000 is 2660 g/mol. This slurry composition is denoted as a polyvinyl butyral-based binder system and the amounts of solvents, dispersant, binder and plasticizers were 33, 1.2, 3.8, 2 wt% for 60 wt% of SZS/LMZBS powder. This composition produces Newtonian type viscosity (Joshi *et al.*, 2002) commonly required for tape casting. All the organic additives were supplied by Richard E. Mistler, Yardley, PA. The tape casting was carried out with a laboratory caster (Unicaster 2000, Leeds, UK) with a single 300 μm wide doctor blade and a casting speed of 0.8 m/min after which the tapes were uniaxially laminated under a pressure of 20 MPa and fired.

Thermal gravimetric analysis (TGA) and differential thermal analysis (DTA) of green tapes were carried out in an atmosphere of nitrogen with 5 ^{o}C/min heating rate using PerkinElmer analyzer (Massachusetts, USA). This gave an estimation of the temperature at which the slurry organics start to burn out and the melting of the glassy phase begins. Furthermore the investigation of the phase and microstructure of the tape samples were performed using XRD and SEM as explained earlier.

The ε_r and tan δ of sintered tapes at cryogenic temperatures were measured using Split Post Dielectric Resonator (SPDR) technique at 20 GHz (Krupka *et al.*, 2001). $TE_{01\delta}$ mode was used for the measurements since this mode is insensitive to the presence of air gaps perpendicular to Z-axis of the resonator. The procedure for cryogenic microwave characterization is well explained in reference (Sudheendran *et al.*, 2009). The measurement system consisted of Network Analyzer (Agilent 8364B), closed cycle

refrigerator (ARS Cryo DE204), temperature controller (Lakeshore 340), vacuum Dewar, PC and the split post dielectric resonator operating in the transmission mode. The cryogenic temperatures are expressed in K rather than ^{o}C for convenience.

4.3.3. Results and discussion

(a) Dry pressed Samples

(i) Effect of glass addition on the sintering temperature

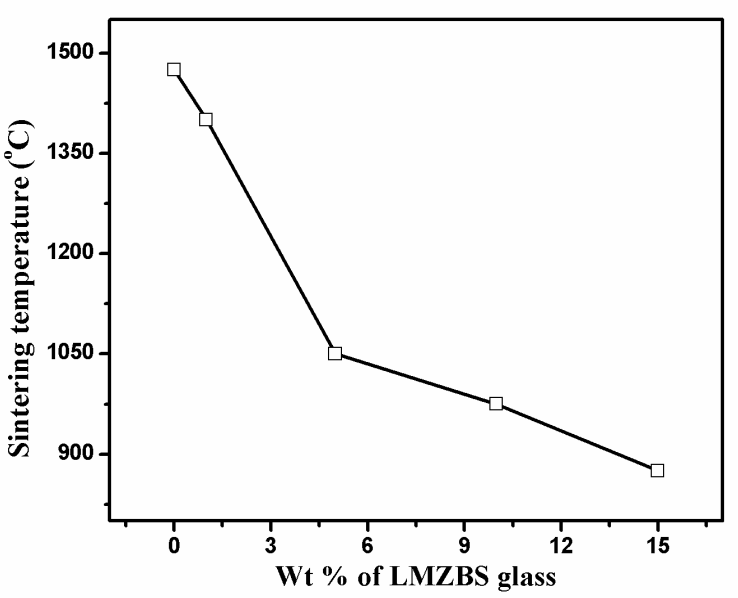

Figure 4.11 The variation of sintering temperature of SZS/glass composites as a function of different wt% of glass addition.

Fig. 4.11 shows the variation of sintering temperature of SZS/glass composites as a function of different wt% of LMZBS glass addition. The figure shows that 15 wt% of LMZBS glass lowers the sintering temperature of the SZS ceramic from 1475 ^{o}C to 875 ^{o}C. The liquid phase formed by the melting of LMZBS glass enhances densification by the process of liquid phase sintering (Joseph, Sebastian, *et al.*, 2010). The decrease in the sintering temperature with glass addition is also evident from the shrinkage characteristics of pure SZS and glass added SZS, which is shown in Fig. 4.12. There is a gradual decrease in the onset of densification temperature with the increase in glass content. A comparison of these curves indicates the lowering of the sintering temperature

of SZS ceramics with the increase in glass loading. For pure SZS, the shrinkage does not start even at 1100 ^{o}C, whereas for 15 wt% glass added SZS shrinkage starts around 800 ^{o}C and is almost complete when the temperature becomes ~900 ^{o}C. A linear shrinkage of ~ 17 % can be observed for the SZS + 15 wt% LMZBS composite.

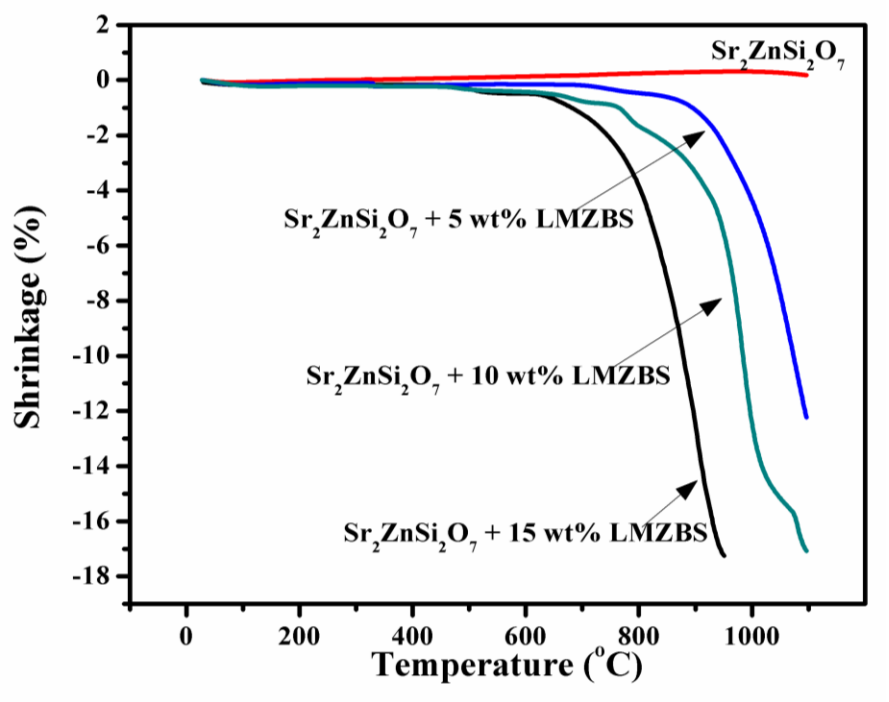

Figure 4.12 The linear shrinkage (%) of SZS/LMZBS composites as a function of temperature for various amount of glass content.

(ii) Analysis of phase and microstructure

Fig. 4.13 (a-c) shows the XRD patterns of LMZBS glass, pure SZS and the composite containing 15 wt% of LMZBS glass. The absence of any additional diffraction peaks other than SZS indicates the amorphous nature of LMZBS. All recognizable reflection peaks of SZS can be readily indexed based on $P\bar{4}21m$ (no. 113) having tetragonal structure with lattice parameters of a = 8.0282 Å and c = 5.1851 Å, which is consistent with the standard data file. Even though large amount of glass (15 wt%) is present, no additional peaks were observed in Fig. 4.13 (b), indicating negligible chemical reactions between the ceramic and LMZBS glass.

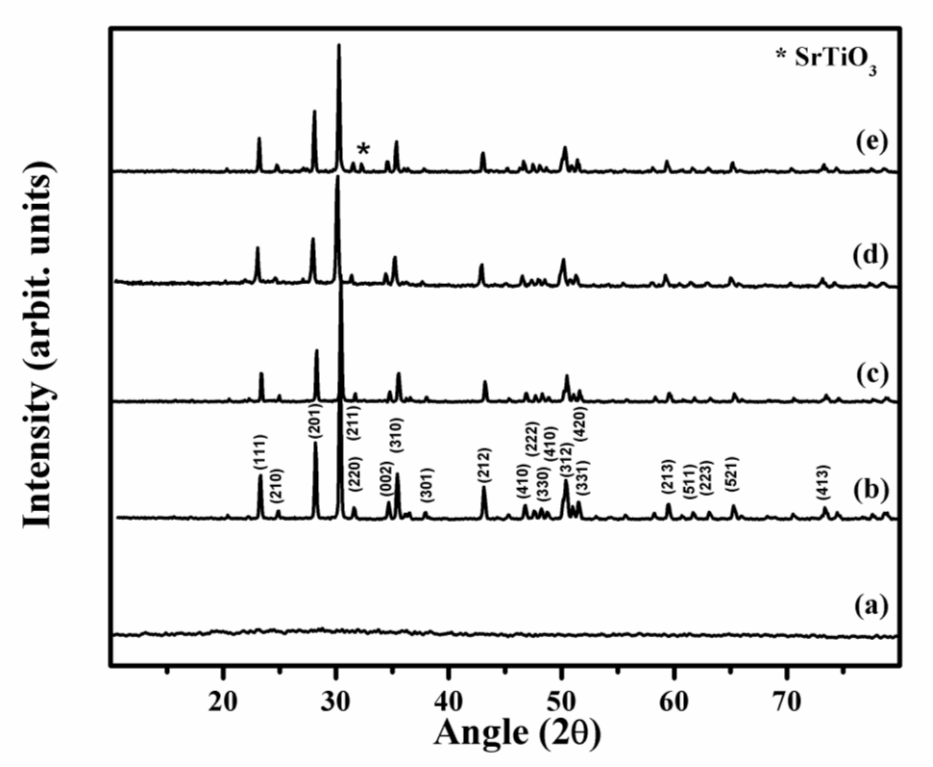

Figure 4.13 Powder XRD patterns for (a) LMZBS glass (b) pure SZS sintered at 1475 ^{o}C/2h (c) SZS + 15 wt% LMZBS sintered at 875 ^{o}C (d) stacked tapes of SZS + 15 wt% LMZBS sintered at 825 ^{o}C (e) SZS + 15 wt% LMZBS + 4 wt% $SrTiO_3$ sintered at 875 ^{o}C.

Fig. 4.14 (a-c) shows SEM images of pure SZS, SZS + 1 wt% LMZBS, and SZS + 15 wt% LMZBS ceramic/glass composites respectively, sintered at optimized temperatures. From Fig. 4.14 (a) it is clear that pure SZS sintered at 1475 ^{o}C has an average grain size of ~ 5-8 μm. The effect of liquid phase on the grain size is apparent from Fig. 4.14 (b-c). Grains of varying size in the range ~2-8 μm are seen in the case of SZS + 1 wt% LMZBS, sintered at 1400 ^{o}C/2h (Fig. 4.13 (b)). However, large amount of LMZBS glass reduced grain growth of the SZS phase considerably. Most of the grains have a size in the range ~1-3 μm when sintered at 875 ^{o}C/2h. The reduction in grain size is mainly due to the decrease of sintering temperature with increase in glass content.

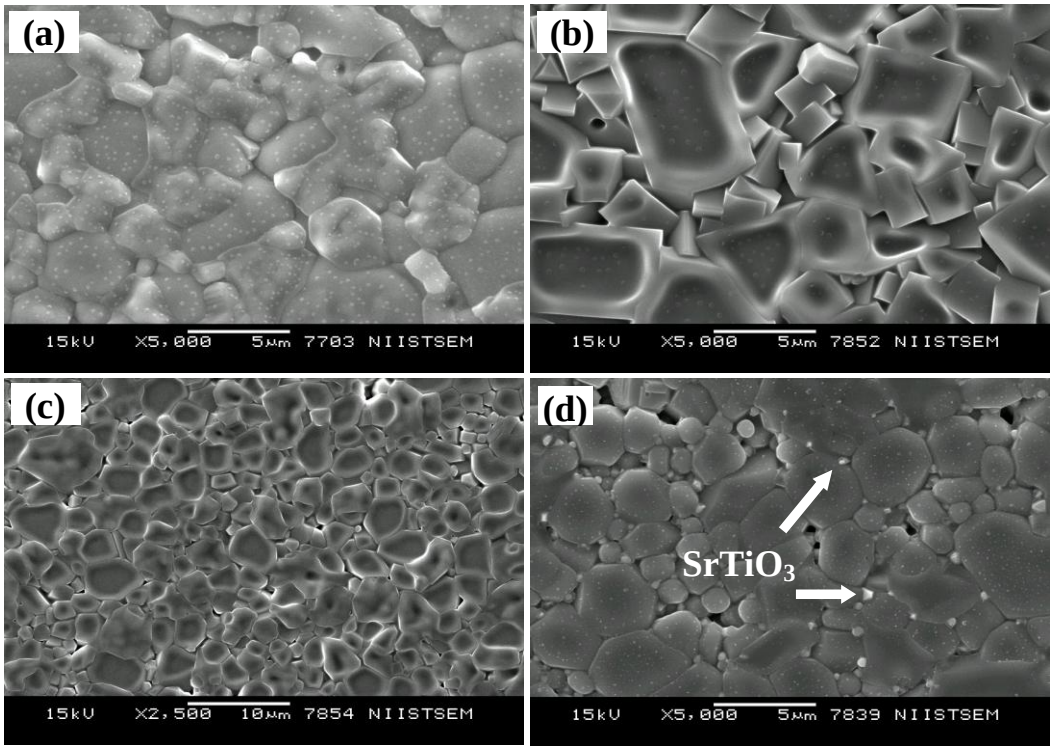

Figure 4.14 SEM images of (a) pure SZS sintered at 1475 ^{o}C (b) SZS + 1 wt% LMZBS sintered at 1400 ^{o}C/2h (c) SZS + 15 wt% LMZBS sintered at 875 ^{o}C/2h (d) SZS + 15 wt% LMZBS + 4 wt% $SrTiO_3$ sintered at 875 ^{o}C.

(iii) Microwave dielectric properties

Fig. 4.15 shows the variation of relative density and permittivity of SZS ceramics with different wt% of LMZBS glass addition. The pure SZS ceramics sintered at 1475 ^{o}C/2 h has a density 3.98 g/cm^3 (relative density of 97 %). The density decreases with increase in glass content and reaches a low value of 3.61 g/cm^3 (relative density of 93.7 %) for 15 wt% LMZBS addition. The decrease in density of the SZS/LMZBS composite can be attributed to the low density of LMZBS glass compared to the SZS ceramics. The variation of relative permittivity as a function of glass content is also of the same nature as that of relative density. Since LMZBS has low relative permittivity (ε_r = 6.9 at 1 MHz) (Renjini *et al.*, 2009) compared to that of SZS, the permittivity of the ceramic/glass composite decreases with the increase in glass content. The pure SZS ceramics sintered at 1475 ^{o}C has ε_r = 8.5, $Q_u \times f$= 105000 GHz (at 12.628 GHz) and τ_f = −51.5 ppm/^{o}C. The SZS + 15 wt% LMZBS has ε_r = 7.9, $Q_u \times f$ = 39000 GHz (at 12.59 GHz), and τ_f = −53.5

ppm/◦C, when sintered at 875 ^{o}C. Addition of glass decreases the $Q_u \times f$ values due to the fact that glasses in general have high dielectric loss (Sebastian *et al.*, 2008).

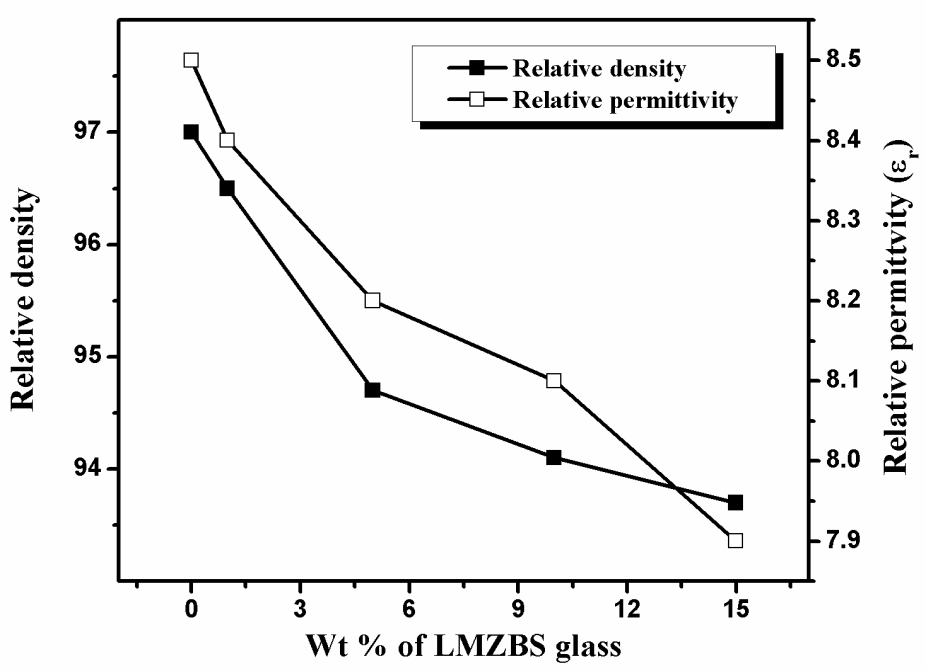

Figure 4.15 Variation of relative density and relative permittivity of SZS/LMZBS composites as a function of different wt% of LMZBS content.

Although the relative permittivity and quality factor obtained are suitable for microwave applications, the τ_f value is very high. Addition of 4 wt% of $SrTiO_3$ having very high positive value of τ_f = +1600 ppm/^{o}C (Wise *et al.*, 2001) to SZS + 15 wt% LMZBS composite improves the τ_f value to -37.7 ppm/^{o}C with ε_r = 8.1 and $Q_u \times f$ = 30100 GHz (at 12.71 GHz). The XRD pattern of SZS + 15 wt% LMZBS + 4 wt% $SrTiO_3$ is shown in Fig. 4.13 (e). Diffraction peaks of SZS and $SrTiO_3$ are visible indicating the absence of extensive chemical reaction between SZS and $SrTiO_3$. The indexing of the peak of $SrTiO_3$ is performed based on ICDD file card No. 86-0179. Only the high intensity peak of $SrTiO_3$ was visible in the XRD pattern, since the amount of $SrTiO_3$ was very small compared to that of the SZS/LMZBS composites. The SEM image of SZS + 15 wt% LMZBS + 4 wt% $SrTiO_3$ also represent two different types of grains of SZS and $SrTiO_3$ along with the glassy phase as shown in Fig. 4.14 (d). This clearly indicates that there is no extensive chemical reaction between SZS/LMZBS composites and $SrTiO_3$.

Thus it will be possible to tune the value of τ_f to ~ 0 ppm/^oC by the addition of appropriate amount of $SrTiO_3$ to SZS/LMZBS. However, large amount of $SrTiO_3$ addition will have detrimental effect in the $Q_u \times f$ values, as $SrTiO_3$ has a low value of $Q_u \times f$ (Wise *et al.*, 2001) and hence the tapes were cast without the addition of $SrTiO_3$ to SZS/LMZBS ceramics.

(iv) Compatibility with Ag

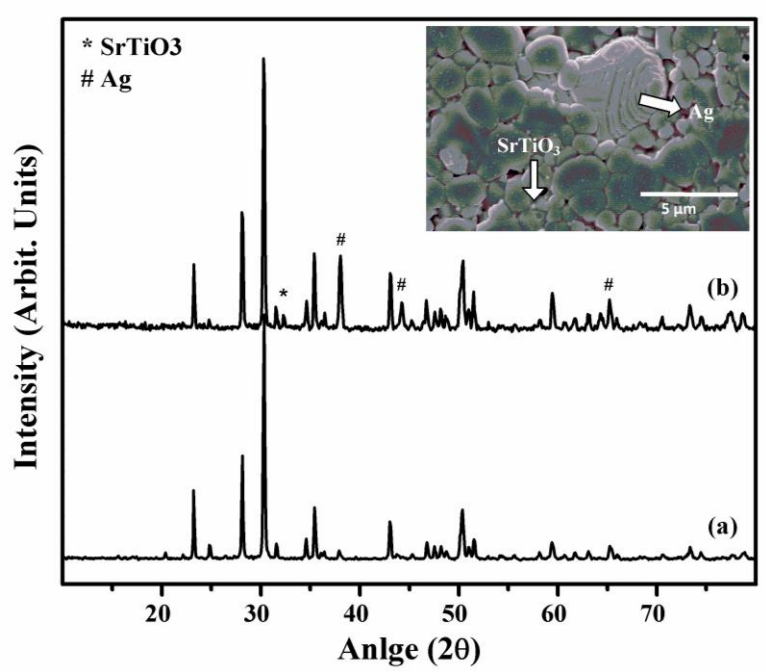

Figure 4.16 XRD patterns of (a) pure SZS sintered at 1475 ^oC/2h (b) SZS + 15 wt% LMZBS + 4 wt% $SrTiO_3$ + 20 wt% Ag sintered at 875 ^oC/2h (SEM image of (b) is shown in the inset).

The reactivity of Ag with SZS/LMZBS glass composites is also tested. 20 wt% of Ag particles were added to a mixture of SZS, LMZBS and $SrTiO_3$ and the analysis was performed with the help of XRD and SEM techniques. The XRD pattern of SZS + 15 wt% LMZBS + 4 wt% $SrTiO_3$ + 20 wt % Ag, sintered at 875 ^oC is shown in Fig. 4.16. The diffraction peaks of pure SZS, $SrTiO_3$ and Ag are visible, indicating the absence of any chemical reaction between the ceramic/glass composite and the Ag particles. The powder diffraction pattern of Ag was indexed based on ICDD file card No. 04-0783. The SEM images of SZS + 15 wt% LMZBS + 4 wt% $SrTiO_3$ + 20 wt% Ag is shown in the inset of Fig. 4.16. This also indicates the absence of reactivity of Ag with the

ceramic/glass composite. A large and bright spherical grain of unreacted Ag can be seen along with very small grains of $SrTiO_3$. Hence it may be concluded that in the case when Ag based LTCC paste is used to fabricate embedded electrodes, interfaces without excess reactions can be achieved.

(v) Coefficient of thermal expansion (α_l)

A mismatch in the values of α_l of the substrate material and Si can cause problems as the temperature is increased during the operation of the electronic device. Fig. 4.17 shows the variation of linear dimensions of SZS and SZS+15 wt% LMZBS with operating temperature. Both of the samples show an increase in their linear dimensions with operating temperature. Glass added ceramic expand more than that of pure ceramic because of the fact that glasses have large value of thermal expansion compared to the ceramics. The values of α_l, calculated in the temperature range 30 ^oC to 500 ^oC using the equation (2.24) are +4.9 ppm/^oC and +5.8 ppm/^oC for SZS and SZS+15wt% LMZBS respectively. The thermal expansion of the SZS/LMZBS composite is comparable to that of Si (~ 4 ppm/^oC) and therefore is suitable for LTCC applications.

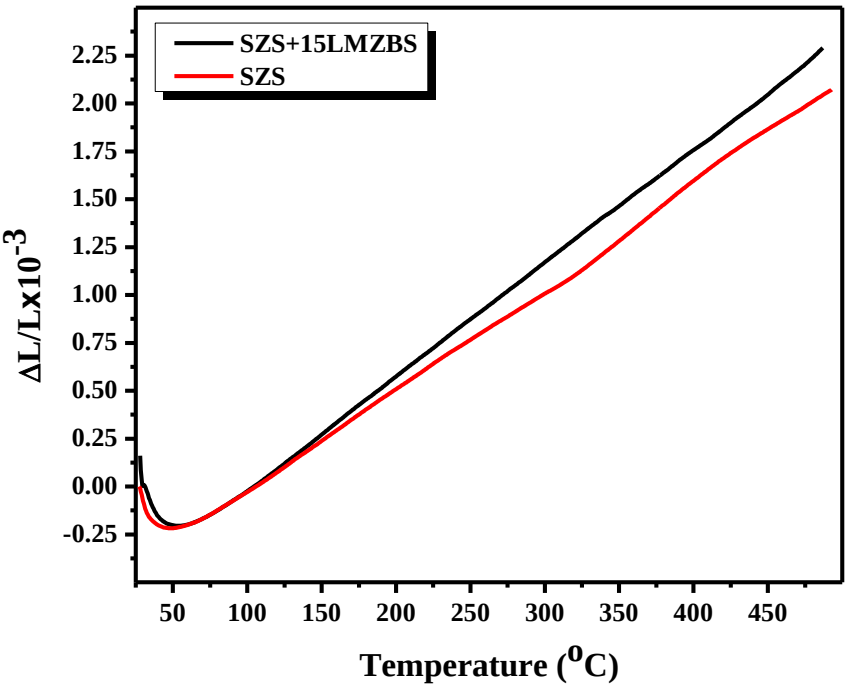

Figure 4.17 Variation of linear dimensions of SZS and SZS+15 wt% LMZBS with operating temperature.

(b) Laminated tapes

(i) Effect of temperature treatment

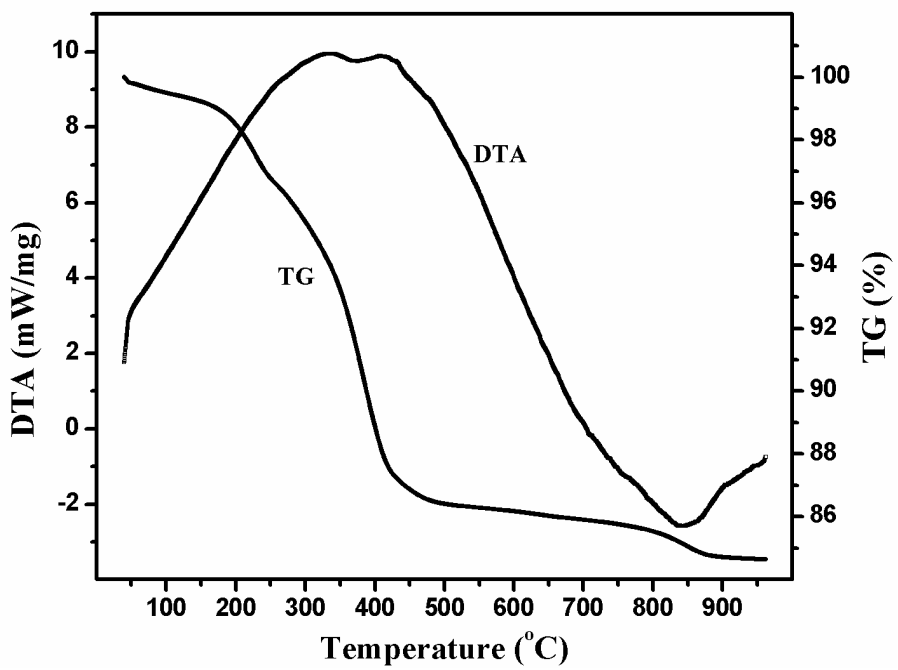

Figure 4.18 TGA/DTA curves of green tape (heating rate 5 ^{o}C/min).

The TGA/DTA result for the cast SZS/LMZBS green tapes are shown in Fig. 4.18. A weight loss up to 10 % is observed in the temperature range 100-500 ^{o}C, which may be due to the burning of organic additives used for the preparation of tapes. A broad endothermic peak can be observed in the DTA curve in the corresponding temperature region due to the absorption of heat energy for burning the additives. A small weight loss of ~ 0.5 % can be observed at 850 ^{o}C. This may be due to the formation of porosity due to the evaporation of LMZBS glass.

Fig. 4.19 shows the variation of density of stacked tapes (8 stacks) as a function of sintering temperature. The results show that as the sintering temperature increases the density of the stacked tapes increases and reaches a maximum value of 3.53 g/cm^3 at 825 ^{o}C. This value is lower than that of the dry pressed ceramic sample (3.61 g/cm^3) sintered at 875 ^{o}C. Further increase in the sintering temperature, however, causes a decrease in the density. This may be due to the escape of LMZBS glass during sintering at temperatures

above 825 ^{o}C. The optimized sintering temperature of stacked tapes is thus 825 ^{o}C compared to 875 ^{o}C for the dry pressed ceramic pellet sample. The presence of several organic additives and the effect of the slurry fabrication process might be the reason for the lowering of sintering temperature of stacked tapes.

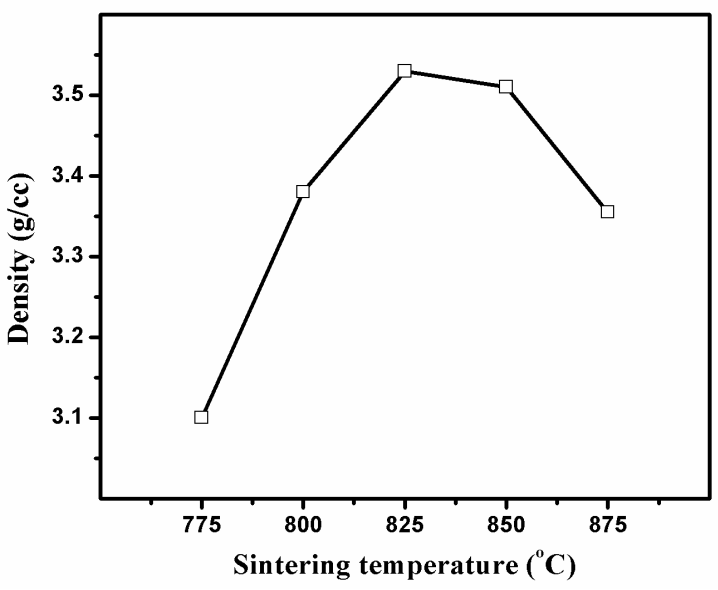

Figure 4.19 Variation of density of the stacked tapes (8 nos.) as a function of sintering temperature.

(ii) Analysis of phase and microstructure

The XRD pattern of SZS + 15 wt% LMZBS tapes sintered at 825 ^{o}C is shown in Fig. 4.13 (d). No additional peaks are observed, revealing the absence of any chemical reaction between the ceramic and glass phase even in the tape form. The microstructures of the green and sintered tapes of SZS + 15 wt% LMZBS are shown in Fig. 4.20. The SEM image of green tape shows a uniform distribution of fine particles with a large amount of porosity as shown in Fig. 4.20 (a). The microstructure of the SZS + 15 wt% LMZBS tape sintered at 825 ^{o}C/2h (Fig. 4.20 (b)) shows that grain growth has occurred during sintering resulting in the elimination of porosity to a large extend. A magnified image of the same tape is shown in the inset of Fig. 4.20 (b), which clearly depicts grains of size in the range ~1-3 μm. Grains of similar size were also visible in the dry pressed sample sintered at 875 ^{o}C/2h, which is an indication of reduction of sintering temperature of the tapes.

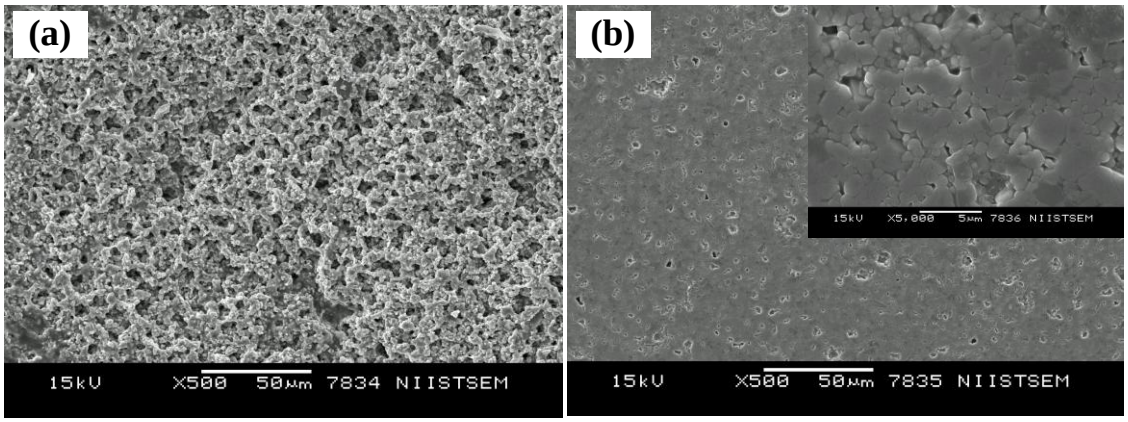

Figure 4.20 SEM images of (a) green tape (b) stacked tapes (8 nos.) sintered at 825 ^{o}C (Image of higher magnification is shown in the inset).

(iii) Microwave dielectric properties at cryogenic temperatures

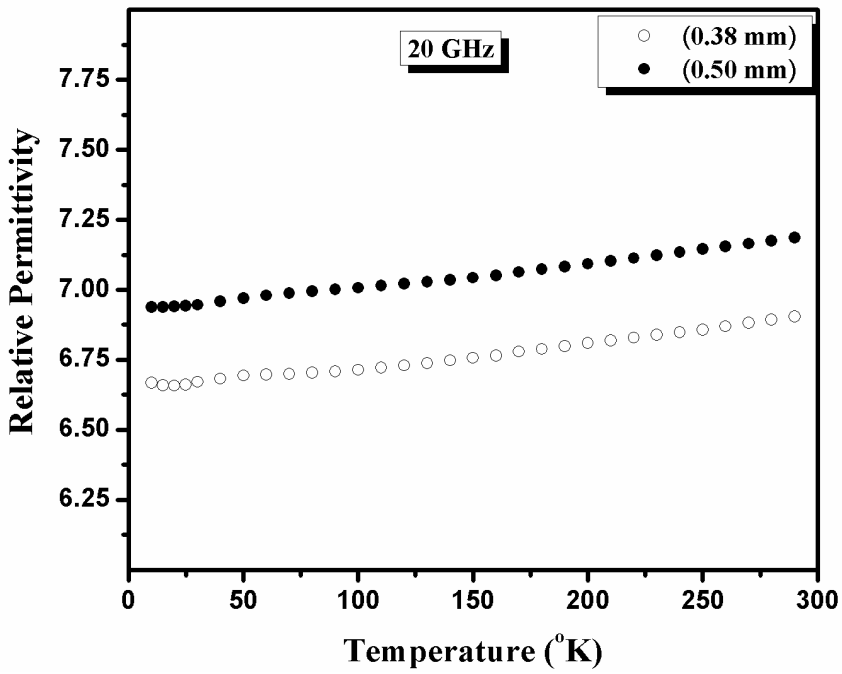

Figure 4.21 Variation of relative permittivity of sintered tapes (825 ^{o}C/2h) of thickness 0.5 mm and 0.38 mm as a function of temperature.

The microwave dielectric properties at very low temperature were measured for two different samples having thickness 0.5 mm (8 stacks) and 0.38 mm (5 stacks). The variation of relative permittivity as a function of temperature is shown in Fig. 4.21. A small increase in the values of relative permittivity is observed with the increase in

temperature from 10 K to 290 K. The percentage increase in relative permittivity is found to be 3.4% for both the tapes as the temperature rises from 10 K to 290 K. The values of ε_r for sintered tapes are lower than that for dry pressed pellet sample of the same composition, possibly due to the inferior densification of the sintered tapes as explained earlier. The sample with thickness 0.5 mm exhibits slightly larger values of relative permittivity. The variation was linear for both of the samples. This increase in ε_r is discussed by Samara in terms of the Clausius–Mossotti relation and is attributed to the change of polarizability with volume (Samara, 1990). The increase in the ε_r with increasing temperature may be due to the increase in magnitudes of the lattice polarizability and anharmonic contributions (Samara, 1968; 1976).

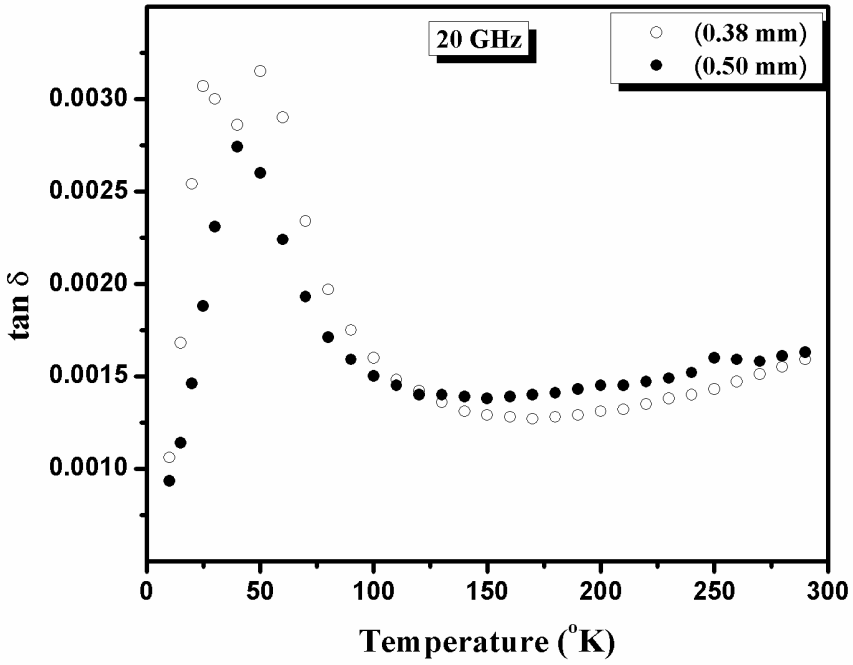

Figure 4.22 Variation of loss tangent (tan δ) of sintered tapes (825 °C/2h) of thickness 0.5 mm and 0.38 mm as a function of temperature.

Fig. 4.22 shows the variation of tan δ as a function of temperature in the range 10 K to 290 K. For T > 100 K, tan δ is almost a constant. The loss tangent below 100 K is characterized by a peak in tan δ at about 40 K. Losses in bulk crystals fall into two categories, intrinsic and extrinsic. Intrinsic losses are dependent on the crystal structure and can be described by relaxation of the non-equilibrium phonon distribution caused by an alternating electric field (Sparks *et al.*, 1982; Braginsky *et al.*, 1987; Gurevich *et al.*,

1991). The intrinsic losses occur under all circumstances and therefore define a lower limit of the loss tangent. This absorption mechanism is the only one to be essentially uninfluenced by defects. Earlier studies show that in the low temperature range the microwave absorption is mainly due to intrinsic contribution, especially the two phonon process for T > 100 K (Sparks *et al.*, 1982; Heidinger, 1994; Zuccaro *et al.*, 1997). Extrinsic losses are associated with imperfections in the crystal structure like impurities, microstructural defects, grain boundaries, porosity, microcracks, and random crystallite orientation etc. The grain boundaries can contribute to the dielectric losses at cryogenic temperatures (Breeze *et al.*, 2009).

Earlier studies have demonstrated the deleterious effects of impurities and it is certainly true that even minor amounts of impurity will cause large increase in dielectric loss (Alford *et al.*, 1996). This is particularly the case in polycrystalline ceramics where the sintering process sweeps impurities to grain boundaries so that impurities and grain boundaries are inextricably linked. The peak in tan δ is the characteristic nature of dipole relaxation, i.e., the relaxation of defect dipoles. This phenomenon has been reported (Zuccaro *et al.*, 1997) in the case of oxygen vacancies in $LaAlO_3$ caused by twin boundary defects in the region 4-12 GHz. The defect dipoles are associated with interstitials. The interstitials can be impurities or lattice ions on interstitial positions. It has been proved that the impurities on interstitial positions are the cause of relaxation losses in quartz crystals (Stevels, 1980). Hence the major factor contributing towards the peak observed in tan δ must be the local motion of ions of lattice or impurity ions on interstitial lattice positions between different equilibrium positions in their own interstice (Stevels, 1980).

4.4 Conclusions

$CaMgSi_2O_6$ (CMS) ceramics sintered at 1300 ^oC/2h has ε_r = 8.3, $Q_u \times f$ = 53,000 GHz (10.20 GHz) and $\tau_f = -45$ ppm/◦C. Various glass powders such as B_2O_3 (B), 30BaO-60B_2O_3-10SiO_2 (BBS), 60ZnO-30B_2O_3-10SiO_2 (ZBS), 40PbO-20B_2O_3-40SiO_2 (PBS), 40MgO-40B_2O_3-20SiO_2 (MBS), 35.14Li_2O-31.66B_2O_3-33.2SiO_2 (LBS), and 20Li_2O-20MgO-20ZnO-20B_2O_3-20SiO_2 (LMZBS) were used in this investigation to reduce the sintering temperature of CMS, out of which only LBS and LMZBS were useful in

lowering the sintering temperature of CMS for LTCC applications. The sintering temperature could be reduced to 925 ^{o}C/2h for CMS+15wt% LBS composite with the dielectric properties ε_r = 8, $Q_u \times f$ = 15,000 GHz (10.17 GHz) and τ_f = −49 ppm/◦C. The CMS+15wt% LMZBS has ε_r = 8.2, $Q_u \times f$ = 32,000 GHz (10.15 GHz) and τ_f = −48 ppm/◦C, when sintered at 900 ^{o}C/2h. The values of α_l in the temperature range 30 ^{o}C to 500 ^{o}C are +5.14 and +5.85 for CMS+15wt% LBS and CMS+15wt% LMZBS respectively, which are close to that of Si. The increase in relative permittivity (at 1 MHz) was less than 3.5% for both of the composition in the temperature range -25 ^{o}C to 75 ^{o}C and hence exhibits good temperature stability of relative permittivity. X-ray diffraction and SEM studies showed that Ag remains unreacted with CMS/glass composites. The τ_f values become more negative with the addition of LBS and LMZBS glasses. The high negative τ_f values obtained for the CMS/glass composites preclude their immediate use in practical applications. Further research is to be carried out to tailor the τ_f values ~ 0 by using materials having high positive τ_f values such as TiO_2, $CaTiO_3$ etc.

The pure SZS ceramics sintered at 1475 ^{o}C has ε_r = 8.5, $Q_u \times f$ = 105000 GHz (at 12.628 GHz) and τ_f = −51.5 ppm/^{o}C. The addition of LMZBS glass was effective in lowering the sintering temperature of SZS ceramics from 1475 ^{o}C to below the melting point of Ag by liquid phase sintering. The composition SZS + 15 wt % LMZBS exhibited ε_r = 7.9, $Q_u \times f$ = 39 000 GHz (at 12.59 GHz), and τ_f = −53.5 ppm/^{o}C, when sintered at 875 ^{o}C and is suitable for LTCC applications. The decrease in ε_r and $Q_u \times f$ of the SZS/LMZBS composite is attributed to the low ε_r and high dielectric loss of the LMZBS phase. XRD and SEM studies showed that Ag is chemically compatible with the SZS/LMZBS composite. Green tapes were cast using SZS + 15 wt % LMZBS composite with the help of suitable additives and solvents. The tapes were stacked, sintered and the dielectric properties investigated in the temperature range 10–290 K. A small increase (< 3.5%) in the values of relative permittivity is observed with the increase in temperature from 10 K to 290 K, which is due to the increased polarizability with volume. The loss tangent below 100 K is characterized by a peak in tan δ at about 40 K, which is consistent with previous reports. In the temperature range 100 K to 290 K, dielectric loss remained of the order of 1.5×10^{-3}.

Chapter 5

Polymer-Ceramic Composites Based on Silicates

5.1 Introduction

During the past decade, the wireless communication industry has emerged as a predominantly military driven market to a cost effective consumer driven commercial market. The cost conscious product miniaturization has been long demanding goals of electronic industries. The growth of telecommunication systems and high-speed digital devices stimulated the scientists to develop new materials, which can deliver improved performance. An ideal substrate material should have low dielectric loss, optimum relative permittivity, high thermal conductivity, matching coefficient of thermal expansion to that of silicon, and good mechanical properties (Bolt *et al.*, 1989; Tummala, 1991; Chung, 1995; Pecht *et al.*, 1999; Xiang *et al.*, 2006; Youngs *et al.*, 2006; Subodh, Pavithran, *et al.*, 2007). In this context, several ceramics with excellent microwave dielectric properties have been developed for practical applications (Surendran, Santha, *et al.*, 2004; Ohsato *et al.*, 2006; Sebastian, 2008). However, they are brittle and have higher processing temperature. Polymeric materials have the advantages of ease of processing, low cost, low dielectric constant, adhesive properties, and high electrical insulation (Agari *et al.*; Cheng *et al.*, 2007). However, the high value of linear coefficient of thermal expansion and low surface energy limits their practical use. Recently, Button *et al.* proposed a composite strategy of combining the advantages of ceramic and polymer to achieve a superior property balance (Button *et al.*, 1989). They offer an attractive combination of processability and properties, which cannot be attained from individual components. Flexible polymer/ceramic composites belongs to the class of soft substrates, which have been widely used due to their ease of fabrication, low cost, and potential applications in substrates and packaging devices (Chen *et al.*, 2003; Hong *et al.*, 2005; Xiang *et al.*, 2006; Subodh, Joseph, *et al.*, 2007; Rajesh *et al.*, 2009). One of the attractive features of the composites is that their dielectric properties can be designed by varying the volume fraction of the filler. Many theoretical models have been proposed (Sihvola *et al.*, 1988; Jayasundere *et al.*, 1993; Wakino *et al.*, 1993; Sareni *et al.*, 1997; Wong *et al.*, 1999; Rao *et al.*, 2000; Jylha *et al.*, 2005; Subodh *et al.*, 2008) for simulating the thermal and dielectric properties of the composites.

Commonly used polymers for substrate fabrication are poly(tetrafluoroethylene), polyethylne, polystyrene, PPS, epoxy, etc. The polymers used in the present study are given in table 1 along with their microwave dielectric properties. The selection of high density polyethylene (HDPE) is based on low dielectric loss and flexibility. Ideally, polyethylene is a non-polar polymer whose main chain is a hydrocarbon, ($-CH_2CH_2-$). It is a semi crystalline with melting temperature of ~160 ^oC. The origin of dielectric loss in polyethylene is dipolar impurities, end groups, chain folds and branch points. The lower the concentration of these groups, the lower will be the dielectric loss. It has been reported that polystyrene has low-processing temperature (~150 ^oC), good flexibility, and excellent microwave dielectric properties compared with polyvinylidene fluoride, polymethyl methacrylate, polyacetylene, and polyanilene (Vo *et al.*, 2002). This polymer, which is considered to be non-polar, does in fact possess a small dipole moment (0.26D) due to the asymmetry at the phenyl side group (Bur, 1985). DGEBA based materials have been widely used in coatings, as encapsulant for electronic components, adhesives, foams used to produce light weight castings for electronic applications and for coating textiles because of their outstanding mechanical, thermal and electrical properties (Lee, 1988; Chen *et al.*, 2003). DGEBA composites have been used extensively over the past thirty years in the microelectronics industry as electronic packaging materials because of its inertness to the electroless plating solution and its compatibility with printed wiring boards (Cheng *et al.*, 2007). The major disadvantages of the polymers described above are their high value of coefficient of thermal expansion and inferior thermal conductivity. These factors have extreme importance when it comes to the electronic packaging applications.

Table 5.1 Microwave dielectric properties of the polymers used in the present investigation.

Polymer	Permittivity	Loss tangent	CTE (ppm/^oC)	TC (W/mK)
HDPE	2.3	~ 10^{-3}	250	0.48
PS	2.1	~ 10^{-3}	100	0.10
DGEBA	3.0	~ 10^{-2}	90	0.19

A variety of ceramic materials can be used to improve the thermal conductivity and coefficient of thermal expansion (CTE) of the polymers. But it should be noted that

low permittivity materials decrease power dissipation, cross talk and when incorporated into the devices, can dramatically decrease the propagation delay (Shamiryan *et al.*, 2004). In order to develop low permittivity composites, the relative permittivity of the ceramic filler should be as small as possible. At microwave frequencies, ionic polarization is dominant and is responsible for the relative permittivity. Lowest relative permittivity at microwave frequency is generally found in predominantly covalently bonded materials (such as silicates) with low atomic number rather than ionic bond materials. Thus with the help of silicates, it is possible to develop low ε_r polymer/ceramic composites even for higher filler loading with a significant improvement in the thermal conductivity and CTE values. In this study for developing low permittivity composite for packaging applications, $Sr_2ZnSi_2O_7$ (SZS) is used as the filler. From chapter 3 it is clear that SZS ceramics has good microwave dielectric properties (ε_r = 8.4, $Q_u \times f$ = 105000 GHz and τ_f = −51.5 ppm/ ^oC) (Joseph and Sebastian, 2010). This work provides with an opportunity for comparison of the dielectric, thermal and mechanical properties of the PS/SZS, HDPE/SZS and DGEBA/SZS composites.

5.2 Theoretical modeling

The dielectric properties of disordered heterogeneous materials have received considerable fundamental attention since nearly the time of Maxwell and these investigations continue to be centrally important for developing a deeper understanding leading to a wide variety of innovative technological applications in many branches of engineering. Although, experiments and simulations are designed to probe the dielectric behavior of composite materials, the prediction of dielectric properties of these media remains an outstanding problem in materials physics. Formulas for the permittivity of hetero-structures were originally discussed by Maxwell and Faraday in the middle of the nineteenth century as part of their comprehensive studies of electricity and magnetism. Later on Clausious (1897) and Maxwell-Garnet (1904) discovered new relations for isotropic dielectric mixtures. In the early 20^{th} century Lichteneker derived a famous logarithmic relation for dielectric composites (Subodh, 2008). Logarithmic relation has been widely used to fit permittivity of various composites. Effective medium approximation was first introduced by Bruggemen in 1935. A twist to the story developed

in the year of 1957 when percolation theory was introduced by Broadbent and Hammersley (Subodh, 2008). The availability of high performance computers made the problem much more interesting and several other models were developed. Various theoretical models for the prediction of relative permittivity, dielectric loss tangent, thermal conductivity and coefficient of thermal expansion are presented in the following section.

5.2.1 Relative permittivity

The dielectric properties of the composites are influenced not only by the relative permittivity of the components but also by other factors such as the morphology, dispersion and the interaction between the two phases. Therefore the prediction of relative permittivity of the composite from the relative permittivity of the components and the volume fraction of the filler is a very important as far as the electronic packaging applications are concerned. The theoretical modeling enables the material scientists to arrive at novel composite systems without much experimental iterations. The following equations are used to calculate the relative permittivity of the composites with low filler content:

Lichtencker equation

$$\log_e \varepsilon_{eff} = v_f \log_e \varepsilon_f + (1 - v_f) \log_e \varepsilon_m \tag{5.1}$$

Jayasundere-Smith equation (Jayasundere *et al.*, 1993)

$$\varepsilon_{eff} = \frac{\varepsilon_m (1 - v_f) + \varepsilon_f v_f \left[\frac{3\varepsilon_m}{\varepsilon_f + 2\varepsilon_m}\right]\left[1 + \frac{3v_f(\varepsilon_f - \varepsilon_m)}{(\varepsilon_f + 2\varepsilon_m)}\right]}{(1 - v_f) + v_f \left[\frac{3\varepsilon_m}{\varepsilon_f + 2\varepsilon_m}\right]\left[1 + \frac{3v_f(\varepsilon_f - \varepsilon_m)}{(\varepsilon_f + 2\varepsilon_m)}\right]} \tag{5.2}$$

Effective medium theory (Rao *et al.*, 2000)

$$\varepsilon_{eff} = \varepsilon_m \left[1 + \frac{v_f(\varepsilon_f - \varepsilon_m)}{\varepsilon_m + n(1 - v_f)(\varepsilon_f - \varepsilon_m)}\right] \tag{5.3}$$

where ε_{eff}, ε_f, and ε_m are the relative permittivity of the composites, SZS and the polymer matrix respectively. v_f is the volume fraction of the $Sr_2ZnSi_2O_7$ ceramics and n is the correction factor to compensate for the shape of the fillers used in polymer/ceramic

composites. The most commonly used equation is the logarithmic law of mixing. It considers the composite system as randomly oriented spheroids that are uniformly distributed in a continuous matrix. Jayasundere–Smith equation which was derived by modifying the well-known Kerner equation by including interactions between neighboring spheres is valid only for low filler concentrations. In this case it is assumed that a bi-phase system consisting of dielectric spheres with permittivity ε_i is dispersed in continuous medium of permittivity ε_m.

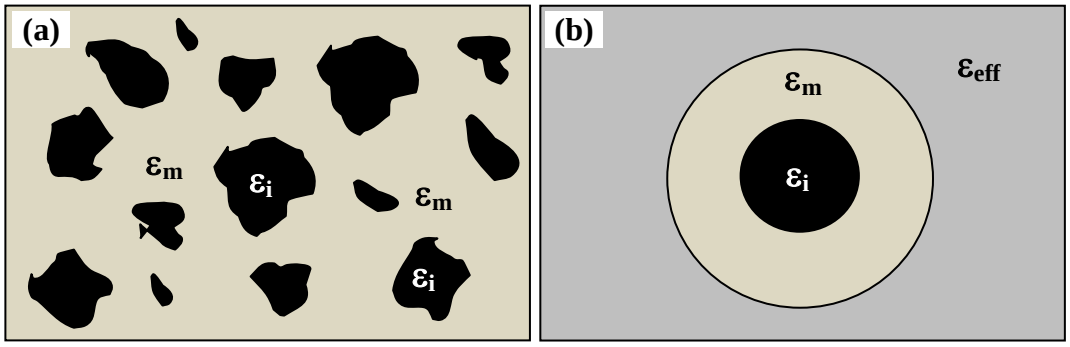

Figure 5.1 Schematic diagram of (a) microstructure of composite materials and (b) Random unit cell embedded in the effective medium.

In the EMT model proposed by Rao *et al.* (Rao *et al.*, 2000), the composite can be treated in terms of an effective medium whose effective ε_r can be obtained by averaging over the relative permittivity of the two constituents. The schematic representation of the microstructure of polymer/ceramic composites is shown in Fig. 5.1 (a). In order to account for the major features of a composite microstructure, a random unit cell of relative permittivity ε_i is defined as core surrounded by a shell of host matrix ε_m as shown in Fig. 5.1 (b) (where ε_i, ε_m and ε_{eff} are the permittivity of ceramics, matrix and composites respectively). In other words the random unit cell can be replaced by a material characterized by ε_{eff}. The basic concept of effective medium is that when a random unit cell is embedded in an effective medium it cannot be detected in the electromagnetic experiment. This model incorporates a ceramic morphology factor n, which is subjected to the shape of ceramic particles. The value of n can be determined empirically. The value of n used should be the same for the polymer/ceramic composites having the same filler.

5.2.2 Dielectric loss

The number of theoretical models available for predicting loss tangent is relatively less, as it is more complicated (Ang *et al.*, 2003). Literatures show that a composite of two low loss materials generally exhibits higher dielectric loss than the constituents. The trend of dielectric loss with different volume fraction of filler in the composite is entirely different from that of permittivity relation. The following relations are used to model dielectric loss tangent of the composites (Wakino *et al.*, 1993; R. Abraham, 2005)

General mixing model,

$$(\tan \delta_c)^{\alpha} = \sum \varphi_i (\tan \delta_i)^{\alpha} \tag{5.4}$$

Bruggemen model,

$$\varepsilon'' = \frac{(\varepsilon_c' - \varepsilon')(\varepsilon_c' + 2\varepsilon_p')\varepsilon'\varepsilon_p''}{(\varepsilon_c' - \varepsilon_p')(\varepsilon_c' + 2\varepsilon')\varepsilon_p'} + \frac{3(\varepsilon' - \varepsilon_p')\varepsilon_c''}{(\varepsilon_c' - \varepsilon_p')(\varepsilon_c' + 2\varepsilon')} \tag{5.5}$$

where $\tan \delta_c$, $\tan \delta_i$, α and φ_i are the loss tangent of the composite, loss tangent of i^{th} material, a constant, and volume fraction of the i^{th} material, respectively. The value of the constant α determines the mixing rule, if $\alpha = -1$ serial mixing and $\alpha = 1$ parallel mixing. In Bruggemen model ε', ε_c', ε_p', ε_p'', ε_c'' represent the effective dielectric constant of composite, dielectric constant of ceramic, dielectric constant of polymer, dielectric loss of polymer and dielectric loss of ceramic respectively.

5.2.3 Thermal conductivity

Determining the thermal conductivity of composite materials is crucial in a number of industrial processes and applications. The effective thermal conductivity of a composite is strongly affected by its composition, structure, intrinsic thermal conductivities, filler particle size, shape, and interfacial thermal resistance. To predict the effective thermal conductivity of composites the following equations are used:

Series mixing rule (Richerson, 2006)

$$\frac{1}{k_c} = \frac{v_f}{k_f} + \frac{v_m}{k_m} \tag{5.6}$$

Parallel mixing rule (Richerson, 2006)

$$k_c = v_f k_f + v_m k_m \quad (5.7)$$

Maxwell model (Sebastian *et al.*, 2010)

$$k_c = k_f \left[\frac{k_f + 2k_m + 2v_f (k_f - k_m)}{k_f + 2k_m - v_f (k_f - k_m)} \right] \quad (5.8)$$

Effective medium theory (Håkansson *et al.*, 1990)

$$v_m \left[\frac{k_m - k_c}{k_m + 2k_c} \right] + v_f \left[\frac{k_f - k_c}{k_f + 2k_c} \right] = 0 \quad (5.9)$$

where k_c is the effective thermal conductivity of the composite, k_m and k_f are the thermal conductivity of matrix and filler, and v_m and v_f are the volume fractions of matrix and filler respectively. The series and parallel models give only a lower and upper limit of the expected thermal conductivity values of the composites respectively. The Maxwell model assumes a dispersion of small spheres within a continuous matrix of a different phase, with the spheres being far enough apart such that the local distortions to the temperature distributions around each of the spheres do not interfere with their neighbours' temperature distributions. The EMT model assumes a completely random distribution of all the phases.

5.2.4 Coefficient of thermal expansion (CTE)

When a composite is heated, polymer matrix will expand more than ceramic fillers. However, if the interfaces are capable of transmitting stress, the expansion of matrix will be reduced (Holliday *et al.*, 1973). The presence of ceramic cause the polymer chains to get arrested and unable to expand with temperature. The theoretical values of CTE can be predicted by the rule of mixtures using the equation:

$$\alpha_c = f\alpha_f + (1-f)\alpha_m \quad (5.10)$$

where α_c, α_f and α_m are the CTE of the composite, filler and polymer respectively.

5.3 Experimental

The $Sr_2ZnSi_2O_7$ (SZS) ceramics were prepared by the conventional solid-state ceramic route (Joseph and Sebastian, 2010). The resulting powder was ground well in a

ball mill for 10 h and sieved using 25 μm sieves. The phase formation was identified using powder X-ray diffraction and the particle size distribution using laser particle size analyzer (Microtrack X-100 model, USA). The filler, SZS was separately mixed with polystyrene (PS) (Nikunj Industries, Mumbai, India) and high density polyethylene (HDPE, Kerala plastics, India) by melt mixing technique using a kneading machine. Different volume fractions (v_f = 0.1–0.5) of SZS ceramics were added to the melted polystyrene and blended at 160 ^oC for 45 min. The composite thus obtained were thermo-laminated under a pressure of 50 MPa and 160 ^oC for 30 min. Bis Phenol A epoxy resin was mixed with curing agent in the 10:1 ratio. Then volume fractions (v_f = 0.05–0.4) of the SZS ceramics was added and mixed mechanically using an agate mortar and pestle. The thoroughly mixed epoxy resin and ceramics were poured into molds of different shapes and then precured at room temperature for 12 h followed by post curing at 75 °C for 2 h.

The density of the composites (ρ) was determined using Archimedes method. The theoretical density (D) of the polymer ceramic composite was calculated using the equation (2.24). The surface morphology of the composites was studied by scanning electron microscope. The low-frequency dielectric properties were measured by LCR meter. The same instrument is used in order to investigate the variation of relative permittivity with temperature. The samples were heated in a uniform temperature enclosure from 25–70 ^oC and the corresponding values of relative permittivity were measured at 1 MHz. The microwave properties (at ~ 5.1 GHz) of the samples were measured using a vector network analyzer (Agilent 8753 ET) by SPDR technique. $TE_{01\delta}$ mode was used for the measurements since this mode is insensitive to the presence of air gaps perpendicular to z-axis of the resonator. The water absorption measurements were conducted following the standard ASTM D570. The samples were weighed and submerged in distilled water at 25 ^oC for 24 h. The samples were removed, wiped, dried and the amount of water absorbed was calculated based on the weight gain of the samples. Photopyroelectric technique was used to determine the thermal conductivity of the composites (Marinelli *et al.*, 1990; Menon *et al.*, 2000). A 70 mW He-Cd laser of wavelength 442 nm, intensity modulated by a mechanical chopper (model SR540) was

used as the optical heating source. A PVDF film of thickness 28 μm, with Ni-Cr Coating on both sides, was used as pyroelectric detector. The output signal was measured using a lock in amplifier (model SR 830). Modulation frequency was kept above 60 Hz to ensure that the detector, the sample and backing medium were thermally thick during measurements. The thermal thickness of the composites was verified by plotting photopyroelectric (PPE) amplitude and phase with frequency at room temperature. Thermal diffusivity (γ) and thermal effusivity (e) were also measured from PPE signal phase and amplitude (Sebastian *et al.,* 2003). From the values of γ and e, the thermal conductivity of the samples was obtained.

The coefficient of thermal expansion (CTE) of the composites was measured using a dilatometer in the temperature range 25–100 ^{o}C. The micromechanical properties of the polymer/ceramic composites were measured using micro hardness tester (Clemex Model 4, Germany). Both the surfaces of the samples were polished to have optically flat surface for indentation. The specimen was subjected to a load of 50 g and dwell time of 10 s. For pure ceramic sample the load was increased to 400 g. A total of four readings were taken to get the average hardness. Dumbbell shaped strips having dimensions as per ASTM D638 standards were made for tensile strength measurements. A Shimadzu (AGS-1000G, Tokyo, Japan) make universal testing machine was used to determine the ultimate tensile strength. The testing was carried out at room temperature with a drawing speed of 10 mm/min.

5.4 Results and discussion

(i) Particle size distribution and microstructure

It is reported that micron sized filler is more suitable than nano-sized fillers to achieve low ε_r and tan δ of the composites (Murali *et al.,* 2009). Owing to high surface area, nano-sized fillers have more polarizability resulting in larger ε_r values of the composites. The lattice strain of the nano-sized fillers will be large, which is one of the reasons for increase in the dielectric loss of the nano-sized ceramic filled composites (Murali *et al.,* 2009). Fig. 5.2 shows the particle size distribution of SZS powder. A wider distribution of particles of size in the range 0.5 – 10 μm (median ~ 3.9 μm) are observed.

Such a distribution is desirable for high packing fraction of filler in the polymer matrix which is particularly important in formulating dense, dimensionally stable polymer/ceramic composite substrate.

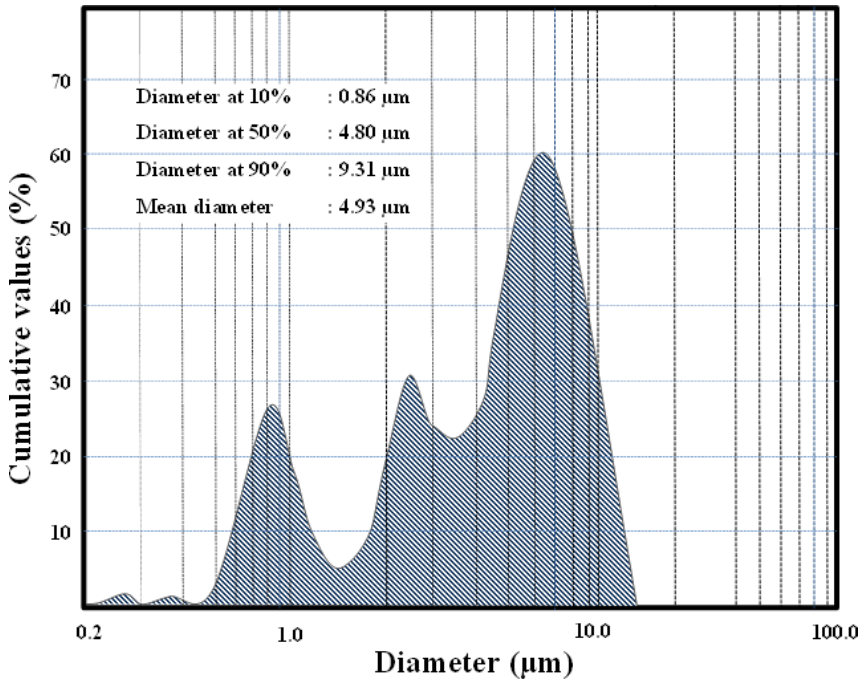

Figure 5.2 Particle size distributions of $Sr_2ZnSi_2O_7$ ceramics.

Fig. 5.3 shows the SEM images of PS/SZS, HDPE/SZS and DGEBA/SZS composites for various filler concentrations. Irregularly shaped particles with average size less than 10 µm are visible in the figure. Fig. 5.3 (a,c,e) represent the images of PS/SZS, HDPE/SZS and DGEBA/SZS composites for 0.2 v_f of filler concentration. Uniform dispersion of the ceramic particles can be observed with good separation between the particles. Hence the major contribution towards the dielectric and thermal properties will be made by the continuous matrix. Fig. 5.3 (b,d,f) represent the images of PS/SZS, HDPE/SZS and DGEBA/SZS composites for 0.4 v_f of filler concentration. Although the ceramic particles are uniformly dispersed in polymer matrix occasional agglomeration can be observed. As the filler content increases, the inter-particle distance decreases, which in turn increases the connectivity among the ceramic particles. The connectivity of the individual components is important because it controls the electric-flux pattern as well as the mechanical and thermal properties (McLachlan *et al.*, 1990).

The aggregation of the ceramic particles with the increase in filler content in the continuous polymer matrix also results in the formation of porosity.

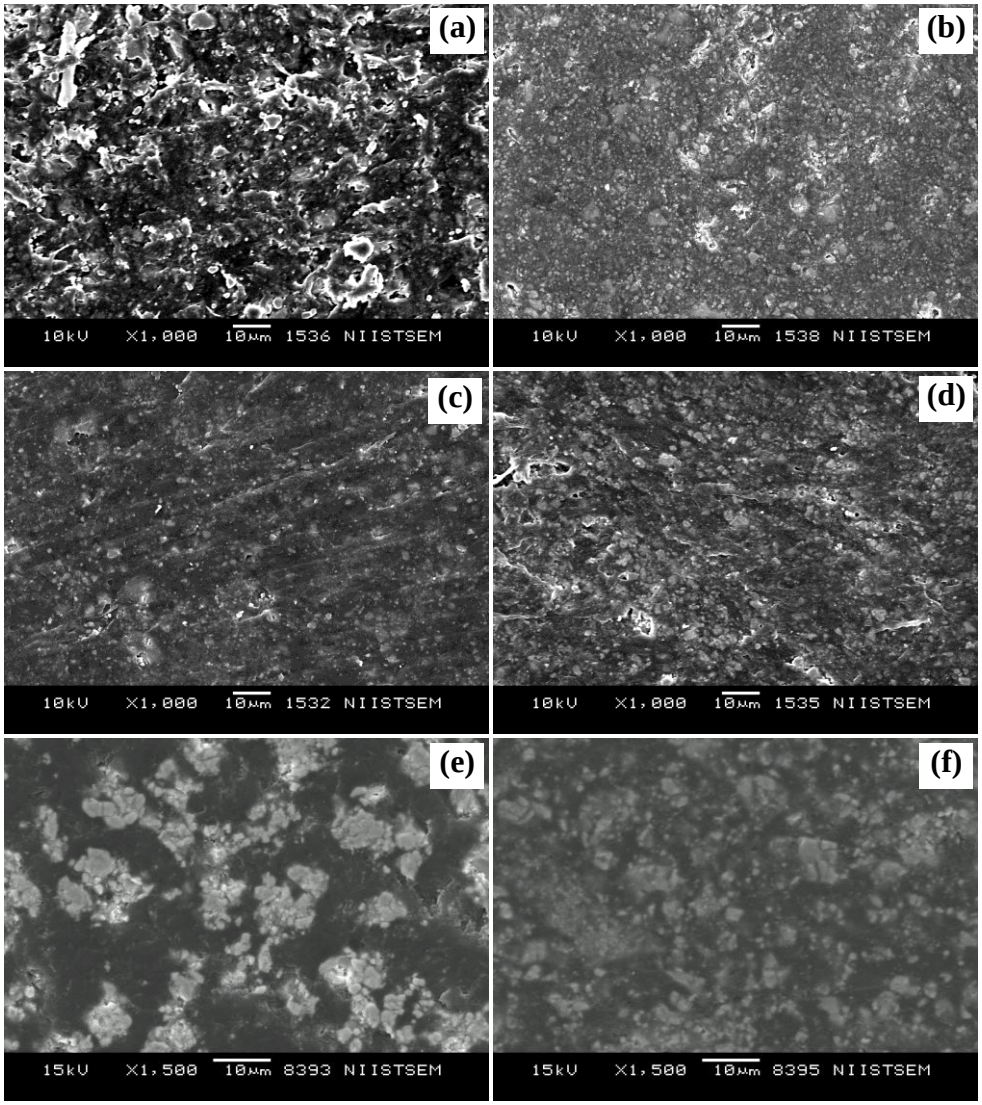

Figure 5.3 SEM images of (a) PS/0.20v_f SZS (b) PS/0.40v_f SZS (c) HDPE/0.20v_f SZS (d) HDPE/0.40v_f SZS (e) DGEBA/0.20v_f SZS (f) DGEBA/0.40v_f SZS.

(ii) Density, porosity and moisture absorption

The densities of the disc shaped samples of PS, HDPE, DGEBA, and SZS measured by Archimedes method are found to be 1.05, 0.95, 1.15 and 4.1 g/cm^3 respectively. Table 5.2 gives an account of the values of density, porosity (%) and moisture absorption (%) of the composites for various v_f of the filler. It is observed that

the density increases with the increase in SZS content, which is quite expected due to the higher density of the filler compared to the polymer matrices. It is found that the experimental density follows the theoretical values at low filler concentrations. However, the difference between them increases marginally as the volume fraction of ceramic increases. This can be due the increase in porosity with increase in filler content. The volume fraction of air in the composites as a function of filler content is also given in table 1, which clearly support the presence of porosity for increased filler concentration. Recently, Doyle and Jacobs (Doyle *et al.*, 1990) reported that clustering of particle in the composite may have significant effect on the effective composite properties. The SEM images of the composites clearly suggest the presence of clustering of ceramic particles at high filler loading. As the volume fraction of filler increases, the agglomeration of ceramic particle results, which leads to porosity (Xiang *et al.*, 2006; Subodh, Joseph, *et al.*, 2007; Anjana *et al.*, 2008; Thornas *et al.*, 2008). Thus, the relative density decreases with increase in the ceramic loading. For low volume fraction, the matrix completely covers the ceramics and hence porosity will be less. However, as the amount of ceramics increases beyond 0.3 volume fraction the packing will be less and hence porosity will be more. The relative density of PS/SZS composites varies from 99.2% to 95.7%, whereas that of HDPE/SZS varies from 99.2% to 96.8% and for DGEBA/SZS composites the variation is from 99.2% to 95.3%.

Sensitivity of polymer ceramic composites to humidity is indeed a serious matter of concern. When subjected to humid environment, the composites can absorb a few weight percentage of water, leading to an overall degradation in the dielectric properties (Gonon *et al.*, 2005). Water is a polar molecule and has high ε_r and tan δ. Hence the values of ε_r and tan δ of the composite increase with moisture absorption (Laverghetta, 1984). Consequent to the absorption of moisture into the composite, mechanical strength also decreases. Hence, moisture absorption is an important parameter to be determined prior to practical use. It can be seen from the table that moisture absorption increases with filler loading. Usually moisture absorption within 0.10 wt% is suitable for packaging materials (Laverghetta, 1984). At 0.40 v_f of filler loading PS/SZS, HDPE/SZS and DGEBA/SZS composites has a moisture absorption of 0.09, 0.06 and 0.14 wt% respectively. Thus DGEBA/SZS composites exhibits high values of moisture absorption

compared to the other two. The molding of the DGEBA/SZS composites for higher ceramic loading is difficult and hence the entrapment of porosity in the samples cannot be eliminated. The high value of porosity of the DGEBA/SZS composites may be responsible for the large moisture absorption of DGEBA/SZS composites. The volume of polymer/ceramic interface increases with filler loading, which in turn promotes moisture absorption. The amount of filler loading has to be optimized to get optimum dielectric, thermal and other desired properties. Under-filled composites suffer from high CTE and inhomogeneous distribution of filler in the polymer matrix whereas over-filled composites result in high porosity, moisture absorption and low mechanical strength. Hence an optimum filler loading in the polymer matrix is preferred for circuit application.

Table 5.2 Density, porosity (%), moisture absorption and dielectric properties (at 1 MHz) of PS/SZS, HDPE/SZS and DGEBA/SZS composites.

Polymer	v_f of SZS	ρ_t (g/cm^3)	ρ_m (g/cm^3)	V_{air} (%)	Relative density (%)	Moisture absorption (wt%)	1 MHz	
							ε_r	tan δ
PS	0.10	1.33	1.32	0.8	99.2	0.054	3.60	0.0020
	0.20	1.63	1.60	1.8	98.2	0.072	3.86	0.0026
	0.30	1.94	1.88	3.1	96.9	0.088	4.21	0.0037
	0.40	2.24	2.16	3.6	96.4	0.097	4.45	0.0053
	0.50	2.54	2.43	4.3	95.7	0.123	4.81	0.0078
HDPE	0.10	1.26	1.25	0.8	99.2	0.032	3.06	0.0009
	0.20	1.57	1.55	1.3	98.7	0.039	3.48	0.0018
	0.30	1.88	1.85	1.6	98.4	0.045	3.89	0.0031
	0.40	2.19	2.14	2.3	97.7	0.062	4.23	0.0053
	0.50	2.50	2.42	3.2	96.8	0.093	4.73	0.0081
DGEBA	0.05	1.30	1.29	0.8	99.2	0.066	4.55	0.0278
	0.10	1.45	1.43	1.4	98.6	0.084	4.76	0.0254
	0.20	1.74	1.69	2.6	97.4	0.102	5.12	0.0248
	0.30	2.04	1.97	3.2	96.8	0.125	5.54	0.0213
	0.40	2.33	2.22	4.7	95.3	0.142	5.85	0.0185

(iii) Dielectric properties

Table 1 also gives the dielectric properties at 1 MHz of the polymer/ceramic composites. A gradual increase in relative permittivity with ceramic loading is observed. The increase in the relative permittivity of the polymer/ceramic composite is due to the relatively high permittivity of SZS (ε_r = 8.6 at 1 MHz) compared to PS (ε_r = 3.20), HDPE (ε_r = 2.62) and epoxy (ε_r = 4.30). When the ceramic filler content is small, the dielectric response is mainly contributed by the continuous matrix, which has low ε_r. As the filler loading increases, the connectivity among the filler particle increases which leads to an increase in the dipole – dipole interaction (Kuo *et al.*, 2004). In addition, the Maxwell-Wagner-Sillars effect appears generally in heterogeneous media due to the accumulation of charges at the interface which leads to the formation of large dipoles (Smaoui *et al.*, 2009). Hence the relative permittivity increases with ceramic loading. Maximum values of ε_r achieved are 4.81, 4.73 and 5.85 for PS/0.50v_f SZS, HDPE/0.50v_f SZS and DGEBA/0.40v_f SZS respectively.

The dielectric loss depends on intrinsic and extrinsic factors (Sebastian, 2008). The intrinsic factors are mainly due to the interaction of ac electric field with phonons. The extrinsic factors such as defects, interfaces, size and shape of the filler and micro-pores also contribute to the dielectric loss. The dielectric loss of PS/SZS and HDPE/SZS composites at 1 MHz increases with the filler content, whereas it decreases for DGEBA/SZS composites. The tan δ values of PS, HDPE and SZS at radio frequencies are of the same order of magnitude and hence the addition of filler does not have a major role in controlling the dielectric loss of the composites. Therefore the increase in the dielectric loss of the composites is attributed to the increase in the heterogeneity of the samples with filler content. As already explained the agglomeration of filler particles and hence the entrapped porosity and moisture absorption have large values for composites with higher filler content. This might be the reason for the increase in tan δ values of PS/SZS and HDPE/SZS composites with the increase in ceramic loading. DGEBA has a large value of tan δ (~ 0.03) compared to SZS. Therefore the addition of SZS to the DGEBA matrix reduces the dielectric loss of the composites as the filler content increases. But the increased inhomogeneity of the samples has an adverse effect on the

dielectric loss as already mentioned. The study of the variation of dielectric loss of the DGEBA/SZS composites indicates that the effect of low dielectric loss of SZS is more pronounced than the inhomogeneity of the samples with high filler loading.

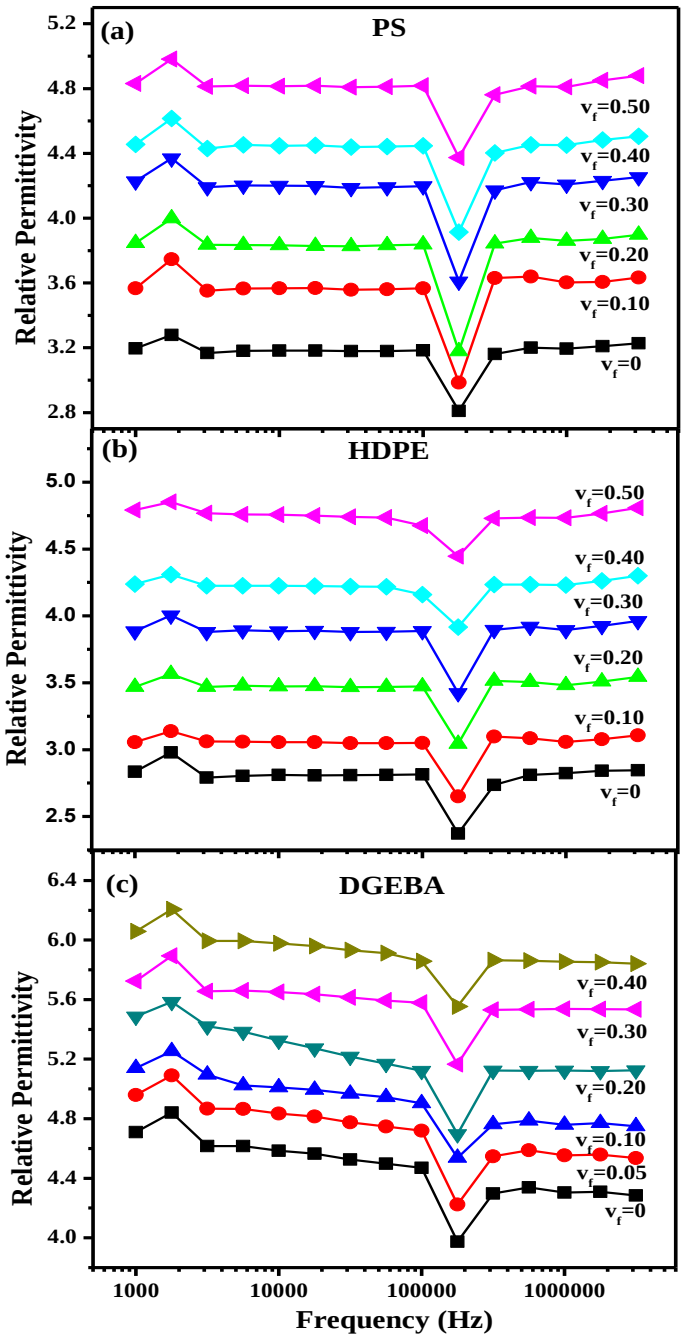

Figure 5.4 Variation of relative permittivity with frequency (a) PS/SZS composites (b) HDPE/SZS composites (c) DGEBA/SZS composites.

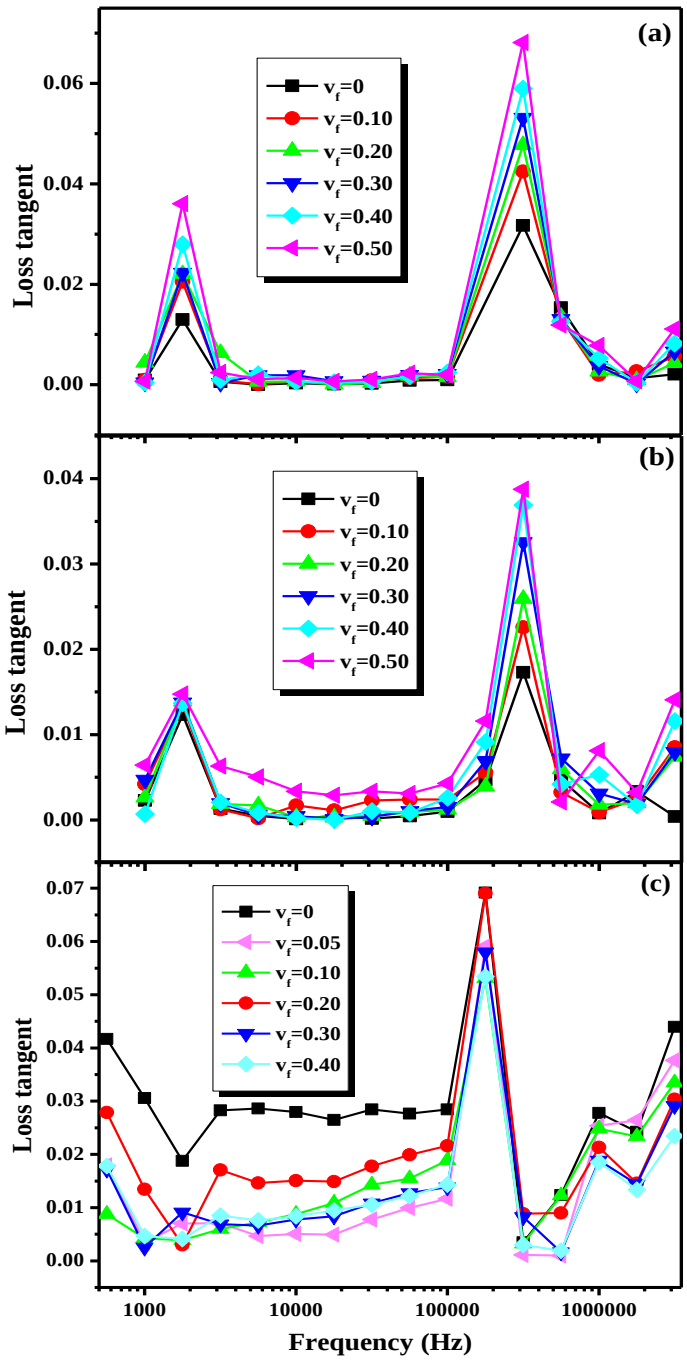

Figure 5.5 Variation of dielectric loss tangent with frequency (a) PS/SZS composites (b) HDPE/SZS composites (c) DGEBA/SZS composites.

The frequency dependence of relative permittivity the composites with the different v_f of SZS filler is studied in the frequency region 0.5 – 3 MHz, which is shown in Fig. 5.4 (a-c). The relative permittivity of each polymer composites increases with filler loading. This is expected as the relative permittivity of the ceramic filler is high compared to the polymer matrices as already explained. In all the volume fractions, permittivity remained almost constant in the measured frequency range except for dispersion at ~ 10^5 Hz. Such relaxation dispersions usually appear in polymers and polymer composites at lower frequencies at room temperatures. George *et al.* (George, Deepu, *et al.*, 2009) made a similar observation while studying the dielectric properties of HDPE/CLNT and PS/CLNT composites. It reveals the good frequency stability of the composites over a wide frequency range.

Fig. 5.5 shows the frequency dependence of dielectric loss of the composites for different v_f of ceramic loading. At a fixed value of operating frequency, dielectric loss increases as the concentration of SZS is increases except for DGEBA/SZS composites. The increase in dielectric loss for higher volume fraction of the filler may be due to the increase in porosity (Kuo *et al.*, 2001). The extent of interfacial polarization is substantially augmented as the loading of SZS is increased, yielding quite a high value of loss at each composition. For each volume fraction, the dielectric loss remains almost a constant. The effect of dispersion, similar to that observed in Fig. 5.4 is observed at ~ 10^5 Hz. In polymer composite materials, interfacial polarization is always present because of the presence of additives, fillers, or even impurities (Yu *et al.*, 2000). It is known that both relative permittivity and dielectric loss depend on electronic, ionic, dipole-orientation, and space charge polarizations. The present systems are mixtures of two dielectrically different materials. Such a mixture with a distinct interphase should be appreciably lossy at low frequencies; it has displayed a large space-charge effect owing to Maxwell–Wagner polarization (Sebastian *et al.*, 2010).

Fig. 5.6 (a) shows the variation of relative permittivity of the composites at microwave frequencies. The relative permittivity shows a similar trend to that obtained at 1 MHz except for the fact that the values obtained at ~ 5 GHz are less than that at radio frequencies. This is due to the absence of certain polarization mechanisms at microwave

frequencies, which are active at radio frequencies. The high relative permittivity of SZS compared to virgin polymer matrices is the reason for the steady increase in relative permittivity with filler content. The variation of relative permittivity is from 2.1 for virgin PS to 4.35 for PS/0.50v_f SZS composite. For HDPE/SZS composites, the variation is from 2.3 to 4.61 in the same range of filler loading, whereas the DGEBA/SZS composites has ε_r = 3.03 (for 0 v_f of SZS) and ε_r = 4.63 (for 0.40 v_f of SZS).

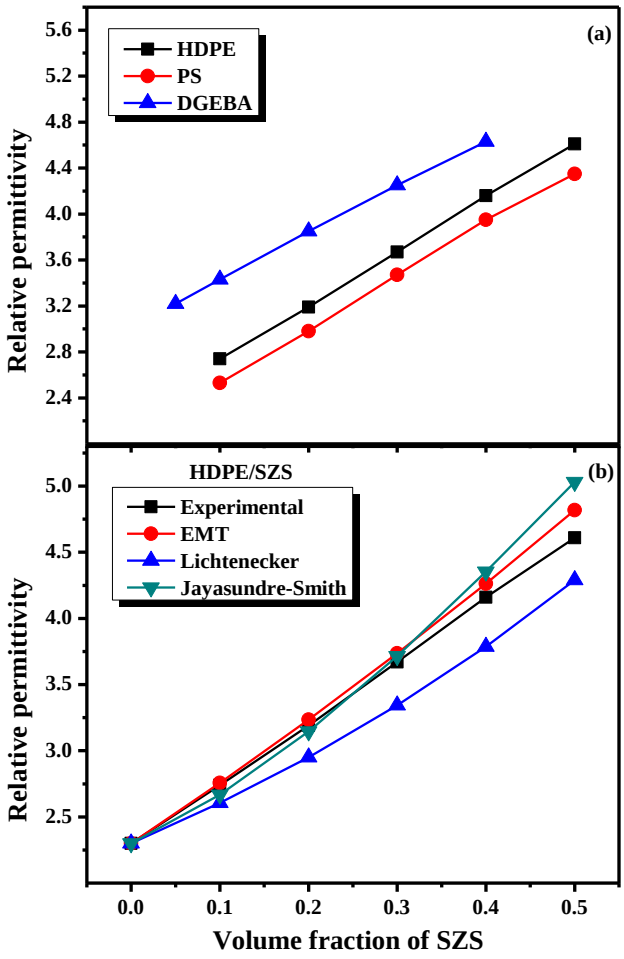

Figure 5.6 (a) Variation of relative permittivity of PS/SZS, PE/SZS and DGEBA/SZS composites (b) Theoretical modeling of relative permittivity of PE/SZS composites as a function of filler loading.

Fig. 5.6 (b) gives a comparison of the experimentally observed values of relative permittivity with the theoretical predictions for HDPE/SZS composites. Theoretical predictions for PS/SZS and DGEBA/SZS composites are given in Fig. 5.7 (a-b).

Jayasundere–Smith equation predicts the permittivity of polymer/ceramic composite by assuming a spherical shape for the fillers. The polymer/ceramic composite is considered as a bi-phase system consisting of dielectric spheres with permittivity ε_i is dispersed in a continuous medium of permittivity ε_m. But the equation fails to give a correct account of the values of ε_{eff} of the composite system by overestimating the values of ε_{eff} beyond 0.30 v_f of filler loading. This can be due to the fact that the used fillers are not exactly spherical, but randomly shaped as seen from the SEM images in Fig. 5.3.

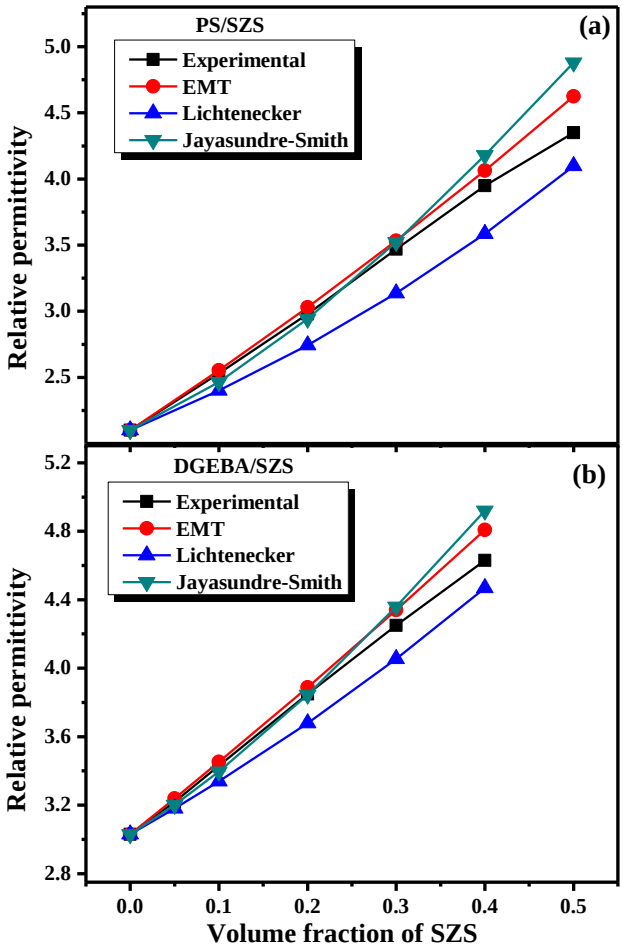

Figure 5.7 Theoretical modeling of relative permittivity of (a) PS/SZS (b) DGEBA/SZS composites.

The Lichtenecker model shows a wide deviation from the experimental values even for low v_f of filler loadings. Lichtenecker model describes the composite system consisting of randomly oriented spheroids inside a continuous matrix. It is reported that

the exponential behavior of Lichtenecker model is best suited for PTFE/ceramic composites because of the non-monotonic variation in relative permittivity of PTFE/ceramic composites due to particle-particle overlap (Joseph, Uma, *et al.*, 2010). However, this model also does not provide an appropriate match to the experimentally observed values of ε_r for PS/SZS, HDPE/SZS and DGEBA/SZS composites.

The EMT model proposed by Rao et al. (Rao *et al.*, 2000) provides a better prediction of the effective ε_r of the composites. In this model, the composite can be treated in terms of an effective medium whose effective ε_r can be obtained by averaging over the relative permittivity of the two constituents. This model incorporates a ceramic morphology factor n, which is subjected to the shape of ceramic particles. The value of n can be determined empirically and is found to be 0.12 (Joseph, Uma, *et al.*, 2010). The theoretical predictions of relative permittivity of PS/SZS and DGEBA/SZS composites also exhibited similar trends. The EMT model with n = 0.12 is found to be very useful in predicting the relative permittivity of all the polymer/ceramic composites with only a small deviation from the experimentally observed values, even at high filler loadings.

The reason for the inconsistency of the theoretical predictions of the values of ε_r of the composites is manifold. Generally, the theoretical predictions are valid only for lower v_f of filler loadings (Sihvola *et al.*, 1988; Wakino *et al.*, 1993; Anjana *et al.*, 2008; Nisa *et al.*, 2008; Thomas, Deepu, *et al.*, 2008). Many theoretical models suggest that the filler particles in a material should ideally be separated, non-interacting, and roughly spherical (Stroud, 1979; Sareni, 1997). However, many composites of interest in practice deviate markedly from this ideal configuration due to increase in porosity and the clustering of filler particles (Bai *et al.*, 2000). This results in the formation of interface regions of polymer/ceramic composite having a relative permittivity significantly different from that of polymer or ceramic phases (Todd *et al.*, 2003). The effective permittivity of the composite, therefore, depends on a number of parameters like the permittivity of each phase in the mixture, their volume fractions, shape, size, porosity, interface polarizability, and volume fractions of interface region. It will be a tedious task to include all these parameters in a single equation and hence an accurate prediction of dielectric properties of such composite becomes awfully challenging. One of the other

reasons for the poor fitting is the difficulty to obtain the correct value of ε_r of the powder. Instead, ε_r of the bulk ceramic is used. The ε_r of the powder may be different from that of the bulk.

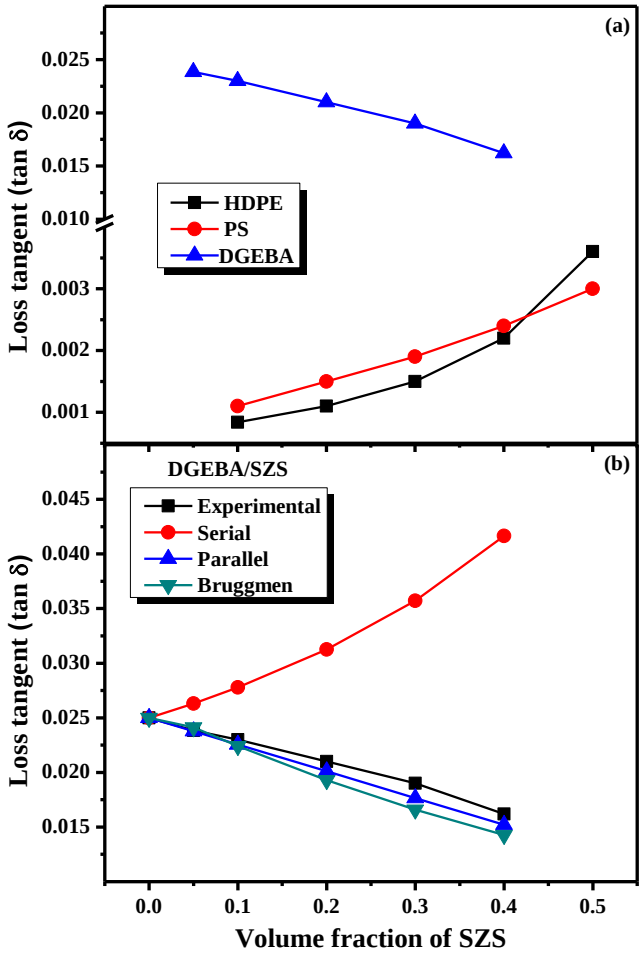

Figure 5.8 (a) Variation of loss tangent of PS/SZS, PE/SZS and DGEBA/SZS composites (b) Theoretical modeling of loss tangent of DEGBA/SZS composites as a function of filler loading.

Fig. 5.8 (a) shows the variation of dielectric loss of the composites at ~ 5 GHz with filler loading. The dielectric loss increases with ceramic loading except for DGEBA/SZS composites. A comparison with the values of tan δ in table 1 shows that, even at microwave frequencies the trend of variation of dielectric loss with filler loading is similar to that at 1 MHz. The increased agglomeration of ceramic particles, entrapped porosity and moisture absorption are the causes of increase in the dielectric loss of the

PS/SZS and HDPE/SZS composites with filler loading. In the case of DGEBA/SZS composites, the major factor controlling the dielectric loss is the extremely low tan δ value of SZS compared to virgin DGEBA matrix. Here the effect of increased inhomogeneity with filler loading is underestimated by the low value of tan δ of SZS ceramics.

Fig. 5.8 (b) shows a comparison between the experimentally obtained and theoretically predicted values of dielectric loss of DGEBA/SZS composites as a function of filler loading. The dielectric loss tangent of pure SZS used for the purpose of modeling is 0.0005, which is measured by the SPDR method. All the theoretical models except serial mixing rule give a relatively good fit to the experimental values of tan δ of the composites for very low filler contents. But for v_f >0.1, the theoretical predictions starts to deviate from the experimentally observed values thereby producing less satisfactory results. In heterogeneous materials such as composites, the intrinsic contributions to the dielectric loss due to the interaction of the ac electric field with phonons are more pronounced. The extrinsic factors such as defects, interfaces, size and shape of the fillers, and micro-pores also have a major effect in controlling the dielectric loss. A new model considering these intrinsic and extrinsic parameters, which affects the loss tangent of the composites, will be able to provide a reasonably good fit for the experimental dielectric loss of the composites for all vol %.

The theoretical predictions of dielectric loss for PS/SZS and HDPE/SZS composites are shown in Fig. 5.9 (a-b). As already discussed, the dielectric loss of SZS does not have a significant role in controlling the dielectric loss of the PS/SZS and HDPE/SZS composites. Instead the extrinsic factors like amount of porosity, moisture absorption and interface region between the polymer and ceramic determine the dielectric loss of the composites. None of these theoretical models takes these factors into account and hence are not valid for the composites involving PS and HDPE. But the above argument is not valid for DGEBA/SZS composites due to a large difference in tan δ of virgin DGEBA and SZS and hence the theoretical predictions are valid at least for small amounts of filler loading.

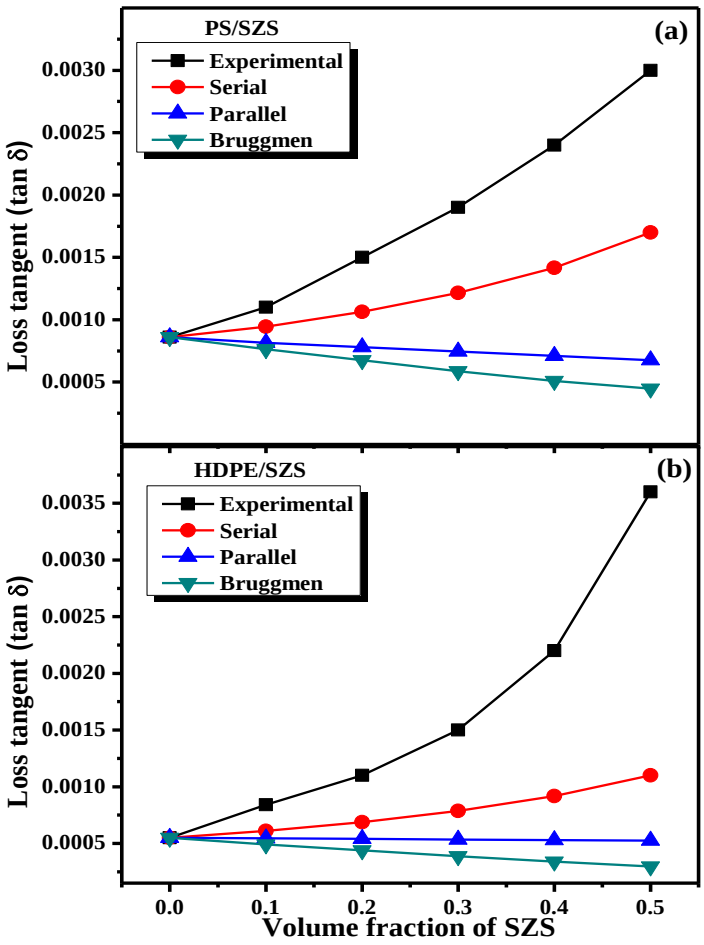

Figure 5.9 Theoretical modeling of dielectric loss of (a) PS/SZS (b) HDPE/SZS composites.

The variation of relative permittivity with temperature is one of the important properties which control the overall performance of the substrate materials. Fig. 5.10 represents the temperature dependence of relative permittivity at 1MHz of PS/SZS, HDPE/SZS and DGEBA/SZS composites for v_f = 0.20 and 0.40. All the compositions exhibit steady values of relative permittivity in the temperature range 20-75 ^{o}C. Therefore relative permittivity is nearly independent of temperature showing a deviation of less than 2 % for all compositions. The composites containing DGEBA matrix show a small increase in relative permittivity with temperature. The increase in temperature leads to the segmental mobility of the polymer molecules which aligns the dipoles parallel to the field which in turn increases the relative permittivity. (Xie *et al.*, 2005) At high

temperatures and for high filler content, the segmental mobility factor increases causing an increase in relative permittivity. Thus it can be concluded that PS/SZS and HDPE/SZS composites exhibit a good temperature stability of relative permittivity compared to that of DGEBA/SZS composites.

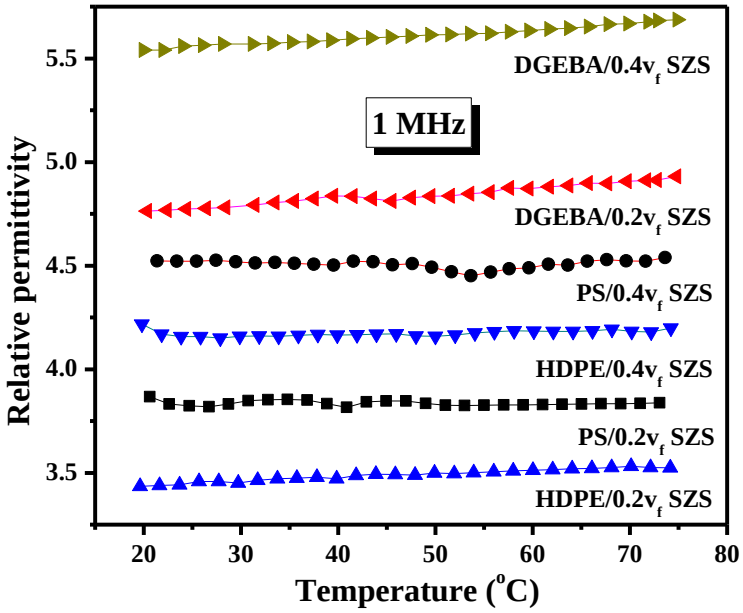

Figure 5.10 Variation of relative permittivity at 1 MHz of polymer/ceramic composites for a filler concentration of v_f = 0.20 and 0.40.

(iv) Thermal conductivity

Fig. 5.11 (a) shows the variation of thermal conductivity of the composites with the volume fraction of the filler. The thermal conductivities of all the polymer composites increase with the filler content. The value of thermal conductivity for SZS ceramic is found to be 16.5 W/mK which is high compared to that of polymers. This would explain the increase in the thermal conductivity values with ceramic loading. The presence of more connecting paths between the filler particles also contribute to the increase in the thermal conductivity of the composites. The HDPE/SZS composites show a high rate of increase in thermal conductivity than PS/SZS and DGEBA/SZS composites. This might be due to the relatively high thermal conductivity of polyethylene (0.45 Wm^{-1} K^{-1}) compared to that of polystyrene (0.08 Wm^{-1} K^{-1}) and DGEBA (0.12 Wm^{-1} K^{-1}). At a filler content of 0.5 v_f, the thermal conductivity of HDPE/SZS composites becomes

nearly six times that of pure polyethylene. This is a much satisfactory result when compared with earlier reports (Zhou *et al.*, 200; Lu *et al.*, 1997). Typical values of thermal conductivity of PS/SZS, HDPE/SZS and DGEBA/SZS composites respectively are 2.06, 0.77 and 1 W/mK for a filler content of 0.40 v_f.

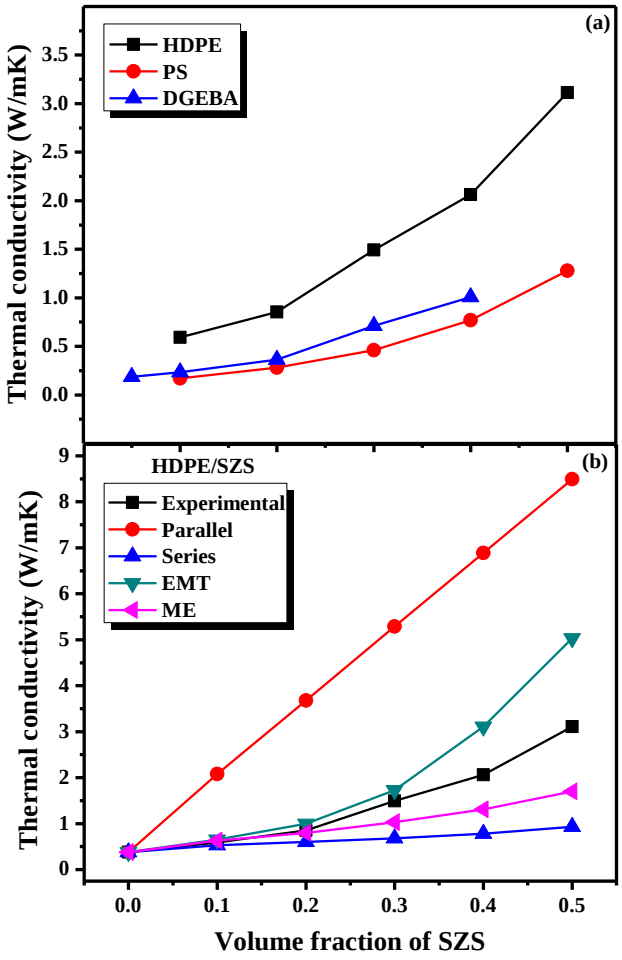

Figure 5.11 (a) Variation of thermal conductivity of PS/SZS, HDPE/SZS and DGEBA/SZS composites (b) Theoretical modeling of thermal conductivity of HDPE/SZS composites as a function of filler loading.

Fig. 5.11 (b) shows a comparative study of the observed value of thermal conductivity of HDPE/SZS composites with that of the theoretical predictions. Fig. 5.12 (a-b) shows the theoretical predictions of thermal conductivity for PS/SZS and DGEBA/SZS composites. The physical structures assumed in the series and parallel models are of layers of the phases aligned either perpendicular or parallel to the heat

flow, as their names imply. The series and parallel models give only a lower and upper limit of the expected thermal conductivity values of the composites respectively. As seen from the Fig. 5.11 (b) and 5.12 (a-b), the observed values of thermal conductivity lie within the range determined by the series and parallel mixing rules.

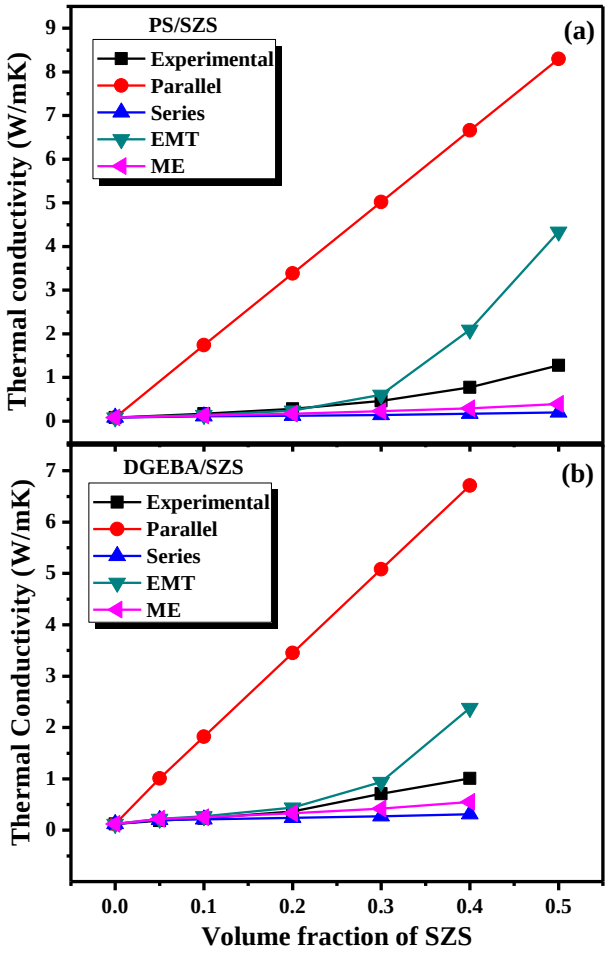

Figure 5.12 Theoretical modeling of thermal conductivity of (a) PS/SZS (b) DGEBA/SZS composites.

The Maxwell model assumes a dispersion of small spheres within a continuous matrix of a different phase, with the spheres being far enough apart such that the local distortions to the temperature distributions around each of the spheres do not interfere with their neighbors' temperature distributions. This assumption is valid only for low ceramic loading and hence the equation gives satisfactory results up to v_f = 0.20 v_f of SZS loading. As the v_f of SZS increases, agglomeration of ceramic particles results as

seen from SEM images in Fig. 5.3, thereby increasing the mismatch between the observed and theoretical values. The EMT model assumes a completely random distribution of all the phases. The EMT model closely follows the observed values up to 0.30 v_f of SZS loading. For higher ceramic loading, however, this model also fails to give a correct account of the observed values of thermal conductivity.

Thus none of the theoretical models used in this study give good results, especially for higher filler concentration of the filler. The wide variations in filler geometry, orientation and dispersion makes it difficult to compare composites filled with different materials. Moreover, the interfacial boundary thermal resistance between the filler particles and the matrix, referred to as Kapitza resistance (Benveniste *et al.*, 1986), is not taken into account while calculating the thermal conductivity of composites. It arises from the combination of poor mechanical or chemical adherence at the interface and a mismatch in CTE. No experimental method seems to be available for the direct measurement of interfacial thermal resistance (Nan *et al.*, 2000). Also the theoretical models explained above do not consider the porosity of the composites. As a result, experimental and theoretical thermal conductivity data are often not in agreement and a single equation for the prediction of thermal conductivity applicable to all systems becomes difficult (Hill *et al.*, 2004).

(v) Coefficient of thermal expansion (CTE)

When a composite is heated, polymer matrix will expand more than ceramic fillers. However, if the interfaces are capable of transmitting stress, the expansion of matrix will be reduced (Holliday *et al.*, 1973). SZS has a coefficient of thermal expansion (CTE) of 5.5 ppm/^oC in the temperature range 25-150 ^oC, while polymers in general have very high values of CTE. Virgin PS, HDPE and DGEBA matrices respectively have CTE values of ~100, 250 and 90 ppm/^oC. Generally, CTE of composites is reduced with an increase of filler content and composites with strong interface exhibit an additional reduction of CTE (Kang *et al.*, 2001). The presence of ceramic causes the polymer chains to get arrested and unable to expand with temperature. Fig. 5.13 (a) depicts the variation of CTE of PS/SZS, HDPE/SZS and DGEBA/SZS composites as a function of filler content. A significant reduction in CTE is observed for all the composites. The

composites PS/SZS and HDPE/SZS exhibit CTE values of 23.5 and 76.2 ppm/^{o}C respectively for a filler concentration of 0.50 v_f. Similarly a value of 36.9 ppm/^{o}C is observed for the composition DGEBA/0.40 v_f SZS.

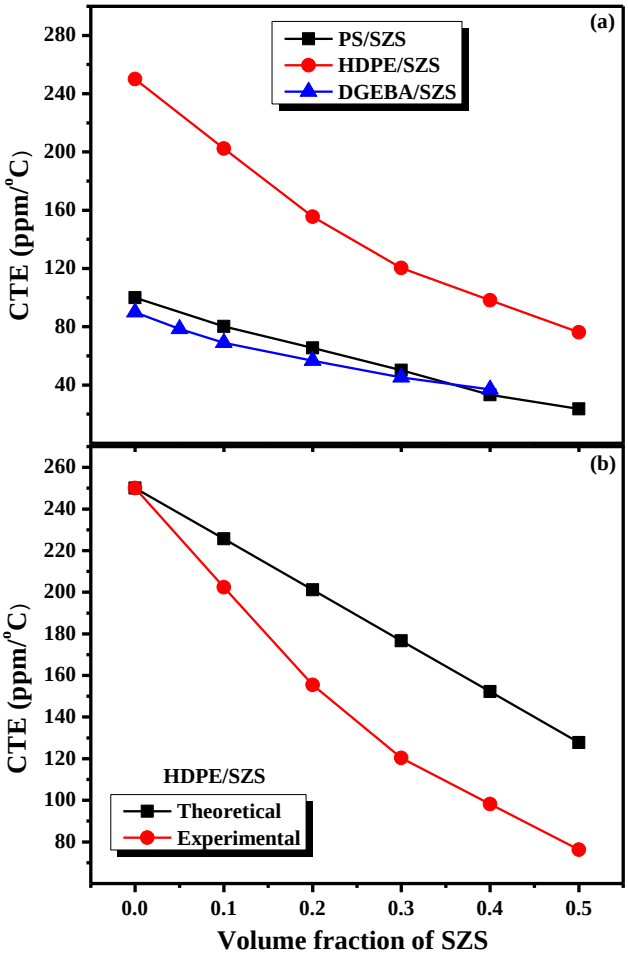

Figure 5.13 (a) Variation of CTE of PS/SZS, HDPE/SZS and DGEBA/SZS composites (b) Theoretical modeling of CTE of HDPE/SZS composites as a function of filler loading.

Fig. 5.13 (b) gives a comparison of the experimental values of CTE and their theoretical predictions for various filler concentrations of HDPE/SZS composites. Fig. 5.14 (a-b) shows the same details for PS/SZS and DGEBA/SZS composites. The theoretical predictions are calculated by using the equation (5.10).

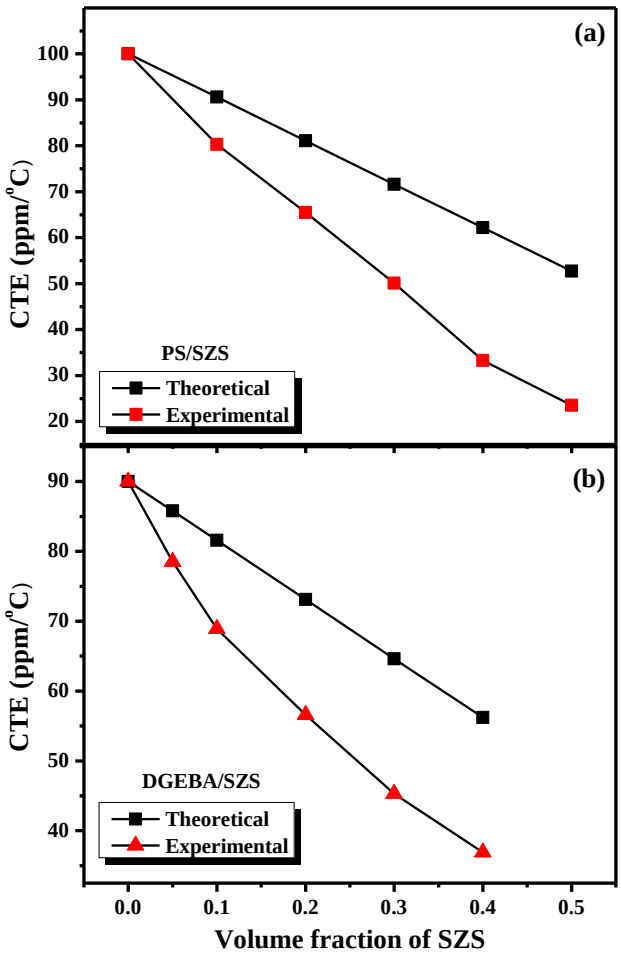

Figure 5.14 Theoretical predictions of CTE of (a) PS/SZS (b) DGEBA/SZS composites.

The CTE of the composites calculated are found to be higher than the experimentally obtained values. The equation gives only a rudimentary approximation of the CTE of the composites because the factors bulk modulus, thermal softening point and microstructure of the polymer and ceramic components are different, which are not taken into account while formulating the theoretical prediction. Also the effect of porosity on the thermal expansion of the samples is not considered in equation (5.10). In actual practice the presence of air in the sample can reduce the coefficient of thermal expansion of the polymer/ceramic composites. This can be the reason for the large deviation of the experimentally observed values of CTE from the theoretical ones, especially at high filler loadings of the ceramic, where the porosity is a maximum.

(vi) Tensile strength

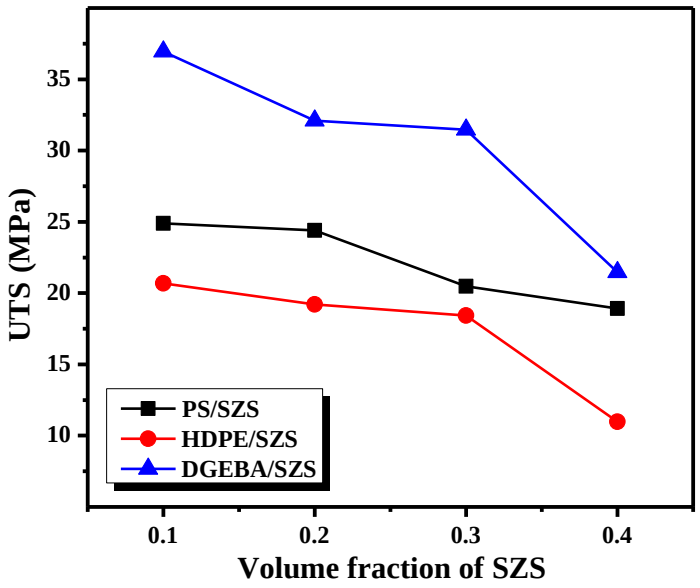

Figure 5.15 Variation of tensile strength of the composites with filler loading.

The ultimate tensile strength (UTS) of the composites studied as a function of filler loading is shown in Fig. 5.15. Earlier studies show that in the case of particulate filled polymers, tensile strength decreases due to poor filler–matrix interface and porosity (Chen *et al.*, 2003; Murali *et al.*, 2009). In the present case also, tensile strength decreases as a result of filler loading in the polymer matrix. When the polymers are loaded with more and more inorganic filler, the deformation area in the matrix decreases which in turn reduces the tensile strength. The interface volume increases at higher filler loading which leads to more filler–filler interaction and there by weakens the filler–matrix interface. The presence of air in the composites also weakens the filler-matrix interface. Weak interface is one of the reasons for reduced tensile strength. An ultimate tensile strength of ~ 19 MPa, 11 MPa, 22 MPa are obtained for PS/SZS, HDPE/SZS and DGEBA/SZS at a filler loading of 0.40 v_f. Thus HDPE/SZS composites exhibited poor mechanical properties compared to the other two. This might be due to the fact that HDPE has relatively low values of the forces of intermolecular interactions. Moreover, its mechanical strength is largely due to its semi-crystalline nature. Incorporation of foreign inclusions in to the polymer induces modifications to the degree of crystallinity and implicitly on its mechanical properties (Rusu *et al.*, 2001).

(vii) Vickers microhardness

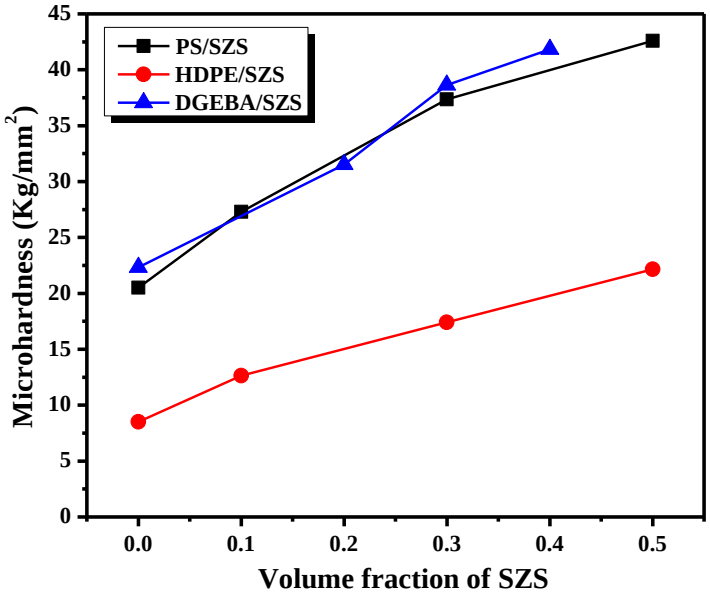

Figure 5.16 Variation of Vickers microhardness of the composites with filler loading.

Microhardness of the composites gives additional information on micromechanical properties with respect to filler loading. Micro indentation technique has been increasingly used in characterizing homopolymers and polymer composites. It is worth to note from the SEM micrographs of the composites that as the volume fraction of ceramics increases the connectivity among the filler ceramics also increases which in turn improves the properties. The variation in microhardness with filler loading is shown in Fig. 5.16. It can be noted that as the ceramic content increases the hardness also increases. This must be due to the high value of microhardness of the SZS ceramic compared to the polymer matrices. The measured value of microhardness of SZS, PS, HDPE and DGEBA are ~ 340, 20.5, 8.5 and 22.5 Kg/mm^2 respectively. The values obtained for the composites PS/0.5v_f SZS, HDPE/0.5v_f SZS and DGEBA/0.4v_f SZS are respectively 42.5, 22.2 and 41.8 Kg/mm^2 respectively.

5.5 Conclusions

Phase pure $Sr_2ZnSi_2O_7$ powder prepared using solid state ceramic route having a median particle size of 3.9 μm were used as a filler to improve the electrical, thermal and mechanical properties of polystyrene, high density polyethylene and DGEBA matrices.

PS/SZS and HDPE/SZS composites were prepared by melt mixing technique and DGEBA/SZS composites by mechanical mixing. Low values of ε_r and tan δ were obtained at microwave as well as radio frequency range for the whole range of filler loading. The theoretical models for the prediction of relative permittivity, thermal conductivity and the coefficient of thermal expansion fail to give an accurate account of the observed values for higher filler loadings. This is attributed to the effect of porosity, interfacial volume and clustering of filler particles with increase in the filler content. It is found that ε_r is nearly stable with variation in the temperature, which is one of the major criterions for packaging applications. An improvement in the CTE of the composites is observed with increase in the filler loading, whereas the moisture absorption resistance decreases. The tensile strength of the composites decreases and the microhardness increases with filler loading. The following table summarizes the major results of the polymer/ceramic composites for 0.4 v_f of filler loading.

Table 5.3 The major results of the polymer/ceramic composites for 0.4 v_f of filler loading.

Properties	**PS/SZS**	**HDPE/SZS**	**DGEBA/SZS**
Density (g/cm^3)	2.16	2.14	2.22
Moisture absorption (wt%)	0.097	0.062	0.142
Relative permittivity (1 MHz)	4.45	4.23	5.85
Dielectric loss tangent (1 MHz)	0.0053	0.0053	0.0185
Relative permittivity (5 GHz)	3.95	4.16	4.63
Dielectric loss tangent (5 GHz)	0.0024	0.0022	0.0162
Thermal conductivity (W/mK)	0.77	2.06	1.01
CTE (ppm/^oC)	33.3	98.2	36.9
Tensile strength (MPa)	18.9	11.0	21.5
Microhardness (Kg/mm^2)	~ 40	~ 20	41.8

Chapter 6

Conclusions and Scopes for Future Works

6.1 Conclusions of the Ph. D thesis

The rapid development in the microelectronic technologies such as wireless LAN, intelligent transport system (ITS) and microwave integrated circuits (MIC) has led to an increase in the utilized frequency from kilometre wave to millimetre wave. The increase in the operating frequency demands the use of materials having low permittivity and low loss in electronic equipments as a result of their immense technological applications. A low value of relative permittivity (< 10) can assure small signal propagation delay and reduced capacitive coupling between the conductor lines of electronic substrates. It can also be useful for the preparation of dielectric resonators at very high frequencies since the size of dielectric resonators prepared using medium or high relative permittivity materials will be too small to be handled. Silicates are found to be suitable for attaining low loss low permittivity materials. Because the predominantly covalent nature of Si-O bond in the SiO_4 tetrahedron, which is the basic building block of all the silicates, restricts rattling of ions thereby giving low values of relative permittivity as well as dielectric loss.

The present investigation, in conclusion, deals with the synthesis, characterization, structure and properties of some silicates their composites for various applications such as dielectric resonators and electronic packaging. The whole work can be divided into three parts as follows

I. Preparation and characterization of silicates having general formula $A_2BSi_2O_7$, A_2SiO_4 and $CaBSi_2O_6$ where A = Ca, Sr, Ba and B = Zn, Mg, Ni, Co, Mn.
II. Lowering of the sintering temperature of selected silicates ($CaMgSi_2O_6$ and $Sr_2ZnSi_2O_7$) by forming composites with Li based borosilicate glasses for LTCC applications.
III. Preparation and characterization $Sr_2ZnSi_2O_7$ based polymer-ceramic composites using three different polymers PS, HDPE and DGEBA for application as soft substrates.

6.1.1 Part I: Development of low loss silicates

Solid solutions $(Sr_{1-x}A_x)_2(Zn_{1-x}B_x)Si_2O_7$ having a tetragonal structure were formed for substitutions A = Ca and B = Mg, Mn, Co in the range $0 \leq x \leq 1$. The composition $(Sr_{0.25}Ba_{0.75})_2ZnSi_2O_7$ had a monoclinic crystal structure. In the case of $Sr_2(Zn_{1-x}Ni_x)Si_2O_7$, a mixture of $SrSiO_3$ and NiO phases resulted when $x > 0.50$. The variation of cell parameters and cell volumes of solid solutions $(Sr_{1-x}A_x)_2(Zn_{1-x}B_x)Si_2O_7$ were according to the size of the substituted ions as expected. The microwave dielectric properties of all the compositions were investigated. Excellent properties $\varepsilon_r = 8.4$, $Q_u \times f = 105000$ GHz and $\tau_f = -51.5$ ppm/◦C were obtained for $Sr_2ZnSi_2O_7$ when sintered at 1475 ^oC/2h. The substitutions at Sr and Zn-sites lowered the $Q_u \times f$ values of $Sr_2ZnSi_2O_7$. The high value of $\tau_f = -51.5$ ppm/◦C of $Sr_2ZnSi_2O_7$ is lowered by adding small amount of $SrTiO_3$. $Sr_2ZnSi_2O_7$ + 2 wt% $SrTiO_3$ sintered at 1450 ^oC/2h has $\varepsilon_r = 8.8$, $Q_u \times f = 60000$ GHz (at 12.585 GHz) and $\tau_f = -13$ ppm/◦C and is a possible material for millimeter wave communication systems and microwave substrates. The thermal expansion coefficient of $Sr_2ZnSi_2O_7$ was found to be +4.9 ppm/^oC in the temperature range 30-500 ^oC.

The formation of Ba_2SiO_4, β-Sr_2SiO_4 and β-Ca_2SiO_4 phases was confirmed by X-ray diffraction studies while investigating the orthosilicates A_2SiO_4. The sintering temperatures of Ba_2SiO_4, Sr_2SiO_4 and Ca_2SiO_4 were 1525 ^oC, 1575 ^oC and 1450 ^oC respectively. The values of ε_r were decreased in the order $Ba_2SiO_4 > Sr_2SiO_4 > Ca_2SiO_4$ due to the decrease in the ionic polarizability of M^{2+} cations. The $Q_u \times f$ values obtained were 17900 GHz, 19100 GHz and 26100 GHz for Ba_2SiO_4, Sr_2SiO_4 and Ca_2SiO_4 respectively. The τ_f of Ba_2SiO_4 was -17 ppm/^oC, whereas Sr_2SiO_4 and Ca_2SiO_4 exhibited high values of τ_f, -205 ppm/^oC and -89 ppm/^oC respectively. Therefore further modification of τ_f is needed before any practical application of these alkaline earth orthosilicates. The values of α_l were +10.3 ppm/^oC for Ba_2SiO_4, +6.2 ppm/^oC for Sr_2SiO_4 and +7.0 for Ca_2SiO_4.

The phase formation of $CaMgSi_2O_6$, $CaCoSi_2O_6$ and $CaNiSi_2O_6$ were identified using the X-ray diffraction analysis, whereas $CaMnSi_2O_6$ and $CaZnSi_2O_6$ did not form. The $CaMgSi_2O_6$ ceramics sintered at 1300 ^oC/2h has $\varepsilon_r = 8.3$, $Q_u \times f = 53000$ GHz and $\tau_f =$ -45 ppm/◦C in the frequency range 8-12 GHz. $CaCoSi_2O_6$ sintered at 1200 ^oC/2h has $\varepsilon_r =$

8.5, $Q_u \times f$ = 28500 GHz and τ_f = -55 ppm/◦C in the same frequency range. Similarly $CaNiSi_2O_6$ sintered at 1300 ^oC/2h has ε_r = 8.3, $Q_u \times f$ = 23200 GHz and τ_f = -41 ppm/◦C. in the frequency range 8-12 GHz. $CaMgSi_2O_6$, $CaCoSi_2O_6$ and $CaNiSi_2O_6$ show small positive values of coefficient of thermal expansion 3.7, 1.9 and 2.0 ppm/^oC respectively. The useful results of the investigations carried out in part (1) can be summarized by the table 6.1.

Table 6.1 Useful results of part (1) of the Ph. D work (development of low loss silicates).

Composition	**Sintering temperature**	**ε_r**	**$Q_u \times f$ GHz**	**τ_f ppm/◦C**
$CaMgSi_2O_6$	1300 ^oC	8.3	53000	−45
$Sr_2ZnSi_2O_7$	1475 ^oC	8.4	105000	−51.5
$Sr_2ZnSi_2O_7$ + 2 wt% $SrTiO_3$	1450 ^oC	8.8	60000	−13

6.1.2 Part II: Development of materials suitable for LTCC applications

Out of the whole compositions described above, two of them were found to have interesting microwave dielectric properties suitable for the substrate as well as DR applications in electronic devices and hence were further investigated for their suitability for LTCC applications. The first one is $CaMgSi_2O_6$ (CMS) ceramics and the second one is $Sr_2ZnSi_2O_7$ (SZS). The major problem with both these ceramics was their high sintering temperature. For LTCC applications low loss metals like Ag, Au etc. have to be co-fired with the ceramics developed for making conductive lines. But the melting points of these metals are less than 1000 ^oC. Hence it was necessary to lower the sintering temperature of these ceramics below the melting point of Ag (in the present work). Thus Part (2) of the work was aimed to reduce the sintering temperature of CMS and SZS ceramics by forming composite of these ceramics with low melting borosilicate glasses.

Among the various glass powders used only $35.14Li_2O$-$31.66B_2O_3$-$33.2SiO_2$ (LBS), and $20Li_2O$-$20MgO$-$20ZnO$-$20B_2O_3$-$20SiO_2$ (LMZBS) were found to be useful in lowering the sintering temperature of CMS. The sintering temperature could be reduced to 925 ^oC/2h for CMS+15wt% LBS composite with the dielectric properties ε_r = 8, $Q_u \times f$

= 15,000 GHz and τ_f = −49 ppm/◦C. The CMS+15wt% LMZBS had ε_r = 8.2, $Q_u \times f$ = 32,000 GHz and τ_f = −48 ppm/◦C, when sintered at 900 ^oC/2h. The values of α_l in the temperature range 30 ^oC to 500 ^oC were +5.14 and +5.85 for CMS+15wt% LBS and CMS+15wt% LMZBS respectively, which are close to that of Si. The increase in relative permittivity (at 1 MHz) was less than 3.5% for both of the composition in the temperature range -25 ^oC to 75 ^oC and hence exhibits good temperature stability of relative permittivity. The compatibility studies showed that Ag remains unreacted with CMS/glass composites. The τ_f values become more negative with the addition of LBS and LMZBS glasses. The high negative τ_f values obtained for the CMS/glass composites preclude their immediate use in practical applications. Further research is to be carried out to tailor the τ_f values ~ 0 by using materials having high positive τ_f values such as TiO_2, $CaTiO_3$ etc.

Table 6.2 Major results of part (2) of the Ph. D work (development of materials suitable for LTCC applications).

Composition	**Sintering temperature**	**ε_r**	**$Q_u \times f$ GHz**	**τ_f ppm/◦C**	**change in ε_r (1 MHz)**	**Reaction with Ag**	**CTE ppm/◦C**
CMS+15wt% LBS	925 ^oC	8.0	15000	−49	3.1%	No	+5.1
CMS+15wt% LMZBS	900 ^oC	8.2	32000	−48	3.3%	No	+5.8
SZS+15wt% LMZBS	875 ^oC	7.9	39000	−53	3.4%	No	+5.8

The addition of LMZBS glass was effective in lowering the sintering temperature of SZS ceramics from 1475 ^oC to below the melting point of Ag. The composition SZS + 15 wt % LMZBS exhibited ε_r = 7.9, $Q_u \times f$ = 39 000 GHz, and τ_f = −53.5 ppm/^oC, when sintered at 875 ^oC. The decrease in ε_r and $Q_u \times f$ of the SZS/LMZBS composite is attributed to the low ε_r and high dielectric loss of the LMZBS phase. Ag is found to be chemically compatible with the SZS/LMZBS composite. Green tapes were cast using SZS + 15 wt % LMZBS composite with the help of suitable additives and solvents. The tapes were stacked, sintered and the dielectric properties investigated in the temperature range 10–290 K. A small increase (< 3.5%) in the values of relative permittivity is

observed with the increase in temperature from 10 K to 290 K, which is due to the increased polarizability with volume. In the temperature range 100 K to 290 K, dielectric loss remained of the order of 1.5×10^{-3}. The values obtained for relative permittivity (~ 8), dielectric loss (~ 10^{-3}) and variation of relative permittivity with temperature (< 3.5%) of the ceramic tapes developed using SZS/LMZBS composites show that it can be used as LTCC material for substrate applications (hard substrates). The major results of work based on developing LTCC materials are summarized in table 6.2.

6.1.3 Part III: Development of polymer/ceramic composites for soft substrates

Table 6.3 The major results part (3) of the Ph. D work for 0.4 v_f of filler loading (development of the polymer/ceramic composites for substrate applications)

Properties	**PS/SZS**	**HDPE/SZS**	**DGEBA/SZS**	**FR4**
Density (g/cm^3)	2.16	2.14	2.22	1.85
Moisture absorption (wt%)	0.097	0.062	0.142	0.10
Relative permittivity (1 MHz)	4.45	4.23	5.85	4.70
Dielectric loss tangent (1 MHz)	0.0053	0.0053	0.0185	0.014
Relative permittivity (5 GHz)	3.95	4.16	4.63	4.35
Dielectric loss tangent (5 GHz)	0.0024	0.0022	0.0162	0.016
Thermal conductivity (W/mK)	0.77	2.06	1.01	0.35
CTE (ppm/^oC)	33.3	98.2	36.9	18
Tensile strength (MPa)	18.9	11.0	21.5	300
Microhardness (Kg/mm^2)	~ 40	~ 20	41.8	--

As already explained $Sr_2ZnSi_2O_7$ had the best microwave dielectric properties out of all compositions studied. Hence it was selected for forming polymer ceramic composites with various polymers like polystyrene (PS), high density polyethylene (HDPE) and Diglycidyl ether of bisphenol A (DGEBA). The suitability of the polymer/ceramic composites for applications as soft substrates was the major concern of part III of the work. Low values of ε_r and tan δ were obtained at microwave as well as radio frequency range for the whole range of filler loading. The theoretical models for the prediction of relative permittivity, thermal conductivity and the coefficient of thermal

expansion fail to give an accurate account of the observed values for higher filler loadings. This is attributed to the effect of porosity, interfacial volume and clustering of filler particles with increase in the filler content. It is found that ε_r is nearly stable with variation in the temperature, which is one of the major criterions for packaging applications. An improvement in the thermal conductivity and CTE of the composites is observed with increase in the filler loading, whereas the moisture absorption resistance decreases. The tensile strength of the composites decreases and the microhardness increases with filler loading. Typical values of important properties of polymer/ceramic composites for 0.4 v_f of filler loading is shown in table 6.3. The properties of the commercially available FR4 (glass filled epoxy) is also given for a comparison. It can be seen that PS/SZS and HDPE/SZS composites are superior to that of FR4 in terms of relative permittivity, dielectric loss and thermal conductivity.

6.2 Scopes for future work

As already seen it was able to develop low permittivity low loss silicates suitable for DR as well as electronic packaging applications, especially $CaMgSi_2O_6$ and $Sr_2ZnSi_2O_7$ ceramics. But the temperature stability of resonant frequency these silicates still remains as an unsolved issue. For instance, $CaMgSi_2O_6$ has τ_f = -45 ppm/^oC and $Sr_2ZnSi_2O_7$ ceramics has τ_f = -51 ppm/^oC. Attempts were made to tune the τ_f value of $Sr_2ZnSi_2O_7$ ceramics by the addition of $SrTiO_3$ having a τ_f value of +1600 ppm/^oC, which were successful upto a certain extend. The addition of 2 wt% of $SrTiO_3$ resulted in a τ_f = -13 ppm/^oC, with a simultaneous deterioration in $Q_u \times f$ values. Further tuning was not possible as the dielectric loss of $SrTiO_3$ is very high. Therefore it is to be attempted to reduce the τ_f value of $Sr_2ZnSi_2O_7$ ceramics to ~ 0 ppm/^oC by forming composites with other compounds like TiO_2 and $CaTiO_3$. The dielectric losses of these compositions are less than that of $SrTiO_3$ and hence may result in higher $Q_u \times f$ values. It should also be noted that TiO_2 can act as a sintering aid thereby lowering the sintering temperature of $Sr_2ZnSi_2O_7$ ceramics, which will be an added advantage. Similar studies should also be performed for $CaMgSi_2O_6$ ceramics as the material is not temperature compensated.

It is seen from the investigations on the LTCC materials that even though glass addition lowers the sintering temperature, the microwave dielectric properties are

adversely affected. Hence chemical synthesizing techniques like hydrothermal, co-precipitation, citrate-gel, sol-gel etc. would be much challenging area towards the development of these silicates. Ceramics tapes were cast and sintered using the composition $Sr_2ZnSi_2O_7$+15wt% LMZBS glass and their microwave dielectric properties investigated. It would be highly appreciable if it is possible to develop electronic devices like flow sensor, gas viscosity sensor, force sensor or micro reactor. Various polymer ceramic composites developed in the present study may be used to fabricate substrates for antenna and printed circuit board applications. Moreover efforts may be made to improve the thermal conductivity of these composites by the addition of suitable amount of AlN. Broadband DRAs of different geometries and DRA array using temperature stable DRs can also be fabricated using the developed DR materials.

BIBLIOGRAPHY

Adams, R. D., Layland, R., Payen, C. and Datta, T. "Syntheses, structural analyses, and unusual magnetic properties of $Ba_2CoSi_2O_7$ and $BaCo_2Si_2O_7$," *Inorg. Chem.*, **35**, 3492 (1996).

Afsar, M. U., Birch, J. R., Clarke, R. N. and Chantry, G. W. "The measurement of the properties of materilas," *Proceedings of the IEEE*, **74**, 183 (1986).

Agari, Y., Tanaka, M., Nagai, S. and Uno, T. "Thermal-conductivity of a polymer composite filled with mixtures of particles," *Journal Of Applied Polymer Science*, **34**, 1429 (1987).

Aitasalo, T., Hölsä, J., Laamanen, T., Lastusaari, M., Lehto, L., Niittykoski, J. and Pellé, F. "Crystal structure of the monoclinic $Ba_2MgSi_2O_7$ persistent luminescence material," *Z. Kristallogr. Suppl.*, **23**, 481 (2006).

Alexander, J. "Cofirable resistors for low-temperature ceramic tape," *1993 International Symposium on Microelectronics*, **2105**, 204 (1993).

Alford, N. M. and Penn, S. J. "Sintered alumina with low dielectric loss," *J. Appl. Phys.*, **80**, 5895 (1996).

Alford, N. M., Wang, X., Penn, S. J., Poole, M. and Jones, A. *Br. Ceram. Trans.*, **99**, 212 (2000).

Ando, M., Himura, K., Tsunooka, T., Kagomiya, I. and Ohsato, H. "Synthesis of high quality forsterite," *Jpn. J. Appl. Phys.*, **46**, 7112 (2007).

Ang, C., Yu, Z., Guo, R. and Bhalla, A. S. "Calculation of dielectric constant and loss of two-phase composites," *J. Appl. Phys.*, **93**, 3475 (2003).

Anjana, P. S. and Sebastian, M. T. "Microwave dielectric properties and low-temperature sintering of cerium oxide for ltcc applications," *J. Am. Ceram. Soc.*, **92**, 96 (2009).

Anjana, P. S., Sebastian, M. T., Suma, M. N. and Mohanan, P. "Low dielectric loss ptfe/ceo_2 ceramic composites for microwave substrate applications," *Int. J. Appl. Ceram. Technol.*, **5**, 325 (2008).

Arai, Y. *Chemistry of powder production*, Chapman and Hall, London (1996).

Bacon, G. E. *X-ray and neutron diffraction*, Pergamon press, Amsterdam (1966).

Bahl, I. J. and Bhartia, P. *Microwave solid state circuit design*, Wiley, New York (1988).

Bai, Y., Cheng, Z. Y., Bharti, V., Xu, H. S. and Zhang, Q. M. "High-dielectric-constant ceramic-powder polymer composites," *Appl. Phys. Lett.*, **76**, 3804 (2000).

Bali, B. E. and Zavalij, P. Y. "Tetragonal form of barium cobalt disilicate, $Ba_2CoSi_2O_7$," *Acta. Cryst.*, **E59**, i59 (2003).

Ballo, D. *Network analyzer basics*, Santa Rosa, Hewlett-Packard Company, CA (1998).

Beke, B. *Principles of Communition*, Akademi Kiado, Budapest (1964).

Benveniste, Y. and Miloh, T. "The effective conductivity of composites with imperfect thermal contact at constituent interfaces," *Int. J. Eng. Sci.*, **24**, 1537 (1986).

Bersaum, M. W. *Fundamentals of ceramics*, Magraw Hill, New York (1997).

Binner, J., Chang, H. and Higginson, R. "Processing of ceramic-metal interpenetrating composites," *J. Eur. Ceram. Soc.*, **29**, 837 (2009).

Bish, D. L. and Post, J. E. "Modern powder diffraction. Reviews in mineralogy, mineralogical association of america, boston.,"**20** (1989).

Bolt, J. D., Button, D. P. and Yost, B. A. "Ceramic-fiber polymer composites for electronic substrates," *Materials Science And Engineering A-Structural Materials Properties Microstructure And Processing*, **109**, 207 (1989).

Braginsky, V. B., Ilschenko, V. S. and S., B. K. " Experimental observation of fundamental microwave absorption in high quality dielectric crystals.," *Appl. Phys. A.*, **120**, 300 (1987).

Breeze, J. D., Perkins, J. M., McComb, D. W. and Alford, N. M. "Do grain boundaries affect microwave dielectric loss in oxides?," *J. Am. Ceram. Soc.*, **92**, 671 (2009).

Bur, A. J. "Dielectric properties of polymers at microwave frequencies: A review," *Polymer*, **26**, 963 (1985).

Button, D. P., Yost, B. A., French, R. H., Hsu, W. Y., Belt, J. D., Subrahmanian, M. A., Zhang, H.-M., Geidd, R. E., Whittacker, A. J. and Onn, D. G. *Ceramic-fiber/polymer laminates :Thermally conductive composites with low dielectric constants*, American Ceramic Society, Westerville, OH (1989).

Cahn, R. W., Haasen, P. and Krawer, E. J. *Structure and properties of composites*, VCH, Tokyo (1993).

Castro, D. F. *Sintering Course, Presented at Centro de Estudios e Investigaciones Técnicas de Gipuzkoa Centro de Estudios e Investigaciones Técnicas de Gipuzkoa, San Sebastián* (2000).

Catti, M., Gazzoni, G. and Ivaldi, G. "Structures of twinned β-Sr_2SiO_4 and α`-$Sr_{1.9}Ba_{0.1}SiO_4$," *Acta Cryst.*, **C39**, 29 (1983).

Cava, R. J. "Dielectric materials for applications in microwave communications," *J. Mater. Chem.*, **11**, 54 (2001).

Chang, M. W., Lyoo, S. H., Choo, H. S. and Lee, J. M. "Properties of glasses based on the CaO-MgO-SiO_2 system for low-temperature co-fired ceramic," *Ceram. Inter.*, **35**, 2513 (2009).

Chaouchi, A., d'Astorg, S., Marinel, S. and Aliouat, M. "$ZnTiO_3$ ceramic sintered at low temperature with glass phase addition for LTCC applications," *Mater. Chem. Phys.*, **103**, 106 (2007).

Chen, L. F., Ong, C. K., NeO, C. P., Varadan, V. V. and Varadan, V. K. *Microwave electronics: Measurement and materials characterization*, John Wiley & Sons, England (2004).

Chen, Y. C., Lin, H. C. and Lee, Y. D. "The effects of filler content and size on the properties of PTFE/SiO_2 composites," *Journal of Polymer Research-Taiwan*, **10**, 247 (2003).

Cheng, K. C., Lin, C. M., Wang, S. F., Lin, S. T. and Yang, C. F. "Dielectric properties of Epoxy resin-Barium Titanate composites at high frequency," *Mater. Lett.*, **61**, 757 (2007).

Chenggang, X., Yi, W. and Smith, B. G. "A novel approach for focusing electron beams using low-cost ceramic grid [field emitter arrays]," *Electron Devices, IEEE Transactions on*, **49**, 324 (2002).

Choi, B. G., Stubbs, M. G. and Park, C. S. "A k-band narrow band pass filter using ltcc technology," *IEEE Microwave Wireless Compon. Lett.*, **13**, 388 (2003).

Choi, Y. J., Park, J. H., Ko, W. J., Hwang, I. S., Park, J. G. and Nahm, S. "Co-firing and shrinkage matching in low- and middle- permittivity dielectric compositions for a low-temperature co-fired ceramics system," *J. Am. Ceram. Soc.*, **89**, 562 (2006).

Chou, C. F., Changrani, R., Roberts, P., Sadler, D., Burdon, J., Zenhausern, F., Lin, S., Mulholland, A., Swami, N. and Terbrueggen, R. "A miniaturized cyclic pcr device--modeling and experiments," *Microelectronic Engineering*, **61-62**, 921 (2002).

Chung, D. L. *Materials for electronic packaging*, Butterworth Heinemann, Washington (1995).

Coble, R. L. "Sintering crystalline solids. I. Intermediate and final state diffusion models," *J. Appl. Phys.*, **32**, 787 (1961).

Cohn, S. B. and Kelly, K. C. "Microwave measurement of high-dielectric-constant materials," *IEEE Trans. Microwave Theory Tech.*, **14**, 406 (1966).

Colla, E. L., Reaney, I. M. and Setter, N. "Effect of structural changes in complex perovskites on the temperature coefficient of the relative permittivity," *J. Appl. Phys.*, **74**, 3414 (1993).

Courtney, W. E. "Analysis and evaluation of a method of measuring the complex permittivity and permeability of microwave insulators," *IEEE Trans. Microw. Theory Technol.*, **MTT-18**, 476 (1970).

Cullity, B. D. and Stock, S. R. *Elements of x-ray diffraction*, Prentice Hall, New Delhi (2001).

Dias, C. J. and Das-Gupta, D. K. "Inorganic ceramic/polymer ferroelectric composite electrets," *Dielectrics and Electrical Insulation, IEEE Transactions on*, **3**, 706 (1996).

Dong, M. Z., Yue, Z. X., Zhuang, H., Meng, S. Q. and Li, L. T. "Microstructure and microwave dielectric properties of TiO_2-doped Zn_2SiO_4 ceramics synthesized through the sol-gel process," *J. Am. Ceram. Soc.*, **91**, 3981 (2008).

Doyle, W. T. and Jacobs, I. S. "Effective cluster model of dielectric enhancement in metal-insulator composites," *Physical Review B*, **42**, 9319 (1990).

Field, R. F. "The formation of ionized water films on dielectrics under conditions of high humidity," *J. Appl. Phys.*, **17**, 318 (1946).

Frohlics, H. *Theory of dielectrics*, Clarendon Press, Oxford (1950).

Fuji, T., Ando, A. and Sakabe, Y. "Characterization of dielectric properties of oxide materials in frequency range from GHz to THz," *J. Eur. Ceram. Soc.*, **26**, 1857 (2006).

Gektin, V., Bar-Cohen, A. and Witzman, S. "Coffin-manson based fatigue analysis of underfilled dcas," *IEEE Transactions on Components, Packaging, and Manufacturing Technology, Part A*, **21**, 577 (1998).

George, S., Anjana, P. S., Deepu, V. N., Mohanan, P. and Sebastian, M. T. "Low-temperature sintering and microwave dielectric properties of Li_2MgSiO_4 ceramic," *J. Am. Ceram. Soc.*, **92**, 1244 (2009).

George, S., Deepu, V., Mohanan, P. and Seabstian, M. T. "Influence of $Ca[(Li_{1/3}Nb_{2/3})_{0.8}Ti_{0.2}]O_{3-\delta}$ filler on the microwave dielectric properties of polyethylene and polystyrene for microelectronic applications," *Polymer Engineering And Science*, **in press** (2009).

German, R. *Fundamentals of particle packing theory*, John Wiley&Sons, Inc., New York, (1996).

Goldberg, L. "Multilayer, low-fire, ceramic substrates sport embedded components, new packaging solutions," *Electronic Design*, **43**, 40 (1995).

Goldsmith, A. *Design and performance of 3G wireless networks and wireless lans*, Springer, US (2005).

Gonon, P., Hong, T. P., Lesaint, O., Bourdelais, S. and Debruyne, H. "Influence of high levels of water absorption on the resistivity and dielectric permittivity of Epoxy composites," *Polymer Testing*, **24**, 799 (2005).

Guo, Y., Ohsato, H. and Kakimoto, K.-I. "Characterization and dielectric behavior of willemite and TiO_2-doped willemite ceramics at millimeter-wave frequency," *J. Eur. Ceram. Soc.*, **26**, 1827 (2006).

Gupta, T. K. "Instability of cylindrical voids in alumina," *J. Am. Ceram. Soc.*, **61**, 191 (1978).

Gurevich, V. L. and Tagantsev, A. K. "Intrinsic dielectric loss in crystals: Low temperature.," *Sov. Phys. JETP*, **64**, 142 (1986).

Gurevich, V. L. and Tagantsev, A. K. "Intrinsic dielectric loss in crystals," *Advances In Physics*, **40**, 719 (1991).

Håkansson, B. and Ross, R. G. "Effective thermal conductivity of binary dispersed composites over wide ranges of volume fraction, temperature, and pressure," *J. Appl. Phys.*, **68**, 3285 (1990).

Hakki, B. W. and Coleman, P. D. "A dielectric resonator method of measuring inductive capacitance in the millimeter range," *IRE Trans. Microwave Theory Tech.*, **MTT-8**, 402 (1960).

Hao, Y. and Wang, Y.-H. "Synthesis and photoluminescence of new phosphors M_2(Mg, Zn)Si_2O_7:Mn^{2+} (M = Ca, Sr, Ba)," *Mater. Res. Bull.*, **42**, 2219 (2007).

Harrop, P. J. "Temperature coefficients of capacitance of solids," *J. Mater. Sci.*, **4**, 370 (1969).

Harrop, P. J. *Dielectrics*, Wiley, Butterworth, London (1972).

Hatton, B. D., Landskron, K., Hunks, W. J., Bennett, M. R., Shukaris, D., Perovic, D. D. and Ozin, G. A. "Materials chemistry for low-k materials," *Materilas Today*, **9**, 22 (2006).

Heidinger, R. "Dielectric measurements on sapphire for electron cyclotron wave systems," *J. Nucl. Mater.*, **212–215,** 1101 (1994).

Herbert, J. M. *Ceramic dielectrics and capacitors*, Gordon and Breach Science Publishers, Reading, U. K. (1985).

Higuchi, Y., Sugimoto, Y., Harada, J. and Tamura, H. "LTCC system with new high-ε_r and high-Q material co-fired with conventional low ε_r base material for wireless communications," *J. Eur. Ceram. Soc.*, **27**, 2785 (2007).

Hill, R. F. and Supancic, P. H. "Determination of the thermal resistance of the polymer-ceramic interface of Alumina-filled polymer composites," *J. Am. Ceram. Soc.*, **87**, 1831 (2004).

Hippel, A. R. V. *Dielectric materials and applications*, Technology Press of MIT, Cambridge (1954).

Holliday, L. and Robinson, J. *J. Mater. Sci.*, **8**, 301 (1973).

Hong, J. I., Winberg, P., Schadler, L. S. and Siegel, R. W. "Dielectric properties of Zinc Oxide/low density polyethylene nanocomposites," *Mater. Lett.*, **59**, 473 (2005).

Hsiang, H.-I., Hsi, C.-S., Huang, C.-C. and Fu, S.-L. "Sintering behavior and dielectric properties of $BaTiO_3$ ceramics with glass addition for internal capacitor of LTCC," *J. Allyos Compd.*, **459**, 307 (2008).

Hu, T., Jantunen, H., Leppavuori, S., Deleniv, A. and Gevorgian, S. "Electricfield-controlled permittivity ferroelectric composition for microwave LTCC modules," *J. Am. Ceram. Soc.*, **87**, 578 (2004).

Hu, T., Uusimaki, A., Jantunen, H., Leppavuori, S., Soponmanee, K. and Sirisoonthorn, S. "Optimization of $MgTiO_3$–$CaTiO_3$ based LTCC tapes containing B_2O_3 for use in microwave applications," *Ceram. Int.*, **31**, 85 (2005).

Huang, C. L., Pan, C. L. and Lee, W. C. "Microwave dielectric properties of mixtures of glass forming oxides Zn-B-Si and dielectric ceramics $MgTiO_3$-$CaTiO_3$ for LTCC applications," *J. Alloys Compd.*, **462**, L5 (2008).

Huang, C. L., Pan, C. L. and Shium, S. J. "Liquid phase sintering of $MgTiO_3$-$CaTiO_3$ microwave dielectric ceramics," *Mater. Chem. Phys.*, **78**, 111 (2003).

Ichinose, N. *Introduction to fine ceramics, applications in engineering*, John Wiley and Sons, New York (1987).

Imanaka, Y. *Multilayered low temperature cofired ceramics (LTCC) technology*, Springer, Japan (2005).

Jantunen, H., Hu, T., Uusimäki, A. and Leppävuori, S. "Tape casting of ferroelectric, dielectric, piezoelectric and ferromagnetic materials," *J. Eur. Ceram. Soc.*, **24**, 1077 (2004).

Jantunen, H., Kangasvieri, T., Vähäkangas, J. and Leppävuori, S. "Design aspects of microwave components with LTCC technique," *J. Eur. Ceram. Soc.*, **23**, 2541 (2003).

Jantunen, H., Leppavuori, S., Turunen, A. and Uusimaki, A. "Multilayer resonators and band pass filters fabricated from a novel low temperature co-fired ceramics," *J. Electron. Mater.*, **31**, 191 (2002).

Jantunen, H., Rautioaho, R., Uusimaki, A. and Leppavuori, S. "Compositions of $MgTiO_3$-$CaTiO_3$ ceramic with two borosilicate glasses for LTCC technology," *J. Eur. Ceram. Soc.*, **20**, 2331 (2000).

Jarvis, J. B., Gayer, R. G., Grosvenor Jr, J. H., Janezic, M. D., Jones, C. A., Riddle, B., Weil, C. M. and Krupka, J. "Dielectric characterization of low-loss materials a comparison of techniques," *IEEE Trans. Dielec. Electrical Insul.*, **5**, 571 (1998).

Jayasundere, N. and Smith, B. V. "Dielectric-constant for binary piezoelectric 0-3 composites," *J. Appl. Phys.*, **73**, 2462 (1993).

Jean, J. H. and Chang, C. R. "Cofiring kinetics and mechanisms of an Ag-metallized ceramic-filled glass electronic package," *J. Am. Ceram. Soc.*, **80**, 3084 (1997).

Jean, J. H. and Gupta, T. K. "Liquid-phase sintering in the glass-cordierite system," *J. Mater. Sci.*, **27**, 1575 (1992).

Jean, J. H. and Lin, S. C. "Low-fire processing of ZrO_2-SnO_2-TiO_2 ceramics," *J. Am. Ceram. Soc.*, **83**, 1417 (2000).

Jean, J. H. and Shen, J. I. "Binary crystallizable glass composite for low-dielectric multilayer ceramic substrate," *Japanese Journal of Applied Physics Part 1-Regular Papers Short Notes & Review Papers*, **35**, 3942 (1996).

Jean, J. H. and Shen, J. I. "Densification inhibitor of low-dielectric binary glass composite," *J. Mater. Sci.*, **31**, 4289 (1996).

Jonscher, A. K. *Universal Relaxation Law*, Chelsea Dielectric, London (1996).

Joseph, T. and Sebastian, M. T. "Microwave dielectric properties of $(Sr_{1-x}A_x)_2(Zn_{1-x}B_x)Si_2O_7$ ceramics (A = Ca, Ba and B = Co, Mg, Mn, Ni)," *J. Am. Ceram. Soc.*, **93**, 147 (2009).

Joseph, T., Sebastian, M. T., Sreemoolanadhan, H. and Nageswari, V. K. S. "Effect of glass addition on the microwave dielectric properties of $CaMgSi_2O_6$ ceramics," *Int. J. Appl. Ceram. Technol.*, **7**, E98 (2010).

Joseph, T., Uma, S., Philip, J. and Sebastian, M. T. "Electrical and thermal propeties of PTFE-$Sr_2ZnSi_2O_7$ composites," *J Mater Sci: Mater. Electron.* In press (2011).

Joshi, S. C., Lam, Y. C., Boey, F. Y. C. and Tok, A. I. Y. "Power law fluids and bingham plastics flow models for ceramic tape casting," *J. Mater. Proc. Technol.*, **120**, 215 (2002).

Jylha, L., Honkamo, J., Jantunen, H. and Sihvola, A. "Microstructure-based numerical modeling method for effective permittivity of ceramic/polymer composites," *J. Appl. Phys.*, **97** (2005).

Kagata, H., Inoue, T., Kato, J. and Kameyama, I. "Low-fire bismuth-based dielectric ceramics for microwave use," *Japanese Journal of Applied Physics Part 1-Regular Papers Short Notes & Review Papers*, **31**, 3152 (1992).

Kaiser, J. W. and Jeitschko, W. "Crystal structure of the new barium zinc silicate $Ba_2ZnSi_2O_7$," *Z. Kristallogr.-New Cryst. Struct.*, **217**, 25 (2002).

Kajfez, D. G., P. *Dielectric resonators*, Noble Publishing Corporation, Atlanta, U. S. (1998).

Kang, S.-J. L. *Sintering, densification, grain growth and microstructure*, Elsevier, Amsterdam (2002).

Kang, S., Hong, S. I., Choe, C. R., Park, M., Rim, S. and Kim, J. *Polymer*, **42**, 879 (2001).

Kaul, S. K. *Millimeterwaves and optical dielectric integrated circuits*, Wiley, New York (1997).

Kiang, J. F. *Novel technologies for millimeter wave applications*. Kluwer academic publications, USA (2003).

Kim, J., Hwang, S., Sung, W. and Kim, H. "Effect of Anorthite and Diopside on dielectric properties of Al_2O_3/glass composite based on high strength of LTCC substrate," *J. Mater. Sci.*, **43**, 4009 (2008).

Kim, J., Hwang, S., Sung, W. and Kim, H. "Thermal and dielectric properties of glass-ceramics sintered based on Diopside and Anorthite composition," *Journal of Electroceramics*, **23**, 209 (2009).

Kim, J. S., Nguyen, N. H., Song, M. E., Lim, J. B., Paik, D. S., Nahm, S., Paik, J. H., Choi, B. H. and Yu, S. J. "Effect of Bi_2O_3 addition on the sintering temperature and microwave dielectric properties of Zn_2SiO_4 ceramics," *Int. J. Appl. Ceram. Technol.*, **6**, 581 (2009).

Kimata, M. "Four-coordinated Co^{2+} cation in $Ca_2CoSi_2O_7$," *Z. Kristallogr.*, **69**, 40 (1982).

Kingery, W. D. "Metal-ceramic interactions: IV, absolute measurement of metal-ceramic interfacial energy and the interfacial adsorption of Silicon from Iron-Silicon alloys " *J. Am. Ceram. Soc.*, **37**, 42 (1954).

Kingery, W. D. "Densification during sintering in the presence of a liquid phase. I. Theory," *J. Appl. Phys.*, **30**, 301 (1959).

Kingery, W. D. *Introduction to ceramics*, John Wiley and Sons, New York (1960).

Kingery, W. D. and Berg, M. "Study of the initial stages of sintering solids by viscous flow, evaporation-condensation, and self-diffusion," *J. Appl. Phys.*, **26**, 1205 (1955).

Kingery, W. D., Bowen, C. R. and Uhlmann, D. R. *Introduction to ceramics*, Wiley, New York (1976).

Kinser, D. L. "Electrical conduction in glass and glass-ceramics," *Physics of Electronic Ceramics, Part A*, 523 (1971).

Knickerbocker, S. H., Kumar, A. H. and Herron, L. W. "Cordierite glass-ceramics for multilayer ceramic packaging," *Am. Ceram. Soc. Bull.*, **72**, 90 (1993).

Kobayashi, Y. and Tanaka, S. "Resonant modes of a dielectric rod resonator short-circuited at both ends by parallel conducting plates," *IEEE Trans. Microwave Theory Tech.*, **28**, 1077 (1980).

Krupka, J. "Precise measurements of the complex permittivity of dielectric materials at microwave frequencies " *Mater. Chem. Phys.*, **79**, 195 (2003).

Krupka, J., Derzakowski, K. D., Riddle, B. and Jarvis, J. B. "A dielectric resonator for measurements of complex permittivity of low loss dielectric materials as a function of temperature," *Meas. Sci. Technol.*, **9**, 1751 (1998).

Krupka, J., Gregory, A. P., Rochard, O. C., Clarke, R. N., Riddle, B. and Baker-Jarvis, J. "Uncertainty of complex permittivity measurements by split-post dielectric resonator technique," *J. Eur. Ceram. Soc.*, **21**, 2673 (2001).

Krupka, J. and Weil, C. "Recent advances in metrology for the electromagnetic characterization of materilas at microwave frequency," *12th international conference on microwaves and radar*, **4**, 243 (1998).

Krzmanc, M. M., Valant, M. and Suvorov, D. "The synthesis and microwave dielectric properties of $Sr_xBa_{1-x}Al_2Si_2O_8$ and $Ca_yBa_{1-y}Al_2Si_2O_8$ ceramics," *J. Eur. Ceram. Soc.*, **27**, 1181 (2007).

Krzmanc, M. M., Valant, M. and Suvorov, D. "A structural and dielectric characterization of $Na_xCa_{1-x}Al_{2-x}Si_{2+x}O_8$ (x=0,1) ceramics.," *J. Eur. Ceram. Soc.*, **25**, 2835 (2005).

Kuo, D. H., Chang, C. C., Su, T. Y., Wang, W. K. and Lin, B. Y. "Dielectric behaviours of multi-doped $BaTiO_3$/Epoxy composites " *J. Eur. Ceram. Soc.*, **21**, 1171 (2001).

Kuo, D. H., Chang, C. C., Su, T. Y., Wang, W. K. and Lin, B. Y. "Dielectric properties of three ceramic/Epoxy composites," *Mater. Chem. Phys.*, **85**, 201 (2004).

Kusaka, K., Hagiya, K., Ohmasa, M., Okano, Y., Mukai, M., Iishi, K. and Haga, N. "Determination of structures of $Ca_2CoSi_2O_7$, $Ca_2MgSi_2O_7$, and $Ca_2(Mg_{0.55}Fe_{0.45})Si_2O_7$ in incommensurate and normal phases and observation of diffuse streaks at high temperature," *Phys. Chem. Miner.*, **28**, 150 (2001).

Laverghetta, T. S. *Microwave materials and fabrication techniques*, Artech House, USA (1984).

Lee, S. M. "Epoxy resin," (1988).

Levinson, L. M. *Electronic ceramics*, New York, Marcel Dekker, Inc. (1987).

Li, J. and Ananthasuresh, G. K. "Three-dimensional low-temperature co-fired ceramic shells for miniature systems applications," *Journal of Micromechanics and Microengineering*, **12**, 198 (2002).

Li, P. L., Yang, Z. P., Wang, Z. J. and Guo, Q. L. "Preparation and luminescence characteristics of Eu^{2+} activated silicate phosphor," *Chin. Phys. B*, **17**, 1135 (2008).

Lin, J. H., Lu, G. X., Du, J., Su, M. Z., Loong, C.-K. and Richardson, J. W. "Phase transition and crystal structures of $BaZn_2Si_2O_7$," *J. Phys. Chem. Solids.*, **60**, 975 (1999).

Liu, J., Duan, C. G., Mei, W. N., Smith, R. W. and Hardy, J. R. "Polymorphous transformations in alkaline-earth silicates," *J. Chem. Phys.*, **116**, 3864 (2002).

Lu, X. and Xu, G. "Thermally conductive polymer composites for electronic packaging," **65**, 2733 (1997).

Marinelli, M., Murtas, F., Mecozzi, M. G., Zammit, U., Pizzoferrato, R., Scudieri, F., Martellucci, S. and Marinelli, M. "Simultaneous determination of specific heat, thermal conductivity and thermal diffusivity at low temperature via the photopyroelectric technique," *Appl. Phys. A. Mater. Sci. and Process.*, **51**, 387 (1990).

Marques, V. M. F., Tulyaganov, D. U., Kothiyal, G. P. and Ferreira, J. M. F. "The effect of TiO_2 and P_2O_5 on densification behavior and properties of Anortite-Diopside glass-ceramic substrates," *Journal of Electroceramics*, **25**, 38 (2010).

Mason, B. and Moore, C. B. *Principles of Geochemisty*, John Wiley & Sons, Inc., New York (1982).

McHale, A. E. *Processing additives, engineering materials handbook, ceramics and glasses*, The Materials Information Society, SC (1991).

McLachlan, D. S., Blaszkiewicz, M. and Newnham, R. E. "Electrical resistivity of composites," *J. Am. Ceram. Soc.*, **73**, 2187 (1990).

Menard, K. P. *Dynamic mechanical analysis; A practical introduction*, CRC Press, Boca Raton (1999).

Menon, C. P. and Philip, J. "Simultaneous determination of thermal conductivity and heat capacity near solid state phase transitions by a photopyroelectric technique," *Meas. Sci. Techno.*, **11**, 1744 (2000).

Mistler, R. E. and Twiname, E. R. *Tape casting: Theroy and practice*. The American Ceramic Society, Westerville, OH (2000).

Molla, J., Gonzalez, M., Vila, R. and Ibarra, A. "Effect of humidity on microwave dielectric losses of porous Alumina," *J. Appl. Phys.*, **85**, 1727 (1999).

Mori, N., Sugimoto, Y., Harada, J. and Higuchi, Y. "Dielectric properties of new glass-ceramics for LTCC applied to microwave or millimeter-wave frequencies," *J. Eur. Ceram. Soc.*, **26**, 1925 (2006).

Murali, K. P., Rajesh, S., Prakash, O., Kulkarni, A. R. and Ratheesh, R. "Preparation and properties of silica filled PTFE flexible laminates for microwave circuit fabrication," *Composites Part A-Applied Science And Manufacturing*, **40**, 1179 (2009).

Nan, C.-W., Li, X.-P. and Birringer, R. "Inverse problem for composites with imperfect interface: Determination of interfacial thermal resistance, thermal conductivity of constituents, and microstructural parameters," *J. Am. Ceram. Soc.*, **83**, 848 (2000).

Nanni, P., Viviani, M. and Buscaglia, V. *Synthesis of dielectric ceramic materials, handbook of low and high dielectric constant and their applications*, Academic Press, New York (1999).

Navias, L. and Green, F. L. "Dielectric properties of glasses at ultra-high frequencies and their relation to composition " *J. Am. Ceram. Soc.*, **29**, 267 (1946).

Newnham, R. E., Skinner, D. P. and Cross, L. E. "Connectivity and piezoelectric-pyroelectric composites," *Mater. Res. Bull.*, **13**, 525 (1978).

Nisa, V. S., Rajesh, S., Murali, K. P., Priyadarsini, V., Potty, S. N. and Ratheesh, R. "Preparation, characterization and dielectric properties of temperature stable srtio$_3$/peek composites for microwave substrate applications," *Comp. Sci. Technol.*, **68**, 106 (2008).

Ochi, Y. "Crystal structure of Sr-akermanite glass–ceramics," *Mater. Res. Bull.*, **41**, 1825 (2006).

Ohsato, H., Tsunooka, T., Kan, A., Ohishi, Y., Miyauchi, Y., Tohdo, Y., Kawai, T., Kakimoto, K. and Ogawa, H. "Microwave-millimeterwave dielectric materials," *Electroceramics in Japan VII*, **269**, 195 (2004).

Ohsato, H., Tsunooka, T., Kan, A., Ohishi, Y., Miyauchi, Y., Tohdo, Y., Okawa, T., Kakimoto, K.-I. and Ogawa, H. "Microwave-millimeterwave dielectric materials," *Key Eng. Mater.*, **269**, 195 (2004).

Ohsato, H., Tsunooka, T., Sugiyama, T., Kakimoto, K. and Ogawa, H. "Forsterite ceramics for millimeterwave dielectrics," *Journal Of Electroceramics*, **17**, 445 (2006).

Onoda, G. Y. and Hench, L. L. *Ceramic processing before firing*, Wiley Interscience, New York (1973).

Park, J. H., Choi, Y. J. and Park, J. G. "Low-fire dielectric compositions with permittivity 20-60 for LTCC applications," *Mater. Chem. Phys.*, **88**, 308 (2004).

Pauling, L. "The nature of Silicon-Oxygen bonds," *Am. Mineralogist.*, **65**, 321 (1980).

Pecht, M., Agarwal, R., McCluskey, F. P., Dishongh, T. J., Javadpour, S. and Mahajan, R. *Electronic packaging materials and there properties*, CRC Press, London (1999).

Penn, S. J., Alford, N. M., Templeton, A., Wang, X. R., Xu, M. S., Reece, M. and Schrapel, K. "Effect of porosity and grain size on the microwave dielectric properties of sintered Alumina," *J. Am. Ceram. Soc.*, **80**, 1885 (1997).

Pennisi, L. *The firing process, engineered materials hand book, ceramics and glasses*, ASM International, The material information society, SC (1991).

Pieper, G., Eysel, W. and Hahn, T. "Solid solubility and polymorphism in the system Sr_2SiO_4-Sr_2GeO_4-Ba_2GeO_4-Ba_2SiO_4," *J. Am. Ceram. Soc.*, **55,** 619 (1972).

Pires, A. M. and Davolos, M. R. "Luminescence of Europium (III) and Manganese (II) in Barium and Zinc Orthosilicate," *Chem. Mater.*, **13**, 21 (2001).

Pozar, D. M. *Microwave engineering*, John Wiley & Songs, New York (1997).

R. Abraham, R. G., A. S. Bhalla *Ferroelectrics*, **1**, 315 (2005).

Rajesh, S., Nisa, V. S., Murali, K. P. and Ratheesh, R. "Microwave dielectric properties of PTFE/rutile nanocomposites," *J. Alloys. Compd.*, **477**, 677 (2009).

Rao, Y., Qu, J. M., Marinis, T. and Wong, C. P. "A precise numerical prediction of effective dielectric constant for polymer-ceramic composite based on effective-medium theory," *IEEE Transactions On Components And Packaging Technologies*, **23**, 680 (2000).

Reaney, I. M., Colla, E. L. and Setter, N. "Dielectric and structural characteristics of Ba-based and Sr-based complex perovskites as a function of tolerance factor," *Japanese Journal of Applied Physics Part 1-Regular Papers Short Notes & Review Papers*, **33**, 3984 (1994).

Renjini, S. N., Thomas, S., Sebastian, M. T., Kiran, S. R. and Murthy, V. R. K. "Microwave dielectric properties and low temperature sintering of $Sm_2Si_2O_7$ ceramic for substrate applications," *Int. J. Appl. Ceram. Technol.*, **6**, 286 (2009).

Richerson, D. W. *Modern ceramic engineering: properties processing and use in design*, Taylor and Francis, CRC press, London (2006).

Rose, H. E. and Sullivan, R. M. *A treatise on the internal mechanics of ball, tube and rod mills*, Chemical publishing, Boston (1958).

Rusu, M., Sofian, N. and Rusu, D. "Mechanical and thermal properties of Zinc powder filled high density polyethylene composites " *Polymer Testing*, **20**, 409 (2001).

Sagala, D. A. and Nambu, S. "Microscopic calculation of dielectric loss at microwave-frequencies for complex perovskite $Ba(Zn_{1/3}Ta_{2/3})O_3$," *J. Am. Ceram. Soc.*, **75**, 2573 (1992).

Samara, G. A. "Temperature and pressure dependence of the dielectric constants of the Thallous Halides," *Phys. Rev.*, **165**, 959 (1968).

Samara, G. A. "Temperature and pressure dependence of the dielectric properties of PbF_2 and the alkaline earth flurides,," *Phys. Rev. B*, **13**, 4229 (1976).

Samara, G. A. "Low temperature dielectric properties of candidate substrates for high temperature superconductors: $LaAlO_3$ and ZrO_2: 9.5 mol% Y_2O_3," *J. Appl. Phys.*, **68**, 4214 (1990).

Sareni, B. "Effective permittivity of composite materials," *Journal De Physique III*, **7**, 793 (1997).

Sareni, B., Krahenbuhl, L., Beroual, A. and Brosseau, C. "Effective dielectric constant of random composite materials," *J. Appl. Phys.*, **81**, 2375 (1997).

Sasikala, T. S., Suma, M. N., Mohanan, P., Pavithran, C. and Sebastian, M. T. "Forsterite-based ceramic-glass composites for substrate applications in microwave and millimeter wave communications," *J. Alloys Compd.*, **461**, 555 (2008).

Schmalzried, H. *Solid state reactions*, New York, Academic Press (1974).

Schwartz, M. *Mobile wireless communications*, Newyork, Cambridge University press (2005).

Sebastian, M. T. *Dielectric materials for wireless communication*, Oxford, U. K, Elseiver Publishers (2008).

Sebastian, M. T. and Jantunen, H. "Low loss dielectric materials for LTCC applications: A review," *Int. Mater. Rev.*, **53**, 57 (2008).

Sebastian, M. T. and Jantunen, H. "Polymer–ceramic composites of 0–3 connectivity for circuits in electronics: A review," *Int. J. Appl. Ceram. Technol.*, **7**, 415 (2010).

Sebastian, M. T., Menon, C. P., Philip, J. and Schwartz, R. W. "Thermal properties of $La_{0.5}Sr_{0.5}Co_{1-x}Ni_xO_{3-\delta}$ ceramics using photopyroelectric technique," *J. Appl. Phys.*, **94**, 3206 (2003).

Shamiryan, D., Abell, T., Lacopi, F. and Maex, K. "Low-k dielectric materials," *Materials today*, 34 (2004).

Shand, E. B. *Properties of glass*, McGraw-Hill, New York (1958).

Shannon, R. D. "Revised effective ionic radii and systematic study of interatomic distances in Halides and Chalcogenides," *Acta Crystallogr.*, **A32**, 751 (1976).

Shannon, R. D. "Dielectric polarizabilities of ions in Oxides and Fluorides," *J. Appl. Phys.*, **73**, 348 (1993).

Sihvola, A. H. and Kong, J. A. "Effective permittivity of dielectric mixtures," *IEEE Transactions On Geoscience And Remote Sensing*, **26**, 420 (1988).

Smaoui, H., Mir, L. E. L., Guermazi, H., Agnel, S. and Toureille, A. "Study of dielectric relaxations in Zinc oxide-epoxy resin nanocomposites," *J. Alloys Compd.*, **477**, 316 (2009).

Soane, D. S. and Martynenko, Z. *Polymers in microelectronics: Fundamentals and applications*, New York, Elsevier (1989).

Song, M. E., Kim, J. S., Joung, M. R. and Nahm, S. "Synthesis and microwave dielectric properties of $MgSiO_3$ ceramics," *J. Am. Ceram. Soc.*, **91**, 2747 (2008).

Soucy, J. W., Haley, J. F. and Marinis, T. F. "An approach to mem sensor array packaging," *2000 International Symposium on Microelectronics*, **4339**, 768 (2000).

Sparks, M., King, D. F. and Mills, D. L. "Simple theory of microwave absorption in alkali halides," *Phys. Rev. B.*, **26**, 6987 (1982).

Sprague, J. L. "Multilayer ceramic packaging alternatives," *IEEE transactions on components hybrids and manufacturing technology*, **13**, 390 (1990).

Stevels, J. M. "Local motion in vitreous systems," *J. Non-Cryst. Solids*, **40**, 69 (1980).

Stroud, D. "Percolation effects and sum rules in the optical properties of composities," *Phys. Rev. B*, **19**, 1783 (1979).

Subodh, G. *Investigations on high permittivity* $Sr_{2+n}Ce_2Ti_{5+n}O_{15+3n}$ *(n<10) based ceramics and their polymer composites for microwave applications*, Ph. D. Theis, University of Kerala. Trivandrum (2008).

Subodh, G., Joseph, M., Mohanan, P. and Sebastian, M. T. "Low dielectric loss polytetrafluoroethylene/TeO_2 polymer ceramic composites," *J. Am. Ceram. Soc.*, **90**, 3507 (2007).

Subodh, G., Manjusha, M. V., Philip, J. and Sebastian, M. T. "Thermal properties of polytetrafluoroethylene/$Sr_2Ce_2Ti_5O_{16}$ polymer/ceramic composites," *Journal Of Applied Polymer Science*, **108**, 1716 (2008).

Subodh, G., Pavithran, C., Mohanan, P. and Sebastian, M. T. "PTFE/$Sr_2Ce_2Ti_5O_{16}$ polymer ceramic composites for electronic packaging applications," *J. Eur. Ceram. Soc.*, **27**, 3039 (2007).

Sucher, M. *Measurement of Q in handbook of microwave measurements*, Polytechnic Press, Brooklyn (1963).

Sudheendran, K., James Raju, K. C. and Jacob, M. V. "Microwave dielectric properties of Ti-substituted $Bi_2(Zn_{2/3}Nb_{4/3})O_7$ pyrochlores at cryogenic temperatures," *J. Am. Ceram. Soc.*, **92**, 1268 (2009).

Sugiyama, T., Tsunooka, T., Kakimoto, K.-I. and Ohsato, H. "Microwave dielectric properties of forsterite-based solid solutions," *J. Eur. Ceram. Soc.*, **26**, 2097 (2006).

Sun, H., Zhang, Q., Yang, H. and Zou, J. "$(Ca_{1-x}Mg_x)SiO_3$: A low permittivity microwave dielectric ceramic system," *Mater. Sci. Eng. B.*, **138,** 46 (2007).

Sun, Y. Y., Zhang, Z. Q. and Wong, C. P. "Influence of interphase and moisture on the dielectric spectroscopy of epoxy/silica composites," *Polymer*, **46**, 2297 (2005).

Surendran, K. P., Bijumon, P. V., Mohanan, P. and Sebastian, M. T. "$(1-x)MgAl_2O_4$-$xTiO_2$ dielectrics for microwave and millimeter wave applications," *Applied Physics A-Materials Science & Processing*, **81**, 823 (2005).

Surendran, K. P., Mohanan, P. and Sebastian, M. T. "The effect of glass additives on the microwave dielectric properties of $Ba(Mg_{1/3}Ta_{2/3})O_3$ ceramics," *J. Solid State Chem.*, **177**, 4031 (2004).

Surendran, K. P., Santha, N., Mohanan, P. and Sebastian, M. T. "Temperature stable low loss ceramic dielectrics in "$(1-x)MgAl_2O_4$-$xTiO_2$ system for microwave substrate applications," *Eur. Phys. J. B*, **41**, 301 (2004).

Takada, T., Wang, S. F., Yoshikawa, S., Jang, S. J. and Newnham, R. E. "Effect of glass additions on BaO-TiO_2-WO_3 microwave ceramics," *J. Am. Ceram. Soc.*, **77**, 1909 (1994).

Takada, T., Wang, S. F., Yoshikawa, S., Jang, S. J. and Newnham, R. E. "Effects of glass additions on (Zr,Sn)TiO_4 for microwave applications," *J. Am. Ceram. Soc.*, **77**, 2485 (1994).

Templeton, A., Wang, X. R., Penn, S. J., Webb, S. J., Cohen, L. F. and Alford, N. M. "Microwave dielectric loss of Titanium Oxide," *J. Am. Ceram. Soc.*, **83**, 95 (2000).

Terada, M., Kawamura, K., Kagomiya, I., Kakimoto, K.-I. and Ohsato, H. "Effect of Ni substitution on the microwave dielectric properties of cordierite," *J. Eur. Ceram. Soc.*, **27**, 3045 (2007).

Thomas, S. *Silicate and aluminate based dielectric ceramic for microwave communication,* Ph. D. Thesis, Cochin university of science and technology, Cochin (2010).

Thomas, S., Deepu, V. N., Mohanan, P. and Sebastian, M. T. "Effect of filler content on the dielectric properties of PTFE/$ZnAl_2O_4$-TiO_2 composites," *J. Am. Ceram. Soc.*, **91**, 1971 (2008).

Thomas, S. and Sebastian, M. T. "Effect of B_2O_3-Bi_2O_3-SiO_2-ZnO glass on the sintering and microwave dielectric properties of 0.83$ZnAl_2O_4$-0.17TiO_2," *Mater. Res. Bull.*, **43**, 843 (2008).

Tinga, W. R., Voss, W. A. G. and Blossey, D. F. "Generalized approach to multiphase dielectric mixture theory," *J. Appl. Phys.*, **44**, 3897 (1973).

Todd, M. G. and Shi, F. G. "Characterizing the interphase dielectric constant of polymer composite materials: Effect of chemical coupling agents," *J. Appl. Phys.*, **94**, 4551 (2003).

Tovar, M., Dinnebier, R. E. and Eysel, W. "The Cu(II)O_4 tetrahedron in the åkermanite structure," *Mater. Sci. Forum.*, **278-281**, 750 (1998).

Tse, D. and Viswanath, P. *Fundametals of microwave communication,* New York, Cambridge University Press (2005).

Tsunooka, T., Androu, M., Higashida, Y., Sugiura, H. and Ohsato, H. "Effects of TiO_2 on sinterability and dielectric properties of high-Q forsterite ceramics," *J. Eur. Ceram. Soc.*, **23**, 2573 (2003).

Tummala, R. R. "Ceramic and glass-ceramic packaging in the 1990s," *J. Am. Ceram. Soc.*, **74**, 895 (1991).

Vizard, D. R. "Millimeter-wave applications: From satellite communications to security systems," *Microwave Journal*, **49**, 22 (2006).

Vo, H. T. and Shi, F. G. "Towards model-based engineering of optoelectronic packaging materials: Dielectric constant modeling," *Microelectronics Journal*, **33**, 409 (2002).

Wahlers, R. L., Stein, S. J., Huang, Y. D. and Heinz, M.R. *Leadfree multilayer dielectric system for telecommunications*, Technical publications of Electro-Science Laboratories, Prussia, PA, USA (2001).

Wakino, K., Okada, T., Yoshida, N. and Tomono, K. "A new equation for predicting the dielectric-constant of a mixture," *J. Am. Ceram. Soc.*, **76**, 2588 (1993).

Wang, H., Zhang, Q., Yang, H. and Sun, H. "Synthesis and microwave dielectric properties of $CaSiO_3$ nanopowder by the sol-gel process," *Ceram. Inter.*, **34**, 1405 (2008).

Wang, H. P., Zhang, Q. L., Yang, H. and Sun, H. P. "Synthesis and microwave dielectric properties of $(Ca_{1-x}Mg_x)SiO_3$ ceramic by sol-gel process," *Acta Physico-Chimica Sinica*, **23**, 609 (2007).

Weil, C. W. *The NIST metrology program on electromagnetic characterization of materials*, The American Ceramic Society, Westerville (1995).

Wersing, W. "Microwave ceramics for resonators and filters," *Current Opinion in Solid State & Materials Science*, **1**, 715 (1996).

West, A. R. *Solid-state chemistry and its applications*, John Wiley, Chichester (1984).

Wise, P. L., Reaney, I. M., Lee, W. E., Iddles, D. M., Cannell, D. S. and Price, T. J. "Tunability of τ_f in perovskites and related compounds," *J. Mater. Res.*, **17**, 2033 (2002).

Wise, P. L., Reaney, I. M., Lee, W. E., Price, T. J., Iddles, D. M. and Cannell, D. S. "Structure–microwave property relations in $(Sr_xCa_{(1-x)})_{n+1}Ti_nO_{3n+1}$," *J. Eur. Ceram. Soc.*, **21**, 1723 (2001).

Wong, C. P. and Bollampally, R. S. "Thermal conductivity, elastic modulus, and coefficient of thermal expansion of polymer composites filled with ceramic

particles for electronic packaging," *Journal Of Applied Polymer Science*, **74**, 3396 (1999).

Wu, J.-M. and Huang, H.-L. "Microwave properties of Zinc, Barium and Lead Borosilicate glasses," *Journal of Non-Crystalline Solids*, **260**, 116 (1999).

Xiang, F., Wang, H. and Yao, X. "Preparation and dielectric properties of Bismuth-based dielectric/PTFE microwave composites," *J. Eur. Ceram. Soc.*, **26**, 1999 (2006).

Xie, S.-H., Zhu, B.-K., Wei, X.-Z., Xu, Z.-K. and Xu., Y.-Y. *Composites Part A*, **36**, 1152 (2005).

Yokoi, A., Ogawa, H., Kan, A. and Nakamura, Y. "Relationship between crystal structure and microwave dielectric properties of Melilite-type ceramic," *J. Eur. Ceram. Soc.*, **27**, 2989 (2007).

Youngs, I. J., Stevens, G. C. and Vaughan, A. S. "Trends in dielectrics research: An international review from 1980 to 2004," *Journal Of Physics D-Applied Physics*, **39**, 1267 (2006).

Yu, S., Hing, P. and Hu, X. "Dielectric properties of polystyrene-aluminum-nitride composites," *J. Appl. Phys.*, **88**, 398 (2000).

Zhang, Q. L., Yang, H. and Sun, H. P. "A new microwave ceramics with low permittivity for LTCC applications," *J. Eur. Ceram. Soc.*, **28**, 605 (2008).

Zhang, Q. L., Yang, H. and Zou, J. L. "Microwave dielectric properties and low temperature sintering of $(Zn_{0.8}Mg_{0.2})_2SiO_4$-$TiO_2$ ceramics with Li_2O-B_2O_3," *J. Mater. Sci: Mater. Electron.*, **20**, 181 (2009).

Zhou, W., Qi, S., An, Q., Zhao, H. and Liu, N. *Mater. Res. Bull.*, **42**, 1863 (200).

Zuccaro, C., Winter, M., Klein, N. and Urban, K. "Microwave absorption in single crystals of lanthanum aluminate," *J. Appl. Phys.*, **82**, 5695 (1997).

CONFERENCES AND WORKSHOPS

1) P. S. Anjana, **Tony Joseph** and M. T. Sebastian, "Microwave dielectric properties of $Ca_{5-x}Mg_xNb_4TiO_{17}$ (x= 0-3) Ceramics," AEMC-2007, Institute of Radio physics and Electronics, University of Calcutta, December 2007 (Published by IEE).

2) P. S. Anjana, **Tony Joseph** and M. T. Sebastian, "Effect of glass addition on the microwave dielectric properties of $Ce_2(WO_4)_3$ ceramics," 5^{th} International conference on Microwave Materials and their Applications-2008, Hangzhou, China, September 2008.

3) **Tony Joseph,** H. Sreemoolanadhan, V. K. Sree Nageswari and M. T. Sebastian , **"**Diopside based low loss low permittivity ceramics for LTCC applications," NSFD-15, Thapar University, Patiala, November 2008

4) **Tony Joseph** and M. T. Sebastian, "Microwave dielectric properties of $(Ca_{1-x}Sr_x)_2Si_2O_7$ ceramics," International seminar on high temperature materials, BHU, Varanasi, February 2009.

5) Jobin Varghese**, Tony Joseph** and M. T. Sebastian, "Synthesis and characterization of $ASiO_4$ ceramics for gate dielectric applications," ICAFM-09, NIIST-Trivandrum, December 2009.

6) **Tony Joseph** and M. T. Sebastian**,** "Microwave dielectric properties of $Ca_{2-x}Sr_xZnSi_2O_7$ Ceramics (x = 0-2)," AEMC-2009, Institute of Radio physics and Electronics, University of Calcutta, December 2009.

7) **Jobin cusat**

8) Workshop in NIIST

PUBLICATIONS

1. D. Guha, S. Biswas, **Tony Joseph** and M.T. Sebastian, *Electron. Lett.*, 44 [14] (2008)

2. **Tony Joseph** and M. T. Sebastian, *J. Am. Ceram. Soc.*, 93 [1] 147–154 (2010)

3. Jobin Varghese, **Tony Joseph**, M. T. Sebastian, M. R. McLaren, A. Feteira, *J. Am. Ceram. Soc.*, 93 [10] 2960–2963 (2010)

4. P. S. Anjana, **Tony Joseph** and M. T. Sebastian, *J. Alloys Compd.*, 490 [1-2] 208–213 (2010)

5. **Tony Joseph**, P.S. Anjana, S. Letourneau, R. Ubic, S. v. Smaalen, M. T. Sebastian, *Mater. Chem. Phys.*, 121 [1-2] 77–82 (2010)

6. P. S. Anjana, **Tony Joseph** and M. T. Sebastian, *Ceram. Int.*, 36 [5] 1535–1540 (2010)

7. **Tony Joseph**, H. Sreemoolanadhan, V. K. Sree Nageswari and M. T. Sebastian, *Int. J. Appl. Ceram. Technol.* 7 [S1] E98–E106 (2010)

8. **Tony Joseph** and M. T. Sebastian, *Mater. Lett.*, 65 [5] 891-93 (2010)

9. **Tony Joseph**, H, Jantunen, M. Jacob, H. Sreemoolanadhan and M. T. Sebastian, *Int. J. Appl. Ceram. Technol.* (2010) Accepted

10. **Tony Joseph**, S. Uma, J. Philip and M. T. Sebastian, *J. Mater. Sci: Mater. Electron.* (2010) Accepted

11. Jobin Varghese, **Tony Joseph** and M. T. Sebastian, *Mater. Lett.* (2010) Accepted